6GNTN

D4.1 REPORT ON UNIFIED AND DATA DRIVEN AIR-INTERFACE FOR 6G-NTN

Revision: v.1.0

Work package	4
Task	Task 4.1
Due date	31/05/2023
Submission date	21/07/2024
Deliverable lead	UNIBO
Version	1.0
Authors	Carla Amatetti (UNIBO), Alessandro Vanelli-Coralli (UNIBO), Musbah Shast (CTTC), Marius Caus (CTTC), Estefania Recayte (DLR), Eduardo Medeiros (ERIS), Chao Zhang C (ERIS) Juan Bucheli (QCM), Mehmet Gurelli (QCM), Nathan Borios (TASF), Dorin Panaitopol (TH-SIX), Sorya Tong (TH-SIX)
Reviewers	Miguel-Ángel Vazquez (CTTC), Joel Grotz (SES), Sebastian Euler (ERIS), Per-Erik Eriksson (ERIS)
Abstract	This deliverable is the first version of the report on unified and data-driven air-interface for 6G-NTN. It provides the preliminary outcomes of the evaluation of a set of waveforms identified by the project as potential candidates for the NTN component of 6G, namely CP-OFDM, WOLA-OFDM, DFT-s-OFDM, F-OFDM, BF-OFDM, UFMC, and OTFS. To this aim, the deliverable contains: i) the selection of the required waveform features and Key Performance Indicators (KPIs) to be used for the waveform assessment and final selection; ii) the review of the state-of-the-art for the TN and NTN waveforms; iii) the characterization of the channel models for the new frequency bands identified by WP3, i.e., C band and Q/V bands, and of the non-linear amplification and phase noise impairments; iv) the initial waveform performance analysis in two scenarios for the C band and one scenario for the Q/V band. The deliverable contains also a detailed description of the numerical results obtained during the calibration phase of the Partners' simulation tools aimed at ensuring a consistent and fair comparison of the Partners' analysis.
Keywords	Waveform, BLER, PSD, channel models, design drivers

www.6g-ntn.eu

Grant Agreement No.: 101096479
Call: HORIZON-JU-SNS-2022

Topic: HORIZON-JU-SNS-2022-STREAM-B-01-03
Type of action: HORIZON-JU-RIA

Document Revision History

Version	Date	Description of change	List of contributor(s)
V0.1	15/02/2023	Creation of the document	Carla Amatetti, Alessandro Vanelli-Coralli (UNIBO)
V0.2	10/06/2024	Document ready for the internal review	UNIBO, CTTC, DLR, ERIS, QLC, TAS-F, TH-SIX
V1.0	21/07/2024	Final version submitted to EC	UNIBO

DISCLAIMER

Co-funded by the European Union

Project funded by

Schweizerische Eidgenossenschaft
Confédération suisse
Confederazione Svizzera
Confederaziun svizra

Swiss Confederation

Federal Department of Economic Affairs, Education and Research EAER
State Secretariat for Education, Research and Innovation SERI

6G-NTN (*6G Non Terrestial Network*) project has received funding from the Smart Networks and Services Joint Undertaking (SNS JU) under the European Union's Horizon Europe research and innovation programme under Grant Agreement No 101096479. Views and opinions expressed are however those of the author(s) only and do not necessarily reflect those of the European Union. Neither the European Union nor the granting authority can be held responsible for them. This work has received funding from the Swiss State Secretariat for Education, Research and Innovation (SERI).

COPYRIGHT NOTICE

Project co-funded by the European Commission in the Horizon Europe Programme		
Nature of the deliverable:	**R**	
Dissemination Level		
PU	*Public, fully open, e.g., web (Deliverables flagged as public will be automatically published in CORDIS project's page)*	✓
SEN	*Sensitive, limited under the conditions of the Grant Agreement*	
Classified R-UE/ EU-R	*EU RESTRICTED under the Commission Decision No2015/ 444*	
Classified C-UE/ EU-C	*EU CONFIDENTIAL under the Commission Decision No2015/ 444*	
Classified S-UE/ EU-S	*EU SECRET under the Commission Decision No2015/ 444*	

* R: Document, report (excluding the periodic and final reports)
DEM: Demonstrator, pilot, prototype, plan designs
DEC: Websites, patents filing, press & media actions, videos, etc.
DATA: Data sets, microdata, etc.
DMP: Data management plan
ETHICS: Deliverables related to ethics issues.
SECURITY: Deliverables related to security issues
OTHER: Software, technical diagram, algorithms, models, etc.

EXECUTIVE SUMMARY

D4.1 is the first version of the deliverable on the unified and data driven air interface for 6G-NTN, whose primary purpose is to provide the initial development related to the design of the flexible waveform for 6G-NTN. More specifically, the objective of this document is to report preliminary outcomes of the evaluation of a set of waveforms identified by the project as potential candidates for the NTN component of 6G.

To achieve such goal, the work is organized in four main activities:

- Definition of the desirable list of features (also known as design drivers) for the 6G NTN waveform and of the Key Performance Indicators (KPIs) for their evaluation.
- A comprehensive state-of-the-art review with the aim to narrow down a pool of waveforms for the preliminary evaluation. This review considered both standardized waveforms, such as Cyclic Prefix (CP) – Orthogonal Frequency Division Multiple Access (OFDM), and non-standardized waveforms proposed in the literature and assessed in other studies.
- Analysis of channel modelling in NTN within the new frequency bands addressed in the project (i.e., C, Q, and V bands), with a particular attention on multipath effects triggered by the propagation environment on the Earth surface. This activity also includes:
  - ray tracing simulations to obtain the rice factor and the delay spread under three different propagation scenarios, i.e., suburban, urban, dense urban, considering elevation angles in the range of [10°, 90°] with random azimuth angle;
  - definition of the hardware (HW) impairments to be considered at the transmitter and the receiver side. Particular attention has been dedicated to the characterization and definition of the High-Power Amplifier (HPA) in C and Q/V bands.
- Performance analysis of the selected waveforms by means of simulations. The selected candidate waveforms are all OFDM-based waveforms, namely CP-OFDM, WOLA-OFDM, DFT-s-OFDM, F-OFDM, BF-OFDM, UFMC, and OTFS. The simulations process consists of:
  - Partners' software tools calibration, with the aim of ensuring that all partners' simulators were aligned for consistent waveform comparison. More in details, an end-to-end analysis of the CP-OFDM and DFT-s-OFDM with 15 kHz and 120 kHz of Sub-Carrier Spacing has been performed by all partners evaluating Bit Error Rate (BER), Block Error Rate (BLER), Power Spectral Density (PSD), and Peak to Average Power Ratio (PAPR) on three scenarios. Results have been then compared and discrepancies identified and fixed.
  - Waveforms evaluation, aiming to assess and compare the candidate waveforms, i.e., CP-OFDM, WOLA-OFDM, DFT-s-OFDM, F-OFDM, BF-OFDM, UFMC, and OTFS. Three different scenarios have been defined, one in Q/V band and two in C band. Results have been compared in terms of BER, BLER, PSD, and PAPR.
    - Simulation results showed that OFDM-based waveforms exhibit nearly identical BER/BLER in AWGN. However, while filtered waveform have similar out-of-band emissions, CP-OFDM, DFT-spread alternatives, and OTFS show higher emissions due to their reliance on sharp rectangular pulses that cause significant spectral regrowth. When the HPA is considered, all OFDM-based waveforms show similar out-of-band emissions, though DFT-s-OFDM demonstrates slightly less PA-related performance degradation because of its improved PAPR. The increased computational complexity of UFMC, BF-OFDM, and F-OFDM does not seem justified by the qualitative or quantitative gains for the studied KPIs, compared to the lower-complexity WOLA-OFDM.

Finally, OTFS provides similar performance to OFDM, except in scenario C3, where it outperforms OFDM thanks to its inherent robustness to the multipath at the expense of higher computational complexity.

It is worth mentioning that in this preliminary analysis, the waveform assessment has been performed under the assumption of ideal channel estimation and synchronisation, and no receiver optimization. In the second release of the deliverable, the robustness against estimation and synchronization non-idealities will be addressed

TABLE OF CONTENTS

.

LIST OF FIGURES

LIST OF TABLES

Co-funded by the European Union

ABBREVIATIONS

3D	Three-Dimensional
6G	Sixth Generation
ACE	Active Constellation Extension
ADC	Analog to Digital Converters
AI	Artificial Intelligence
AWGN	Additive White Gaussian Noise
BER	Bit Error Rate
BFN	Beam Forming Network
BLER	Block Error Rate
BT	Bandwidth Time
CDF	Cumulative Distributed Function
CP	Cyclic Prefix
CPFSK	Continuous-Phase Frequency Shift Keying
CPM	Continuous-Phase Modulation
CQI	Channel Quality Indicator
CSI-RS	Channel State Information Reference Signal
DAC	Digital to Analog Conversion
DD	Delay-Doppler
DFT-s-OFDM	Discrete Fourier Transform spread OFDM
DL	Downlink
DMRS	Demodulation Reference Signal
DRA	Direct Radiating Antenna
DVB-S2	Digital Video Broadcasting Second Generation
DVB-S2X	Digital Video Broadcasting Second Generation - eXtension
F-OFDM	Filtered OFDM
FBMC	Filter Bank Multi-carrier
FDD	Frequency Division Duplex

FDE	Frequency Domain Equalization
FER	Frame Error Rate
FFT	Fast Fourier Transform
FMT	Filtered multitone
FWD	Forward Link
G-OFDM	Generalized OFDM
GI	Guard Interval
GMSK	Gaussian Minimum Shift Keying
GNSS	Global Navigation Satellite System
GSO	Geostationary Orbit
HPA	High Power Amplifier
HW	Hardware
IBO	Input Backoff
ICI	Inter-Carrier Interference
ISFFT	Inverse Simplistic Finite Fourier Transform
ISI	Inter-Symbol Interference
KPIs	Key Performance Indicators
LDPC	Low Density Parity Check
LEO	Low Earth Orbit
LLR	Log Likelihood Ratio
LMMSE	Linear Minimum Mean Square Error
LoS	Line-of-Sight
MCS	Modulation and Coding Scheme
MIMO	Multiple Input Multiple Output
MP	Message Passing
MRC	Maximum-Ratio Combining
MSE	Mean Square Error
MSK	Minimum Shift Keying
MSR	Multiple Signal Representation

NGSO	Non-Geostationary Orbit
NLoS	Non-Line of Sight
NR	New Radio
NTN	Non-Terrestrial Network
OBO	Output Backoff
OFDM	Orthogonal Frequency Division Multiplexing
OOB	Out-of-band emissions
OTFS	Orthogonal Time-Frequency Space
PA	Power Amplifier
PAPR	Peak to Average Power Ratio
PBCH	Physical Broadcast Channel
PDSCH	Physical Downlink Shared Channel
PN	Phase Noise
PSD	Power Spectral Density
PSS	Primary synchronization signal
PTRS	Phase Tracking Reference Signal
PTS	Partial Transmit Sequences
PUSCH	Physical Uplink Shared Channel
RAT	Radio Access Technology
RCS	Return Channel Satellite
RIC	Radio Intelligent Controller
RRM	Radio Resource Management
RS	Reference Signal
RTN	Return Link
RX	Receiver
SC-FDE	Single Carrier FDE
SC-QAM	Single Carrier-Quadrature Amplitude Modulation
SFN	Single Frequency Network
SoA	State of the Art

SSS	Secondary Synchronization Signal
SW	Software
TDD	Time Division Duplex
TDE	Time Domain Equalization
TF	Time-Frequency
TN	Terrestrial Network
TRP	Transmission/Reception Points
TX	Transmitter
UAV	Unmanned Aerial Vehicle
UE	User Equipment
UFMC	Universal Filtered Multi-carrier
UL	Uplink
UW DFT-s-OFDM	Unique Word DFT-s-OFDM
WOLA	Weighted Overlap and Add
ZC	Zadoff-Chu
ZT DFT-s-OFDM	Zero-tail DFT-s-OFDM

1 INTRODUCTION

The broaden ambition of the 6G-NTN project is the design of a Non-Terrestrial Network (NTN) component fully integrated into future 6G infrastructure which allows to meet the vertical industry's needs and consumer market expectations thanks to its greater coverage, increased resilience, and improved sustainability.

In order to achieve this objective, the 6G-NTN project will research and develop a revolutionary three-dimensional (3D) network infrastructure concept for 6G with the ambition to provide, through unification with the Terrestrial Network (TN) component, a ubiquitous coverage with high data rate communication at quasi ultra-low latency while providing a disruptive concept of high accuracy and reliable location service. This infrastructure will leverage: i) more effective terminals in terms of cost, size, and power consumption, compatible with both TN and NTN access; ii) flexible software defined payloads; iii) a flexible waveform; iv) Artificial Intelligence (AI)-enhanced Radio Intelligent Controller (RIC) to provide effective Radio Resource Management (RRM) solutions; and v) solutions relying on cloud native architecture and open interfaces mainly focused on securing the communication scheme

Deliverable D4.1 is the first deliverable on the unified and data driven air interface for 6G-NTN, and its updated version will be produced by the end of the project. The general purpose of this document is to provide the initial insights and guidelines related to the design of the flexible waveform of 6G NTN.

1.1 OBJECTIVE OF THE DOCUMENT

The objective of D4.1 is to identify a set of potential waveforms for 6G NTN and to report a preliminary performance evaluation. The preliminary selection and evaluation of the candidate waveforms is based on the following steps:

- Identification of the desirable list of features (also known as design drives) and the set of Key Performance Indicators (KPIs) to evaluate the waveforms.
- Review of the state-of-the-art, including both standardized waveforms, such as Cyclic Prefix (CP) – Orthogonal Frequency Division Multiple Access (OFDM), and non-standardized waveforms studied in the scientific literature and projects.
- Identification and modelling of the hardware impairments to be considered in the evaluation process.
- Software calibration to ensure that all partners' simulators are aligned for fair and consistent waveform comparisons.
- Performance evaluation of the selected waveforms through numerical simulations.

In parallel, the definition of wireless propagation models for non-terrestrial networks within the new frequency bands addressed in the project (i.e., C, Q, and V bands) by means of an extensive literature review and ray tracing simulations of specific scenarios has been conducted.

1.2 STRUCTURE OF THE DOCUMENT

The document is organized in the following way:

- Section 2 provides a description of the KPIs and design drivers of the waveform.

- Section 3 presents the state of the art of the waveforms.
- Section 4 is dedicated to description of the NTN channel models in C band and Q/V band and reports the outputs of the ray tracing simulations and the description of the hardware impairments.
- Section 5 provides the method and the results of the software calibration.
- Section 6 reports the simulation results of the selected waveforms.
- Section 7 concludes the deliverable highlighting the major results and work that will be performed in the next deliverable.

2 AIR INTERFACE/WAVEFORMS FEATURES AND KPIS

To evaluate the candidate waveforms for the NTN component of 6G, which are intended to meet the requirements identified in this project, specifically in D2.3 'Report on system requirements', a comprehensive list of desirable features is presented in this chapter. Then, a set of KPIs has been selected to rigorously assess the candidate waveforms. The KPIs were carefully chosen to provide a robust framework for assessing the performance of each waveform candidate in meeting the specific demands and objectives of the NTN scenario.

In Section 2.1, the set of features is introduced and their relationship to the project's objectives are detailed. In Section 2.2 the set of KPIs is described.

2.1 WAVEFORM DESIGN FEATURES

In this section, we provide an outline of the desired features based on their importance level attributed by the project consortium. The rationale for considering specific features when choosing the waveform is provided, along with an explanation of how waveform design affects these features. Following this discussion, Table 1 presents a summary of the prioritized features and their implications in NTN waveform design.

- F1: Compatibility with terrestrial network

Compatibility with the terrestrial network refers to the capability for the waveform to be utilized in both TN and NTN in the context of 6G to seamlessly coexist and interact. This compatibility holds significance as it ensures several key functionalities and advantages within the 6G ecosystem. Firstly, it facilitates seamless handover between terrestrial and non-terrestrial networks, ensuring seamless connectivity for users moving between different coverage areas or network types. Secondly, it promotes device compatibility, i.e., enabling devices (i.e., User Equipment - UE) to operate seamlessly across both terrestrial and non-terrestrial networks without necessitating significant modifications or additional hardware (i.e., using the same chipset), thereby enhancing user experience and device versatility. Finally, utilizing a compatible waveform across TN and NTN components simplifies hardware design and implementation, reducing overall complexity and cost associated with network deployment and maintenance.

- F2: Possibility for spectrum sharing

The possibility for spectrum sharing, facilitated by a flexible waveform design, denotes the capability to allocate and utilize available frequency bands efficiently across both TN and NTN. This feature enables a sharing of spectrum resources under various scenarios and use cases, enhancing spectrum utilization efficiency and accommodating diverse network requirements. Spectrum sharing between TN and NTN needs a compatible design of waveform for seamless coordination and allocation of spectral resources between TN and NTN networks, allowing for optimized utilization with minimal interference or degradation of service quality.

- F3: Robustness to co-channel interference

Robustness to co-channel interference refers to the network's ability to maintain reliable and effective communication when facing interference from signals transmitted on the same frequency channels. This ensures that the NTN system can provide a large coverage in a cost-effective manner, while also enabling the possibility to properly coexist with terrestrial network deployments.

- F4: Possibility for seamless connectivity

This feature ensures continuous and reliable connectivity for UE across diverse deployment scenarios and geographical regions, regardless of the type or location of the NTN platform being accessed. A well-designed waveform for NTN facilitates seamless connectivity by enabling efficient handovers and seamless transition between TN and NTN, thus ensuring good end-user experience throughout the coverage area.

- F5: Ability to provide an additional link margin

The ability to provide an additional link margin (specially in C band, where regular smartphones are expected to operate) refers to the air interface's capability to improve the signal strength and reliability, particularly to accommodate users in light indoor and in-vehicle environments in NTN. These scenarios typically involve increased penetration loss, requiring an enhanced link margin to ensure reliable communication.

- F6: Support of accurate network-based positioning

Support of accurate network-based positioning refers to one waveform’s capacity to facilitate robust localization capabilities, allowing network operators to accurately track the geographic locations of UE devices for various applications, such as emergency services, location-based services, and network optimization. This could entail, for example, the provision of dedicated pilot symbols or reference signals within the waveform to enable precise timing and phase measurements for accurate estimation of UE positions within the network infrastructure. Furthermore, waveform parameters, such as symbol duration, subcarrier spacing, and transmission power levels, can be carefully optimized to balance between localization accuracy and spectral efficiency.

- F7: Support to UE without Global Navigation Satellite System (GNSS) receiver

The support for UE without GNSS refers to the air interface's capability to enable UE connectivity to NTN for UEs without GNSS support or in scenarios where GNSS signals are unavailable or unreliable, such as indoor environments or areas with limited GNSS visibility. This feature ensures that UE can establish and maintain communication with NTN platforms without relying on GNSS-based location services. In 5G NTN, the UE uses its position and satellite ephemeris information to compensate for Doppler shift, introducing a dependency on GNSS availability.

- F8: Backward compatibility with 5G

Backward compatibility with 5G refers to the ability of the air interface to integrate with and support existing 5G New Radio (NR) standards. This feature ensures that 6G NTN can leverage the infrastructure, devices, and protocols established by 5G deployments, promoting smooth migration paths from 5G to 6G. By maintaining backward compatibility, the air interface promotes immediate compatibility with 5G smartphones and devices, enabling efficient utilization of existing network resources and enhancing the user experience across both 5G and 6G networks.

- F9: Support of Frequency Division Duplexing (FDD) and Time Division Duplexing (TDD)

By supporting both FDD and TDD, the air interface enables flexibility in spectrum utilization. The choice between FDD and TDD modes depends on specific deployment scenarios and use cases, with each mode offering distinct advantages in terms of spectral efficiency, coverage, and latency management.

- F10: Computational complexity

Computational complexity in the context of air interface design refers to the level of computational resources required for the signal processing, e.g., modulation, demodulation, error correction, and other algorithms needed for efficient communication within the network.

This aspect is crucial as it directly impacts the efficiency, performance, and scalability of the network infrastructure. For NTN, the computational complexity may influence the payload design and overall capacity, since satellites may be power limited. Minimizing computational complexity ensures that the network operates effectively, meeting communication demands while optimizing resource utilization and minimizing energy consumption.

TABLE 1: SUMMARY OF THE WAVEFORM FEATURES

Name	Definition
Compatibility with terrestrial network	If TN and NTN 6G components have a compatible waveform, that would improve 1) seamless handover between the networks, 2) device compatibility, 3) potential to integrate and use 5G/6G infrastructure, 4) coexistence 5) hardware complexity
Possibility for spectrum sharing	It is desirable to have a waveform design that allows efficient spectrum sharing between TN and NTN.
Robustness to co-channel interference	The network should be able to maintain reliable and effective communication in the presence of interference from signals transmitted on the same frequency channels.
Possibility for seamless connectivity	The air interface should support seamless connectivity to NTN platforms including flying nodes, NGSO satellites, and GEO satellites.
Ability to provide an additional link margin (especially in C band)	To serve smartphone users in light indoor and in-vehicle conditions, the air interface should be able to provide additional link margin to combat extra penetration loss.
Support of accurate network-based positioning	Dedicate pilot signals or reference symbols to facilitate accurate timing and phase measurements for accurate positioning.
Support to UE without GNSS	UE should still be able to connect to NTN when GNSS is not available or unreliable, such as indoor environment.
Backward compatibility with 5G	3GPP 5G NR specifications support NTN since Release 17. An air interface having backward compatibility with 5G will benefit from 5G flexibility and immediate compatibility with 5G smartphones.
Support of FDD and TDD	Supporting both FDD and TDD enables more deployment possibilities when spectrum is scarce (or only available for one type of duplexing). The choice of using FDD or TDD is dependent on scenarios and use cases.
Computational complexity	The air interface design should ensure that the network operates effectively while minimizing the demand on processing resources.

2.2 WAVEFORMS KPIS

In the previous section, we present the desired features within the NTN framework, which can be addressed by having a flexible waveform design. To assess the performance of waveform candidates, we have carefully chosen several KPIs, and ordered them based on their importance levels (from high to low). By using these KPIs, researchers and stakeholders can systematically evaluate different waveform candidates and make decisions regarding their

Co-funded by the European Union

suitability. Additionally, these KPIs offer valuable insights into the trade-offs involved in waveform design, helping to refine the process for optimal performance and functionality.

Below we provide the definitions of various KPIs selected in the project. Table 2 summarizes the information presented in the text and the metric used to evaluate the KPI.

- K1: Spectral efficiency

Efficient utilization of the spectrum is essential to meet demanding data rate requirements. In this project, we consider operating frequency bands including C band and Q/V band. These frequency bands are limited and possibly shared among multiple services. Evaluating waveform spectral efficiency helps maximize the utilization of available spectrum resources, enabling more efficient communication, and accommodating more users within the allocated frequency bands.

- K2: Robustness to Doppler

NTN is used under high Doppler environment (as opposed to TN). It is particularly important to test the 6G-NTN waveform against high Doppler to choose the most adapted 6G-NTN waveform with high resilience to Doppler. In NTN, UE must calculate the relative speed and Round-Trip Time (RTT) of the service link, for timing and Doppler resolution. There is also a proposition to connect UEs to NTN without relying on GNSS support. Instead, UEs can be localized using standalone Radio Access Technology (RAT) methods, thereby establishing a connection with NTN. Enhancing the waveform design to exhibit improved robustness to Doppler in the NTN scenario can significantly increase the feasibility of UEs connecting to NTN without GNSS support.

- K3: Flexibility/scalability

Waveform flexibility refers to the ability of a communication system to adapt and adjust its waveform parameters to meet varying requirements, conditions, or constraints. A flexible design of waveforms in NTN system allows the network to operate in multiple frequency bands, different bandwidth, various scenarios, etc. The flexible design can also enhance network scalability, i.e., increase the coverage, harmonize different use cases and improve the resource management of the NTN system.

- K4: Robustness to Timing error

Timing error variation for NTN has to be considered especially for Low Earth Orbit (LEO) satellite scenarios. It is particularly important to test the 6G-NTN waveform against timing errors. Furthermore, in TDD setups, a waveform design resilient to timing errors leads to notable enhancements in synchronization performance. This improvement, in turn, enhances overall performance in TDD networks. By addressing timing error challenges through appropriate waveform design, NTN can achieve heightened efficiency, accuracy, and reliability, particularly in LEO scenarios and TDD networks.

- K5: PAPR/PA backoff

Power amplifiers can introduce non-linear distortion when operating near their saturation point. High Peak to Average Power Ratio (PAPR) signals may exceed the amplifier's linear range, leading to distortion and intermodulation products. Evaluating PAPR allows for determining the required Power Amplifier (PA) backoff, which ensures the amplifier operates within its linear range, minimizing distortions and maintaining signal quality. The performance of the PA is evaluated by comparing its Output Backoff to Input Backoff (OBO-IBO) characteristics. This is particularly important in non-terrestrial networks where signal degradation due to non-linear distortion can have a significant impact on system performance. Specifically, this improvement in the link budget will be particularly advantageous in scenarios such as light indoor environments or when users are in vehicles, where additional penetration loss occurs due to the material blockage.

➲ K6: Robustness against phase noise

Phase noise refers to the random fluctuations in the phase of a signal, which can occur due to various factors such as imperfections in oscillators or frequency synthesizers. Phase noise affects all types of transmitters and receivers, but especially where high-quality oscillators may not be feasible for economical or other reasons.

Phase noise levels increase with carrier frequency. In this project, we have a candidate frequency band i.e., Q/V band, operating at mm-wave bands, where signals are more sensitive to phase noise.

By designing waveforms that are robust to phase noise, NTNs can maintain reliable communication links and efficient deployment of communication systems in space.

➲ K7: Out-of-band emissions (OOE)

Non-terrestrial networks often coexist with other communication services and systems, such as terrestrial wireless networks, other satellite systems, or radio astronomy observatories. Evaluating out-of-band emissions helps ensure that the non-terrestrial network's emissions do not cause harmful interference to these coexisting services. This coexistence is crucial for maintaining harmonious operation, preventing service degradation, and fostering efficient utilization of the radio spectrum. This will also impact the co-channel interference since the co-existence of 6G-NTN and 6G-TN is also within the scope of the study of the project.

➲ K8: Robustness to frequency-selective channels

The use of very narrow beams in NTNs can substantially reduce the frequency selectivity of the channel. By tightly focusing the transmission beams, the received signal experiences less multipath propagation and reduces the effects of frequency-selective fading. In scenarios where Line-of-Sight (LoS) propagation is dominant, the channel may reduce to a single tap, indicating minimal frequency selectivity.

On the contrary, extreme bandwidths can increase the frequency selectivity of the channel. A wider bandwidth results in a larger range of frequency components, potentially leading to greater variations in attenuation and phase distortion across the frequency spectrum.

The impact and importance of frequency selectivity for waveform design in NTN are strongly dependent on the specific use case.

➲ K9: Robustness to time-selective channels

Generally, a propagation channel is time selective when the transmitted signal is reflected and scattered (multi-path propagation) and not stationary. In NTN scenarios, in most cases the propagation path can be seen as a LoS for outdoor users, making the channel less time selective. However, due to the interest in ubiquitous coverage it is desirable to serve users in Non LoS (NLoS) conditions, with high time-dispersion as well. Good candidate waveforms are expected to provide high robustness to time-selective channels.

TABLE 2: SUMMARY OF THE WAVEFORM KPIS

Name	**Metrics for evaluation**	**Definition**
Spectral efficiency	Bit/s/Hz	To maximize data throughput while ensuring efficient spectrum use.
Robustness to Doppler	BER, BLER	The fast movement of LEO satellites and high carrier frequency create large Doppler shifts in NTN system.
Flexibility/scalability	-	The ability to operate in multiple frequency bands, different bandwidths, various scenarios in NTN system.
Robustness to timing error	BER, BLER	In TDD, precise time synchronization is required to ensure system performance in NTN.
PAPR/HPA IBO-OBO	BER, BLER for a given IBO level	Power amplifiers can introduce non-linear distortion when operating near their saturation point. High PAPR signals may exceed the amplifier's linear range, leading to distortion and degraded performance.
Robustness to phase noise	BER, BLER	Phase noise levels increase with carrier frequency. Choosing waveforms that are robust to phase noise is crucial for reliable operation and increased coverage.
Out of Band Emission	ACLR, SEM	Evaluating out-of-band emissions helps ensure that the NTN's emissions do not cause harmful interference to coexisting services (e.g., coexist with TN).
Robustness to frequency selective channel	BER, BLER	Frequency selective fading becomes more prominent in NTN scenarios due to high mobility and/or dynamic channel conditions. Techniques such as adaptive modulation, coding and MIMO compatibility are crucial in waveform design to combat the issue.
Robustness to time selective channel	BER, BLER	The movement of satellites and the high operating frequency, such as in the Q/V band, introduces time selectivity to the channel.

3 STATE OF THE ART FOR WAVEFORM/AIR INTERFACE

This section is devoted to the State-of-the-Art (SoA) of the waveforms/air interface to identify the most suitable candidate waveforms. It is organized in two main sub-sections: i) SoA on standardized air interface and ii) SoA on non-standardized air interface proposed in the literature and in other studies. Both multicarrier and single-carrier waveforms are analysed.

3.1 3GPP AIR INTERFACE

This section will provide a description of the standardized waveforms in 5G NR, including frame structure, modulation, OFDM and DFT-s-OFDM baseband signal generation.

In 3GPP, the document specifying the 5G NR waveform for terrestrial networks is the Technical Specification (TS) 38.211 – Physical Channels and Modulation [1]. It outlines the specifics of physical channels and modulation techniques. The same waveform specification is valid for 5G-NTN.

3.1.1 NR Frame Structure

The NR frame structure is specified in [1]. The design of the frame and slot structure ensures efficient time and frequency resource allocation for both uplink and downlink transmissions in 5G NR, with support for different numerologies and configurations. The frame structure in 3GPP 38.211 is a fundamental aspect of how data and control information is organized and transmitted in 5G networks.

The downlink transmission waveform is the conventional OFDM using a Cyclic Prefix (CP). The uplink transmission waveform is the conventional OFDM using a CP with a transform precoding function performing Discrete Fourier Transform (DFT) spreading that can be disabled or enabled. Downlink and uplink transmissions are organized into frames with 10 ms duration, consisting of ten 1 ms subframes. Each frame is divided into two equally sized half-frames of five subframes each. The slot duration is 14 symbols with normal CP and 12 symbols with extended CP, and scales in time as a function of the used sub-carrier spacing so that there is always an integer number of slots in a subframe.

In the following, we will provide a summary on the key elements of the frame structure defined in [1].

3.1.1.1 Subcarrier spacing

In 5G NR, the subcarrier spacing can vary from 15 kHz to 960 kHz[1] as specified in [1]. The larger subcarrier spacings allow for lower latency and support higher-frequency bands, while smaller spacings are suitable for lower-frequency bands and increased coverage. The term "numerology" describes the selection of specific subcarrier spacing configurations (and other parameter settings), enabling the system to adapt and optimize its parameters for various 5G communication scenarios.

---

[1] Most commercial deployments are based on 15, 30 and 120 kHz subcarrier spacings, though.

Table 3 shows the mapping between numerology (parameter μ) and subcarrier spacing. The numerology μ = 0 represents $\Delta f_{\mu=0} = 15\text{kHz}$, which is the same as LTE. The subcarrier spacing of the other numerologies is derived from $\Delta f_{\mu=0}$ by scaling up in the power of 2.

TABLE 3: SUPPORTED TRANSMISSION NUMEROLOGIES

μ	$\Delta f = 2^{\mu} \cdot 15[\text{kHz}]$
0	15
1	30
2	60
3	120
4	240
5	480
6	960

3.1.1.2 Slot length

As mentioned previously, downlink and uplink transmissions are organized into frames with T_f= $(\Delta_{fmax}N_f/100)\cdot T_c$ duration, where T_c is the time unit for NR, Δf_{max} is the subcarrier spacing, N_f is the Fast Fourier Transform (FFT) size which equals to 4096. Hence, each consisting of ten subframes of T_f= $\left(\frac{\Delta_{fmax}N_f}{100}\right)\cdot T_c = 1\,ms$ duration.

Having the mapping between numerology and subcarrier spacing in mind, we can easily calculate the slot length for different numerologies (shown in Table 4). Note that the general tendency is that slot length gets shorter as subcarrier spacing gets wider.

TABLE 4: SLOT LENGTH FOR DIFFERENT NUMEROLOGIES

μ	$N_{\text{slot}}^{\text{subframe},\mu}$	**Slot length [ms]**
0	1	1
1	2	0.5
2	4	0.25
3	8	0.125
4	16	0.0625

Co-funded by the European Union

For subcarrier spacing configuration μ, slots are numbered $n_{\mathrm{s}}^{\mu} \in \left\{0, \ldots, N_{\mathrm{slot}}^{\mathrm{subframe},\mu} - 1\right\}$ in increasing order within a subframe and $n_{\mathrm{s,f}}^{\mu} \in \left\{0, \ldots, N_{\mathrm{slot}}^{\mathrm{frame},\mu} - 1\right\}$ in increasing order within a frame. There are $N_{\mathrm{symb}}^{\mathrm{slot}}$ consecutive OFDM symbols in a slot where $N_{\mathrm{symb}}^{\mathrm{slot}}$ depends on the cyclic prefix as given by Table 5 and Table 6. The start of slot n_{s}^{μ} in a subframe is aligned in time with the start of OFDM symbol $n_{s}^{\mu} N_{\mathrm{symb}}^{\mathrm{slot}}$ in the same subframe.

TABLE 5: NUMBER OF OFDM SYMBOLS PER SLOT, SLOTS PER FRAME, AND SLOTS PER SUBFRAME FOR NORMAL CYCLIC PREFIX [1]

μ	$N_{\mathrm{symb}}^{\mathrm{slot}}$	$N_{\mathrm{slot}}^{\mathrm{frame},\mu}$	$N_{\mathrm{slot}}^{\mathrm{subframe},\mu}$
0	14	10	1
1	14	20	2
2	14	40	4
3	14	80	8
4	14	160	16
5	14	320	32
6	14	640	64

TABLE 6: NUMBER OF OFDM SYMBOLS PER SLOT, SLOTS PER FRAME, AND SLOTS PER SUBFRAME FOR EXTENDED CYCLIC PREFIX [1]

μ	$N_{\mathrm{symb}}^{\mathrm{slot}}$	$N_{\mathrm{slot}}^{\mathrm{frame},\mu}$	$N_{\mathrm{slot}}^{\mathrm{subframe},\mu}$
2	12	40	4

3.1.1.3 Supported channels

Not all numerologies are applicable to every physical channel and signal in the 5G NR system. Each physical channel has specific numerologies assigned to it, although most numerologies can be utilized across various physical channels. Table 7 illustrates the mapping of numerologies to specific physical channels.

TABLE 7: SUPPORT CHANNEL TYPES FOR DIFFERENT NUMEROLOGIES [2]

μ	**Supported for Data** **(PDSCH, PUSCH etc)**	**Supported for Sync** **(PSS,SSS,PBCH)**
0	Yes	Yes

1	Yes	Yes
2	Yes	No
3	Yes	Yes
4	No	Yes
5	Yes	Yes
6	Yes	Yes

3.1.1.4 SYMBOL DURATION

The symbol duration in 5G NR is inversely proportional to the subcarrier spacing. A larger subcarrier spacing results in a shorter symbol duration, enabling faster data transmission and lower latency. Table 8 reports key parameters of the 5G network's physical layer OFDM, CP, and total symbol duration for different numerologies (μ).

The numerology values range from 0 to 6, corresponding to subcarrier spacings of 15, 30, 60, 120, 240, 480 and 960 kHz respectively. A larger numerology indicates a wider subcarrier spacing. As the numerology increases, the OFDM symbol duration and the cyclic prefix duration decrease, resulting in a shorter overall OFDM symbol duration (including the cyclic prefix).

TABLE 8: OFDM SYMBOL DURATION FOR DIFFERENT NUMEROLOGIES

μ	**Subcarrier Spacing [kHz]**	**OFDM Symbol Duration [μs]**	**CP Duration [μs]**	**OFDM Symbol including CP [μs]**
0	15	66.67	4.69	71.35
1	30	33.33	2.34	35.68
2	60	16.67	1.17	17.84
3	120	8.33	0.57	8.92
4	240	4.17	0.29	4.46
5	480	2.08	0.14	2.22
6	960	1.04	0.07	1.11

3.1.1.5 Modulation mapper

Modulation mapper schemes are specified in Section 5.1 of [1]. The modulation step transforms the block of scrambled bits to a corresponding block of complex modulation symbols. The specification outlines seven modulations schemes, including π/2-BPSK, BPSK, QPSK, 16QAM, 64QAM, 256QAM and 1024QAM. Here we only consider PUSCH and PDSCH channels which are responsible for transferring data.

Choosing a suitable modulation scheme is important. High order modulations are necessary to improve the bandwidth efficiency for the communication system. Thus, high modulation orders are used to transfer high throughputs in good coverage, while low modulation orders are used to maximize the coverage. Both PUSCH and PDSCH support QPSK, 16QAM, 64QAM, 256QAM and 1024QAM. For the uplink π/2-BPSK is supported in the case the DFT-precoding is used, to improve PA efficiency, especially for coverage-limited scenarios. BPSK is only used for PUCCH.

3.1.2 OFDM based signal generation

In 5G NR, 3GPP has selected CP-OFDM as a waveform for downlink. In uplink, both CP-OFDM and DFT-s-OFDM are supported. In this section, the CP-OFDM is introduced as specified in [1] Section 5.3. Following, the transform precoding operation that is used to transmit with DFT-s-OFDM is described.

The cyclic prefix is a copy of the symbol's end portion, which is appended to the beginning of the symbol. In conjunction with the DFT operation, it is used to mitigate the effects of multipath propagation and channel delay spread.

In the following part, the OFDM baseband signal generation for all channels except PRACH and Remote Interference Management – reference Signal (RIM-RS) is provided.

For each numerology and carrier, a resource grid of $N_{\text{grid,x}}^{\text{size,μ}} N_{\text{sc}}^{\text{RB}}$ subcarriers and $N_{\text{symb}}^{\text{subframe,μ}}$ OFDM symbols is defined, starting at common resource block $N_{\text{grid}}^{\text{start,μ}}$ indicated by higher-layer signalling. There is one set of resource grids per transmission direction (uplink, downlink) with the subscript x set to DL and UL, respectively.

For uplink and downlink, the carrier bandwidth $N_{\text{grid}}^{\text{size,μ}}$ for subcarrier spacing configuration μ is given by the higher-layer parameter *carrierBandwidth* in the *SCS-SpecificCarrier* IE. The starting position $N_{\text{grid}}^{\text{start,μ}}$ for subcarrier spacing configuration μ is given by the higher-layer parameter *offsetToCarrier* in the *SCS-SpecificCarrier* IE.

The time-continuous signal $s_l^{(p,\mu)}(t)$ on antenna port p and subcarrier spacing configuration μ for OFDM symbol $l \in \left\{0,1,\ldots,N_{\text{slot}}^{\text{subframe},\mu} N_{\text{symb}}^{\text{slot}} - 1\right\}$ in a subframe for any physical channel or signal except PRACH is defined as [1]:

$$s_l^{(p,\mu)}(t) = \begin{cases} \displaystyle\sum_{k=0}^{N_{\text{grid},x}^{\text{size},\mu} N_{\text{sc}}^{\text{RB}}-1} a_{k,l}^{(p,\mu)} e^{j2\pi\left(k+k_0^\mu - N_{\text{grid},x}^{\text{size},\mu} N_{\text{sc}}^{\text{RB}}/2\right)\Delta f\left(t-N_{\text{CP},l}^\mu T_{\text{c}} - t_{\text{start},l}^\mu\right)} & t_{\text{start},l}^\mu \leq t < t_{\text{start},l}^\mu + T_{\text{symb},l}^\mu \\ 0 & \text{otherwise} \end{cases}$$

where

$$k_0^\mu = \left(N_{\text{grid},x}^{\text{start},\mu} + N_{\text{grid},x}^{\text{size},\mu}/2\right) N_{\text{sc}}^{\text{RB}} - \left(N_{\text{grid},x}^{\text{start},\mu_0} + N_{\text{grid},x}^{\text{size},\mu_0}/2\right) N_{\text{sc}}^{\text{RB}} 2^{\mu_0-\mu}$$

$$T_{\text{symb},l}^\mu = \left(N_{\text{u}}^\mu + N_{\text{CP},l}^\mu\right) T_{\text{c}}$$

When $t = 0$ at the start of the subframe,

$$N_{\mathrm{u}}^{\mu} = 2048\kappa \cdot 2^{-\mu}$$

$$N_{\mathrm{CP},l}^{\mu} = \begin{cases} 512\kappa \cdot 2^{-\mu} & \text{extended cyclic prefix} \\ 144\kappa \cdot 2^{-\mu} + 16\kappa & \text{normal cyclic prefix, } l = 0 \text{ or } l = 7 \cdot 2^{\mu} \\ 144\kappa \cdot 2^{-\mu} & \text{normal cyclic prefix, } l \neq 0 \text{ and } l \neq 7 \cdot 2^{\mu} \end{cases}$$

- p is the antenna port;
- $\mu \in \{0, 1, 2, 3, 4\}$ is the subcarrier spacing configuration (numerology);
- $\Delta \mathrm{f} = 2^{\mu} \cdot 15$ kHz is the subcarrier spacing;
- With k_0^{μ}=0, the subcarrier index is generated by subtracting half of the total number of subcarriers from k. So first half of the subcarriers have negative index, second half of the subcarriers have 0 or positive index.
- μ_0 is the largest μ value among the subcarrier spacing configurations by the higher-layer parameter *scs-SpecificCarrierList*;
- $N_{\mathrm{grid}}^{\mathrm{size},\mu}$ is the number of Resouce Blocks given by the higher-layer parameter *carrierBandwidth* related to numerology and frequency offset;
- $N_{\mathrm{grid}}^{\mathrm{start},\mu}$ is the start Resource Block index given by the higher-layer parameter *offsetToCarrier* related to numerology and frequency offset;
- x can be uplink or downlink;
- $a_{k,l}^{(p,\mu)}$ is the content of Resource Element (subcarrier k and symbol l);
- $N_{\mathrm{sc}}^{\mathrm{RB}} = 12$ is the number of consecutive subcarriers in the frequency domain;
- The constant $\kappa = 64$ is the ratio between T_s and T_c;
- $\mathrm{T_c} = 1/(\Delta \mathrm{f_{max}} \cdot \mathrm{N_f}) = 1/(480 \cdot 10^3 \cdot 4096) = 0.5086$ ns is the basic time units for NR.
- $N_{\mathrm{CP},l}^{\mu}$ is the cyclic prefix length;
- k is subcarrier index relative to a reference.

The starting position of OFDM symbol l for subcarrier spacing configuration μ in a subframe is given by:

$$t_{\mathrm{start},l}^{\mu} = \begin{cases} 0 & l = 0 \\ t_{\mathrm{start},l-1}^{\mu} + \left(N_u^{\mu} + N_{\mathrm{CP},l-1}^{\mu}\right) \cdot T_c & \text{otherwise} \end{cases}$$

The time index has two parts, first is $N_{\mathrm{CP},l-1}^{\mu}$ which is used to generate the cyclic prefix. The second part is $t_{\mathrm{start},l-1}^{\mu}$ which is the start time of each symbol.

3.1.3 DFT-s-OFDM based signal generation

In [1], Section 6.3.1.4 specifies the transform precoding procedure to create DFT-s-OFDM waveform. The DFT-spread operation spreads the uplink data across subcarriers and time, introducing additional diversity and better Peak to Average Power Ratio (PAPR). Thereby, the operation enables higher PA efficiency. Conditions for transform precoding being enabled are specified in TS 38.214 Section 6. Transform precoding shall be applied according to the equation specified in Section 6.3.1.4 (of TS 38.214) when conditions are met.

Figure 1 illustrates the simplified block diagram for CP-OFDM and DFT-S-OFDM signal generation. For DFT-S-OFDM, an extra procedure called transform precoding is implemented, which basically performs DFT process.

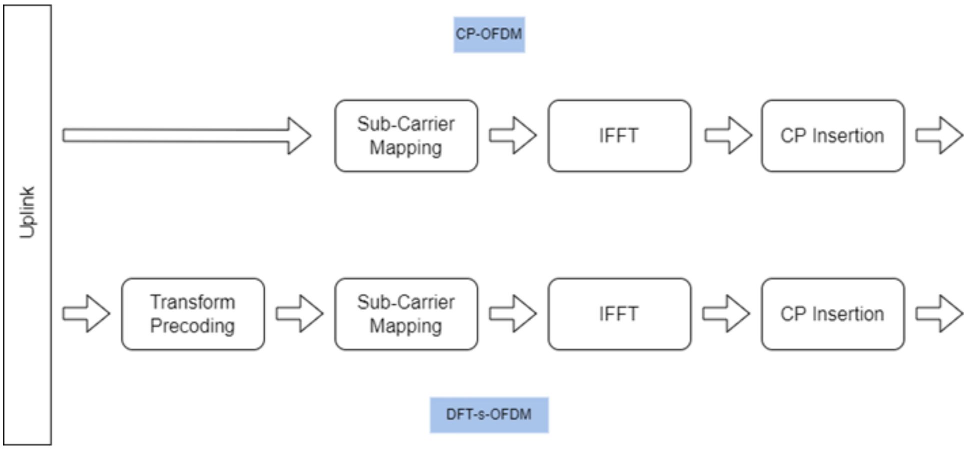

FIGURE 1: SIMPLIFIED BLOCK DIAGRAM OF THE CP-OFDM AND DFT-S-OFDM

In [1], transform precoding shall be applied according to:

$$y^{(0)} = (l \cdot M_{sc}^{PUSCH} + k) = \frac{1}{\sqrt{M_{sc}^{PUSCH}}} \sum_{i=0}^{M_{SC}^{PUSCH}-1} \tilde{x}^{0}(l \cdot M_{sc}^{PUSCH} + i) e^{\frac{-j\,2\pi ik}{M_{sc}^{PUSCH}}}$$

$$k = 0, \dots, M_{sc}^{PUSCH} - 1$$

$$l = 0, \dots, \frac{M_{symb}^{layer}}{M_{sc}^{PUSCH}} - 1$$

resulting in a block of complex-valued symbols $y^{(0)}(0), \dots, y^{(0)}\left(M_{\text{symb}}^{\text{layer}} - 1\right)$.

The variables:

- $M_{\text{symb}}^{\text{layer}}$ is the number of modulation symbols per layer
- $M_{\text{RB}}^{\text{PUSCH}} = 2^{\alpha_2} \cdot 3^{\alpha_3} \cdot 5^{\alpha_5}$, represents the bandwidth of the PUSCH in terms of resource blocks
- $\alpha_2, \alpha_3, \alpha_5$ is a set of non-negative integers for defining DFT sizes
- $M_{\text{sc}}^{\text{PUSCH}} = M_{\text{RB}}^{\text{PUSCH}} \cdot N_{\text{sc}}^{\text{RB}}$ is the total number of subcarriers across the whole allocated PUSCH bandwidth

3.1.4 Advantages and disadvantages of CP-OFDM and DFT-s-OFDM

As previously mentioned, the two basic waveforms, CP-OFDM and DFT-s-OFDM, have been the waveforms of choice for 4G and 5G systems due to their many desirable features. For CP-OFDM, these features include the following:

- Efficient transmitter and receiver implementations using FFT operations.

- Avoidance of Inter-Carrier Interference (ICI) and Inter-Symbol Interference (ISI) in time-invariant multipath channels where the delay spread is smaller than the CP duration. In this case, the multipath may become beneficial due to diversity gain, which may be utilized by systems such as Single Frequency Network (SFN) and multi-Transmission/Reception Points (TRP). ICI is avoided thanks to the orthogonality of subcarriers.
- Use of frequency-domain equalization: due to cyclic convolution that results from the CP, equalization can be performed conveniently in the frequency-domain. Compared to time-domain equalization, this is typically much simpler because the frequency domain equalization is simply a per-subcarrier multiplication with a complex coefficient.
- Simple and flexible placement of RS tones in frequency domain, and correspondingly simple channel and noise plus interference estimation and equalization in frequency-domain using RS tones.
- Efficient and flexible Multiple Input Multiple Output (MIMO) configuration and associated receiver processing for spatial multiplexing gains.
- Flexible resource allocation to users in frequency, time, and spatial domains, as well as in power-domain. Flexible modulation and code-rate assignments in frequency/time/space domains. Avoidance of narrow-band interferers in frequency domain via resource assignment.
- Flexible numerologies, including subcarrier spacing, that may be chosen according to use case.
    - Higher numerologies can accommodate larger frequency synchronization errors and phase noise, but less delay spread and timing errors. Terrestrial networks, on the one hand, make use of high numerologies in higher bands, along with narrow antenna patterns, resulting in less multipath and ultimately a reduced delay spread. In NTN, however, time and frequency synchronization errors may both be simultaneously large, creating the dilemma that higher numerologies may be better for frequency synchronization errors, but could only be used at the expense of the time counterparts.

Disadvantages of CP-OFDM waveforms include:

- High PAPR is one of the main disadvantages of the CP-OFDM waveform which requires sufficient power backoff in PA operation and also high Digital to Analog Conversion (DAC) range/resolution. These result in power inefficiencies. Many PAPR reduction techniques available in the literature will be reviewed in this section.
- Slowly decaying OOB emissions envelope results in interference in the presence of unsynchronized (in time and/or frequency) adjacent channel transmitters. This can be alleviated to some degree by using WOLA and/or narrow-band filtering. Note that in addition to the inherently high OOB emissions, CP-OFDM waveforms suffer from an additional source of OOB emissions which is non-linear distortions in the transmitter (PA, DAC) due to high PAPR.
- Sensitivity to Doppler-spread and frequency errors which may cause ICI. This may be partially mitigated by using a sufficiently large subcarrier spacing. It is worth

mentioning that Doppler shift alone can be pre-compensated or post-compensated.

- Sensitivity to timing errors which may cause both ISI and ICI.
- CP overhead, although arguably reasonable, is a loss if the delay spread is much shorter than the CP length. Conversely, if the delay spread is larger than the CP length, there will be ISI introduced.

Alternatively, in the case of DFT-s-OFDM, its desirable features are:

- Reduced PAPR relative to CP-OFDM which helps with energy efficiency, especially in link budget limited scenarios. Consequently, OOB emissions caused by transmitter non-linearities are less of a concern.
- Like CP-OFDM, efficient implementation using FFT operations.
- Like CP-OFDM, ISI can be avoided in a time-invariant multi-path channel so long as the delay-spread is smaller than the CP duration.
- Like CP-OFDM, equalization can be performed in frequency-domain, however, since the symbols in a DFT-s-OFDM waveform are embedded in time-domain, the intra modulation symbol ISI may not be fully avoidable.
- Like CP-OFDM, flexible resource allocation.
- Like CP-OFDM, flexible numerologies.

On the contrary, the disadvantages of DFT-s-OFDM waveforms include:

- Unlike CP-OFDM, the insertion of RS tones is not straightforward in DFT-s-OFDM given the inherent placement of symbols in the time-domain [3].
- Like CP-OFDM, slowly decaying OOB emissions inherent to the waveform is an important concern, making co-existence with unsynchronized systems challenging.
- Like CP-OFDM, sensitivity to Doppler spread and frequency errors is a concern.
- Like CP-OFDM, sensitivity to timing errors is a concern.
- Like CP-OFDM, fixed overhead of CP is a concern.
- Unlike CP-OFDM, resource allocation to a user may be more restricted in DFT-s-OFDM due to the requirement of low PAPR.

3.2 DVB AIR INTERFACE: COMPARISON WITH 5G NR

The ETSI Technical Report (TR) 103.886 [4] provides an initial technical comparison of the Digital Video Broadcasting Second Generation - eXtension (DVB-S2X) and the DVB – Return Channel Satellite (RCS), i.e., two native satellite air interfaces, with the 5G NR air interface adapted to the satellite channel.

Therefore, this section aims to summarize the primary outcomes of this technical report, comparing the performance of DVB-S2X and DVB-RCS2 vs PDSCH and PUSCH (with DFT-s-OFDM as waveform), respectively. For detailed information on the DVB-S2X and DVB-RCS standards, readers can refer to the appendix.

In [4], the reference scenario is based on a single Geostationary (GSO) satellite system offering broadband services through multi-beam coverage. The satellite payload is transparent, and the end-to-end RF link is composed of the user link and the feeder link, both established in the Ka band.

The baseline multi-beam payload architecture is based on an active antenna, which can be either a Direct Radiating Antenna (DRA) or parabolic antenna with active sources. It relies on a Beam Forming Network (BFN) -digital, analog or hybrid- and multiple High-Power Amplifiers (HPA).

The study compares DVB-S2X against NR PDSCH and DVB-RCS against NR PUSCH, both at link and system level in terms of:

- Physical layer demodulation performances
- Spectral efficiencies
- PAPR
- Intermodulation noise

3.2.1 Channel impairments and assumptions

For the link level simulations, the propagation channel on both service and feeder links is considered as a LoS, non-frequency selective, and time invariant. This is justified by the assumption related to the fixed directive terminal type considered in the study.

The Doppler impact in the frequency and time domain is considered negligible in the scenarios under study since the terminals are considered fixed on the ground and the GSO satellite on-orbit velocity is usually inferior to 1,5 m/s.

In terms of hardware impairments, the gain variation and the group delay of the filters (Figure 2), the Phase Noise (PN) on the Forward Link (FWD) and Return Link (RTN) (Figure 3), and the HPA in Ka band (Figure 4) are considered.

Notably, in the study HPA non linearities are not taken into account for the computation of the demodulation performances for both air interfaces. They are instead considered for the computation of the intermodulation noise.

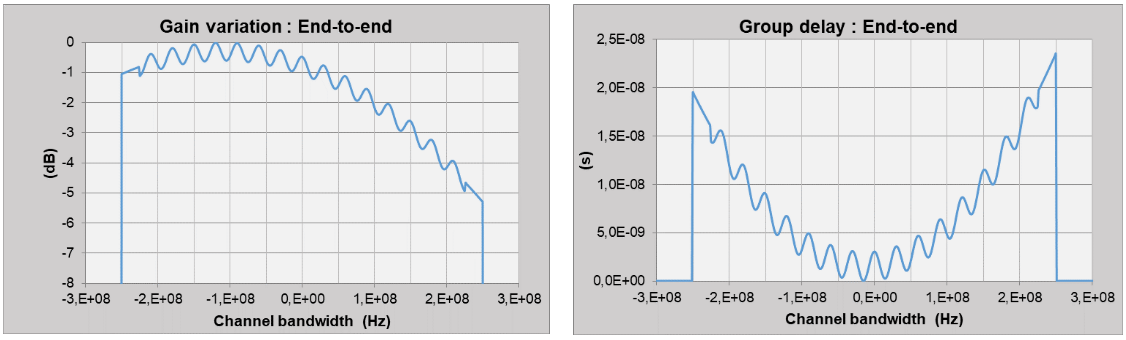

FIGURE 2: AGGREGATED GAIN VARIATION AND GROUP DELAY

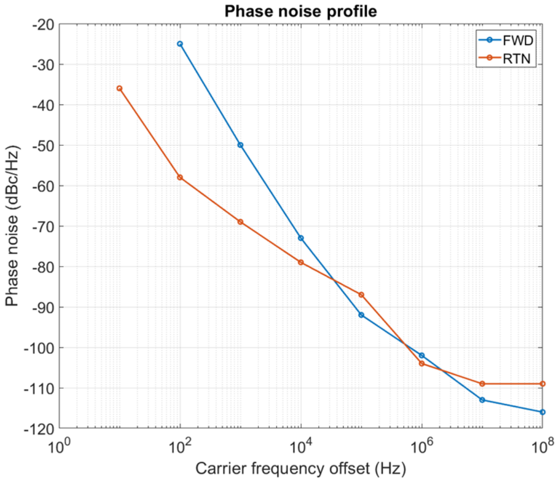

FIGURE 3: SINGLE SIDEBAND AGGREGATED FWD AND RTN PHASE NOISE PROFILE

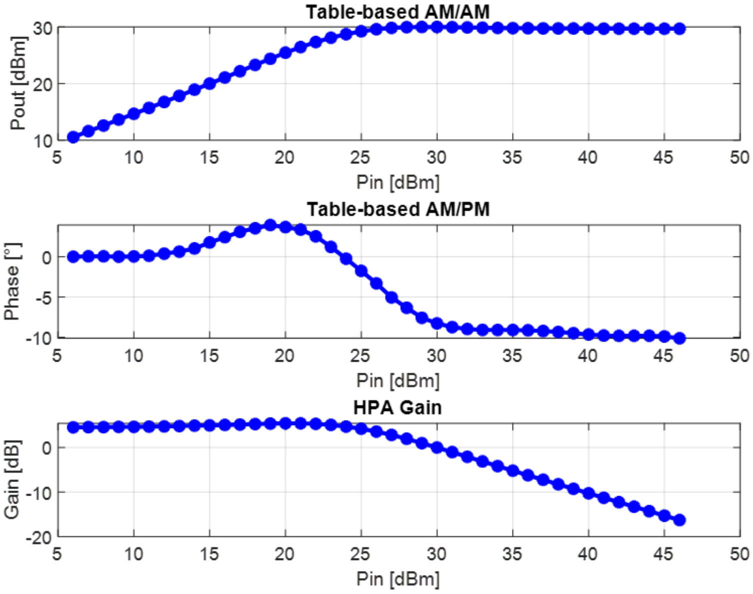

FIGURE 4: AM/AM, AM/PM, AND GAIN CHARACTERISTICS OF THE HPA IN KA BAND

Two channels are considered (Table 9): i) the Additive White Gaussian Noise (AWGN) with no HW impairments, and ii) Type A channel (according to Table 9) with HW impairments and LoS frequency selective and non-time variant propagation channel.

TABLE 9: CHANNEL MODELS IN THE MARINA PROJECT

Channel types	**Impairments**		**HPA**	**Propagation Channel**
	Phase Noise	GF/GD		
AWGN	No PN	Not Considered	No amplifier	LOS non-frequency selective and non-time variant No Doppler AWGN

Type A	FWD	RTN	Figure 2	FWD	RTN	LOS non-frequency selective and non-time variant No Doppler AWGN
	Figure 3	Figure 3		Figure 4	Ka Band GaAs amplifier	

3.2.2 Results

Performance have been evaluated in terms of the required Es/N0 threshold for each modulation and coding scheme to ensure a certain target Frame Error Rate/ Block Error Rate (FER/BLER), and spectral efficiency.

- For the DVB-S2X, the following elements have been considered:
  - BaseBand (BB) framing efficiency, which takes into account the BB header overhead;
  - Physical Layer (PL) framing efficiency, which takes into account the pilots and the PL header overhead
  - Carrier roll-off which characterizes the spectral occupancy of the carrier
  - Guard bands which are often required between adjacent DVB-S2X carriers due to operational constraints
- For the DVB-RCS2:
  - Frame Protocol Data Unit (PDU) CRC which may induce significant loss in the burst ID with the smallest size in terms of number of information bits.
  - Burst framing efficiency taking into account the pilots, preamble and postambule overhead.
  - Guard Times which are necessary to avoid inter-user interference between successive transmissions and maintain the close time synchronization loop between the baseband demodulator and the user terminals.
  - Carriers roll-off which characterizes the spectral occupancy of the Multi-Frequency Time Division multiple Access (MF-TDMA) burst transmission.
- For NR PDSCH/PUSCH:
  - Demodulation Reference Signal (DMRS) and Phase Tracking reference Signal (PTRS) occupancy which are essential to the receiver for synchronization and demodulation.
  - The cyclic prefix which is an essential feature of NR to deal with multipath channel and enable one tap equalization.
  - Standardized guard band which have been defined in the standard to enable good co-existence conditions between two systems operating in adjacent channel carriers.

Finally, it is worth mentioning that the Hybrid Automatic Repeat reQuest (HARQ) has been disabled for NR.

3.2.3 DVB-S2X vs NR PDSCH

3.2.3.1 Demodulation performance

Figure 5 and Figure 6 present the demodulation performance comparison between DVB-S2X spectral efficiencies with respect to NR PDSCH spectral efficiencies (both expressed in terms of bits/s/Hz). This comparison is firstly done in AWGN conditions, then in channel Type A.

In an AWGN, to meet a FER/BLER target of 1e-3, there is a 0-2 dB difference between the two air interfaces, with DVB-S2X being more efficient. For a FER/BLER target of 1e-5, the difference is 0-2.5 dB, again in favour of DVB-S2X, indicating that 5G NR requires higher Es/N0 to achieve the same spectral efficiency.

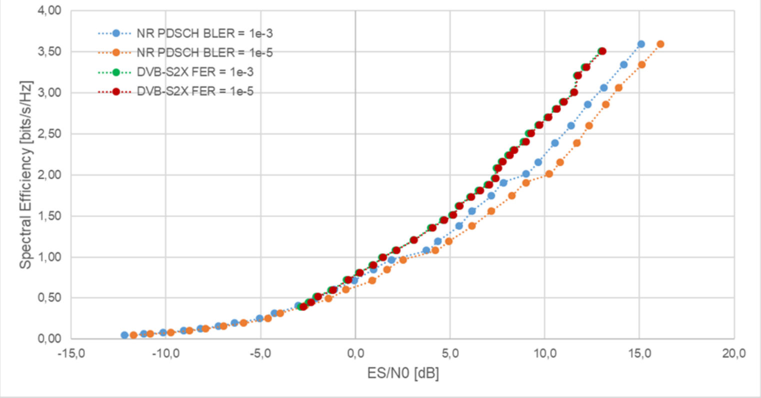

FIGURE 5: DVB-S2X VS NR PDSCH - COMPARISON OF REQUIRED ES/N0 IN CHANNEL TYPE AWGN – SPECTRAL EFFICIENCY IN BITS/S/HZ

The performance gap remains unfavourable for 5G NR when considering the Type A channel without HPA. The observed SNR degradation needed to achieve the same spectral efficiency ranges from 0 to 3 dB for a FER/BLER target of 1e-3, and from 0 to 3.2 dB for a FER/BLER target of 1e-5. Consequently, the effects of spectral occupancy and framing efficiency tend to widen the performance gap between the two air interfaces.

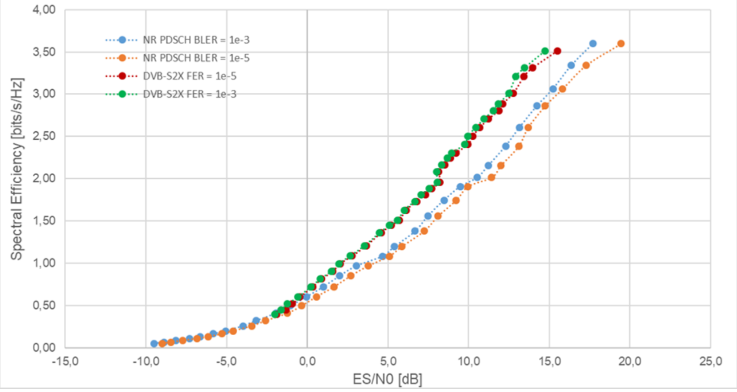

FIGURE 6: DVB-S2X VS NR PDSCH - COMPARISON OF REQUIRED ES/N0 IN CHANNEL TYPE A CONDITIONS WITHOUT NON LINEAR AMPLIFIER – SPECTRAL EFFICIENCY IN BITS/S/HZ

The observed performance gaps in favour of DVB-S2X are mainly explained by the following factors:

- The lower performance of the NR Low Density Parity Check (LDPC) coding scheme especially at low FER/BLER targets. The reason is twofold:

  - NR was not primarily designed to reach such low BLER targets in a single transmission and therefore does not implement concatenated coding scheme unlike DVB-S2X;
  - the lower number of information bits per LDPC code block in case of NR transport block transmissions varies approximatively from 1200 to 4000 bits depending on the Modulation Coding scheme (MCS) index considered, while the number of information bits inside a DVB-S2X NORMAL BBFRAME varies approximatively from 15000 to 55000 depending on the MODCOD considered.

- ➲ The NR lower framing efficiency due to higher reference symbol overhead specifically for the high MCS indexes for which the PTRS overhead may become significant as well as CP related efficiency loss.
- ➲ The higher impairments sensitivity and implementation losses for NR. This seems to be the factor with the least impact on the performance gap.

However, several NR PDSCH optimizations can be foreseen to reduce the performance gap observed at the physical layer level w.r.t. DVB-S2X:

- ➲ Optimization of the DMRS and PTRS configuration for each MCS to find the best compromise between the induced overhead and the level of degradation due to impairments and channel estimation inaccuracy.
- ➲ Enhancement of the NR receiver in order to take advantage of the past PDSCH demodulations and the periodical broadcast of channel state information reference signal CSI-RS.
- ➲ Adjustment of the NR PDSCH allocation to target a higher number of information bits per code block.

3.2.3.2 PAPR

With the active antenna payload architecture and the multi-beam coverage assumptions, it is reasonable to assume that each satellite amplifier manages tens of carriers in case of DVB-S2X based transmissions or thousands of OFDM subcarriers in case of 5G NR based transmissions. Moreover, since the payload design is based on an active antenna and satellite beamforming capabilities, the carriers amplified within the same amplifier will even share the same frequency resources when they have been applied different beamforming coefficients.

Furthermore, the power envelope fluctuation to cope with at the amplifier input is very similar for OFDM based signal and multi DVB-S2X carriers based signal as soon as the number of uncorrelated DVB-S2X carriers in the amplified bandwidth is higher than ten, as shown in Figure 7.

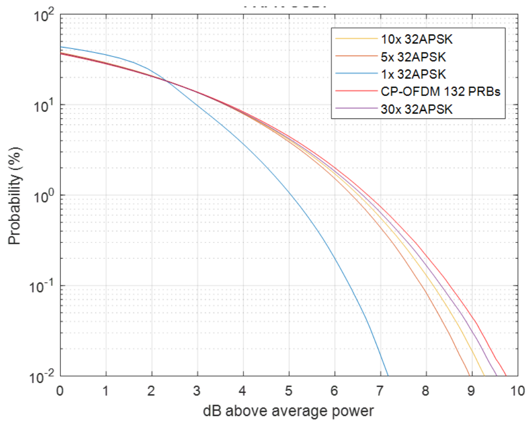

FIGURE 7: COMPARISON OF PAPR DISTRIBUTION OF CP-OFDM TRANSMISSION AND SINGLE/MULTI DVB-S2X CARRIER TRANSMISSION

In conclusion, the power envelope fluctuation to cope with at the high-power amplifier chain input is waveform agnostic (in case of satellite payload designs based on active antenna). Therefore, the performance in terms of intermodulation noise level at the HPA output is expected to be very similar both for DVB-S2X and for NR PDSCH.

However, for the use cases for which the number of carriers (NR or DVB-S2X) per satellite amplifier is lower, then the PAPR is going to be lower for DVB-S2X with respect to NR. In these conditions, depending on how the amplifier is operated, one can expect less nonlinear distortions and/or better power efficiency in favor of DVB-S2X.

3.2.3.3 Intermodulation noise

The achievable performance in terms of power Carrier over Intermodulation Noise (C/Im) are based on different points of operation regarding the satellite HPA characteristics. The input signal is either composed of several hundreds of NR CP-OFDM subcarriers or 32 DVB-S2X carriers.

Due to the satellite active antenna architecture and the multi-beam coverage assumptions, it is assumed that a gain of 5 dB can be expected between conducted and radiated C/Im.

The results are summarized in Figure 8.

It is possible to observe that the C/Im performance are very similar for both cases with small gain of 0.1 to 0.3 dB in favour of DVB-S2X. It is expected that increasing the number of DVB-S2X carriers in the amplifier will make this gain disappear.

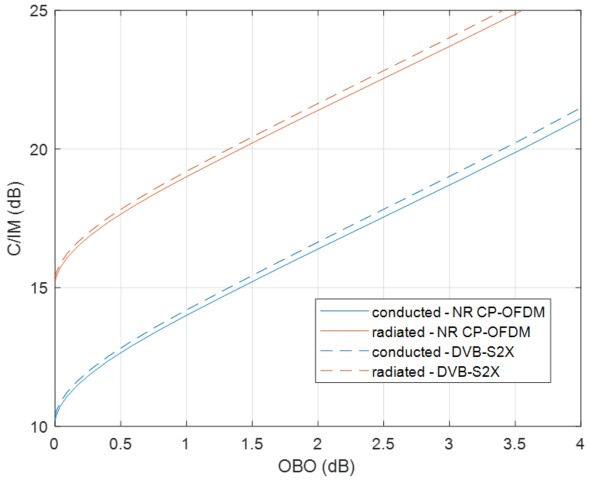

FIGURE 8: C/IM VS OBO PERFORMANCE COMPARISON BETWEEN NR CP-OFDM AND DVB-S2X

3.2.4 DVB-RCS vs NR PUSCH

3.2.4.1 Demodulation performance

Figure 9 and Figure 10 present the demodulation performance comparison between DVB-RCS2 spectral efficiencies with respect to NR PUSCH spectral efficiencies (both expressed in terms of bits/s/Hz). This comparison is firstly done in AWGN conditions, then in channel Type A conditions.

Under AWGN conditions, the observed SNR degradation for DVB-RCS2 to achieve the same spectral efficiency of NR PUSCH ranges from 0 to 2.5 dB for a FER/BLER target of 1e-3, and from 0 to 1.7 dB for a FER/BLER target of 1e-5.

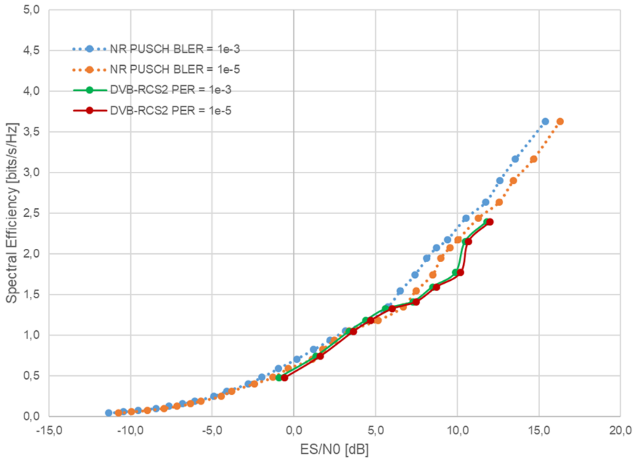

FIGURE 9: DVB-RCS2 VS NR PUSCH - COMPARISON OF REQUIRED ES/N0 IN CHANNEL TYPE AWGN – 28 MHZ ALLOCATED BANDWIDTH – SPECTRAL EFFICIENCY IN BITS/S/HZ.

The performance gap remains generally in favour of NR PUSCH when considering the channel Type A without HPA. For spectral efficiencies below 1.4 bits/s/Hz, both air interfaces exhibit similar performance. However, for spectral efficiencies above 1.4 bits/s/Hz, NR PUSCH shows better performance compared to DVB-RCS2. The SNR degradation required to achieve the same spectral efficiency ranges from 0.5 to 2.2 dB for a BLER target of 1e-3, and from 0.1 to 1.6 dB for a BLER target of 1e-5.

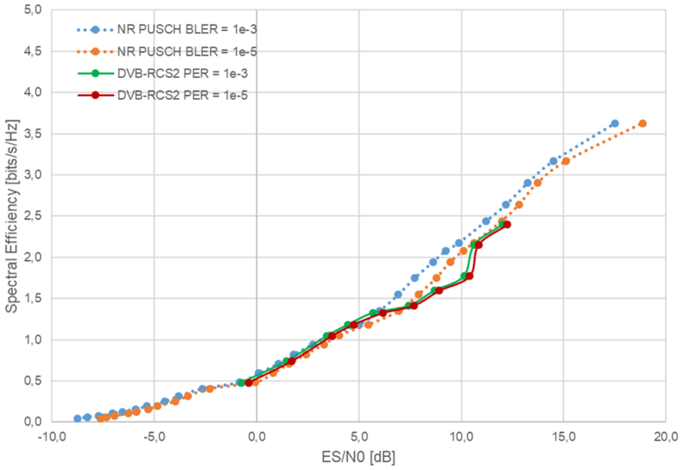

FIGURE 10: DVB-RCS2 VS NR PUSCH – COMPARISON OF REQUIRED ES/N0 IN CHANNEL TYPE A – 28 MHZ ALLOCATED BANDWIDTH – SPECTRAL EFFICIENCY IN BITS/S/HZ

The observed performance gaps between DVB-RCS2 and NR PUSCH are mainly explained by the following factors:

- Better FEC performance of NR PUSCH due to the DVB-RCS2 lower framing efficiency especially the higher roll-off overhead as illustrated by the Figure 9.
- Same demodulation performance in channel Type A conditions between the two air interface for spectral efficiencies below 1.4 bits/s/Hz as illustrated by the Figure 10.
- Better demodulation performance in channel Type A conditions of the NR PUSCH with respect to DVB-RCS2 for spectral efficiencies above 1.4 bits/s/Hz as illustrated by the Figure 10.

3.2.4.2 PAPR

The PAPR distributions of NR PUSCH transmissions and single DVB-RCS2 carrier transmissions are compared in Figure 11.

The following observations are made:

- PAPR < 4.7 dB for 99.9% of the time for the single DVB-RCS2 carrier transmissions in QPSK.
- PAPR < 6 dB for 99.9% of the time for the DFT-OFDM based transmissions in QPSK.
- PAPR < 5.7 dB for 99.9% of the time for the single DVB-RCS2 carrier transmissions in 16QAM.
- PAPR < 6.6 dB for 99.9% of the time for the DFT-OFDM based transmissions in 16QAM.

In conclusion, these results show that the power envelope fluctuation is approximately 0.9 to 1.3 dB higher in case of DFT-based transmissions with respect to single DVB-RCS2 carrier transmission with a roll-off factor of 0.2 depending on the modulation considered.

Therefore, it is expected that the terminal amplifier IBO shall be increased in case of NR PUSCH transmission to get the same intermodulation noise level at the amplifier output. It will result in the terminal effective EIRP reduction. The other way around, if the same IBO configuration is applied for both waveforms, then the non-linear distortion impact on the signal will be higher in case of NR PUSCH transmissions w.r.t. DVB-RSC2.

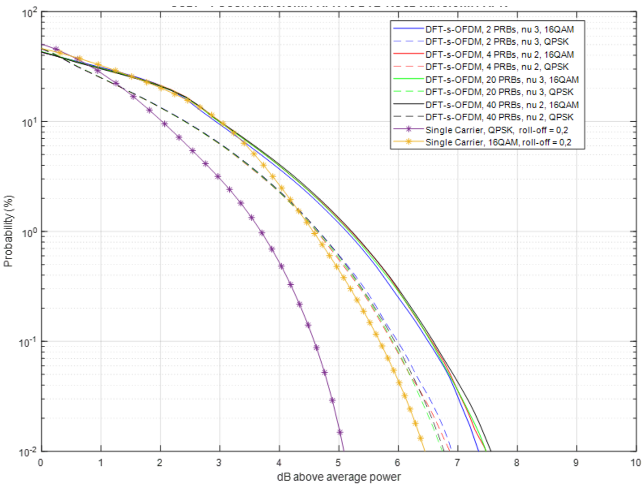

FIGURE 11: COMPARISON OF DFT-OFDM BASED NR PUSCH TRANSMISSIONS AND SINGLE CARRIER TRANSMISSIONS PAPR DISTRIBUTION

3.2.4.3 Intermodulation noise

The achievable performance in terms of conducted C/Im assuming the User Terminal HPA characteristics have been evaluated for different points of operation. The input signal is either composed of several hundred NR subcarriers (assuming DFTs-OFDM precoding is used) or a single DVB-RCS2 carrier. Several configurations of modulations are compared.

Referring to Figure 12, assuming a point of operation with an OBO of 0 dB (which has been analysed as the optimal configuration for both technologies assuming a required SNR inferior to 12 dB), the following observations are made:

- DVB-RCS2 QPSK and 8PSK C/Im equals 24 dB.
- DVB-RCS2 16QAM C/Im equals 19.7 dB.
- NR DFT-s-OFDM QPSK C/Im equals 21.2 dB that is a degradation of 2.8 dB with respect to DVB-RCS2 QPSK.
- NR DFT-s-OFDM 16QAM C/Im equals 18.7 dB that is a degradation of 5.3 dB with respect to DVB-RCS2 8PSK and a degradation of 1 dB with respect to DVB-RCS2 16QAM.
- NR DFT-s-OFDM 64QAM C/Im equals 17.95 dB that is a degradation of 1.75 dB with respect to DVB-RCS2 16QAM.

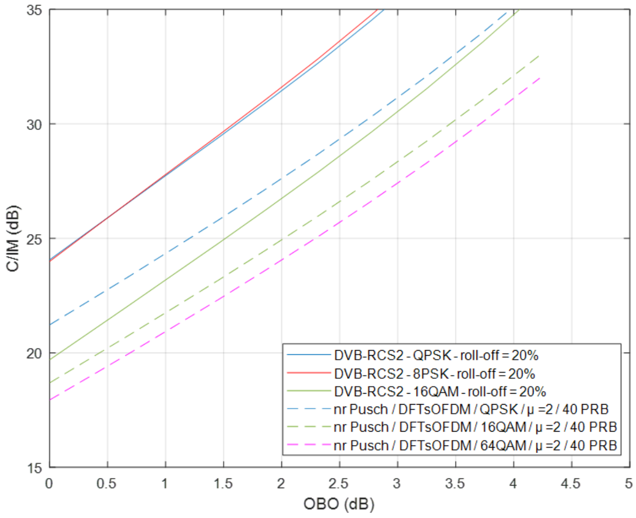

FIGURE 12: C/IM VS OBO PERFORMANCE COMPARISON BETWEEN NR DFT-S-OFDM AND DVB-RCS2

3.3 SCIENTIFIC LITERATURE

This section is devoted to the analysis of waveforms mainly addressed in the literature.

3.3.1 OFDM-based waveforms

This section provides a general overview of OFDM-based waveform studies in the literature. Moreover, a brief review of PAPR reduction methods for OFDM-based waveforms is given. There are plenty of references in the literature that provide a thorough view of OFDM-based waveforms. The interested reader is referred to [5]-[10].

As discussed in Section 3.1.4, high OOB emission and high PAPR are major concerns with CP-OFDM. Particularly, in NTN, the tight link budget (i.e., compared to terrestrial systems) brings power efficiency and PAPR to the forefront. As an alternative, the DFT-s-OFDM counterpart provides a reduction to the PAPR, while still suffering from OOB emissions as related to the common OFDM basic pulse.

Likewise, in the context of NTN, ISI and ICI due to frequency and timing misalignments become a challenge. Both frequency and timing errors arise from inaccuracies in satellite ephemeris information and in UE position.

Several variants of both CP-OFDM and DFT-s-OFDM with improved properties in terms of OOB emissions and PAPR will be discussed in the rest of the current section.

Weighted Overlap and Add (WOLA) is one of the techniques used to reduce the inherent OOB emissions related to the transmitted waveform, as well as reducing the sensitivity of the receiver to unsynchronized adjacent channel transmissions. WOLA can be applied to CP-OFDM, DFT-s-OFDM, and other OFDM-based waveforms that use CP as discussed later in this section.

The definition of the OFDM waveform in the specifications involves an instantaneous transition of phase and amplitude at OFDM symbol boundaries. This is one of the major problems with OFDM OOB emissions. The reduction of OOB emissions is a major goal for 6G-NTN waveform, where asynchronous operation with other transmitters in co-existence scenarios is of importance.

Practical implementations may use TX WOLA, which suppresses OOB emissions of the transmitted signal, at the cost of reducing the effectiveness of the CP. Note that Tx WOLA may also have some impact on PAPR around OFDM symbol boundaries.

The receiver may implement RX WOLA to reduce the sensitivity of the receiver to unsynchronized (in frequency and/or time) adjacent channel transmissions. The Transmitter (TX) and Receiver (RX) WOLA concepts are illustrated in Figure 13. In addition to WOLA, several filtered versions of OFDM-based waveforms with reduced OOB emissions will be discussed in what follows.

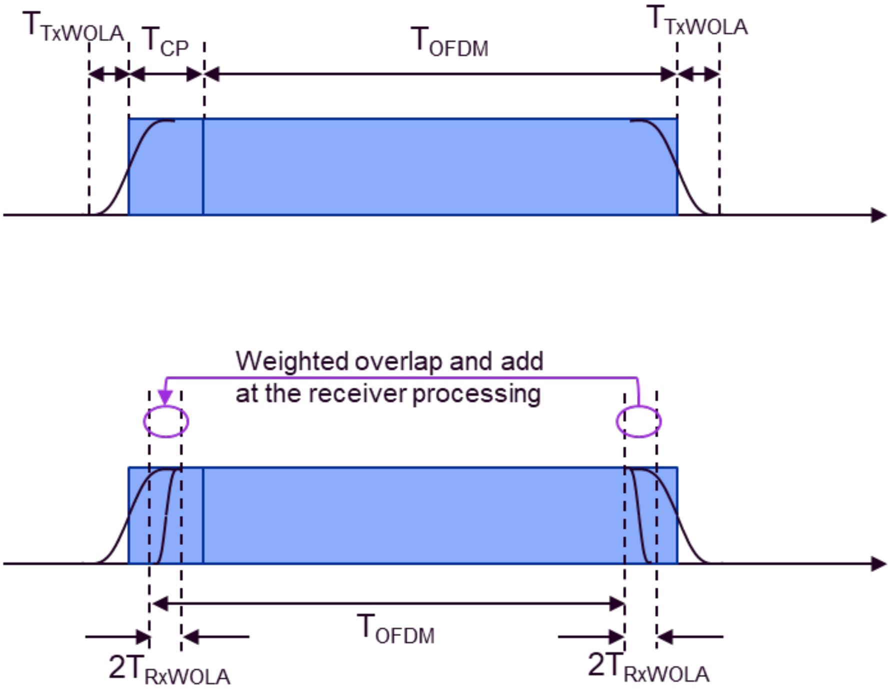

FIGURE 13: THE TX AND RX WOLA CONCEPTS

In TX WOLA, the CP + OFDM symbol is cyclically extended and windowed by T_{TxWOLA} using an odd-symmetric window, such as a raised-cosine window. The extended parts of the OFDM symbols overlap among adjacent OFDM symbols, thus reducing the supportable delay spread by the CP by an amount equal to $2T_{TxWOLA}$.

Tx WOLA suppresses OOB emissions by smoothing the transitions between adjacent OFDM symbols. Rx WOLA on the other hand suppresses interference picked up by the receiver from un-synchronized interferers by reducing the sidelobes of the receive filter.

Note that Tx WOLA applies to entire OFDM symbol including the CP, whereas RX WOLA applies to the FFT window only (i.e., the selected part of the OFDM symbol free of ISI). Thus, we can define roll-off factors as:

$$\beta_{tx,rolloff} = 2\,\frac{T_{TxWOLA}}{T + T_{CP}}$$

$$\beta_{rx,rolloff} = 2\,\frac{T_{RxWOLA}}{T}$$

Co-funded by the European Union

Similar to Tx WOLA, Rx WOLA reduces the delay spread supported by the CP by an amount equal to $2T_{RxWOLA}$. Thus, the available part of CP to support delay spread is given by $T_{CP} - 2 \times (T_{TxWOLA} + T_{RxWOLA})$.

Note that WOLA cannot mitigate OOB emissions caused by transmitter non-linearities, such as those associated with PA and DAC. Low-PAPR waveforms, such as DFT-s-OFDM and its variants discussed later in this section, have better immunity to non-linearity induced OOB emissions. DFT-s-OFDM can also benefit from WOLA by suppressing transitions at symbol boundaries.

Another important aspect in the study of waveforms for 6G-NTN is the compatibility with existing 5G waveforms, given that 6G and 5G will likely to co-exist and may even share spectra. Various levels of compatibility may be listed as:

- **Slot duration and sampling rates:** compatible slot durations, FFT block sizes, and sampling rates, such as the same set of values among 5G and 6G or values related by powers of two, would help UE implementations to re-use existing hardware/software at front-end blocks. The same goes for aspects relating to gNB implementation.
- **Symbol duration:** some of the waveforms discussed in this section do not have CP or overlap over multiple OFDM symbols. However, waveform-specific time considerations could be brought up front. For example, in 5G NR, a slot contains 14 CP-OFDM symbols. As the sum of CPs over 14 symbols add up to one additional symbol worth of time resources, if a waveform without CP is selected, a slot could therefore fit exactly 15 symbols.
- **Orthogonality:** time and frequency synchronization among systems is challenging. However, in applications such as spectrum sharing, one may assume that a gNB maintains synchronization among 5G and 6G UEs. In addition, waveforms with well-suppressed OOB, such as FBMC, are valuable of consideration as they do not suffer as much from unsynchronized interferers.

The time-frequency phase-space lattice representation is a useful representation of the allocation of symbols in such domains (see [11] for example). Figure 14 shows a time-frequency phase-space lattice representation for allocation in OFDM.

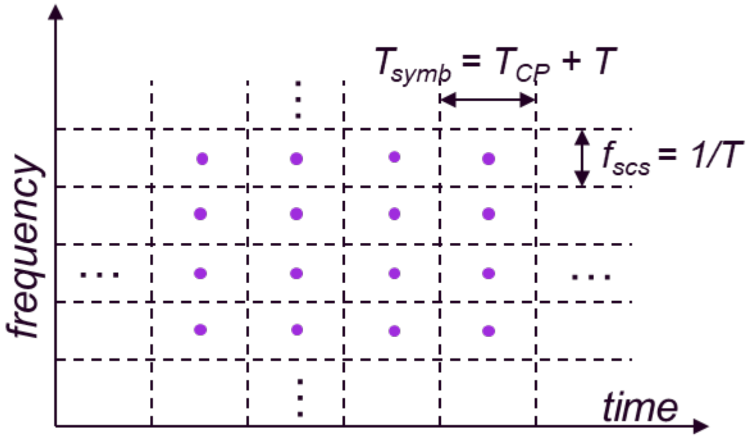

FIGURE 14: TIME FREQUENCY PHASE SPACE LATTICE

Each purple dot represents a complex-valued symbol, namely: a modulation symbol in CP-OFDM or a DFT-transformed symbol in the DFT-s-OFDM alternative. As explained, every symbol is orthogonal to its neighbours by virtue of the basic pulse definition.

As highlighted in the figure above, both CP-OFDM and DFT-s-OFDM allow for one complex symbol per area of $T_{symb} f_{scs}$. In other words, the area occupied per complex symbol is larger than unity by an amount of $T_{CP} f_{scs}$. The latter means that the *symbol density* [11] in the time-frequency domain is less than one ($\eta = T_{symb}^{-1} f_{scs}^{-1}$) or, equivalently, that less than one complex-valued symbols can be transmitted per unit area in time-frequency domain.

3.3.1.1 OFDM variants

The presented OFDM variants may be conveniently classified according to the OFDM-related drawback they aim at alleviating, namely high out-of-band emissions and PAPR, as illustrated in Figure 15.

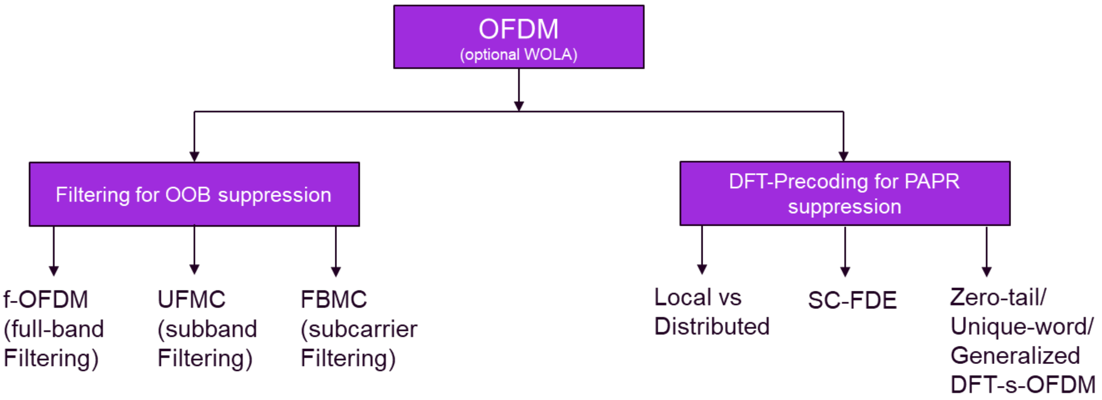

FIGURE 15: OFDM BASED WAVEFORMS CLASSIFICATION

Particularly, in relation to techniques for spectrum containment, Filtered-OFDM (f-OFDM) is a variant of OFDM where the whole transmission band is filtered with the objective of suppressing out of band emissions, whereas Filter Bank Multi-carrier (FBMC) is an alternative where this is carried out at a per-subcarrier basis. In the middle ground, Universal Filtered Multi-carrier (UFMC) is a compromise between f-OFDM and FBMC where the transmission band is divided, and filtering applied to each of the resulting sub-bands.

In relation to the so-mentioned alternatives, it is important to note that the length of the filter (and with it the induced dispersion) is inversely proportional to the band (f-OFDM), subcarrier (FBMC), and sub-band (UFMC) bandwidths. Consequently, FBMC results in filtering that has the length of multiple OFDM symbols, while f-OFDM and UFMC filters can be accommodated within CP/ Guard Interval (GI). In general, long filters reduce the effectiveness of CP or guard intervals between OFDM symbols; however, some waveforms (such as FBMC) do not make use of CP or GI.

When a guard interval is used instead of a CP between symbols, the receiver may overlap and add the last part of the symbol to the beginning to effectively emulate a CP.

Although OOB resulting from the waveform itself can be suppressed via filtering, the part of emissions due to other sources, such as those induced by PA non-linearity, may still be of concern. Importantly, transmitter non-linearities not only cause OOB emissions, but they also do increase the levels of in-band distortion. In such cases, DFT precoding applies as a means of PAPR and, with it, reduction of the impact of PA non-linearities.

The DFT-s-OFDM alternative and its variants shown on the right-hand branch of Figure 15 rely on precoding to produce a signal that resembles a single-carrier time-domain waveform, thus reducing the PAPR relative to the previously introduced OFDM variants.

A reduction of PAPR is beneficial for power efficiency as it allows the system to operate at a lower PA backoff without sacrificing the linear operation. Power efficiency is especially relevant for battery operated devices, such as a handheld UE on uplink transmissions, but may also be important for satellite operation both in uplink and downlink.

The so-mentioned DFT precoding can be applied, and subcarriers allocated either in a localized or a distributed manner. In the localized alternative, a subset of contiguous subcarriers is assigned at a UE basis. In the distributed counterpart, uniformly spaced subcarriers are assigned over the entire system bandwidth. Different considerations such as frequency diversity and the availability of Channel Quality Indicator (CQI) determine the best choice. Protection from ISI due to multipath is ultimately accomplished by use of CP or GI.

Methods for ISI mitigation are summarized in the Table 10.

TABLE 10: METHODS FOR ISI MITIGATION

Waveform	**Method**
CP-OFDM	Fixed CP length to protect from delay-spread less than CP length.
DFT-s-OFDM	Fixed CP length to protect from delay-spread less than CP length.
Zero Tail (ZT) DFT-s-OFDM	Flexible CP length while preserving symbol alignment.
Unique Word (UW) DFT-s-OFDM	Flexible CP length while preserving symbol alignment.
FBMC	None
UFMC	Guard Interval
F-OFDM	Similar to CP-OFDM, the extra delay due to filtering is minimal.

A summary of Reference Signals in OFDM based waveforms is listed in the Table 11.

TABLE 11: REFERENCE SIGNALS IN OFDM BASED WAVEFORMS

Waveform	**Reference signal**
CP-OFDM	DMRS subcarrier insertion, flexible configuration in time/frequency/space.
DFT-s-OFDM	Insertion of DMRS in frequency domain detrimental to low PAPR. Several alternatives for insertion in time domain have been proposed in the literature, e.g.,[12].

ZT DFT-s-OFDM	Low-power constraint of head and tails impacts properties of DMRS sequences. Requires tailored receiver processing [13].
UW DFT-s-OFDM	Low correlation DMRS sequences can be readily used in unique word head/tail while preserving cyclicity [13].
FBMC	Additional techniques, such as the insertion of auxiliary pilots, are required to mitigate the imaginary interference for accurate channel estimation [14]
UFMC	Similar to CP-OFDM [15].
F-OFDM	Similar to CP-OFDM.

Filtered Bank Multi-Carrier (FBMC)

The principles of FBMC will be illustrated based on a specific subcarrier filtering method described in [16] in what follows. A more thorough discussion on the filter design process can be found in [11] but will be omitted here for the sake of brevity.

As explained above, FBMC consists of filtering the waveform on a per-subcarrier basis, ultimately causing the corresponding responses to be long. In comparison, the time domain impulse responses have a length of *KT*, where *K* is a design parameter referred to as the *overlapping factor* and *T* is the duration of a single OFDM symbol. Therefore, each FBMC symbol occupies *K* OFDM symbol durations, albeit avoiding the need for a CP.

Instead of a rectangular window (such as in the CP/DFT-S-OFDM case), FBMC uses real-valued and symmetric half-Nyquist pulses. Consequently, the related matched filter per subcarrier at the receiver is equal to the transmit filter. Likewise, the convolution of the transmit and receive filters for a given subcarrier are therefore real, symmetric, and observe the Nyquist property: *T*-spaced samples at the output of the receive filter are free of inter-symbol interference within a given subcarrier.

Note that the so-mentioned filtering operations are performed in the frequency domain (via a sliding FFT window of duration KT) both at the transmitter and receiver sides.

Figure 16 shows the frequency response H_k of the transmit filter for K=4 and Table 12 provides the values for K=2,3,4 (only half of the frequency response is provided due to symmetry), consisting of 2K-1 non-zero taps. Due to the FFT window duration of KT, the frequency bins are spaced by f_{scs}/K. The modulation symbols are mapped to every *K*'th subcarrier (thus resulting in f_{scs} spacing between consecutive modulation symbols in frequency domain) and the intervening samples are interpolated by frequency-domain convolution with H_k.

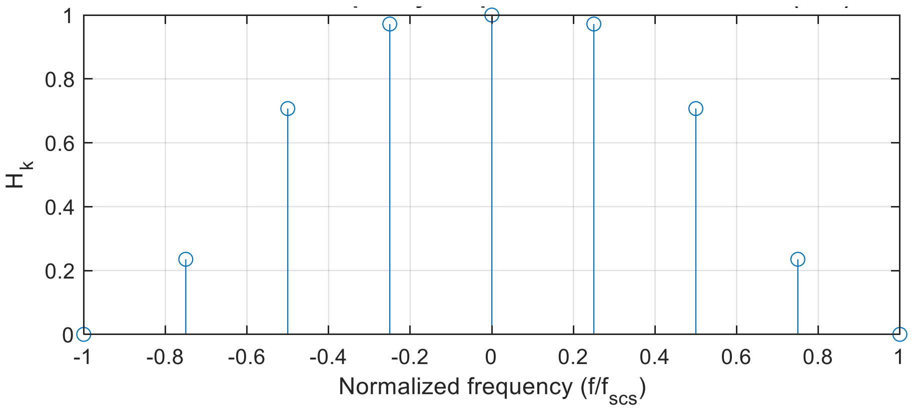

FIGURE 16: FREQUENCY RESPONSE OF THE TX FILTER WITH K = 4

TABLE 12: VALUES OF THE FREQUENCY RESPONSE OF THE TX FILTER

K	H_0	H_1	H_2	H_3
2	1	$1/\sqrt{2}$	-	-
3	1	0.911438	0.411438	-
4	1	0.971960	$1/\sqrt{2}$	0.235147

The transmit filter for the DC subcarrier, $h_{tx}(t)$, is a real-valued symmetric “half” or “square-root” Nyquist filter that can be obtained as:

$$h_{tx}(t) = \sum_{k=-(K-1)}^{K-1} H_k e^{j2\pi kt/(KT)}$$

where T denotes the FFT window duration for one OFDM symbol. The transmit filter or basic pulse is illustrated in Figure 17 (a), and the matched filter at the receiver $h_{rx}(t)$ is therefore equal to the TX filter.

The convolution of h_{tx} and h_{rx} corresponds to the so-called *signal-path impulse response*, which is a Nyquist filter, is illustrated in Figure 17 (b) below. Noteworthy, it is real-valued and has zero crossings at T-spaced intervals on either side of the peak.

The interference from lower and upper neighbouring subcarriers can be found by convolving the receive filter h_{rx} with the TX filters corresponding to the lower and upper subcarriers, which are simply frequency shifted versions of h_{tx} by $-f_{scs}$ and f_{scs}, respectively, where $f_{scs}=1/T$.

Note that the real and imaginary part of the so-called *interference-path impulse response* has zero crossings at odd multiples of T/2 and integer multiples of T, respectively. This is a consequence of real and symmetric nature of H_k, which results in a real valued $H_k H_{k-K}$ (symmetric around $-f_{scs}/2$) and similarly real valued $H_k H_{k+K}$ (symmetric around $f_{scs}/2$). Thus, the time-domain response has a complex sinusoidal factor at a frequency of $f_{scs}/2$.

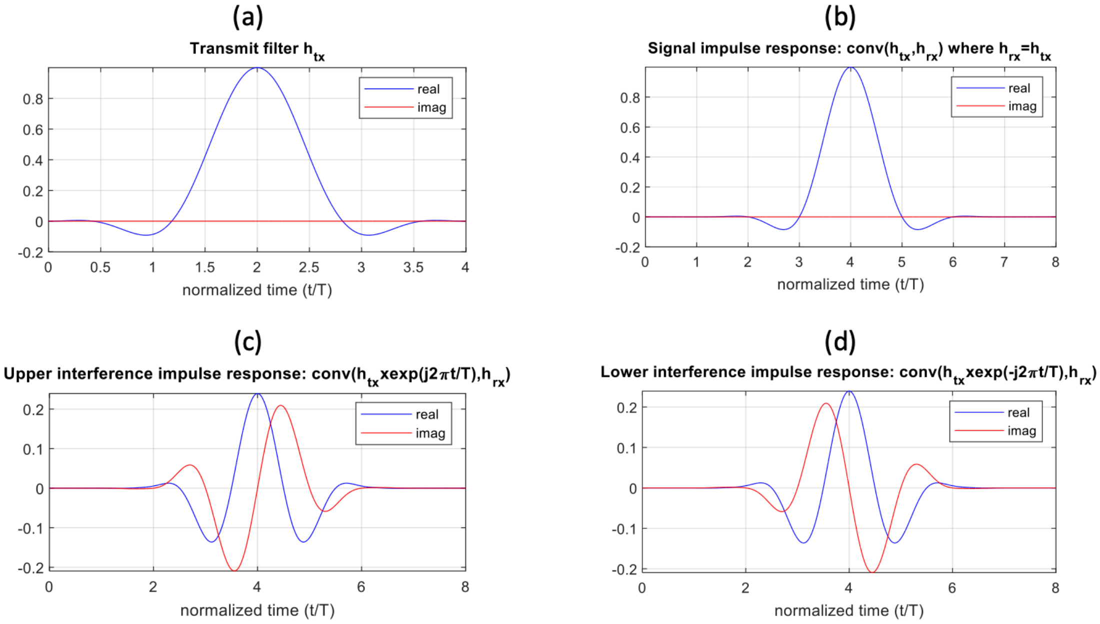

FIGURE 17: IMPULSE RESPONSE

From the preceding discussion, it can be seen that complex-valued modulation symbols can be mapped at a time-domain spacing of T without ISI. Likewise, subcarriers that are at least $2f_{scs}$ apart do not interfere due to the bandlimitedness of transmit filters.

However, there would be interference from adjacent subcarriers that are f_{scs} away. Thus, one way to map complex-valued (e.g., QPSK) modulation symbols in frequency-time domain in an interference-free manner would be as shown in Figure 18. That is, by subcarrier spacing that is double that of CP-OFDM, but with $T=1/f_{scs}$ spacing in time-domain, rather than $T_{CP}+1/f_{scs}$ spacing. This results in half of a complex-valued modulation symbol per unit-area in frequency-time domain representation, which is less efficient than conventional CP-OFDM.

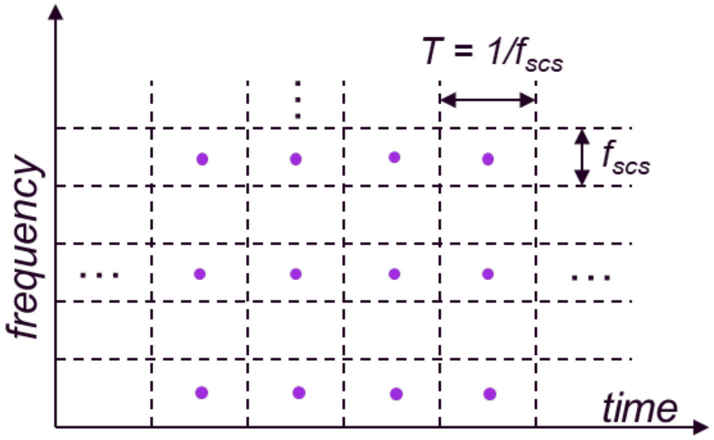

FIGURE 18: EXAMPLE OF MAPPING OF COMPLEX-VALUED MODULATION SYMBOLS IN FREQUENCY-TIME DOMAIN IN AN INTERFERENCE-FREE MANNER

Now, consider the frequency-time mapping shown in Figure 19 where blue dots represent purely real and yellow dots represent purely imaginary modulation symbols.

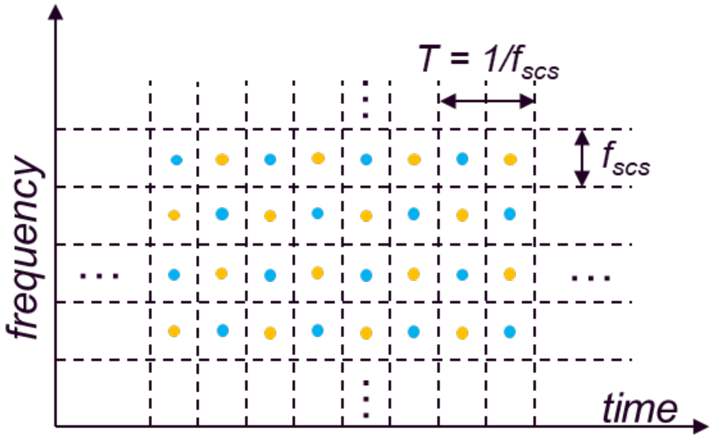

FIGURE 19: EXAMPLE OF MAPPING OF COMPLEX-VALUED MODULATION SYMBOLS IN FREQUENCY-TIME DOMAIN

Both the time and the frequency domain densities are doubled compared to the mapping of complex-valued data (purple dots) shown in the previous figure. Hence, the scheme results in two real-valued, or equivalently one complex-valued modulation symbol, per unit area which is better than CP-OFDM.

Note that the data points shown in Figure 19 either do not interfere with each other, or they do interfere entirely out-of-phase (i.e., orthogonally), in particular:

- Dots of same colour in any given subcarrier are T-spaced, hence they don't interfere in the time domain by Nyquist property of the signal-path filter. They are free of ISI.
- Dots of opposite colour interfere with each other on a given subcarrier. However, there is only a real component to the overall *signal-path impulse response* that can be easily removed, and thus ISI avoided.
- Dots of same colour across adjacent subcarriers do interfere but there is only an imaginary component to the overall *interference-path impulse response* at odd multiples of T/2 that can be easily removed, and thus ICI avoided.
- Dots of opposite colour across adjacent subcarriers do interfere but there is only a real component to the overall *interference-path impulse response* at multiples of T that can be easily removed, and thus ICI avoided.
- Dots separated by more than one subcarrier do not interfere because of the band-limited subcarrier filter.

An implementation of the so-called offset-QAM (OQAM) transmitter for FBMC based on KN-point FFT is shown Figure 20 [5]:

Co-funded by the European Union

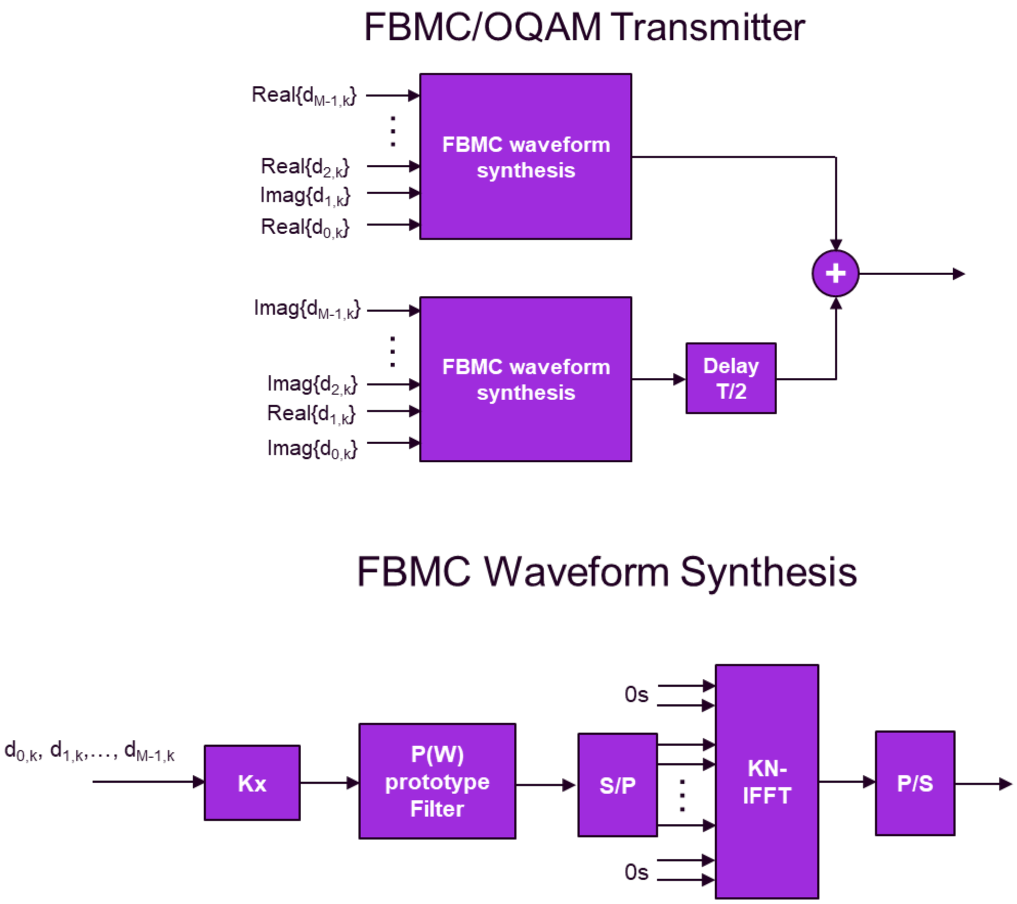

FIGURE 20: IMPLEMENTATION OF OQAM TRANSMITTER FOR FBMC BASED ON KN-POINT FFT

The receiver structure for FBMC is illustrated in Figure 21. The receiver consists of a matched filtering implemented by a KN-point FFT with matched filtering performed in frequency-domain by H_r and sampling by T/2-spaced sliding window operation. Samples are collected and vectorized over a KN-point window and transformed into frequency domain. The prototype window is applied around each subcarrier and outputs are collected to N-point vector, which is then serialized. Based on the frequency-time domain mapping of real and imaginary parts of complex-valued modulation symbols, the received “soft” versions of the complex-valued modulation symbols are re-constructed. These are then passed to Log Likelihood Ratio (LLR) computation.

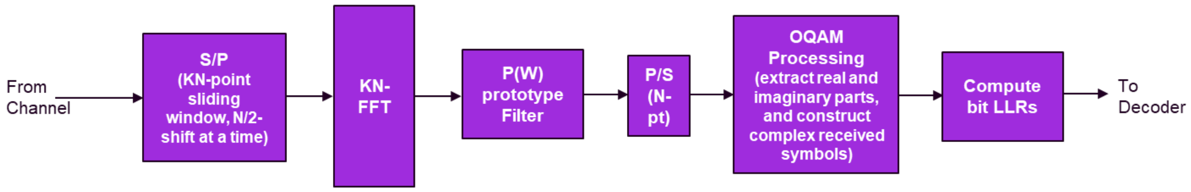

FIGURE 21: FBMC RECEIVER

More general filtering options are described in [11], and efficient architectures based on N-point FFT using poly-phase filter structures are described in [16]. On the other hand, regarding channel estimation, pilot symbols cannot be as easily inserted as in CP-OFDM due to the indeterminacy induced by imaginary interference. Consequently, different methods have been devised in the literature to mitigate such imaginary interference and enable accurate channel estimation [14].

The FBMC waveform makes efficient use of the available resources by removing the CP. Despite such removal, time alignment with 5G NR can be maintained simply by considering 15 symbols per slot, further making sampling rates compatible with 5G NR.

Additionally, OOB emissions are reduced by the appropriate design of the subcarrier filter. Importantly, OOB emissions related to PA non-linearities and DAC are not diminished by such a waveform.

Also, as the so-mentioned filter spans multiple OFDM durations, FBMC is inefficient for short packet transmissions, low-latency transmissions, and frequent Uplink (UL)/Downlink (DL) switching [8] but, as explained above, it is more efficient than CP-OFDM for long sequences [11] [16].

Although MIMO is straightforward in the complex version of FBMC [17], the efficient version using OQAM does not lend itself so easily for MIMO implementation as orthogonality of the symbols only holds in the real field. Several methods have been developed to deal with this limitation [18]. Importantly, most of the techniques developed for MIMO-OFDM are not applicable owing to the specifics of OQAM.

Lapped-OFDM

Lapped-OFDM is a FBMC-OQAM variant with a particular prototype filter. Its name is derived from the lapped orthogonal transform as defined in [19]. The lapped transform can be implemented with a 2N-FFT followed by a sine filter having the 2 coefficients: [1, −1]. The lapped-OFDM filter is defined on a shorter duration L = 2N. In other works, the overlapping factor of lapped-OFDM is K = 2.

FBMC-OQAM and lapped-OFDM belong to the same waveform class with two different prototype filters, PHYDYAS for FBMC-OQAM and Sinus for Lapped-OFDM, as shown in Figure 22.

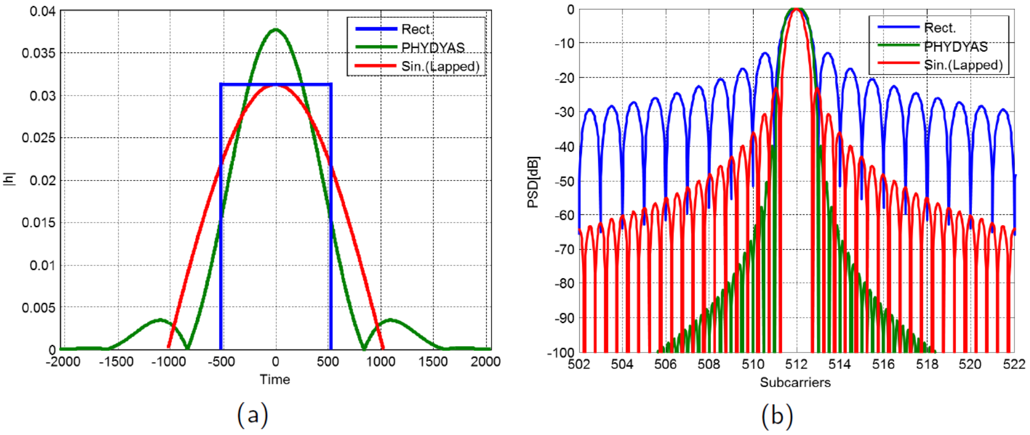

FIGURE 22: LAPPED-OFDM FILTER COMPARISON IN TIME (A) AND FREQUENCY (B) WITH PHYDYAS FILTER

The response of lapped-OFDM is more localized in the time domain compared to other forms of FBMC-OQAM although it spreads on higher number of subcarriers compared to FBMC-OQAM (more than 9 subcarriers instead of 3 for FBMC-OQAM).

The study in [20] compared Lapped-OFDM with other OFDM-based waveforms in terms of latency, complexity, PSD, and Mean Square Error (MSE). Due to shorter prototype filter duration (K=2), Lapped-OFDM has lower spectrum decaying than FBMC-QAM, FBMC-OQAM, and Filtered Multi-Tone (FMT). The authors showed that a very small number of edge subcarriers are affected by interference thanks to the good spectral containment of FBMC-OQAM and Lapped-OFDM signals.

Block-Filtered-OFDM (BF-OFDM)

Block-filtered-OFDM [21] is part of the FBMC family. It can be seen as an improved version of FFT-FBMC, which is a derivative of FBMC-OQAM.

One of the drawbacks of FBMC-OQAM mentioned earlier is its orthogonality in the real domain which is a problem for MIMO implementation due to the added complexity. BF-OFDM is able to keep orthogonality in the complex domain while having very good frequency localizations similar to FBMC-OQAM ones.

The transmitter scheme for BF-OFDM is illustrated in Figure 23. It consists of a pre-distortion stage followed by pre-coding and filter bank. The precoding scheme is performed by means of CP-modulators (of size N) consisting of Inverse Fourier Transforms (IFTs) and CP insertion. The filtering operation uses a PolyPhase Network (PPN) (of size M) as for FFT-FBMC.

BF-OFDM differs from FFT-FBMC with the addition of a filter pre-distortion stage on the transmitter side. This stage allows to compensate the distortion induced by the filter bank in both amplitude and phase in order to attenuate the transmitted signal spectrum inside the carrier bandwidth. Thanks to the pre-distortion stage, no filtering is required at the receiver side which can be reduced to a MN/2-point FFT preceded by a CP removal (Figure 24).

It can be noted that complexity on the transmitter side is influenced by the number of active RBs. On the other hand, the receiver has low complexity due to its similarity to the CP-OFDM receiver.

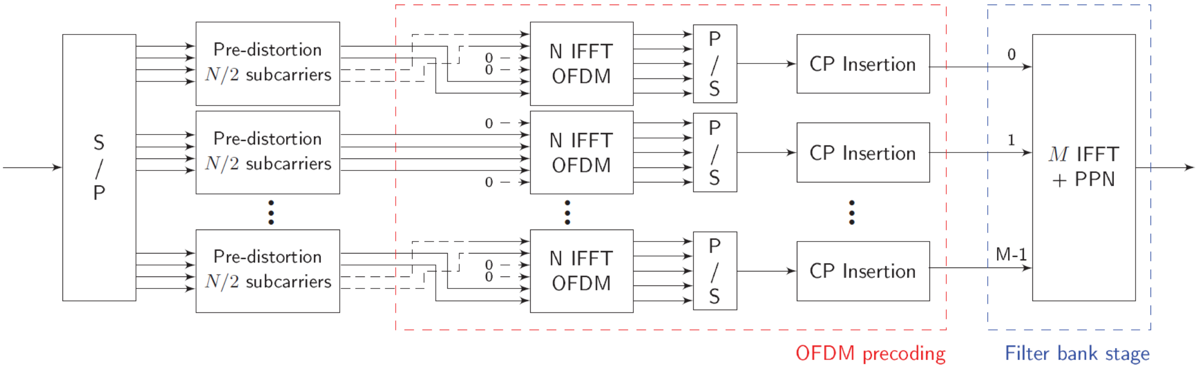

FIGURE 23: BF-OFDM TRANSMITTER SCHEME

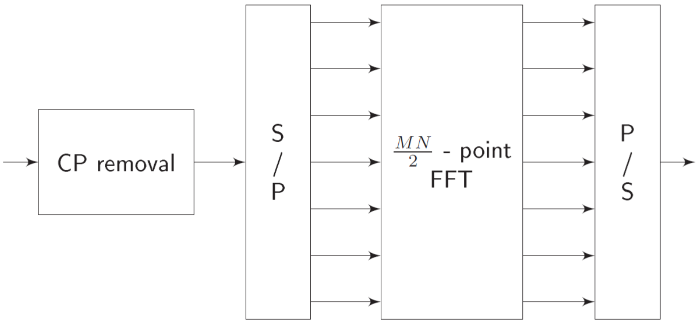

FIGURE 24: BF-OFDM RECEIVER SCHEME

The study in [20] compared BF-OFDM to other OFDM-based waveforms in terms of PSD and synchronization with timing and frequency errors due to inter-user interference. It must be noted that the timing and frequency offsets tested are quite low (±33.33 μs and ±1.5 kHz respectively). BF-OFDM provides excellent PSD performances thanks to the use of filterbank on the transmitter side. However, the BF-OFDM rectangular receiver filter brings an important amount of interference from the coexisting asynchronous user. BF-OFDM MSE is higher than FFT-FBMC when the timing errors are outside the CP-region, since BF-OFDM receiver corresponds to the classical CP-OFDM through the use of FFT. FFT-FBMC receiver is better in that regard since the filtering performed by the analysis filterbank significantly reduces the asynchronous interference. When errors are within the CP-region, BF-OFDM performs better than FFT-FBMC since the prototype filter is designed to minimize the degradation in negligible timing offset case. The MSE for BF-OFDM with different carrier frequency offsets is also high in the regions outside the CP.

Universal Filtered Multi-Carrier (UFMC)

Universal Filtered Multi-Carrier [22]-[24] can be seen as a middle ground between f-OFDM and FBMC. In f-OFDM, the entire band is filtered, whereas in FBMC individual subcarriers are filtered.

On the contrary, UFMC divides the transmission band into smaller sub-bands and applies filtering to each of them, hence reducing the filter length compared to FBMC. Importantly, the filter dispersion can be confined to a guard interval, making UFMC better suited to short packet transmissions in comparison to FBMC [8]. Additionally, UFMC rely on QAM modulation and can therefore reuse conventional MIMO techniques.

The UFMC transmitter can be implemented as shown in Figure 25 [5].

The full band is thus divided into sub-bands, e.g., resource blocks, each one having a fixed number of subcarriers. At each sub-band, an N-point IFFT spanning the full band is relied upon, with only the corresponding sub-band allocation present and zero power at all other subcarriers.

Following the IFFT stage, an all-zero guard is attached in the time domain, and the resulting sequence is ultimately filtered. Different filters per sub-band can be applied. Sub-band filters may be rotated versions of the same prototype filter, i.e., rotated versions to place the frequency response at the sub-band centre.

Co-funded by the European Union

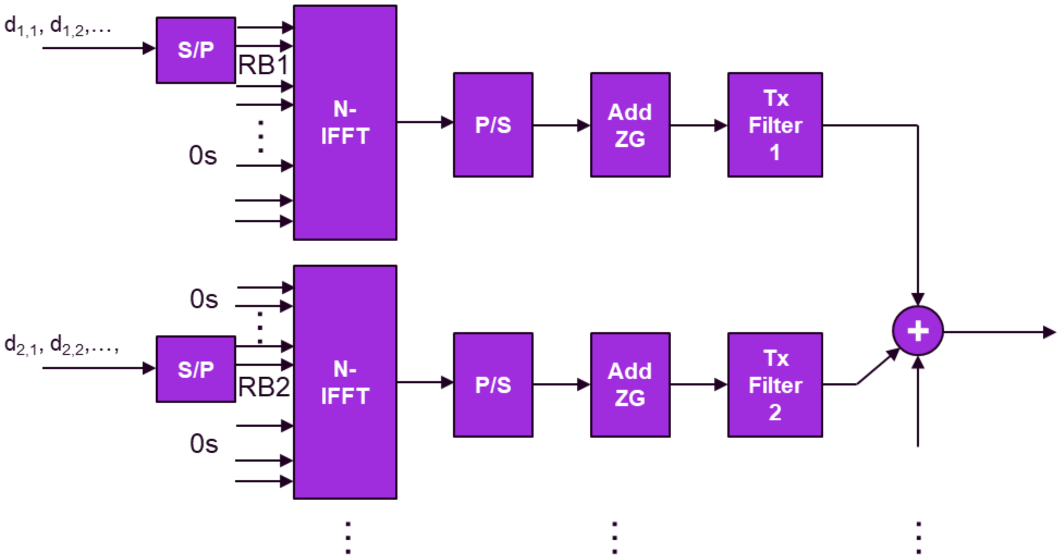

FIGURE 25: UFMC TRANSMITTER

In [22], Chebyshev filter is used with desired attenuation level and filter length as inputs to filter design. The filter outputs are summed and converted to Radio Frequency (RF) band for transmission over the channel.

Figure 26 further illustrates the UFMC time-domain signal processing.

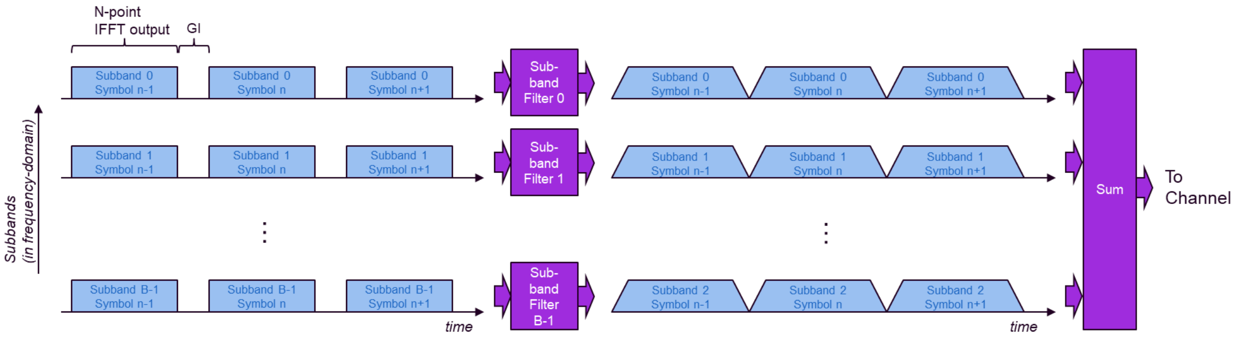

FIGURE 26: UFMC TIME-DOMAIN SIGNAL PROCESSING

An implementation of the UFMC receiver is shown in Figure 27 [5].

The samples corresponding to symbol *n* are extracted using a window larger than the transit FFT size as a means to capture the filter-related tails. then, zeroes are appended to make the length equal to twice the original FFT window size.

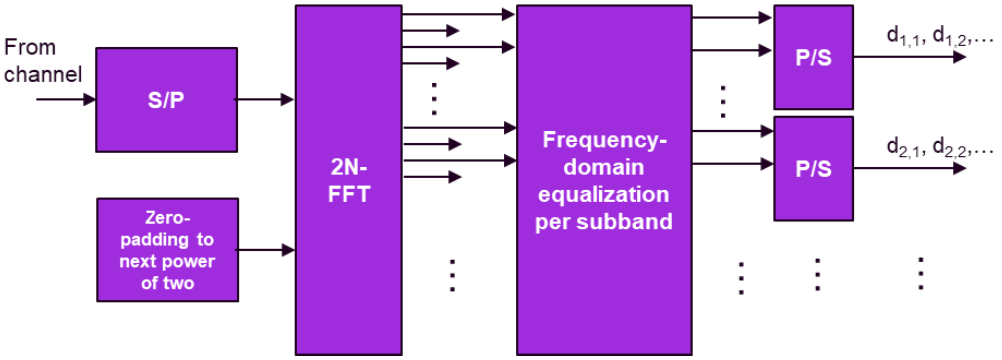

FIGURE 27: UFMC RECEIVER

As presented in Figure 28, a 2N-point FFT is applied but only even-indexed outputs are kept. Thus, at the FFT output, the effect of sub-band filtering and multipath appears as a multiplicative channel in frequency-domain (circular convolution in time-domain), which is then estimated and equalized using 1-tap equalizer. The remainder of the process is the same as in CP-OFDM.

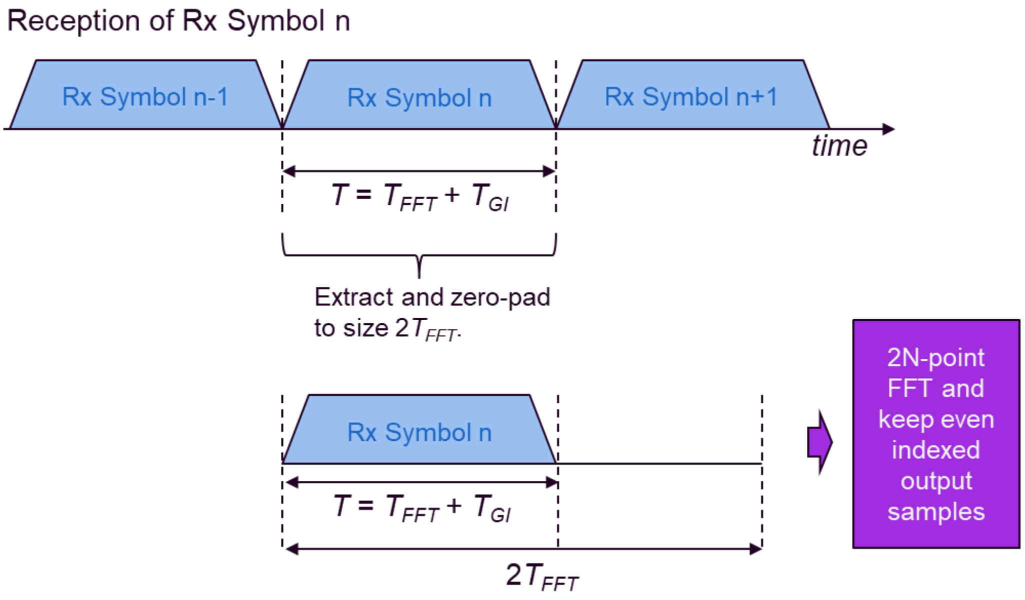

FIGURE 28: RECEPTION OF N-TH UFMC SYMBOL

For additional in-depth references of UFMC in the literature, the reader is referred to [23] and [24].

Filtered Orthogonal Frequency Division Multiplexing (F-OFDM)

As aforementioned, the f-OFDM transmitter and receiver structures are similar to those of CP-OFDM except for the use of full-band filtering to reduce out-of-band emissions [25]. Compared to UFMC, the length of the designed filter can be designed longer than the CP, and resulting ISI further reduced by soft windowing.

As is the case in CP-OFDM, the time-frequency efficiency of f-OFDM is less than one due to the use of CP and QAM modulation (as well as MIMO) can be relied upon. Additionally, DFT spreading can be further used to reduce PAPR as in the DFT-s-OFDM variant discussed above.

Co-funded by the European Union

Diagrams of typical transmitter and received architectures for f-OFDM are illustrated Figure 29 and Figure 30. As expected, the receive signal is matched filtered by the transmit filter, and then processed similar to CP-OFDM.

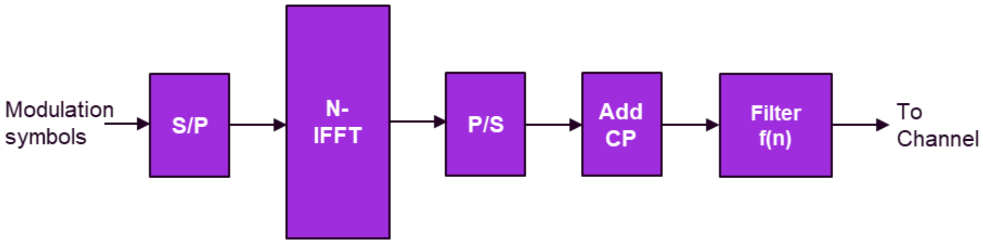

FIGURE 29: F-OFDM TRANSMITTER

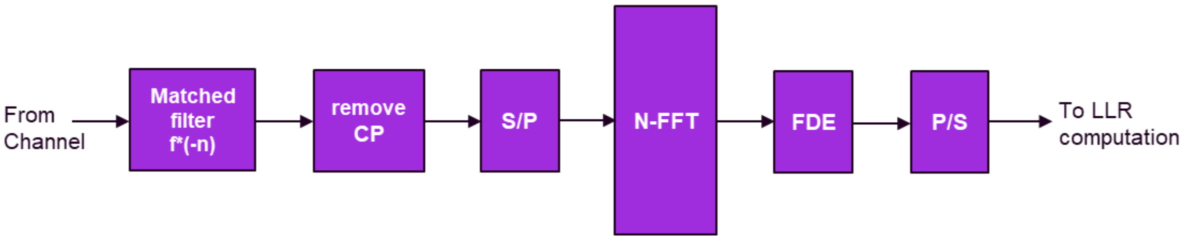

FIGURE 30: F-OFDM RECEIVER

The time-domain filter should have the following properties:

- Flat passband response within the transmission band,
- High attenuation in the stopband (outside the transmission band).
- Sharp transition between passband and stop-band.

In [25], a systematic approach is proposed to provide a reasonable balance between frequency and time-localization of the filter:

- Start with a filter with rectangular frequency response as the prototype filter (sinc impulse response p(n), with appropriate bandwidth).
- Apply a time-domain mask w(n) on p(n): f(n) = p(n) x w(n).
- Then shift the filter in frequency domain to be centred at the desired frequency.

The windowing mask has smooth transitions to zero at both ends, avoiding abrupt jumps. The windowing provides a reasonable time-localization for the filter's impulse response.

A candidate for windowing is the Hanning window of duration T_w:

$$w(t) = \begin{cases} 0.5[1+\cos(2\pi|t|/T_w)] & |t| \le T_w/2 \\ 0 & else \end{cases}$$

For additional in-depth references of f-OFDM in the literature, the reader is referred to [25] [26].

Generalized Frequency Division Multiplexing (GFDM)

Generalized Frequency Division Multiplexing (GFDM) can be seen as a renewal of the traditional filter bank multi-carrier concept in the digital domain [27]-[30]. Unlike the OFDM counterpart, GFDM allows for a loss in the orthogonality among subcarriers, and therefore some level of ISI and ICI interference are observed. Nonetheless, using CP, as well as an appropriately chosen protype filter, time and frequency dispersion can be contained to obtain the same symbol error rate performances as OFDM [27].

Importantly, GFDM with its reliance on filter banks allows to limit OOB emissions by choosing a filter with good spectral contention. It also improves the spectral efficiency relative to conventional CP-OFDM as it requires a single CP per block (unlike OFDM where one CP per symbol is used). The latter comes at the expense of an increase in the computational complexity and delay related to the block-based operations. Nevertheless, shorter blocks can also be considered, if application's latency becomes stringent.

Additionally, GFDM does provide a typically lower PAPR than OFDM given that fewer subcarriers are observed [28]. The latter is explained by the reduction of the amount of superimposed sinusoidal waves and, consequently, of the fast variations due to their constructive and destructive superposition, ultimately improving the PAPR.

Lastly, given that symbols on GFDM can be encoded through conventional QAM, and an FFT-based Frequency Domain Equalization (FDE) can be exploited, many existing techniques available over MIMO-OFDM can be easily ported to GFDM. In fact, as highlighted in [27], the flexible GFDM architecture can be seen as one with both CP-OFDM and Single Carrier FDE (SC-FDE) as special cases.

The GFDM TX and RX architectures [28] are presented below in Figure 31 and Figure 32.

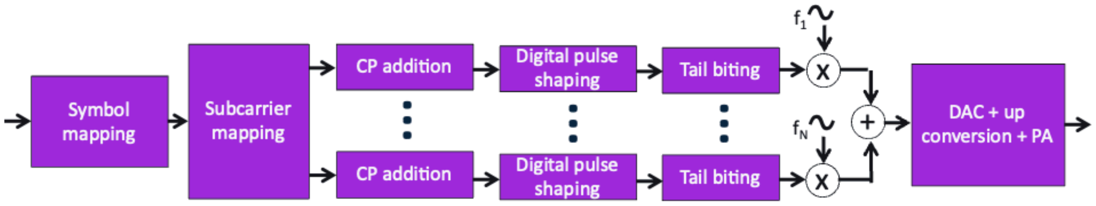

FIGURE 31: GFDM TRANSMITTER

As we can see from Figure 31 and Figure 32, every subcarrier is processed independently allowing for a per sub-carrier configuration of bandwidth and prototype filter, as well as contiguous or non-contiguous spectrum allocation.

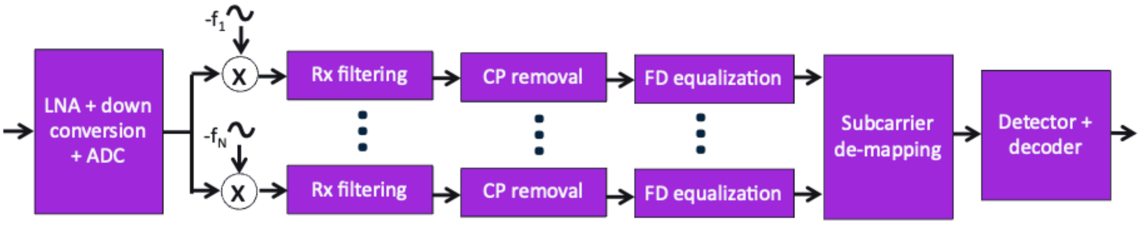

FIGURE 32: GFDM RECEIVER

In the architecture presented above, the tail biting technique was used to reduce the required length of the CP by the length of the Tx filter. The latter, as the CP would conventionally need to accommodate for the Tx filter, channel, and Rx filter related dispersions.

Generalized DFT-s-OFDM (G-DFT-s-OFDM)

Several generalizations of DFT-s-OFDM [13], [31],[32]-[36] will be discussed in the following. These variants use either CP or GI, with the latter being dynamically configurable by the transmitter based on individual channel requirements or system-level timing-error observations.

In fact, CP-based waveforms suffer from:

- Limited flexibility: due to predefined CP duration, channels with high delay spread may suffer ISI/ICI, while channels with low delay spread may observe unnecessarily long overhead.
- Poor spectral containment: due to sudden changes in amplitude/phase at symbol boundaries. Spectral containment issues affect asynchronous users allocated at adjacent channels.

Special cases of Generalized DFT-s-OFDM include:

- ZT DFT-s-OFDM [34]: the internal guard period is composed of low power samples.
- UW DFT-s-OFDM [13] [35] [36]: Predefined known word is used at the tail of the signal.

Overall, by reusing the same sequence at the tail and head of every symbol, transitions at symbol boundaries can be smoothened producing:

- An improved spectral containment compared to DFT-s-OFDM,
- A PAPR that can be close to that of DFT-s-OFDM.

The zero tail and header with flexible duration is useful in providing gaps for UL/DL switching in the ZT DFT-s-OFDM case. Although these tend to increase the PAPR with respect to other variants, the waveform still observes a significant benefit over CP-OFDM of close to 2.5 dB of PAPR improvement (cf. 3 dB in the case of DFT-s-OFDM).

Additionally, the adoption of identical header and tail samples for all OFDM symbols enforces a continuity at symbol boundaries that reduces OOB emission, while preserving the DFT-s-OFDM benefit of PAPR reduction.

Compared to waveforms based on cyclic prefix, the head/tail guard-interval based alternative allows as well to better cope with diverse time dispersions in the system. The latter translates into an improved spectrum efficiency as the length of the tail, that is meant to absorb the channel dispersion, can adapt to specific channel requirements [13].

Using the same tail samples (i.e., either zeros or unique words) at the end of each symbol provides periodicity by generating the same dispersion at the beginning of each symbol. Maintaining the same head samples preserves continuity by avoiding the first data samples from wrapping around to the end due to cyclicity. Thus, the waveform emulates cyclicity and, consequently, a simplified one-tap equalizer in the frequency domain can be used.

For UW DFT-s-OFDM, reference symbols can be made up of Zadoff-Chu (ZC) sequences. Continuity between UW DFT-s-OFDM symbols and reference symbols is achieved by using the Nh first samples of the time-domain RS sequence as the header for the UW DFT-s-OFDM symbol, and similarly, using N_t last samples as the tail.

The transmitter and receiver structures of generalized DFT-s-OFDM are shown in Figure 33.

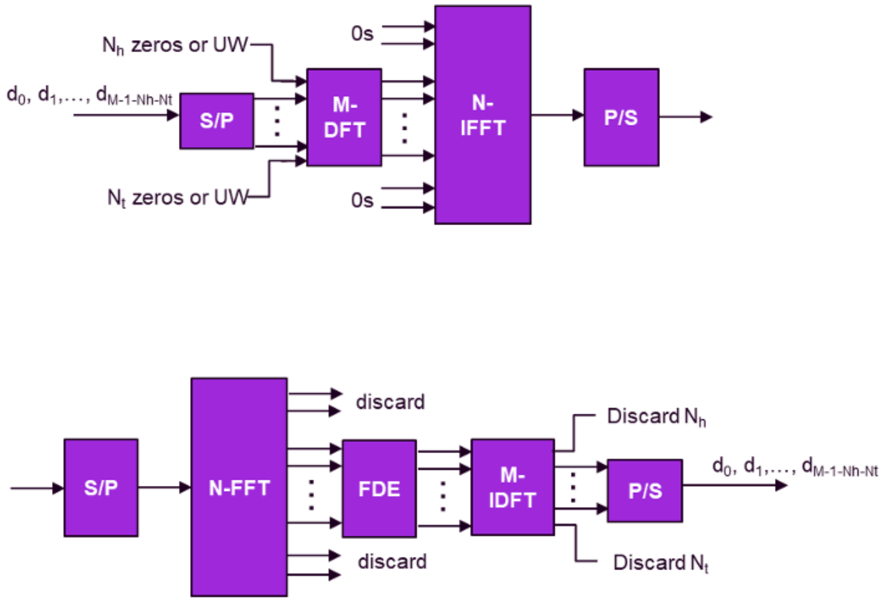

FIGURE 33: ZT/UW DFT-S-OFDM TRANSMITTER (TOP) AND RECEIVER (DOWN)

3.3.1.2 PAPR reduction techniques and Partial Transmit Sequences (PTS)

Since the advent of OFDM and its popularity as the core technology of many standards, the high PAPR has been identified as one of its main intrinsic limitations [37]-[48]. Particularly, a high PAPR impacts by requiring HPA with a large input back-off power, and complex DAC and Analog to Digital converters (ADC) [37]. Thus, if not properly accounted for, it may dramatically impact the Bit Error Rate (BER) and cause spectrum leakages, in addition to the high cost and low efficiency of power amplifiers at such operating regimes.

Consequently, plenty of techniques have been devised to reduce its impact, among which two broad kinds can be identified, namely**:** *signal distortion techniques* and *signal scrambling techniques*. The former (including clipping, peak windowing, Active Constellation Extension (ACE), among others), considerably reduces the PAPR at the expense of some in-band distortion and out-of-band emissions related to the removal of the time-domain peaks of the signal prior to the HPA stage.

Unlike signal distortion techniques, the signal scrambling counterpart does not generally produce degradation of BER nor unwanted emissions. On the other hand, it may suffer of an increase in computational complexity, as well as a decrease in the spectrum efficiency due to extra side information needed to be sent over to the receiver side for correct decoding.

The signal scrambling techniques can be further grouped into three categories: coding techniques, Multiple Signal Representation (MSR) techniques and constellation shaping techniques. The rest of the current section will focus on Partial Transmit Sequences (PTS), a member of the MSR group within the signal scrambling category of the PAPR reduction techniques.

The MSR techniques rely on the production of several representations of the same OFDM waveform, out of which the one with the lowest PAPR is to be selected. As such, the PTS

Co-funded by
the European Union

corresponds to a type of MSR in which the input data is partitioned into disjoint frequency domain subsets, all of which are linearly combined via rotation phasors (an operation that can be easily undone by a receiver with sufficient information). A PTS-OFDM architecture looks like the one in Figure 34.

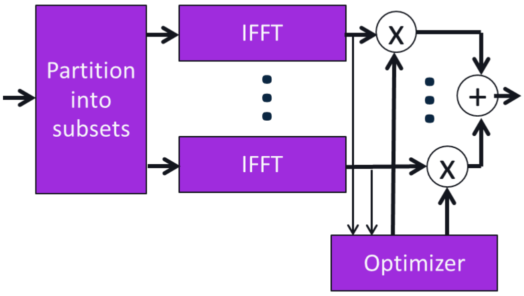

FIGURE 34: PTS-OFDM TRANSMITTER

Several subset partitioning and optimization schemes have been proposed and studied in the literature, thus providing an array of configurations with different computational complexities and PAPR reduction performances [41]-[48].

As shown via simulation in [37], analysing dozens of modified configurations to the one presented above, the PTS technique can provide up to 2 dB improvement in the median PAPR and 3 dB on the top 1% of the PAPR distribution. Factors such as the PAPR requirements, the allowed spectrum efficiency loss, and computational complexity are identified as key to determine one specific implementation.

3.3.1.3 Orthogonal time frequency space (OTFS)

The Orthogonal Time-Frequency Space (OTFS) modulation is a recently proposed waveform that aims to overcome the OFDM limitations in high mobility environments [49]. The OTFS waveform has been conceived to achieve robustness against Doppler frequency shifts in fast time-varying multipath propagation channels. The resulting channel is doubly selective, i.e., time and frequency selective. These effects are typically found in scattering environments where transmission and reception points are embedded in mobile platforms, e.g., planes, trains, vehicles, Unmanned Aerial Vehicle (UAVs) or Non-Geostationary (NGSO) satellites.

The main characteristic of OTFS stems from encoding the information in the Delay-Doppler (DD) domain rather than in the Time-Frequency (TF) plane. Interestingly, if the channel has a small number of multipath components, then it follows that the channel impulse response on the DD domain is sparse. Furthermore, the channel taps remain constant on the DD plane over the frame transmission. Hence, to all modelling effects, channel gains are constant for all the symbols that are arranged in the frame. This is crucial to simplify symbol detection. Remarkably, in presence of time and frequency selectivity, the channel impulse response is neither sparse nor constant on the TF plane.

OTFS modulation and demodulation

The OTFS modulation is divided into two stages [49]. First, a set of symbols in the DD domain are converted to the TF domain through an Inverse Simplistic Finite Fourier Transform (ISFFT). In the second stage, the transmitted signal is obtained from the TF modulated sequence using the Heisenberg transform. Remarkably, a form of Heisenberg transform can be implemented by a multicarrier modulator, which generates the time domain signal that is transmitted over the channel. At the other end of the link, the stages are reversed. Hence, the OTFS demodulator maps the received symbols into the DD domain. First, the received samples are fed into the Wigner transform and next, the SFFT is applied. The Wigner transform is a generalization of the demodulator that maps the received signal into the modulated symbols on the TF plane. The Wigner transform can be implemented in the form of a multicarrier demodulator. The concept is illustrated in Figure 35. It is important to remark that the grid of the DD plane corresponds to Delay and Doppler resolutions.

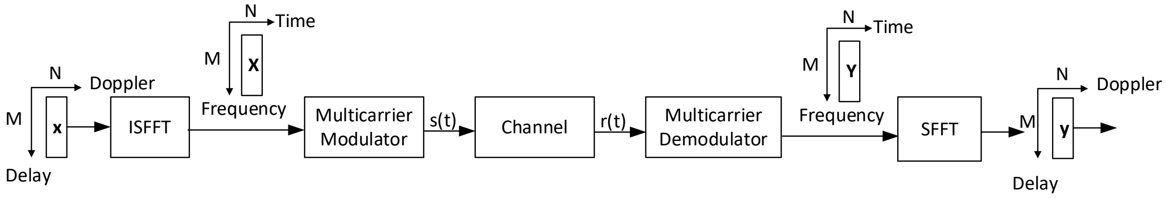

FIGURE 35: OTFS TX AND RX BLOCK DIAGRAM

As described in the previously, the transmitter first maps the symbols $\{x[m,n]\}$ from the DD domain to TF domain using the ISFFT, i.e.

$$X[l,k] = \frac{1}{\sqrt{NM}} \sum_{n=0}^{N-1} \sum_{m=0}^{M-1} \boldsymbol{x}[m,n] e^{j2\pi\left(\frac{nk}{N} - \frac{ml}{M}\right)}$$

for $l = 0, \dots, M-1, k = 0, \dots, N-1$. Let $\boldsymbol{X} \in \mathbb{C}^{M\times N}$represents the matrix form of the TF domain modulated symbols $\{\boldsymbol{X}[l,k]\}$. Note that the ISFFT is a 2D transformation that perform an M-point DFT of the columns of $\boldsymbol{X}$ and N-point inverse DFT (IDFT) of the rows of $\boldsymbol{X}$.

To obtain a continuous time waveform, the subcarrier signals are shaped with the transmit waveform $g_{tx}(t)$. Then, the output of the TF modulator, aka Heisenberg transform, which convert the $\{X[l,k]\}$ samples to a continuous-time waveform, can be written as

$$s(t) = \sum_{k=0}^{N-1} \sum_{l=0}^{M-1} X[l,k] g_{tx}(t-kT) e^{j2\pi l\Delta f(t-kT)}$$

The symbols are spaced T in time and $\Delta\mathrm{f}$ in frequency. The symbol density is $T\Delta\mathrm{f} = 1$. Therefore, $M \times N$ symbols are transmitted in NT seconds and span a bandwidth $\mathrm{M}\Delta_f$. Once the signal $s(t)$ is transmitted over the channel, the received signal $r(t)$ at the receiver is passed through $g_{rx}(t)$ .The output can be expressed as the cross-ambiguity function $A_{g_{rx},r}(f,t)$ as

$$Y(f,t) = A_{g_{rx},r}(f,t) \triangleq \int r(\acute{t})\, g_{rx}^{*}(\acute{t}-t) e^{-j2\pi f(\acute{t}-t)} d\acute{t}$$

By sampling $Y(f,t)$ on the TF grid points, the demodulated symbols can be arranged in the matrix $\boldsymbol{Y} \in \mathbb{C}^{M\times N}$ with entries

$$Y[l,k] = \left. Y(f,t)\right|_{f=l\Delta f,\ t=kT}$$

for $l = 0, \dots, M-1, k = 0, \dots, N-1$. Note that the last two equations are referred to as Wigner transform.

In the final step, the SFFT is applied to $\boldsymbol{Y}$ leading to $\boldsymbol{y} \in \mathbb{C}^{M\times N}$. The symbols received in the DD bins are expressed as

$$y[m,n] = \frac{1}{\sqrt{NM}} \sum_{k=0}^{N-1} \sum_{l=0}^{M-1} Y[l,k] e^{-j2\pi(\frac{nk}{N} - \frac{ml}{M})}$$

Note that the SFFT is a 2D transformation which takes an M-point IDFT of the columns of $\boldsymbol{Y}$ and an N-point DFT of the rows of $\boldsymbol{Y}$.

Let τ_{max} and υ_{max} denote the maximum delay and Doppler of the channel. The pulses $g_{tx}(t)$ and $g_{rx}(t)$ are said to be ideal if satisfy $A_{g_{rx},g_{tx}}(nT - \tau, m\Delta f - \upsilon) = \delta(n)\delta(m)$, for $-\tau_{max} \leq \tau \leq \tau_{max}$ and $-\upsilon_{max} \leq \upsilon \leq \upsilon_{max}$. This condition is referred to as the bi-orthogonal robust condition [49]. When the pulses are ideal, and if the noise term is omitted, the TF domain signal can be written as

$$Y[l,k] = H_{tf}[l,k]X[l,k],$$

for $l = 0, \ldots, M-1, k = 0, \ldots, N-1$. The TF domain channel matrix is expressed as

$$H_{tf}[l,k] = \iint e^{-j2\pi\upsilon\tau} h(\tau,\upsilon) e^{j2\pi l\upsilon T} e^{-j2\pi k\Delta f\tau} d\tau d\upsilon$$

where $h(\tau,\upsilon)$ represents the channel impulse at delay τ and Doppler υ. According to [49], the DD input-output relation can be written as

$$y[m,n] = \sum_{k=0}^{N-1} \sum_{l=0}^{M-1} x[l,k] H_{dd}[m-l, n-k]\,,$$

where $H_{dd}[m-l,n-k]$ is a sampled version of $h_w(\tau,\upsilon)$, i.e.,

$$H_{dd}[m-l,n-k] = h_w(\tau,\upsilon)\big|_{\upsilon = m - \frac{l}{NT},\ \tau = kT}$$

with

$$h_w(\tau,\upsilon) = \iint e^{-j2\pi\upsilon\tau} h(\tau',\upsilon') \omega(\tau-\tau',\upsilon-\upsilon') d\tau' d\upsilon'$$

$$\omega(\tau,\upsilon) = \sum_{k=0}^{N-1} \sum_{l=0}^{M-1} e^{-j2\pi(\upsilon kT - \tau l\Delta f)}\,.$$

In practical scenarios, it's challenging to attain perfect orthogonality, but one can employ pulse shaping techniques to mitigate the impact of biorthogonality loss. Typically, the use of narrower pulses can approximate biorthogonality in the time-frequency domain, although this might come at the expense of time-frequency resource efficiency.

Practical implementation of OTFS

In the following, practical OTFS structures, as the ideal pulses introduced in the previous section cannot be realized in practice. In this regard, it is common practice to consider the OFDM technology to implement the multicarrier modulation scheme. Depending on the placement of the CP redundancy blocks, two OFDM-based OTFS schemes can be differentiated.

- OTFS with per-symbol CP

This scheme is based on applying a 2D transform to the symbols that are fed into the OFDM modulator [51]. It is important to remind that OFDM in its basic form can be efficiently implemented with an inverse fast Fourier transform (IFFT) block. At reception, the inverse transforms are applied. The structure of the transmitter and the receiver is shown in Figure 36.

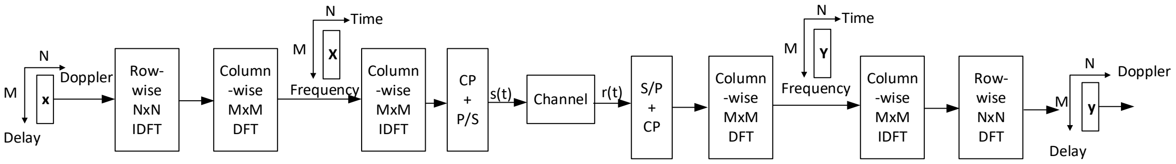

FIGURE 36: OTFS WITH CP TX AND RX BLOCK DIAGRAM

➲ OTFS with per-frame CP

A remarkable feature of this scheme is that a single CP block is shared by a bundle of multicarrier symbols [52]. This enhances the spectral efficiency and reduces the required transmission power. However, the complexity of detection is generally lower in the OTFS with per-symbol CP than in OTFS with per-frame CP [53]-[57]. This variant of OTFS transmits with lower overhead than OFDM.

➲ Pulse-shaped OTFS

Utilizing the perfect pulse shaping waveform in OTFS that adheres to the orthogonality requirement in both time and frequency domains is practically unattainable [49][51][52]. The conventional approach within OTFS systems resorts to employing a rectangular pulse shape spanning a single symbol duration [49][51][52]. Nevertheless, the rectangular pulse exhibits an exceedingly pronounced OOB emission, consequently leading to a substantial rise in adjacent channel interference. It is worth mentioning that the ISFFT precoder prevents the application of the conventional OOB suppression schemes adopted in OFDM as for example spectral guarding or frequency domain precoding based OOB emission mitigation techniques will break the inherent connection between the DD and TF domain signals [58].

Within the context of [52], the authors advocate for the adoption of a frequency-localized pulse as recommended in [59] spanning a single symbol duration. Regrettably, the utilization of this extended pulse gives rise to non-orthogonality, thus causing a deterioration in the performance of the BER. In their work presented in [60], the researchers put forth Gaussian and raised cosine pulse shaping alternatives. Nevertheless, it is essential to note that these alternatives are accompanied by a significant upsurge in the PAPR. Authors in [61] proposed a circular Dirichlet pulse shaped OTFS which reduces the OOB emission as well as PAPR over rectangular pulse shaped OTFS.

OTFS detection and channel estimation

Single-tap equalizer, similar to the commonly employed detector in OFDM, can also be adopted for OTFS in very slow time-varying channels. Although that this single-tap equalizer has very low complexity, it works only for static or very low mobility wireless channels which is not the case for NTN as the Doppler spread caused by high mobility introduces ICI which degrades the performance [53]. Linear Minimum Mean Square Error (LMMSE) detector for OTFS can offer good performance in both static and high mobility channels. Nevertheless, it comes with the trade-off of increased complexity. When M and N are in order of 100's, the complexity of LMMSE receiver becomes extraordinarily large and hence, low complexity design of LMMSE receiver for OTFS has been presented in [54]. Message Passing (MP) detection presents a more favorable trade-off, delivering superior performance compared to LMMSE detection with significantly reduced complexity. This method can be applied to various OTFS variants, as discussed in [50] [62]. Another attractive option is Maximum-Ratio

Combining (MRC) detection, offering performance on par with MP detection but at a considerably lower complexity level [63]. Comprehensive analyses and strategies for expediting detector convergence can be explored in [64][65]. Furthermore, additional equalization techniques have been explored in [55][56][66] while iterative detection methods are discussed in [56][67][68]. For a comprehensive overview of low-complexity detectors for OTFS, refer to the in-depth survey available in [69].

Regarding channel estimation, embedded pilot-based channel estimation techniques for OTFS are put forth in [70]-[72] for both the delay-Doppler and delay-time domains. However, a noteworthy challenge associated with these methods is the substantial PAPR, attributed to the high pilot power and the guard zeros enveloping it. Superimposed pilots- based channel estimation techniques were introduced in [73][74]. Nevertheless, these approaches entail more intricate channel estimation and data detection processes due to potential interference between the data and pilot signals, and they are susceptible to PAPR performance degradation stemming from the high power of the superimposed pilots. Preamble-based pilots are also deployed for channel estimation in OTFS [75][76]. The main issue with these techniques is that it suffers from channel ageing issue. Novel embedded pilot structure with significantly reduced PAPR has been proposed in [77]. Throughout the literature, one can explore a wide array of channel estimation methods tailored for OTFS systems with massive number of antennas [78][79], and scenarios involving multiple users [76].

OTFS in NTN

Table 13 reports the main outcomes of the state of the art of OTFS in NTN. As can be seen from the table, the OTFS is mainly addressed in downlink communication. From this SoA, it can be inferred that, it generally provides better communication rate mainly because of the presence of a per block guard interval rather than a per symbol cyclic prefix as in OFDM. This of course comes at the cost of a more complex channel estimation scheme, working on large block-wise operations. Moreover, OTFS is insensitive to the magnitude of the Doppler shifts, while the performance of OFDM degrades significantly even under small-to-moderate Doppler values if the number of subcarriers increases. Therefore, OTFS is a good candidate for high mobility systems in rural environments or aerial environments, where Doppler shifts may be large, and the propagation channel contains typically the line-of-sight and a few other reflection components, and it is therefore sparse in the Doppler-delay domain.

TABLE 13: SOA OF OTFS IN NTN FOR THE DOWNLINK SCENARIO

Topic	Reference	Metric	Comments
Satellite diversity	[80]	Pragmatic capacity	OTFS provides significant performance improvements than OFDM with two satellites
	[81]	Spectral efficiency and Uncoded BER	OTFS outperforms OFDM in both the metrics with 2 satellites
Resiliency to high Doppler shift	[82]	Uncoded BER	OTFS outperforms OFDM and satellite diversity is exploited
	[83]	Uncoded BER	BER performance only slightly deteriorates toward higher SNRs when increasing the relative speeds from the subsonic regime M=0.5 (617.4 km/h) to the supersonic regime M=4 (4939.2 km/h)
	[84]	MSE	The MSE of the CFO obtained through the proposed method estimation tends to decline as the MSE energy increases

Channel estimation	[85]	Uncoded BER	• Joint channel estimation and data detection algorithm • Type of waveforms: bi-orthogonal waveforms and rectangular waveforms
	[86]	Uncoded BER	1) Type of waveform: Zero Prefix-OTFS 2) LMMSE detection performs better than MRC algorithm in case of QPSK modulation across all the channel models 3) MCR is better with higher value of SNR

3.3.2 Non OFDM-based waveforms

This section is dedicated to the State of the Art of non-OFDM based waveforms.

3.3.2.1 Single carrier constant-envelope

Minimum Shift Keying (MSK) is an example of single carrier constant envelope modulation, and it has been adopted by IEEE 802.15.4. The modulation uses half cycle sine wave instead of rectangular pulse wave. MSK is a special case of Continuous-Phase Frequency Shift Keying (CPFSK) which is a special case of a general class of modulation schemes known as Continuous-Phase Modulation (CPM). As CPM is a non-linear modulation, by extension MSK is a non-linear modulation as well. It can also be generated from Offset Quadrature Phase Shift Keying (OQPSK), which is a special case of Phase Shift Keying (PSK), thus making it a linear modulation scheme.

One variant of MSK is Gaussian Minimum Shift Keying (GMSK) which has been adopted by GSM and Bluetooth. Compared to MSK, GMSK has better interference rejection against adjacent channels thanks to various Bandwidth Time (BT) factors, as well as good side lobe suppression, achieving better spectral efficiency compared to MSK and less demodulator complexity.

The constant envelope of both of MSK and GMSK make them resilient to non-linear distortion. The signal can be amplified without distortion by a non-linear amplifier operating near the saturation point, reducing cost and achieving more efficiency compared to a linear amplifier. The advantages of these constant envelope waveforms also include 0dB PAPR and the possibility of asynchronous multiplexing.

However, both GMSK and MSK have lower spectral efficiency compared to other existing waveforms. MSK has been shown to be less resistant to ICI than OFDM, with Spectral Separation Coefficient (SSC) almost 10 dB higher than those of OFDM signals [87] for a 20MHz pre-filtering bandwidth. The study in [87] compared OFDM and MSK with several currently used modulations in GNSS such as BPSK, BOC and MBOD signal. The worst performance in average multipath-caused bias in the realistic channel model was caused by MSK. The phase continuity between bit transitions makes the Power Spectral Density (PSD) of MSK compact, falling off rapidly with increased frequency. The main lobe of MSK is larger than BPSK and OFDM, which means that most of the energy of MSK modulation is concentrated within the main lobe, while the side lobes magnitude decreases rapidly. Therefore, it is less vulnerable to ACI caused by other closely spaced signal sources in the frequency domain.

The conclusion in [87] was that the OFDM multipath error envelope was smaller than that of MSK for signals that require pre-filtering bandwidths larger than 2MHz, while MSK modulation was better suited for pre-filtering bandwidth below 2 MHz where it exhibits the largest Gabor bandwidth.

3.3.2.2 Single-carrier Non-Constant envelope

- SC-QAM (Single Carrier-Quadrature Amplitude Modulation) has been adopted by EV-DO (Evolution-Data Optimized) and UMTS. Its main advantages are high spectral efficiency, low PAPR at low spectral efficiency and simple waveform synthesis. It is possible to use asynchronous multiplexing. However, SC-QAM has limited flexibility in spectral assignment and the support for MIMO is non-trivial [88]
- SC-CP-FDE (SC-Frequency Domain Equalization), a variant of SC-QAM but with the addition of CP, has been adopted by IEEE 802.11ad. It is equivalent to SC-QAM with CP, however the problem with SC-QAM with TDE (Time Domain Equalization) is that it shows limited performance when the channel is subject to strong frequency-selective fading, even with a receiver of high complexity. FDE can be used instead to improve the transmission reliability. One way to do this is to insert CP into the waveform [89][90]. The signal thus be reliably demodulated at the receiver with relatively low complexity. The reception is more complicated in SC-FDE than in OFDM due to the presence of an additional IDFT after the two FFTs. It also has a lower PAPR than OFDM. It is possible to do FDE processing. However, SC-FDE suffers from the same drawbacks as SC-QAM and has ACLR similar to DFT-s-OFDM.
- SC-ZP-FDE**,** by replacing CP with ZP to remove interblock interference, blocked SC-ZP-FDE signals can be easily handled by FDE [91] [92].
- SC-FDMA (Single Carrier Frequency Division Multiple Access) SC-FDMA is used in the uplink mode of 3GPP-LTE to solve the problem of the high PAPR in CP-OFDM, which negatively affects transmit power efficiency and the power amplifier. SC-FDMA has also been adopted as one of the waveforms for the satellite profile of DVB-NGH (Next Generation Handheld). It is based on classic CP-OFDM but differs from it with its precoding stage. The precoding stage at the transmitter consists of a DFT applied before the IFFT stage. At the receiver, the reverse operation is applied with the use of an IDFT after the FFT.

  The study in [93] assessed the performance of SC-FDMA in the context of Geostationary (GEO) satellites in Ku/Ka band in the satellite return link. The comparison with SC-TDM (DVB-S2X) and TDMA (DVB-RCS2) at the physical layer showed that for comparable spectral and power efficiency, the use of SC-FDMA allows for decreased receiver complexity (especially for the equalizer) with its per-subcarrier equalization in the frequency domain. SC-FDMA allows for multiplexing with OFDMA. However, it doesn't support asynchronous multiplexing. It suffers from link budget loss for large number of simultaneous users.

3.3.2.3 FMT (Filtered MultiTone)

FMT is a multicarrier modulation technique that has been specifically developed for DSL applications **Error! Reference source not found.**. FMT modulation mitigates interference due t o echo and near-end crosstalk signals, and increases the system throughput and reach.

In FMT, a conventional method of frequency division multiplexing is used, i.e. the subcarrier bands are juxtaposed. Each band can be seen as a traditional single carrier modulation which respects the Nyquist criteria. It is well known that the optimal repartition (in terms of Signal to Noise Ratio at the demodulation input) of the Nyquist filter is a square-root Nyquist filter at both emission and reception sides.

3.4 OTHER STUDIES

This section provides an insight on the waveform related topics addressed by other funded projects.

Within the Phase 1 projects of the SNS-JU Stream B, two other projects, HEXA-X-II and ETHER, focus on NTN and explore waveforms applicable to both terrestrial and non-terrestrial systems. Additionally, numerous H2020-funded projects have evaluated waveforms, which are different from CP-OFDM and DFT-s-OFDM, for NTN.

3.4.1 HEXA-X-II

Regarding HEXA-X-II [96], one of the project goals is to study the feasibility of the mainstream 6G waveforms – primarily designed for lower frequency bands – for sub-THz frequencies. The analysis focuses on the suitability of the waveforms for sub-THz frequencies, considering requirements such as increased energy efficiency, Phase Noise (PN) tolerance, and scalability over high bandwidths and different frequency band combinations. The candidate waveforms include OFDM and SC-based waveforms, i.e., DFT-s-OFDM and known-tail discrete Fourier transform spread orthogonal frequency division multiplexing (KT-DFT-s-OFDM).
The key KPIs considered are the waveform’s energy and spectral efficiency, PN tolerance, and scalability over different frequency bands. Network densification is another aspect affecting sub-THz deployment, and this will be considered as a KPI while studying the candidate waveforms for the sub-THz.
In order to be resistant to PN and doppler shift, a design combining polar constellations with a multicarrier waveform, such CP-OFDM, is under investigation. The proposed constellation is related to energy-optimized services use case, mainly for implementing low-cost electronics and precise oscillators. The goal is to avoid increasing the cost of electronics and then develop algorithm to compensate this lack.
Furthermore, OFDM and DFT-s-OFDM are considered as a strong candidate for Joint communication and sensing (JCAS). This aspect is also investigated in the project.

It is worth mentioning that this project is ongoing, and the results of the investigations have yet to be fully reported.

3.4.2 ETHER

One of the targets of ETHER (sElf-evolving terrestrial/non-Terrestrial Hybrid nEtwoRks) project is to design a uniform waveform for high channel impairment robustness to provide context-aware waveform adaptation. For different communication scenarios, a Machine Learning (ML)-based decision on whether to apply either OFDM or OTFS multiplexing scheme will be used, including trade-offs between different factors, such as saturation of power amplifiers, sufficient Signal to Noise Ratio (SNR), Doppler shift sensitivity, or channel estimation complexity.

3.4.3 HEXA-X

Hexa-X [97][98] is one of the 5G-PPP projects under the EU Horizon 2020 framework and it is a flagship project that develops a Beyond 5G (B5G)/6G vision. In particular, the project aimed to create a vision for 6G technology and define its key components, including potential use cases, architectural concepts, and technological requirements. Research also focused on analysis of 6G waveforms, particularly identifying main waveform design KPIs and study of design of hardware-aware waveforms. While the study of the waveform was not focusing an NTN scenario, insight of the impact of HW impairments on the performance of single-carrier frequency domain equalization (SC-FDE) and DFT-s-OFDM was presented.

3.4.4 BATS

Within the BATS (Broadband Access via Integrated Terrestrial & Satellite Systems) project a brief study of terrestrial mobile waveforms in the return link of GEO satellites was conducted, as documented in [99]. The following three waveforms were considered:

- Orthogonal Frequency Division Multiple Access (OFDMA) for its high spectral efficiency.
- SC-FDMA, for its power efficiency gain of more than 2 dB as compared to state-of-the-art TDMA and robustness to satellite channel in terms of nonlinearity and synchronization.
- FBMC for the following reasons:
  - ability to cope with asynchronous access;
  - flexible spectrum allocation;
  - improved power and spectral efficiency when carrier frequency offset is added, and guard subcarriers inserted
  - Spectral efficiency comparable to TDMA

3.4.5 5G-ALLSTAR

The 5G-ALLSTAR (5G AgiLe and fLexible integration of SaTellite And cellular) project [100][101] aims at proving the viability of the two following System-level concepts:

- Possibility of NTNs seamless integration into 5G TNs. In this framework, direct access using the 5G NR waveform instead of a standard Satellite-optimized waveform (i.e. DVB S2/RCS) and in the same frequency bands as the ones allocated to the TNs is performed over Service Links (Forward and Return).
- NTNs complementing TNs to bring an improvement to Service Qualities and/or User Experience Quality, such as better data rates, or better availabilities.

BF-OFDM was investigated for the terrestrial link [102]. The main findings and properties of the waveform under examination can be summarized as follows:

- (BF)-OFDM is fully compatible with a 5G NR receiver.
- high out-of-band rejection levels facilitate efficient spectrum sharing.
- It can be configured in real-time per sub-band, supporting multiservice scenarios.
- Ability to dynamically set sub-bands to zero allows the creation of spectrum holes.
- Exhibition of excellent spectral localization with enhanced side-lobe rejection, similar to Filtered OFDM or Pulse Shaped OFDM.
- Better performance than CP-OFDM in frequency-selective channel environments.
- Scalability, offering dynamic network capabilities based on demand.

In the project, a satellite testbed was used to validate 5G NR satellite radio access. Features were developed to adapt the NR procedures to long delay scenarios, such as GEO satellite channels.

3.4.6 5G CHAMPION

5G CHAMPION (Communication with a Heterogeneous, Agile Mobile network in the Pyunchang wInter Olympic competioN) [103] proposed a direct communication between the devices and the satellites. In terms of interface, the Narrow-Band IoT with a new proposed waveform named as coplanar turbo-FSK has been considered and analyzed.

Indeed, NB-IoT exhibits good performance in terms of capacity but can lead to relatively high peak-to average power ratio when based multi-carriers OFDMA or SC-FDMA. Therefore, it has also been proposed to consider FSK modulation with a simple accumulator code, called coplanar turbo-FSK. This waveform can be used on top of OFDM signals, and exhibits a constant envelope, making it therefore a good candidate for uplink communications. The accumulator code allows for a better use of redundancy than in pure repetition scheme but necessitates soft FSK detector to determine the probabilities of each codeword. Block-filtered OFDM instead of OFDM is in fact considered as it allows for flexible and efficient use of non-contiguous spectrum targeting heterogeneous mobile network deployment scenarios. Through simulations, results have shown that the proposed turbo-FSK exhibit slightly higher performance to the NB-IoT solution in terms of capacity in an AWGN or frequency selective channel, while showing better performance in terms of envelope variations compared to multi-carriers OFDMA and SC-FDMA waveform.

For low throughput scenarios, Turbo-FSK is the best compromise due to its constant envelope property, which sets it apart from OFDM and SC-FDMA. SC-FDMA performs similarly to OFDM in AWGN and mobility scenarios because of the high redundancy in this context, with fewer envelope variations. However, the Zero Forcing (ZF) equalizer used in SC-FDMA under static ETU conditions reduces its performance, and the necessary precoding-FFT algorithm increases complexity at the receiver. For high throughput scenarios, OFDM and SC-FDMA exhibit the same performance, achieved by merely reducing the repetition factor. Turbo-FSK, when considered for higher throughput, undergoes modifications of the scheme that significantly impact performance and complexity, highlighting differences in the orthogonal alphabet choice. For low throughput and energy-constrained communication, Turbo-FSK is recommended, whereas SC-FDMA is preferred for higher throughput at the cost of lower energy efficiency due to the Transmitter PA requiring a 4 to 6 dB back-off. Consequently, a new mode based on Turbo-FSK, with constant envelope and PA optimization, can bridge the gap, facilitating seamless adaptation to both satellite and terrestrial networks for cellular IoT.

3.4.7 SaT5G

SaT5G (Satellite and Terrestrial Network for 5G) proposed a study of 5G NR applied to satellite. The work was concentrated on identifying challenging points in the process of initial synchronization and random access. Simulations results showed that modifications are needed in the uplink random access process and timing advance to cope with the satellite delay and Doppler, and the large cells created by satellite.

3.5 CONCLUSION ON THE SOA

In this third section of the deliverable, we provided a comprehensive state of the art of the waveforms/air interface, and we mainly subdivided them in two categories: i) standardized and non-standardized waveforms/air interface, and ii) multi-carriers and single-carrier waveforms. We then report the main outcomes of the other projects.

On the one hand, standardized waveforms are easily to be adopted thanks to the established ecosystem in terms of protocol and technologies which lead to interoperability between different manufacturers. Moreover, standardized waveforms ensure backward compatibility with the previous generations. On the other hand, the NR air interface, in downlink shows reduced performance when compared with state-of-the-art satellite air interface, i.e., DVB-

S2X. These lead to the investigation and the assessment of other variants of OFDM-based waveforms to cope with the NTN channel.

Regarding the second category, the main difference between single carrier-type waveforms and OFDM-based multi-carrier waveform lies in the symbol sequencing domain: for single carrier waveforms, symbol sequencing is done in the time domain whereas it is done in the frequency domain for OFDM-based waveforms.

Single carrier waveforms have typically lower PAPR leading to high PA efficiency and extended battery life. Equalizer is needed to achieve high spectral efficiency in the presence of multipath.

Advantages of OFDM based waveforms over conventional single carrier approaches include improved network capacity, bandwidth, and reliability; improved spectrum efficiency and mitigation of multipath propagation interference that causes data errors and loss of signal. Another benefit of OFDM based waveforms is that equalization on a narrow band subcarrier needs less complexity than broadband non-OFDM schemes. Moreover, non-OFDM single carrier scheme operating at the same rate of an OFDM based waveform with guard interval protection would more easily encounter ISI. For the same data rate, the single carrier would have to carry more symbols than OFDM-based waveforms, resulting in reduced distance for the reflected signal to travel. It thus becomes easier for one symbol to overlap a later symbol resulting in ISI.

On the other hand, multi-carrier waveforms are sensitive to carrier frequency offset, which requires sophisticated synchronization mechanisms to guarantee the orthogonality between subcarriers.

Regarding the OTFS, it presents three main advantages compared to the OFDM, i) the non-sensitivity to Doppler shifts in high mobility scenarios; ii) a reduced CP, which can lead to improved throughput in case of LoS communications, and iii) separability of the channel paths in the delay-Doppler domain, which supports full diversity in time frequency domain leading to improved link reliability. This last point allows to leverage the multi-satellite diversity to ensure uniform throughput and enhance system reliability against unexpected obstructions. However, the complexity of OTFS detection algorithms is one of the major challenges when it comes to practical implementation on hardware platforms. The two-step conversion from Delay-Doppler domain to time-frequency domain using the ISFFT results in a high-dimensional equivalent Delay-Doppler channel which becomes even larger in MIMO-OTFS systems. Current computational complexity of OTFS detection algorithms is therefore much higher than in case of OFDM. In addition, OTFS with rectangular pulses induce OOB emissions causing adjacent channel interference which in turn degrades system performance.

Based on these observations and the preliminary analyses/outcomes of the other projects, the following waveforms have been retained for simulations and assessment in the 6G-NTN identified scenarios:

- CP-OFDM
- WOLA-OFDM
- DFT-s-OFDM
- F-OFDM
- BF-OFDM
- UFMC
- OTFS

To be specific, several aspects were considered to determine these main waveform candidates, namely:

- Compatibility with current specifications: frame structure, numerology, and RB-level bandwidth allocation.
- Leveraged power amplifier efficiency (i.e., as related to PAPR performance)
- Propensity to generate in-band distortion and out-of-band emissions (i.e., as related to PAPR performance and frequency containment).
- Leveraged latency either via symbol-level or block-level operation.

As such, waveforms relying on symbol-level operation were prioritized, except for OTFS due to its robustness at high-speed scenarios, a particularly relevant consideration for NTN. Consequently, block-based GFDM was discarded as its benefits may be leveraged via symbol-level based OFDM variants.

With regards to the candidate OFDM-based waveform variants, elementary variations were considered to analyze their added value in isolation. Thus, although WOLA and DFT-s-OFDM may be fused to combine their low OOB emission and PAPR advantages, respectively, the current deliverable focuses on their separate gains.

As a reference, F-OFDM, requiring few modifications to CP-OFDM, is considered in this deliverable despite its inherent limitation over non-contiguous bandwidth allocations.

Finally, the BF-OFDM and UFMC OFDM-variants are adopted in this study due to their RB-level granularity for bandwidth allocation and spectrum fragmentation, all while creating low interference to adjacent channels. On the contrary, FBMC is discarded because, first, its sub-carrier level frequency allocation comes at the expense of pulses that extend multiple symbols and, second, the required OQAM results in an increase in complexity and a reduction of flexibility.

4 CHANNEL MODEL AND IMPAIRMENTS

As a matter of fact, waveforms effectiveness for satellite communications also depends on the properties of the propagation channel, i.e., on the impairments experienced by the propagating signals as they travel over the earth-space link. Existing studies and recommendations mainly concern the S and the Ka bands [104], and cannot be automatically extended to different bands as electromagnetic propagation is known to be frequency dependent. This section is therefore devoted to some discussion about wireless propagation in non-terrestrial networks in the new frequency bands mostly addressed in the project (i.e., C, Q and V bands).

4.1 LARGE SCALE PROPAGATION IN NTN

According to [104], large scale channel characterization in wireless networks refers to the evaluation of the attenuation experienced by wireless signals over the travelled propagation path. In [104], the signal attenuation is computed as:

$$PL[dB] = PL_b + PL_a + PL_s + PL_e$$

where:

- PL_b: “basic” path loss [dB];
- PL_a: attenuation due atmospheric effect [dB]. It mainly accounts for absorption from gases and rain.
- PL_s: attenuation due to scintillation effects, either in the troposphere or in the ionosphere [dB].
- PL_e: building entry loss [dB].

4.1.1 Basic path loss

The basic path loss id computed as follow:

$$PL_b[dB] = FSPL + SF + CL$$

being:

- *FSPL - free space loss*: from the Friis equation:

$$FSPL(d, f) = 32.45 + 20log_{10}(f_{GHz}) + 20log_{10}(d_m)$$

- *SF - shadow fading loss*: it usually accounts for extra-loss due to the possible obstruction of the wireless link coming from large obstacles like buildings or hills. Although satellite communications are expected to occur in LoS most of the time, NLoS may be nevertheless experienced, especially at lower elevation angles and/or for hand-held reception at ground level. Shadowing loss is usually modelled as a normal random variable $N(0, \sigma_{SH})$, i.e., the value of σ_{SH} must be provided to fully characterize the shadow loss.
- *CL: clutter loss*: it basically includes further extra-loss related to the presence of smaller items close to the ground equipment and not included in the shadowing loss factor.

Free space attenuation can be of course easily computed at any target frequency, and the FSPL equation clearly shows that heavier loss must be expected at greater frequency. On the other hand, similar, closed form formulas are instead not simply available for SF and CL, which are just provided as tabular data in [104] for S and ka bands only. Nevertheless, both SF and CL are likely to be heavier at greater frequency, at least according to what claimed and shown in [105] and in [104], respectively. Therefore, shadowing and clutter losses in Q and V band should be greater than what reported in [104] for Ka band. With reference to C band, it is so close to S band that the same values might be approximately considered for the two bands in lack of any further specific analysis.

4.1.2 Atmospheric losses

These losses usually refer to the attenuation introduced by the presence of oxygen, water vapor (atmospheric absorption) and rain. Other effects can be considered (e.g. through cloud attenuation), but they usually represent minor contributions. The impact of the atmosphere on wireless communications is known to be negligible up to a threshold frequency, often set equal to 10 GHz [106][107]. Atmospheric effects are therefore expected to mostly impair satellite communications in the Q and V bands, with rather limited effect in the C band.

➲ Atmospheric Absorption: the Earth-to-space additional loss accounting for energy absorption from atmospheric gases like oxygen and water vapour can be easily computed as [104]:

$$PL_G[dB] = \frac{PL_{zenith}(f)}{sin\ (\vartheta)}$$

being θ the elevation angle and PL_{zenith} the attenuation experienced by a vertical link (i.e., θ=90°).

The zenith loss is frequency sensitive and can be estimated by the following Figure 37.

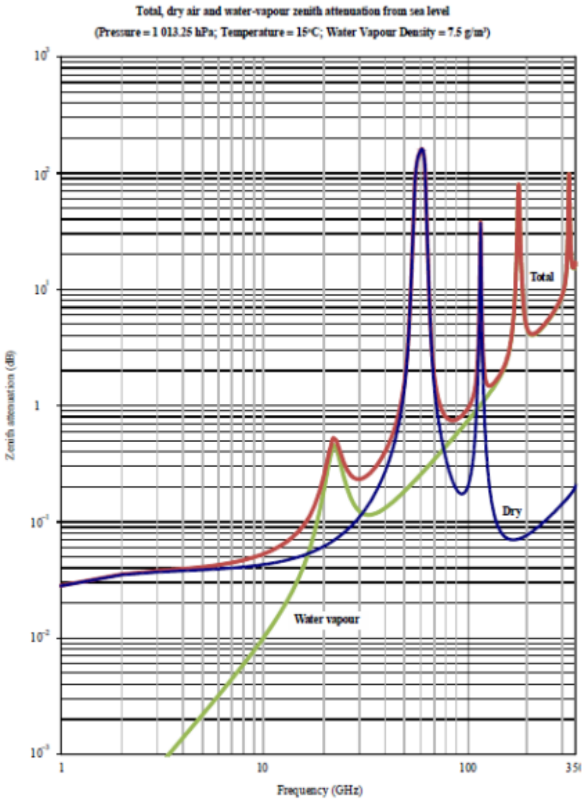

FIGURE 37: ZENITH ATTENUATION VS. FREQUENCY THROUGH THE WHOLE ATMOSPHERE (REF. [96])

The atmospheric absorption losses are then represented in Figure 38 in different frequency bands and for different elevation. Clearly, absorption phenomena are negligible in C band regardless of the elevation[2], and are in general heavier at larger frequency. Interestingly, absorption is slightly greater in the Ka band compared to the Q band, and this is explained by the presence of an absorption peak around 22 GHz (Figure 38).

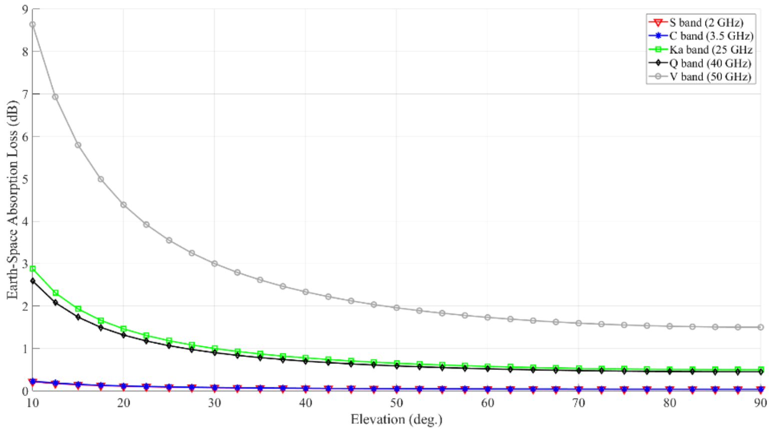

FIGURE 38: ABSORPTION LOSS IN DIFFERENT FREQUENCY BANDS

It is worth pointing out that the values reported in Figure 38 estimate the attenuation experienced by an electromagnetic wave propagating through the

---

[2] In general, they are often claimed negligible at any frequency lower than 10 GHz

whole atmosphere, i.e. they refer to the communication between an earth station and a satellite (either GEO or LEO). In case the flying station is a drone or a high-altitude platform station, Figure 38 is unreliable as the atmospheric loss are then likely to be negligible irrespective of both the elevation and the communication band.

- Rain Loss: it is usually computed as:

$$PL_R[dB] = \gamma_R \cdot L_E$$

being γ_R the rain specific loss [dB/km] and L_E an effective[3] path length. Details on the procedure suggested by ITU-R for the evaluation of γ_R and L_E can be found in [109]. Rain losses in Ka, Q and V bands are for instance compared in Figure 39, where PL_R is plotted against elevation for different polarization and for a target outage probability p=0.01. It can be noted that the rain loss in Q band is roughly 10dB heavier than its value in the Ka band, almost regardless of the elevation angle. Similarly to atmospheric absorption, rain losses are commonly neglected at frequency lower than 10 GHz, i.e. their impact on satellite communications in C band is expected to be very light.

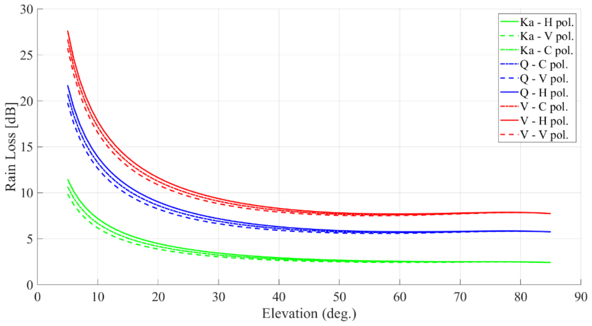

FIGURE 39: RAIN LOSS ACCORDING TO ITU-R MODEL, COMPARISON IN DIFFERENT FREQUENCY BANDS

4.1.3 Scintillation losses

Scintillation includes unexpected, fast fluctuations of the received signal amplitude and phase that may occur in the ionosphere and/or in the troposphere. Although ionospheric scintillation has been observed up to 10 GHz, it is commonly neglected above 6 GHz. By contrast, tropospheric scintillation becomes increasingly important at larger frequency, and especially above 10 GHz [104]. Therefore, the impact of ionospheric scintillation must be investigated in the C band only, as it is not expected in the Q and V bands. Conversely, the assessment of tropospheric scintillation effects can be limited to Q and V bands, with no attention paid to C band.

- Tropospheric scintillation: it can be taken into account by means of an additional loss term to be included in the link budget equation:

$$PL_{TS}[dB] = a(p) \cdot \sigma(f_{GHz}, \vartheta_{el}, N_{wet})$$

---

[3] To take into account that rain in general is not present all over the earth-space link.

being p the target outage probability, f_{GHz} the communication frequency, θ the elevation angle and N_{wet} a coefficient related to the (median) radio refractivity, i.e. to the tropospheric conditions. Details can be found in [109]. Some results returned by the model are presented in the following.

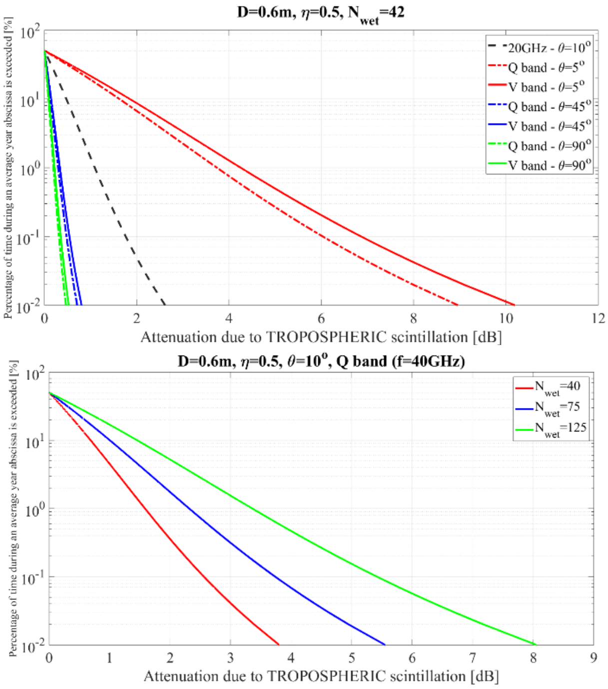

FIGURE 40: TROPOSPHERIC SCINTILLATION LOSS. ACCORDING TO [97], D AND η REPRESENT THE GROUND ANTENNA DIAMETER AND ITS EFFICIENCY

Based on Figure 40, the following general trend can be highlighted:

- Tropospheric scintillation loss increases at larger frequency
- Tropospheric scintillation loss decreases as the elevation of the satellite link gets larger, to the extent that in Q and V bands it is likely to be important just at quite low elevation (around 5°)
- Tropospheric scintillation loss seems quite affected by radio refractivity through the N_{wet} coefficient.

In the worst case (i.e., θ=5°, N_{wet}=150), $PL_{TS,dB}$ at 50GHz can amount to 10dB.

With reference to ionospheric scintillation, a baseline model for the evaluation of the corresponding loss below 6 GHz and low latitude is based on the peak-to-peak fluctuation (P_{fluc}) level at 99% of the P3 curve in Figure 41 [104], which is roughly equal to 1.1. Then, signal loss due to ionospheric scintillation can be easily computed as $PL_{IS}[dB] = {P_{fluc}}/{\sqrt{2}}$. Since P_{fluc} is also known to scale in frequency as $(1/f)^{\upsilon}$, $\upsilon \in [1,2]$ [104] [110], the ionospheric scintillation loss at any frequency lower than 6 GHz and at low latitude can be finally computed as [104], [110]:

$$PL_{IS}[dB] = \frac{P_{fluc}(4\ GHz)}{\sqrt{2}} \left(\frac{4}{f_{GHz}}\right)^{1.5} \approx \frac{1.1}{\sqrt{2}} \left(\frac{4}{f_{GHz}}\right)^{1.5}$$

Accordingly, the scintillation loss corresponding to f = 3.5GHz (C band) is equal to just 0.95 dB.

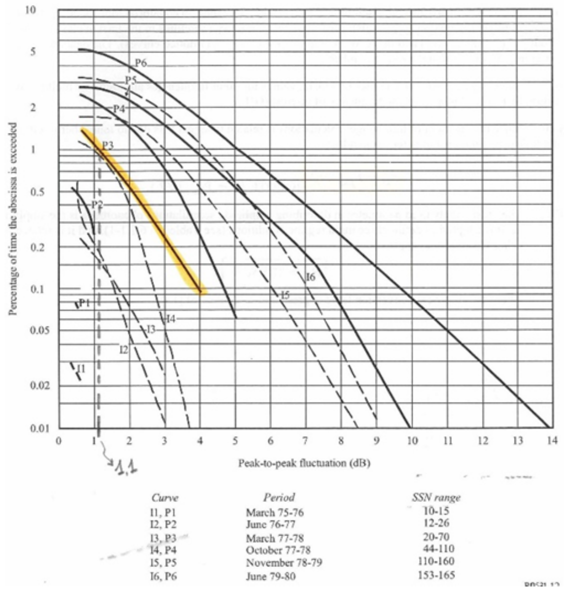

Curve	Period	SSN range
I1, P1	March 75-76	10-15
I2, P2	June 76-77	12-26
I3, P3	March 77-78	20-70
I4, P4	October 77-78	44-110
I5, P5	November 78-79	110-160
I6, P6	June 79-80	153-165

FIGURE 41: CDFS OF PEAK-TO-PEAK FLUCTUATIONS AT 20O ELEVATION (P CURVES) AND 30O ELEVATION (I CURVES)

4.1.4 Building Entry Loss (BEL)

The simple model included in [111] may represent a starting reference for the computation of the BEL at the frequencies of interest:

$$PL_e = 5 - 10log_{10}\left(p_g 10^{-0.1 \cdot L_{glass}} + p_c 10^{-0.1 \cdot L_{concrete}}\right)$$

where:

- p_g and p_c represent the percentage of glass and concrete on the façade of the illuminated wall (p_g+p_c=1)
- $L_{glass} = \begin{cases} 2 + 0.2 \cdot f, & standard\ glass \\ 23 + 0.3 \cdot f, & infrared\ reflecting\ (IRR) glass \end{cases}$
- $L_{concrete}$= 5 + 4·f

Building entry loss is plotted against frequency in Figure 42 for p_g=0.3 (higher loss case) and p_g=0.7 (lower loss case). The difference between C band and Q/V bands amounts to roughly 10 dB.

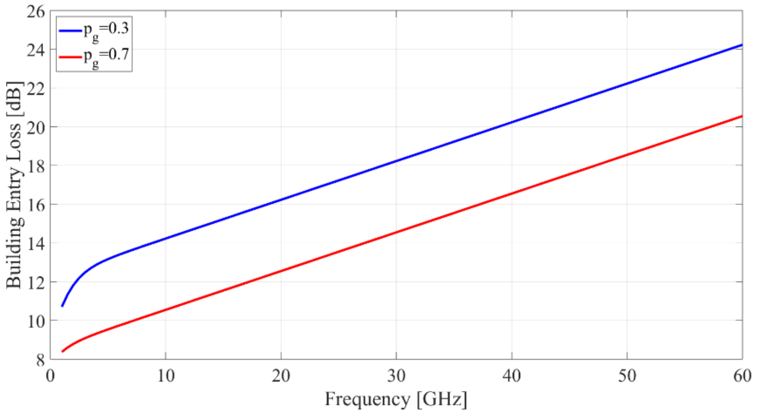

FIGURE 42: BUILDING ENTRY LOSS MODEL

It is worth pointing out that standard glass is assumed in Figure 42, that means the diffusion of IRR glass (e.g., to contrast climate change) may result in a harsh problem for indoor wireless coverage in NTN.

Since one of the target scenarios of the 6G-NTN project is light indoor scenario, where users are inside the car, we also provided a state of the art on the loss due to the outdoor to in vehicle penetration loss [112], [113], [114]. Table 14, Table 15, and Table 16 report the outcome of the measurements.

TABLE 14: UWB CAR ATTENUATION MEASUREMENTS [112]

Frequency range	**BMW 2 (with metal)**	**BMW 1(with metalized window)**	**BMW (w/o metal)**
3-6 GHz	13-16 dB	9-14 dB	7-8 dB
6-9 GHz	12-19 dB	9-14 dB	7-9 dB

TABLE 15: IN CAR MOBILE SIGNAL ATTENUATION MEASUREMENTS [113]

Frequency	**Dash**	**Console**	**Footwell**
2.6 GHz	5.2 dB	10 dB	13.6 dB

TABLE 16: IN CAR PENETRATION LOSS MEASUREMENTS [114]

Freq.	**TX illuminates the rear**				**TX illuminates the front**				**All**	
2.4 GHz	Ver Rx in		Hor RX in		Ver Rx in		Hor RX in			
	μ[dB]	σ[dB]	μ [dB]	σ[dB]	μ [dB]	σ [dB]	μ [dB]	σ [dB]	μ [dB]	σ [dB]
	13.79	4.09	19.86	4.21	5.25	4.06	15.88	4.24	13.68	6.76

4.2 MULTIPATH EFFECTS IN NTN

Although line of sight often occurs in satellite communications with greater probability compared to terrestrial networks, multipath propagation can nevertheless affect the quality of service. The reason is – at least – twofold: *(i)* the atmosphere is not spatially uniform, i.e., the signal spreading from the transmitter can reach the receiver through different curved trajectories over the air, resulting in final multipath effects; *(ii)* the ground footprint of the satellite transmission is in general very large, that means the transmitted signal can experience multiple interactions also at ground level, further contributing to multipath propagation. In the following, the attention is focused on multipath effects triggered by the propagation environment on the Earth surface. The intensity of multipath effects can be evaluated by means of several parameters. Rice factor and delay spread are in particular addressed here in.

- *Rice Factor (K)*: from a mathematical point of view, the Rice factor represents the coefficient of the Rice distribution. When referred to multipath propagation channels, it can be also regarded as the ratio between the intensity of signal arriving at the receiver through the dominant path[4] and the overall intensity coming from all the other paths (often referred to as scattering contribution).
- *Delay Spread (DS)*: it accounts for the channel dispersion properties in the delay domain. In presence of multipath, the same data of course reach the receiver through the different paths, but each path has its own delay. Therefore, the symbol energy of each individual transmitted symbol arrives at the receiver spread over a time period in general longer than the symbol time. The value of the delay spread is an estimate of such spreading.

Rice factor and delay spread have been estimated in three different propagation scenarios (dense urban, urban and suburban) for different elevation of the earth-space link and by means of Ray Tracing (RT) simulations. The main features of the RT tool are described in [115][116]. Besides standard electromagnetic interactions, like reflection and diffraction, the model also includes diffuse scattering according to the "Effective Roughness" (ER) approach [116]. The ER model aims at effectively accounting for the multipath contributions generated by the urban clutter, i.e., by those medium-size items usually present along the streets or on the building walls (like cars, road signs, street lamps, rain pipes, balconies, widows frames, etc.) but not included in any digital representation of the urban layout. Especially at greater elevation, where the wireless signal from the satellite basically drops down from roof level straight to the ground terminals, i.e. with limited or even without obstruction, the multipath pattern is expected to be mostly affected by scattering from the objects surrounding the ground stations.

For each map, twenty ground locations have been spread all over the area (Figure 43). Each location actually corresponds to a grid of 15 × 15 uniformly spaced receivers. Eight different elevation angles have been considered for the satellite, that was placed far away from the urban map with random azimuth angle. The main parameters describing the simulation environment are reported in Table 17.

TABLE 17: MAIN PARAMETERS OF THE SIMULATED ENVIRONMENTS

	Dense Urban	**Urban**	**Suburban**
Map size	0.3 km × 0.3 km	0.4 km × 0.4 km	0.5 km × 0.5 km
No. of buildings	199	187	183
Mean buildings height	17 m	12.6 m	7.8 m
Elevation range	10°, 20°, 30°, 40°, 50°, 60°, 70°, 80°		
Grid size	4.5 m		

---

[4] It basically consists of the cluster of signal contributions carrying the greatest power to the receiver

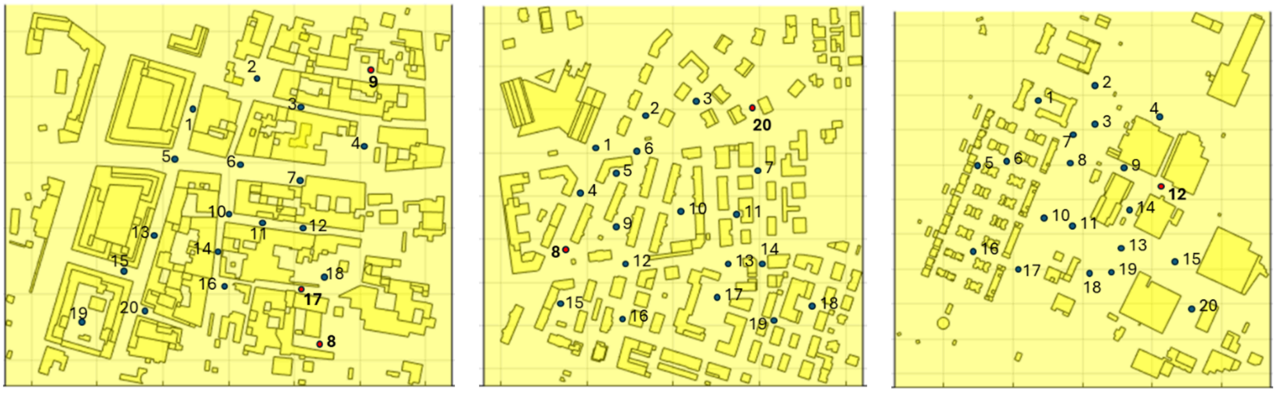

FIGURE 43: DIGITAL REPRESENTATION OF THE URBAN SCENARIOS: DENSE URBAN (LEFT), URBAN (CENTRE) AND SUBURBAN (RIGHT)

RT simulations have been then run between each position of the satellite and each ground terminal inside each grid, according to the simulation parameters outlined in Table 18. At this stage of the activity, isotropic antennas have been assumed at both link ends for the sake of simplicity.

If M different paths have been tracked between a [satellite, ground terminal] pair, and P_i, τ_l represent the intensity and the propagation delay of the i-th path, respectively, the DS value at the k-th ground location has been then computed as:

$$DS_k = \sqrt{\sum_{i=1}^{M} \frac{P_i}{P} \cdot (\tau_i - <\tau>)^2}$$

where P = $\sum_{i=1}^{M} P_i$ and $<\tau> = \sum_{i=1}^{M} P_i/P \cdot \tau_i$.

Assuming that signal fluctuations over each grid are due to fast fading effect only, fast fading samples have been collected by normalizing each received signal amplitude by the spatial signal average over the grid. Finally, a maximum likelihood estimating procedure has been set-up in order to compute the K value of the best Rice distribution that optimally fit the empirical distribution of the fast-fading samples returned by the RT simulations.

TABLE 18: MAJOR SIMULATION PARAMETERS

	C band (3.5 GHz)	**Q band (40 GHz)**	**V band (50 GHz)**
Building relative electrical permittivity (ε_R)	5	5.5	5.5
Building electrical conductivity (σ)	0.01	0.4	0.4
Scattering coefficient [101]	0.4	0.6	0.6
No. reflection alone	3		
No. diffraction alone	1		
No. scattering alone	1		
No. reflection with diffraction	1		

No. reflection with scattering	1
Antennas radiation pattern	isotropic

Results are shown in Figure 44 and Figure 45, where the Rice factor K and the average of $\log_{10}(DS_k)$ over the ground locations are respectively plotted against the satellite elevation for the three considered scenarios.

Rice factor exhibits an increasing trend with elevation regardless of the propagation environment, whereas it is the opposite for the delay spread. This looks quite physically sounded, as larger elevation always means greater LoS probability, i.e., the presence of a powerful, short-delayed received signal contribution, that exactly contributes to increase the Rice factor and to reduce the delay spread.

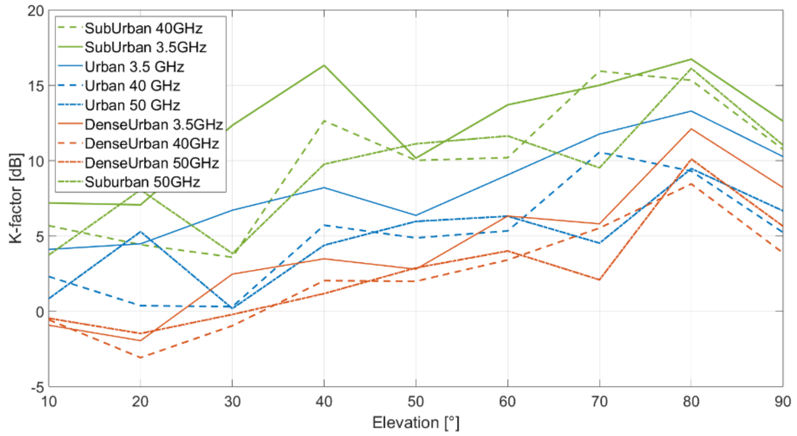

FIGURE 44: RICE FACTOR VS. SATELLITE ELEVATION

Figure 44 shows that Rice factor is also related to the urban density, as greater building density corresponds to lower K values. In fact, a greater building density often entails a greater multipath richness, that means a greater received overall scattered power and this can bring a lower Rice factor. With reference to delay spread, things are a little bit more complicated. At small elevations, it’s harder to have multipath contributions coming from far, large scatterers, almost irrespective of the type of environment. At the same time, LoS occurrence can be not negligible in suburban areas, whereas it is likely to be zero in the dense urban case. This straight leads to delay spread in suburban scenarios lower than it is in dense urban contexts, with the urban case of course in the middle. As elevation increases, LoS probability approaches 1 for every urban layout, whereas long-delayed but still powerful echoes can show up in the suburban case more likely compared to (dense) urban. Therefore, suburban delay spread can result similar – or even larger – compared to the (dense) urban layouts.

Co-funded by the European Union

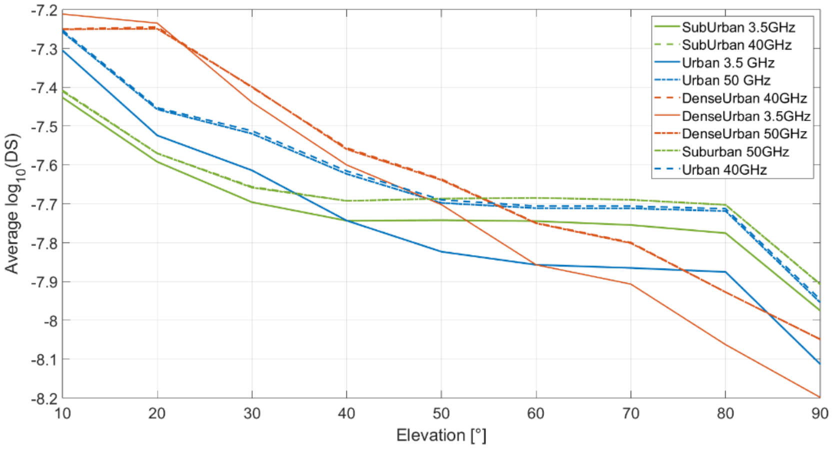

FIGURE 45: DELAY SPREAD VS. SATELLITE ELEVATION

Finally, although both delay spread and Rice factor don't seem so much sensitive to frequency, K values in C band are on the average few dBs greater than they are in Q/V bands, whereas the situation is reversed as far as delay spread is concerned.

4.3 HARDWARE IMPAIRMENTS

The nonideal behaviour of RF hardware imposes boundaries and limitations on system performance. The envisioned use of high carrier frequencies (Q/V bands) and wide signal bandwidths introduces additional challenges for RF design.

RF nonidealities that reduces the signal quality are quantization noise of the converters, IQ-imbalance, phase noise, thermal noise, and PA nonlinearity. In this first version of the deliverable, we focused on the phase noise and the PA nonlinearities.

4.3.1 High Amplifiers Models

Power amplifiers are non-linear. As the carrier power applied to the input of an amplifier is increased, there is a region of quasi-linear operation at low level after which the output power no longer increases in proportion to the input power. The maximum output power corresponds to saturation. When operating with several sub-carriers, intermodulation products appear at frequencies corresponding to linear combinations of the input carrier frequencies and when the carriers are modulated, the intermodulation products which fall within the useful bandwidth of the amplifier behave as noise. This noise is characterized within the bandwidth of each carrier by the value of the intermodulation power spectral density $(N0)_{IM}$. To limit intermodulation noise when several carriers are amplified simultaneously to a value compatible with the overall link budget requirement, it is advisable to operate the amplifier below the saturation region. The OBO, defined as the ratio of the output power delivered on one of the n carriers (P_{on}) to the saturation power, determines the position of the operating point. The power delivered at the amplifier output for the carrier concerned is thus equal to:

$$P_{on} = P_{sat} \cdot OBO\ [W]$$

The value of the back-off depends on the minimum allowed value of the receiver's contributions to the carrier power to intermodulation power spectral density ratio $(C/N_0)_{IM}$ of the link, the number of carriers, and the input-output characteristic of the amplifier.

In order to model the nonlinear behaviour of the amplifier, a few simple models can be considered. A more rigorous model would include the Volterra series expansion which can model complex non-linearities such as memory effects. Among the simpler models, the Rapp model, Saleh model, and the Ghorbani model can be considered. Combinations of pure polynomial models and filter models are also often referred to as fairly simple models, among which the Hammerstein model could be mentioned.

The advantage of the simpler models is usually related to the need of very few parameters to model the non-linear behaviour. The drawback is that such a model only can be used in conjunction with simple architecture amplifiers such as the basic Class A, AB, and C amplifiers. Amplifiers such as the high efficiency Doherty amplifier can in general not be modelled by one of these simple models.

In addition, to properly capture the PA behaviour for the envisaged large bandwidths, it is essential to use PA models capturing the memory effects. Such models would require an extensive set of empirical measurements for proper parameterization.

➲ Rapp Model

A widely accepted solid state amplifier model encompassing the amplitude clipping, is the Rapp model. The latter is designed based on the following equation and it produces a smooth transition for the envelope characteristics as the input amplitude approaches saturation. Amplitude distortion (AM/AM) and Phase distortion (AM/PM) are obtained as follow:

$$F_{AM-AM} = \frac{Gx(t)}{\left(1 + \left|\frac{Gx(t)}{A_{sat}}\right|^{2P}\right)^{\frac{1}{2P}}}$$

$$F_{AM-PM} = \frac{Ax(t)^q}{1 + \left(\frac{x(t)}{B}\right)^q}$$

where A_{sat} is saturation output amplitude, $x(t)$ is complex envelope of the input signal, G is the signal gain, while P controls the smoothness of the transition from a linear region to a saturation region.

If signal measurements of the input/output relationship are available, the parameters of the model may be readily found for a particular amplifier, e.g. with regression techniques.

The strength of the Rapp model lies in its simple and compact formulation, and that gives an estimation of the saturation characteristics of an amplifier. The drawback of this simple model is of course that it cannot model higher order classes of amplifiers such as the Doherty amplifier. It also lacks the ability to model memory effects of an amplifier.

In conclusion, RAPP model, similarly to other memoryless models, would capture some aspects in relation to waveform design but could not serve as a complete and comprehensive PA model covering all the effect possibly affecting the waveform design.

➲ Saleh Model

Saleh's nonlinear models are widely used in the behavioural modelling of modern RF nonlinear solid-state power amplifiers (SSPAs), particularly when the PA can be assumed to be memoryless—typically true only over a narrowband—or when an equivalent memoryless (EM) model is sufficient.

Its original 4-parameter generic model, is given by:

$$F_{AM-AM} = \frac{\alpha\, x(t)^{\eta}}{(1+\beta x(t)^2)^{\nu}}$$

with $\eta = 1{,}2, or\ 3$ and $\nu = 1\ or\ 2$. The variable $x(t)$ represent the envelope of the mem-oryless PA's input signal. The parameters η and ν are preselected. The model's other two parameters, the approximating coefficients α and β, may be extracted usinga Least Squares (LS) approximation to minimise the relative error between the envelope measurements of the target and the values predicted by the model.

From this, the well-known '2-parameter' AM-AM and AM-PM distortion relation are found to be as:

$$F_{AM-AM} = \frac{\alpha_a x(t)}{1+\beta_a x(t)^2}$$

$$F_{AM-PM} = \frac{\alpha_\varphi x(t)^2}{1+\beta_\varphi x(t)^2}$$

Where x is the envelop of the complex signal fed into the amplifier, and α/β are real-valued parameters that can be used to tune the model to fit a particular amplifier.

- Modified Saleh model

The modifications to Saleh's model include allowing η to take the value of zero and introducing a new 'offset phase shift parameter ε as a means to cater for non-zero initial AM-PM. The latter leaves α 'free' to function as a scaling parameter of $x(t)^{\eta}$ attenuated by a monotonic denominator, and help eliminate the danger of the pole instabilities occurring. A second new parameter γ is also introduced to allow greater variability at the denominator. This improves the range of curves which can be matched and likely accuracy of such matching. The new generic model can be written as:

$$F_{AM-AM} = \frac{\alpha\, x(t)^{\eta}}{(1+\beta x(t)^{\gamma})^{\nu}}$$

- Ghorbani Model

The Ghorbani model also gives expressions similar to the Saleh model, where AM-AM and AM-PM distortion is modelled. The AM/AM and AM/PM distortion functions are:

$$F_{AM-AM} = \frac{x_1 r(t)^{x_2}}{1+x_3 r(t)^{x_2}} + x_4 r$$
$$F_{AM-PM} = \frac{y_1 r(t)^{y_2}}{1+y_3 r(t)^{y_2}} + y_4 |r(t)|$$

In the expressions above, r is the amplitude of the input signal and the actual scalars $x_{1\text{-}4}$ and $y_{1\text{-}4}$ have to be extracted from measurements by curve fitting or some sort of regression analysis.

4.3.1.1 C band UE amplifier model

The proposed PA model at UE side corresponds to a modified Saleh model.

For an input signal $s = |x(t)|\, e^{j\theta}$ and output $T(x(t))e^{j(\theta+\Phi(a))}$, the AM-AM model is given by:

$$T(x) = \frac{\alpha\, x(t)^{\eta}}{(1+\beta\, x(t)^{\gamma})^{\nu}}$$

α=16, η =1, $\beta = \alpha$ /1.9, γ=2.2, ν=1/ γ

The phase distortion $\Phi(a)$ may be neglected (as it can be precomputed and cancelled).

Figure 46 presents an example implementation of the AM-AM model following adjustment of the saturation power (Psat) to 30 dBm and linear amplification gain to 0 dB, via input and output scaling of the PA model above.

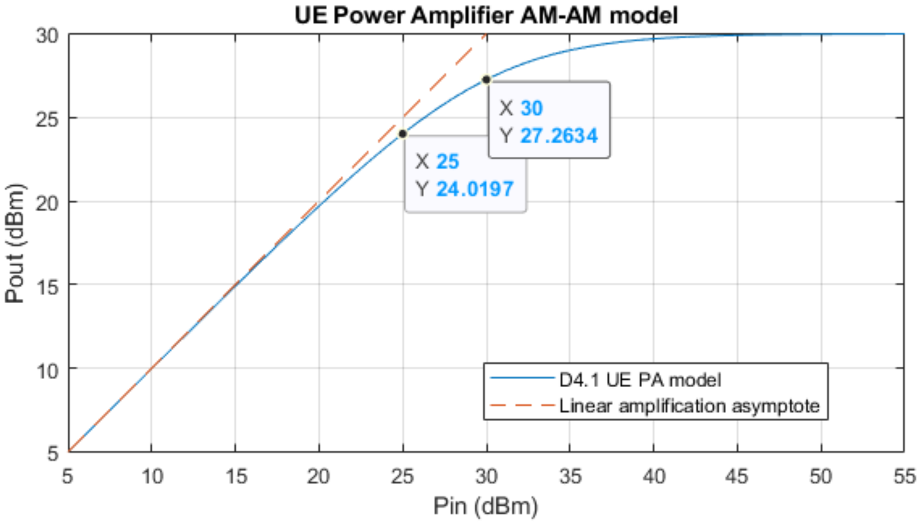

FIGURE 46: EXAMPLE IMPLEMENTATION OF THE AM-AM MODEL FOLLOWING ADJUSTEMENT OF THE SATURATION POWER

Importantly, as input and output scaling of the model corresponds simply to a translation of the AM-AM power representation, without loss of generality, the 1 dB and 3 dB compression points can be expressed in terms of the adopted saturation power. As evidenced in Figure 46, the 1dB and 3 dB compression points of the suggested UE PA model correspond approximately to an output power of Psat – 6 dB and Psat – 3 dB, or 24 dBm and 27 dBm in the example above, respectively.

4.3.1.2 Q band UE amplifier model

The UE amplifier model in Q/V band is based on advanced circuit simulation of a CMOS PA research prototype at 28 GHz and it has been proposed in [117]. In particular, the model is based on the following Generalized Memory Polynomial (GMP) model:

$$y_{GMP}(n) = \sum_{k\in K_a}\sum_{l\in L_a} a_{kl}x(n-l)|x(n-l)|^{2k} + \sum_{k\in K_b}\sum_{l\in L_b}\sum_{m\in M} b_{klm}x(n-l)|x(n-l-m)|^{2k}$$

Where $y_{GMP}(n)$ and $x(n)$ represent the complex baseband equivalent output and input, respectively, of the model. The first term represents the double sum of so-called diagonal terms where the input signal at time shift $l, x(n-l); l \in L_a$, is multiplied by different orders of the time aligned input signal envelope $|x(n-l)|^{2k}$; $k \in K_a$. The triple sum represents cross terms, i.e., the input signal at each time shift is multiplied by different orders of the input signal envelope at different time shifts. The GMP is linear in the coefficients, a_{kl} and b_{klm} which cater for robust estimation based on input and output signal waveforms of the PAs to be characterized. As a complement to the above, also memoryless polynomial models have been derived based on:

$$y_P(n) = \sum_{k \in K_p} a_k x(n)|x(n)|^2$$

The memoryless model has -32.1 dB Normalized Mean Square Error (NMSE) and is defined by:

$a_k, k \in [0,1,..,7]$: `[0.491576+0.870835i; -1.26213+0.242689i; 7.11693+5.14105i; -30.7048-53.4924i; 73.8814+169.146i; -96.7955-253.635i; 65.0665+185.434i; -17.5838-53.1786i]`

The corresponding GMP model has -41.7 dB NMSE and is defined by:

$a_k, k \in [0,1,..,7]$:

$l = 1$:

[-0.0109821+0.00313982i; -0.00397658-0.0427409i; -0.171194+0.151692i; 0.879844-0.0235651i; -1.97684-0.862044i; 2.32524+1.99694i; -1.34472-1.77602i; 0.289959+0.559338i]

$l = 0$:

[0.473465+0.860276i; -0.953417+0.640666i; 1.9899-2.3847i; 7.5417+6.38381i; -64.8415-60.8762i; 159.01+189.579i; -167.466-225.579i; 65.4247+92.5967i]

$l = -1$:

[0.0164844+0.00671299i; -0.0198519+0.177212i; 0.669594-0.543745i; -2.98038-0.279477i; 6.6717+4.50511i; -8.26935-9.04627i; 5.42365+7.52782i; -1.47259-2.32623i]

Figure 47 and Figure 48 show the gain and phase characteristics of the GMP and static model using the same OFDM signal that was used for model estimation.

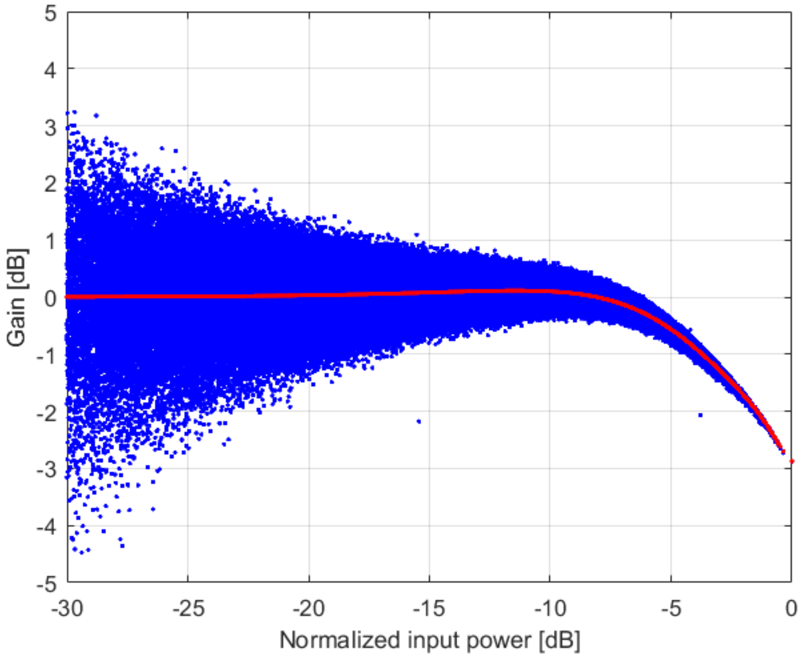

FIGURE 47: GAIN CHARACTERISTICS: GMP MODEL (BLUE), STATIC MODEL (RED)

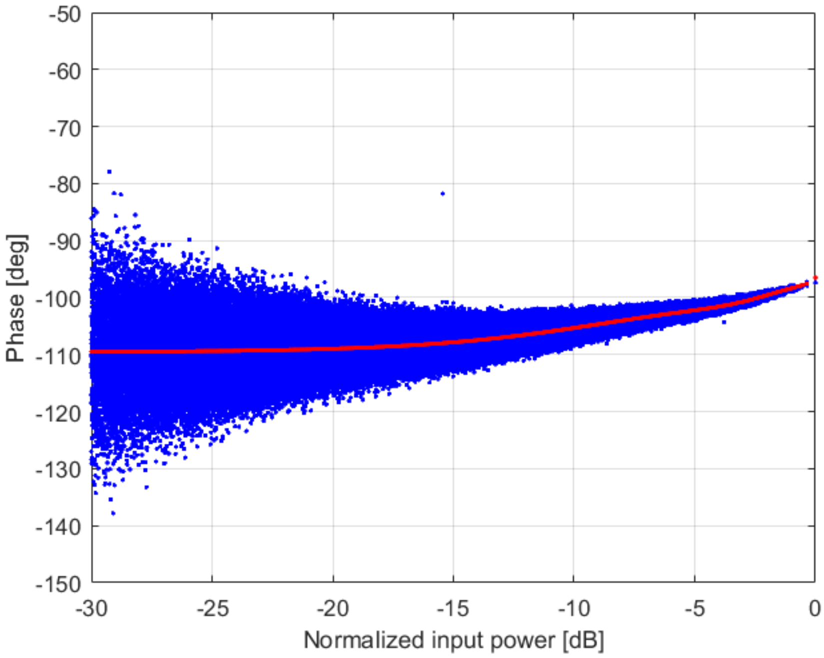

FIGURE 48: PHASE CHARACTERISTICS: GMP MODEL (BLUE), STATIC MODEL (RED)

4.3.1.3 C band satellite amplifier model

The AM/AM and AM/PM characteristics of the satellite amplifier model in C band are obtained by means of measurements.

Table 19 and Figure 49 represent the amplifier model of a single radiating element in C band.

TABLE 19: AM/AM AND AM/PM CHARACTERISTICS OF THE SATELLITE AMPLIFIER IN C BAND

Input power (dBm)	Output power (dBm)	Phase (°)
-35,0	16,485	-19,132
-34,0	17,537	-19,020
-33,0	18,525	-18,940
-32,0	19,488	-19,198
-31,0	20,460	-18,203
-30,0	21,475	-18,567
-29,0	22,394	-20,139
-28,0	23,350	-18,540
-27,0	24,267	-18,004
-26,0	25,151	-16,626
-25,0	26,027	-16,050
-24,1	26,877	-16,048
-23,0	27,795	-14,384
-22,0	28,778	-13,913
-21,0	29,797	-11,809

-20,0	30,806	-9,754
-19,0	31,760	-10,004
-18,0	32,605	-8,331
-17,0	33,333	-7,515
-16,0	33,944	-6,840
-15,0	34,458	-5,354
-14,0	34,784	-1,210
-13,0	34,954	2,015

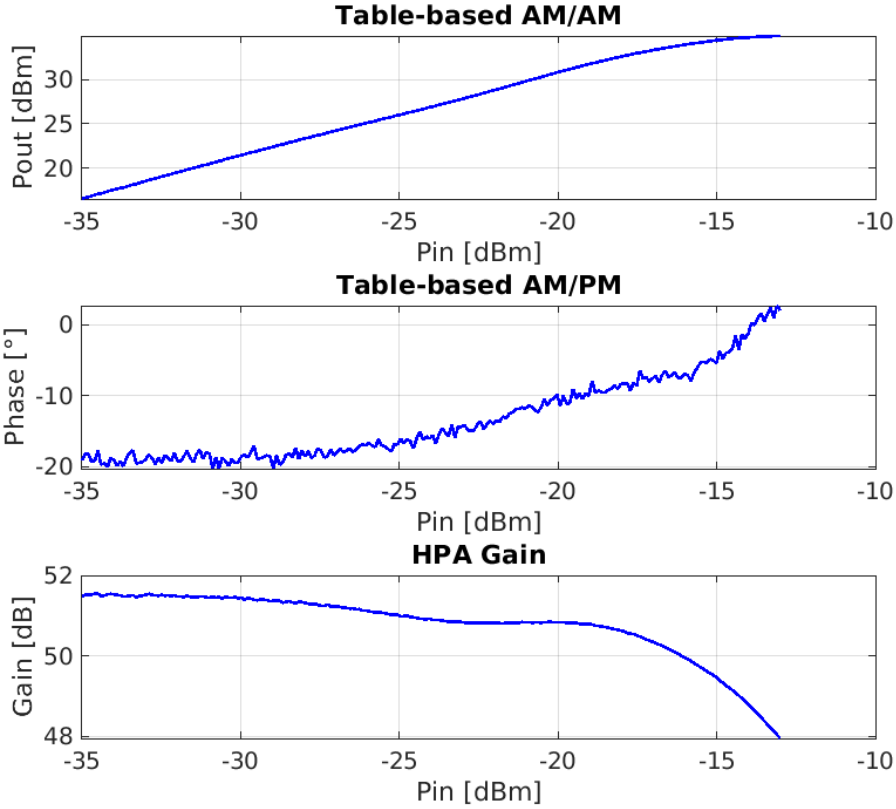

FIGURE 49: NON-LINEAR AMPLIFIER HPA CHARACTERISTICS IN C BAND

4.3.1.4 Q band satellite amplifier model

The AM/AM and AM/PM characteristics of the satellite amplifier model in Q/V bands are obtained by means of measurements.

Table 20 and Figure 50 represent the amplifier model of a single radiating element in the Q band.

TABLE 20: AM/AM AND AM/PM AMPLIFIER RESPONSE FOR Q BAND MODEL

Input power (dBm)	Output power (dBm)	Phase (°)
-20,00	1,90	0,00
-19,00	2,90	-0,10
-18,00	3,90	-0,20
-17,00	4,90	-0,30
-16,00	5,90	-0,50

-15,00	7,00	-0,70
-14,00	8,00	-1,00
-13,00	9,00	-1,40
-12,00	10,00	-1,80
-11,00	11,00	-2,30
-10,00	12,10	-2,90
-9,00	13,10	-3,60
-8,00	14,10	-4,50
-7,00	15,20	-5,50
-6,00	16,20	-6,70
-5,00	17,30	-8,20
-4,00	18,30	-10,10
-3,00	19,30	-12,30
-2,00	20,30	-14,70
-1,00	21,10	-17,40
0,00	21,80	-20,10
1,00	22,40	-22,30
2,00	22,90	-24,20
3,00	23,40	-26,30
4,00	23,70	-28,80
5,00	24,00	-31,40
6,00	24,20	-34,20
7,00	24,40	-37,20
8,00	24,50	-40,00
9,00	24,70	-42,60
10,00	24,90	-45,30

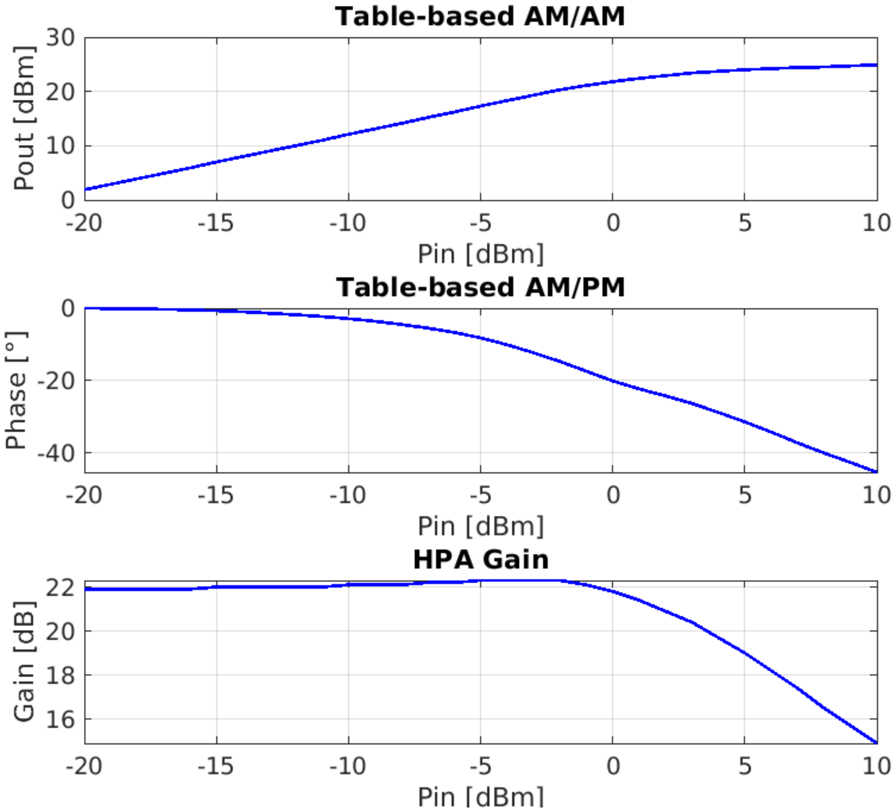

FIGURE 50: PAYLOAD NON-LINEAR AMPLIFIER HPA CHARACTERISTICS IN THE Q BAND

4.3.2 Phase Noise

Phase noise is recognized as one of the primary non-idealities that constrain the performance of wideband 6G systems operating at high carrier frequencies [97].

The choice of waveforms and the frame structure significantly affects the system's overall performance under phase noise. Specifically, the impact of phase noise on various waveforms depends on how phase synchronization is achieved in the receiver and how data and pilot sequences are distributed within the time domain signal relative to phase jitter characteristics. In multi-carrier waveforms, lower offset frequency components of phase noise cause Common Phase Error (CPE) due to long symbol durations, which can be mitigated in the receiver using appropriate phase noise tracking reference signals. Higher offset frequencies and the flat portion of the phase noise contribute to inter-symbol interference, generally limiting the achievable Signal to Noise Ratio (SNR). For single-carrier waveforms, the symbols are short in the time domain, so potential phase drift over a single symbol is primarily dominated by flat phase noise, assuming a fast symbol rate. The impact of lower offset frequency components of phase noise also depends on the signal length.

Given the importance of assessing the performance of the waveforms when affected by the phase noise, in the work we adopted the phase noise profiles proposed in [4]. The latter are representative of the total aggregated phase noise contribution generated by the main elements (i.e., the satellite and the terminal) on the FWD, i.e., from the gNB (satellite) to the UE, and RTN links, i.e., from the UE to the gNB (satellite).

Table 21 and Table 22 present the phase noise profiles considered in this study.

TABLE 21: SINGLE SIDEBAND AGGREGATED FWD PHASE NOISE PROFILE

Offset from Carrier Frequency	Forward link (dBc/Hz)
10 Hz	NA
100 Hz	[-25]
1 kHz	[-50]
10 kHz	[-73]
100 kHz	[-92]
1 MHz	[-102]
10 MHz	[-113]
100 MHz	[-116]

TABLE 22: SINGLE SIDEBAND AGGREGATED RTN PHASE NOISE PROFILE

Offset from Carrier Frequency	Return link (dBc/Hz)
10 Hz	[-36]
100 Hz	[-58]
1 kHz	[-69]
10 kHz	[-79]
100 kHz	[-87]
1 MHz	[-104]
10 MHz	[-109]
100 MHz	[-109]

Co-funded by
the European Union

5 CALIBRATION

In order to compare the different waveforms in a fair way, the software calibration has been performed. To achieve this objective, project's partners have worked together in order to consolidate each partner simulator to be able to deliverable comparable results.

In particular, we proceeded with the calibration of the following blocks:

- Phase noise.
- HPA models for the UE and the gNB satellite considering both C band and Q/V band.
- Tapped Delay Line (TDL) channel model.

5.1 CALIBRATION PROCESS

5.1.1 Phase Noise

The phase noise is modelled using the filtered Gaussian phase noise approach. This method aims to represent the equivalent power spectral density of the phase noise. Consequently, the actual time-domain model used in simulations is derived from an inverse Fourier transform of the spectral model, assuming the spectrum is conjugate symmetric.

Figure 51 illustrate the Single Side Band (SSB) phase noise spectra of the return link, where the PSD is given in logarithmic scale.

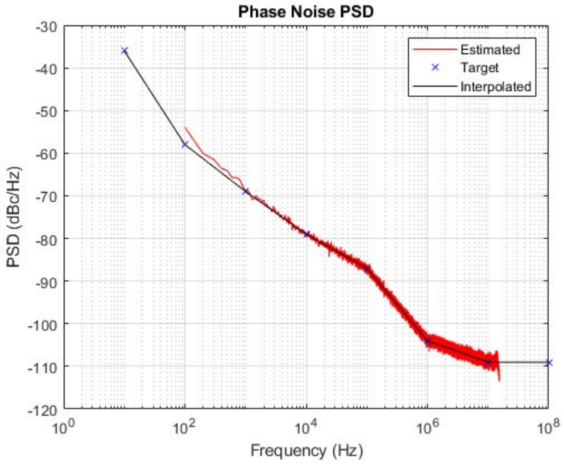

FIGURE 51: SSB PSD OF THE PHASE NOISE OF THE RTL

5.1.2 High Power Amplifiers

In order to apply the HPA model to the transmitted signal, the input and output of the PA-specific AM/AM and AM/PM models are scaled so that two conditions are met:

1. The resulting model saturates at an output power equal to the average power of the input signal leaving a gap equal to the input backoff (IBO), i.e., $P_{sat} = 10 * \log_{10}(12 * N_{PRB}) + IBO$, where $12 * N_{PRB}$ corresponds to the average power according to the normalization in 3.1.2.

2. The gain of the resulting model corresponds to 0 dB at the linear region of amplification.

The conditions above are achieved by effectively applying a vertical and horizontal translation of the log representation of the AM/AM and AM/PM power models introduced above. Equivalently, they correspond to scaling the input and output signals prior and following the PA model stage, respectively.

Importantly, input and output scaling may be achieved either numerically or analytically depending on the nature of the adopted PA model, namely, if available in closed form or obtained from measurements.

In the following, the different models adopted for the calibration and evaluation phases after input and output scaling will be presented for the purpose of illustration.

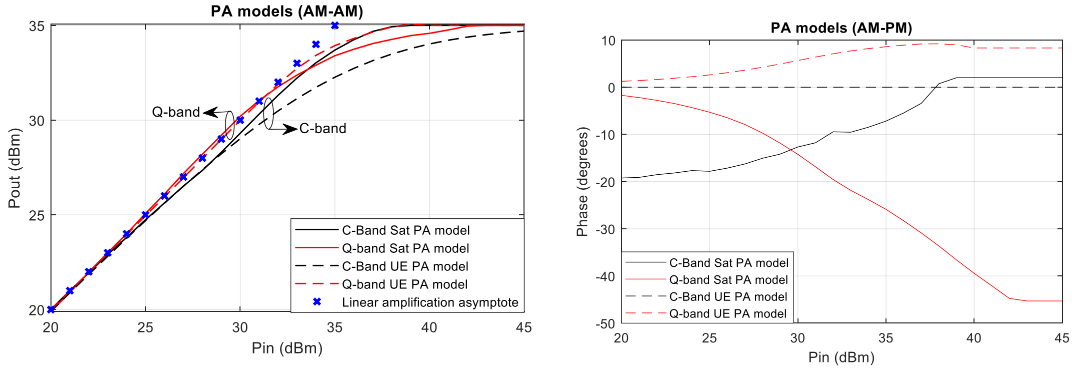

FIGURE 52: AM/AM AND AM/PM NORMALIZED CHARACTERISTICS

Figure 52 shows the AM/AM and AM/PM characteristics of the adopted C/Q-band power amplifier models for an arbitrary saturation power of 35 dBm. As observed, the models vary depending on the direction of the transmission (downlink with continuous line spec vs. uplink in dashed line spec) and the band of use (C-band in black-coloured line vs. Q-band in red-coloured line).

Particularly, it can be observed that the Q-band PAs closely approach the clipping model (which tracks the linear asymptote until saturation) but suffer from a higher phase distortion compared to C-band PAs, especially in the case of downlink.

5.1.3 TDL Channel models

The considered channel model is a TDL model from [104]. In particular, TDL-A 50 ns, TDL-A 100 ns, and TDL-D 50 ns have been considered, where TDL-A represents the channel profiles for NLoS communications, while TDL-D is defined for LoS communication. The values of the normalized delays and power for the two profiles are reported in Table 23 and Table 24, respectively.

TABLE 23:NTN-TDL-A. ELEVATION ANGLE 50°

Tap #	Normalized delay	Power [dB]	Fading Distribution
1	0	0	Rayleigh
2	1.0811	-4.675	Rayleigh

3	2.8416	-6.482	Rayleigh

TABLE 24: NTN- TDL-D. ELEVATION ANGLE 50°

Tap #	Normalized delay	Power [dB]	Fading Distribution
1	0	-0.284	LOS path
2	0	-11.991	Rayleigh
3	0.5596	-9.887	Rayleigh
4	7.3340	-16.771	Rayleigh
The first tap follows a Ricean distribution with a K-factor of K1 = 11.707 dB and a mean power of 0 dB.			

It is worth emphasizing that in this first version of the deliverable, NTN-TDL-A and NTN-TDL-D have been considered for the preliminary evaluation of the waveforms. When a more consolidated channel model in C band and Q/V band will be available within the consortium it will be used for testing the selected waveform.

5.2 CALIBRATION SCENARIOS

The calibration process is performed in an end-to-end fashion considering the CP-OFDM and DFT-s-OFDM waveforms. The link level simulation chain for the CP-OFDM is illustrated in Figure 53.

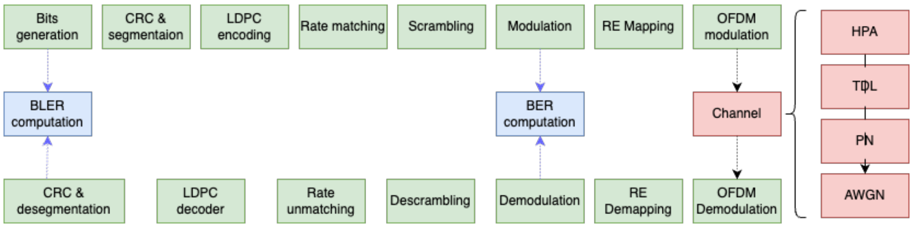

FIGURE 53: CP-OFDM LINK LEVEL SIMULATION CHAIN FOR CALIBRATION

The bits are randomly generated through a bit generator and enter the chain of baseband signal processing blocks: segmentation, cyclic redundancy check (CRC), and scrambling. The FEC scheme is the LDPC. After that, the bits are mapped into the constellation symbols, which are then mapped on the different resource elements. Following, the OFDM modulation is performed and the OFDM modulated signal enters the channel block, which consists of the HPA, TDL, PN, and AWGN. At the receiver side, the reverse path is followed. A dedicated block compares the initially generated bits with the estimated bits and computes the Block Error Rates (BLER), while the BER is evaluated after the demodulation by means of the LLR bits.

The parameters used for the calibration are listed in Table 25.

Co-funded by the European Union

TABLE 25: CALIBRATION SCENARIOS

Parameters				**Downlink**		**Uplink**
				Case1 **10 MHz**	**Case2** **50 MHz**	**Case3** **5 MHz**
TX	**FFT size**			8192		
	Sub-carrier spacing (SCS)			15kHz	120kHz	15kHz
	Number of resource blocks			52	32	25
	Modulation			QPSK CP-OFDM		QPSK DFT-s-OFDM
	Code rate			526/1024	679/1024	379/1024
	Rv			0		
	# OFDM symbols			12 (Symbols 2-13)		14 (Symbols 0-13)
	TBS			7372 bits	5856 bits	2886 bits
	# DMRS			1 (Symbol 2: 6RE/RB for DMRS, 6RE/RB for Data)		1 (Symbol 2: 6RE/RB for DMRS, 6RE/RB not used)
HW impairments	**HPA**	**UE model**	IBO			2 dB, 5 dB
			Model params.			C/Q-V-band UE HPA model
		Satellite model	IBO	2 dB, 5 dB		
			Model params.	C/Q-V-band satellite HPA model		
		Clipping	IBO	2 dB, 5 dB		
	Phase noise		Profile	RTN Profile		
			Sampling Freq.	Fs = 120e3 x 8192 x 3 Hz		
Channel	**AWGN**		SNR values	NOTE1		
	Fading channel	**NTN TDL A**	Delay spread	50ns, 100ns NOTE2		
			K factor	N/A (Rayleigh)		
		NTN TDL D	Delay spread	50ns NOTE4		
			K factor	11.707 dB		
Receiver	**Channel Estimation**		Algorithm	Genie		
	Equalizer		Algorithm	LMMSE		

NOTE1: SNR (dB) values are aligned to integer values and swept in steps of 1 dB.

NOTE2: Tap delays are quantized to sampling interval corresponding to 8192 FFT size for simpler modelling.

As observed in Table 25, three main cases have been devised, each with two variants of HPA model (clipping and UE/satellite as specified above), two different values for the IBO (2 dB and 5 dB) and three variants of channel models (TDL-A with delay spread of 100 ns, and TDL-A and TDL-D with delay spread of 50 ns), for a total of 36 sets of simulation parameters.

5.3 CALIBRATION RESULTS

The PAPR, defined as the ratio of the per-symbol-duration largest instantaneous power value to the average power, is presented below for the three cases. Given that the PAPR is computed prior to amplification, the following curves, shown in Figure 54, remain the same for C-band and Q-band, as per the calibration specifications introduced in the last section.

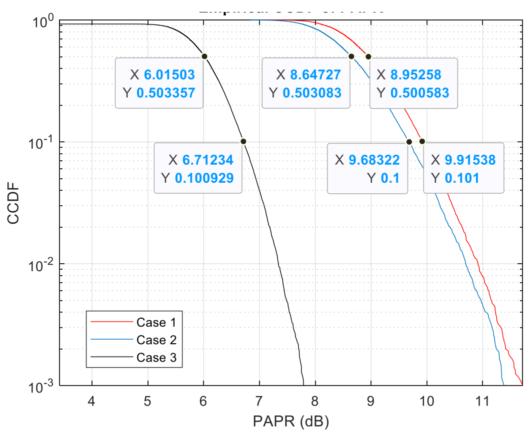

FIGURE 54: EMPIRICAL CCDF OF PAPR FOR CALIBRATION

From the obtained results, the expected improvement of 2.5 to 3 dB [32] in the PAPR for DFT-s-OFDM-based waveform of Case 3 can be evidenced relative to Case 1 and Case 2. Likewise, a minor improvement of ~0.3 dB in the PAPR for the configuration of Case 2 relative to that of Case 1 can also be evidenced and attributed to the lower number of allocated subcarriers as, consequently, it approaches more closely that of a single-carrier transmission [27].

5.3.1 C band calibration results

The results corresponding to calibration in C-band are found in Table 26 and Table 27 according to the case number (row), channel model (line colour), and PA model (line spec). Calibration results were obtained over $5\text{x}10^4$ channel realizations and 20 slots per simulated transmission as means of reducing the variance of the BER/BLER estimates.

TABLE 26: CALIBRATION RESULTS (BER) IN C BAND

	Calibration BER (IBO = 5 dB)	Calibration BER (IBO = 2 dB)

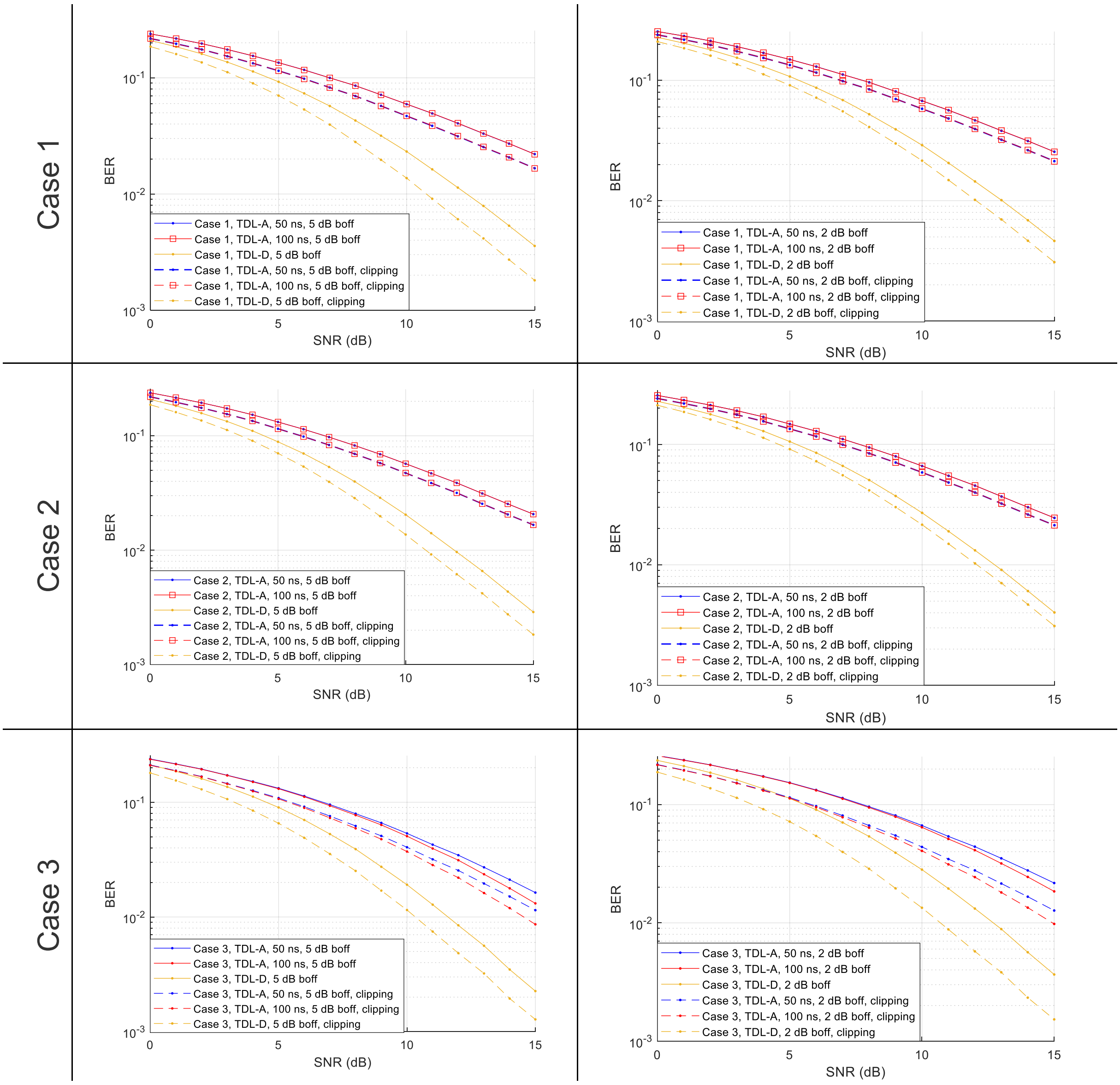

The LoS-based TDL-D channel model exposes a better performance than the NLoS TDL-A alternative, owing to the reliability provided by its 10 dB K-factor. Additionally, it can be observed that DFT-s-OFDM is able to outperform, even if by a small margin, in the case of smaller coherence bandwidths (resp. larger delay spreads) owing to the leveraged frequency diversity via symbol spreading across subcarriers.

The BER performance of the clipping model is shown consistently superior to any other PA model due to its ideal linear amplification up until reaching saturation and its undistorted phase profile.

It is also observed that, as expected, the lower the input power-backoff the larger the extent of the compression and, with it, the BER loss. Relying on the 10% BER as a reference, a loss corresponding to multiple decibels (i.e., 2-3 dB) can be observed on the 2-dB backoff cases (right hand column) relative to those of 5 dB (left hand column), except at the low-PAPR DFT-spread-based Case 3.

Besides, the detriment induced by the further PA amplitude and phase distortions shows consistency with an SNR shift relative to clipping common across cases that share PA specifications. Particularly, the greater loss of Case 3 relative to Case 1 and Case 2 is attributed to the lower compression point of the UE PA model compared to that of the satellite one.

TABLE 27: CALIBRATION RESULTS (BLER) IN C BAND

	Calibration BLER (IBO = 5 dB)	Calibration BLER (IBO = 2 dB)
Case 1	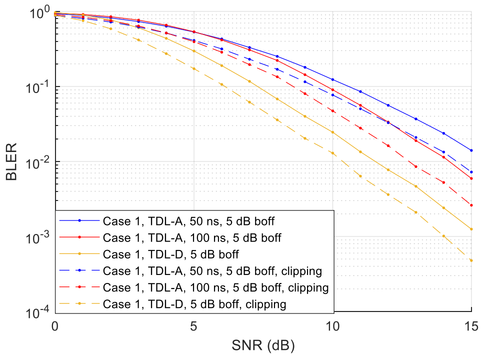	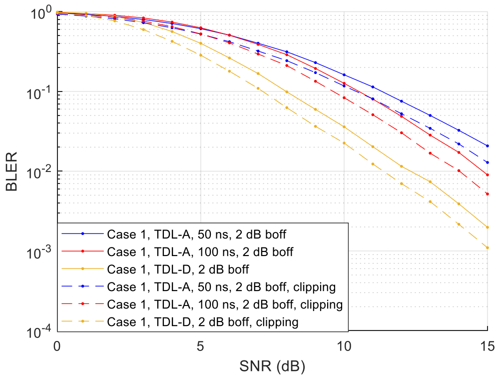
Case 2	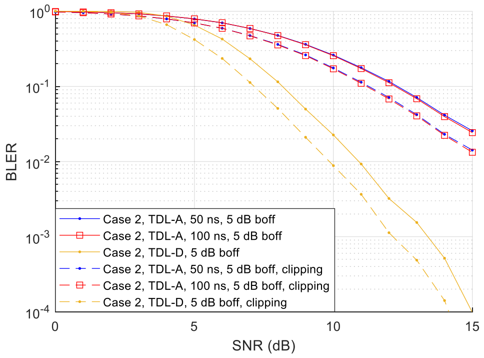	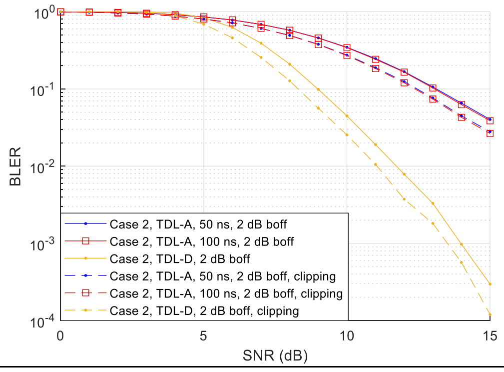
Case 3	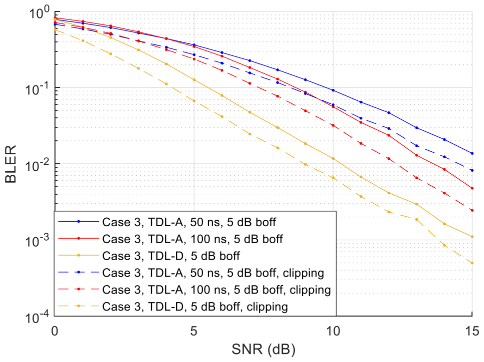	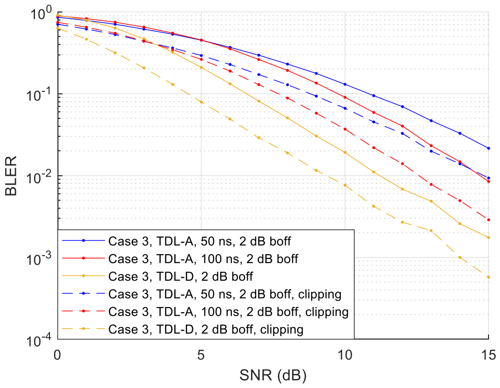

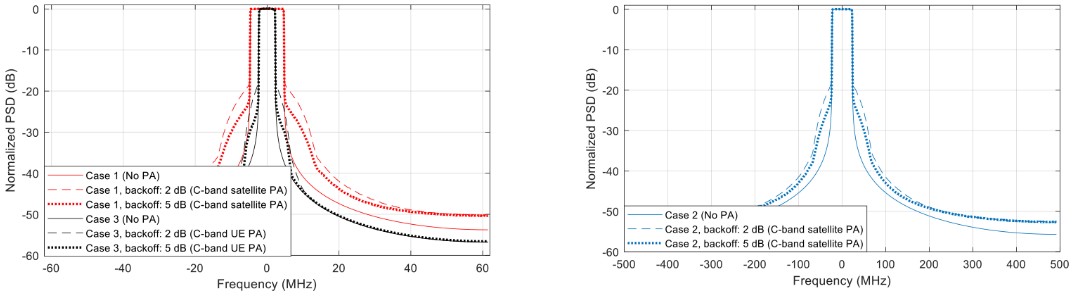

FIGURE 55: ONE SIDE POWER SPECTRAL DENSITY FOR CASE 1 AND CASE 2

The computed PSDs (illustrated in Figure 55) expose that the satellite power amplifier creates larger out-of-band emissions compared to the UE amplifier, in specific, relative to the bandwidth and at components nearby the allocated sub-carriers. These also show that, unlike in the satellite PA case, the UE PA-model related emissions reduce rapidly with the frequency until approaching the emissions inherent to the waveform itself (i.e., the emissions without PA) which constitutes a low bound.

Likewise, and as expected, the greater compression related to the 2 dB backoff cases creates higher out-of-band emissions compared to the alternative 5 dB ones.

It may be pointed out that, despite suffering from lower out-of-band emissions relative to bandwidth (attributed to the distortion-free phase profile at the UE and DFT-spreading related low PAPR), Case 3 suffers of high in-band distortion as evidenced on a similar, and even larger, PA-to-clipping BER/BLER loss relative to Case 1 and Case 2. Once again, the preceding observation is attributed to the lower compression point of the UE PA.

5.3.2 Q band calibration results

Calibration results over this band are reported in Table 28 and Table 29 and they are based on the specifications introduced in the previous section, namely, by adjusting the power amplifier related non-linearities according to the presented Q band PA models. Therefore, clipping results (and their related considerations) remain unchanged.

It may be highlighted that, unlike for the proposed C-band alternatives, the adopted UE PA model has better characteristics both in terms of its amplitude and phase distortions relative to those of the satellite in the Q-band proposals.

TABLE 28: CALIBRATION RESULTS (BER) IN Q/V BAND

	Calibration BER (IBO = 5 dB)	Calibration BER (IBO = 2 dB)
Case 1	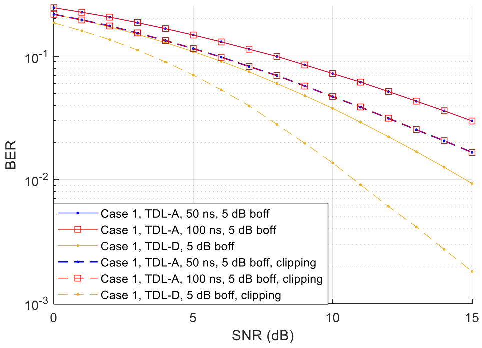	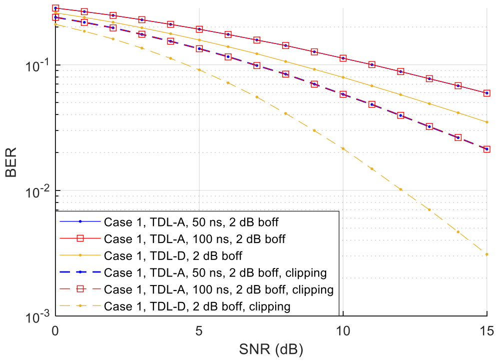

Case 2	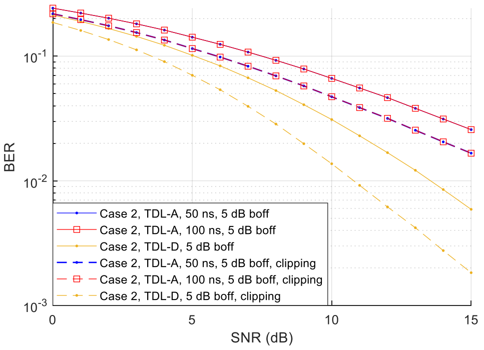	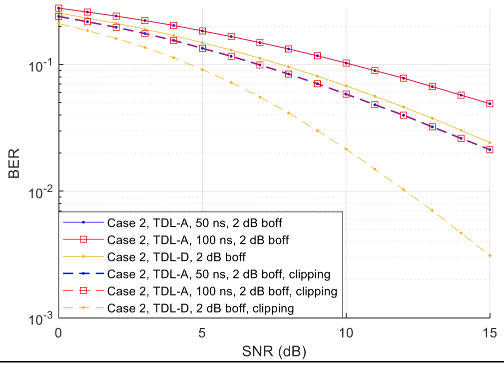
Case 3	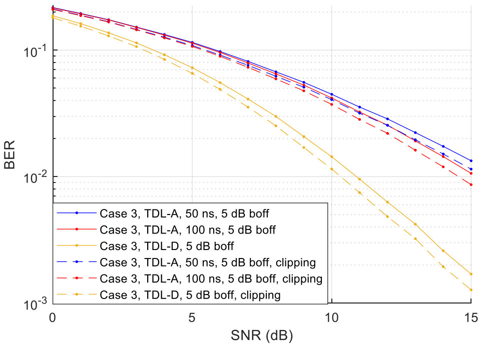	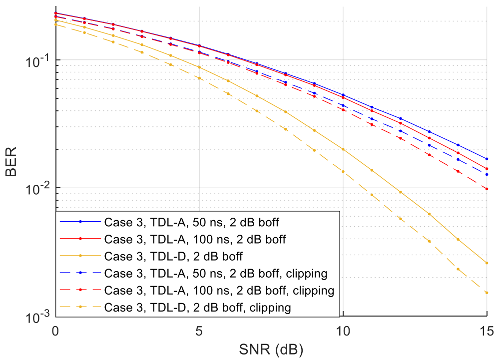

As it might be anticipated, the main BER/BLER trends carry over from the calibration over the C band of the preceding section. Nonetheless, the loss with respect to clipping gets larger (and to a greater extent in the 2 dB backoff case) for downlink Cases 1 and 2, relative to uplink Case 3. This is due to the superiority of the UE PA relative to the satellite PA.

TABLE 29: CALIBRATION RESULTS (BLER) IN Q/V BAND

	Calibration BLER (backoff = 5 dB)	Calibration BLER (backoff = 2 dB)
Case 1	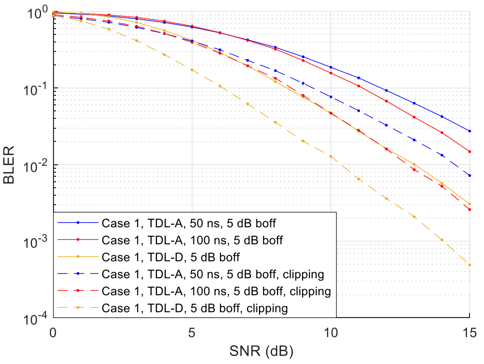	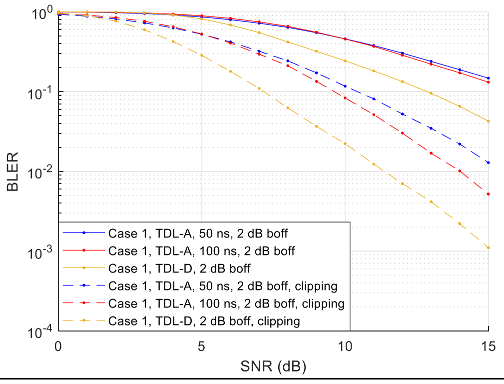
Case 2	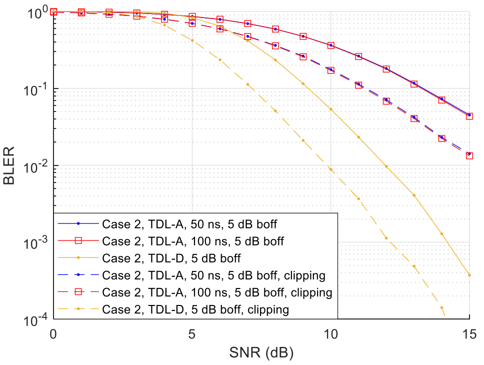	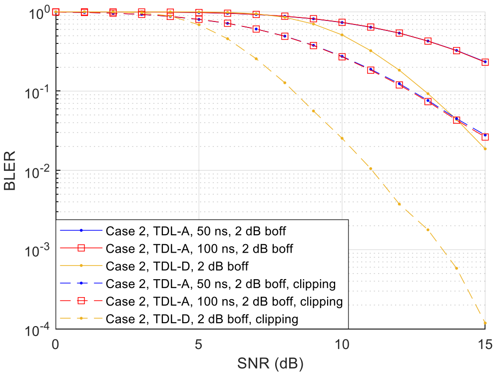

Case 3

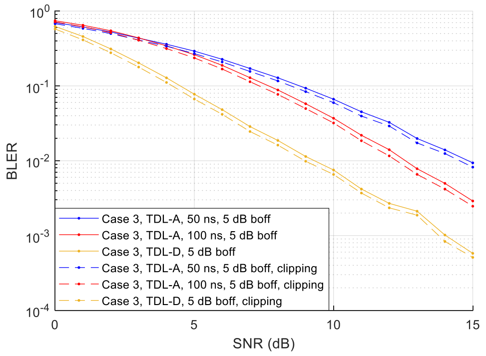
BLER
SNR (dB)
10^0
10^{-1}
10^{-2}
10^{-3}
10^{-4}
0
5
10
15
Case 3, TDL-A, 50 ns, 5 dB boff
Case 3, TDL-A, 100 ns, 5 dB boff
Case 3, TDL-D, 5 dB boff
Case 3, TDL-A, 50 ns, 5 dB boff, clipping
Case 3, TDL-A, 100 ns, 5 dB boff, clipping
Case 3, TDL-D, 5 dB boff, clipping

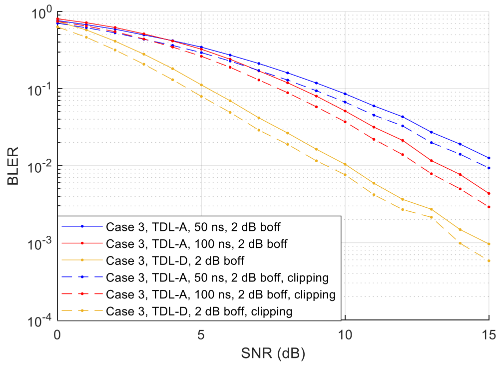
BLER
SNR (dB)
10^0
10^{-1}
10^{-2}
10^{-3}
10^{-4}
0
5
10
15
Case 3, TDL-A, 50 ns, 2 dB boff
Case 3, TDL-A, 100 ns, 2 dB boff
Case 3, TDL-D, 2 dB boff
Case 3, TDL-A, 50 ns, 2 dB boff, clipping
Case 3, TDL-A, 100 ns, 2 dB boff, clipping
Case 3, TDL-D, 2 dB boff, clipping

6 FLEXIBLE WAVEFORMS EVALUATION AND COMPARISON: FIRST ITERATION

In this section, the simulation results in the form of BER, BLER, PAPR, and PSD, of the chosen waveforms are reported.

6.1 SIMULATION SCENARIOS

In order to perform this preliminary round of simulations, three main scenarios, illustrated in Table 30, have been identified, namely Q1, C1, and C3. For each of them, both uplink and downlink were considered. It is worth mentioning that the carrier frequencies are those adopted in D3.5 as well as the Outdoor to Indoor penetration loss. Table 31 lists the parameters used for each scenario, including the hardware and the channel scenario. In C band, the PN model proposed is the Section 4 has not been considered since it is in Ka band. Notably, the purpose of this simulation campaign is to compare the performance of the waveforms. Therefore, at the receiver side a genie aided approach for the channel estimation is considered.

TABLE 30: SIMULATION SCENARIOS

Scenario	Bandwidth	Frequency
Q1	50 MHz	UL: 50 GHz DL 40 GHz
C1	5 MHz	UL: 3.9 GHz DL 3.5 GHz
C3	50 MHz	UL: 3.9 GHz DL 3.5 GHz

TABLE 31: SIMULATION PARAMETERS

Parameters		**Q1**		**C1**		**C3**	
		DL	UL	DL	UL	DL	UL
TX	SCS	120kHz		30 kHz			
	# PRBs	32		11		133	
	Modulation	QPSK					
	Code rate	679/1024	379/1024	679/1024	379/1024	679/1024	379/1024
	Rv	0					
	# OFDM symbols	12	14	12	14	12	14
	# DMRS	1					

HW impairments	HPA	UE model	IBO [dB]	2 and 5					
			Parameters of the model		UE PA model in Q/V band		UE PA Model in C band		UE PA Model in C band
		Sat model	IBO [dB]	2 and 5					
			Parameters of the model	Sat PA model in Q/V-band		Sat PA model in C-band		Sat PA model in C-band	
	Phase noise		Profile	FWD Profile	RTN Profile				
			Sampling Freq.	120e3 x 8192 x 3 Hz					
Channel	AWGN		SNR values	Step of 0.2 [dB]					
	Fading channel	NTN TDL A	Delay spread					50ns, 100ns	
			K factor					N/A	
		NTN TDL D	Delay spread					50ns	
			K factor					First tap K=11.707dB	
	Impairments		Doppler	Maximum Differential Doppler shift					
			O2I penetration loss			10 dB			
RX	Synchroniz.		Algorithm	Not considered					
	Channel Estimation		Algorithm	MMSE					
	Equalization		Algorithm	MMSE					

We chose to simulate the highest differential Doppler shift within a single beam of the satellite coverage area. Since pre-compensation at the beam center can be implemented, only the differential component remains, which impacts system performance. Figure 56 shows the one-way delay, differential delay, the Doppler shift, and the differential Doppler shift obtained with the LEO constellation proposed in D3.5.

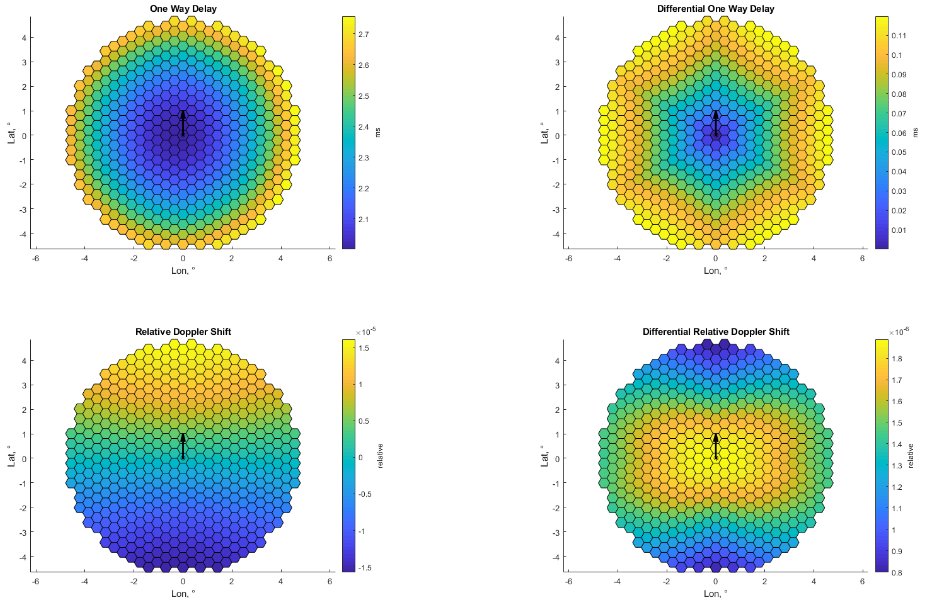

FIGURE 56: LEFT SIDE: ONE WAY DELAY AND DOPPLER SHIFT. RIGHT SIDE: DIFFERENTIAL DELAY AND DIFFERENTIAL DOPPLER. THE BLACK ARROW REPRESENTS THE DIRECTION OF THE MOVEMENT OF THE SATELLITE, WHILE THE BLACK DOT IS THE SUB SATELLITE POINT.

According to the designed constellation and coverage, the worst-case differential values within a beam are:

- Delay: 0.12 ms
- Doppler fraction: 1.9x 10^{-6}

Please note that the Doppler fraction needs to be multiplied by the carrier frequency in order to obtain the differential Doppler shift, as follows:

$$fd_{differential} = fd_{fraction} \times f_c$$
$$fd_{fraction} = fd_{shift,max} - fd_{shift,BC}$$
$$fd_{shift,max} = (v_{sat}/c) \times (\frac{R}{R+h} \cos(\varepsilon_{min}))$$
$$fd_{shift,BC} = (v_{sat}/c) \times (\frac{R}{R+h} \cos(\varepsilon_{BC}))$$

Where f_c is the carrier frequency, v_{sat} is the speed of the satellite, BC refers to beam center, $fd_{shift,max}$ is the maximum Doppler shift experienced at the beam edge (thus with the minimum elevation angle ε_{min}), and $fd_{shift,BC}$ is the Doppler shift at the beam center with elevation angle ε_{BC}.

The differential delay is computed as the differential slant range between the user at the beam edge at the user at the beam center:

$$\Delta\tau = \frac{\Delta D}{c} = \frac{D_{edge} - D_{beam}}{c}$$

6.2 WAVEFORM DESIGN SPECIFICATIONS

The current section provides a view of waveform-specific considerations adopted for the upcoming simulation results. Given the number of degrees of freedom associated to the waveform design of some variants, separate heuristics were applied to determine the configurations hereby adopted. Such heuristics are omitted in this deliverable for the sake of conciseness, but their further enhancement in upcoming deliverables is not barred of consideration, among others, via an end-to-end optimization strategy.

- **CP-OFDM:**

  As in calibration phase. Aligned to 3GPP spec.

- **WOLA-OFDM:**

  WOLA has been implemented both at transmitter and receiver sides. A pulse with soft and short edges is considered since it provides a sharp side-lobe decay in frequency domain, while producing negligible inter-symbol interference. A raised cosine pulse is thus adopted owing to its good performance and simple implementation [119]. Characterized by the roll of factor, the values of 0.03 and 0.008 were selected at the transmitter and receiver sides, respectively.

- **DFT-s-OFDM:**

  As in calibration phase. DFT size corresponds to BW allocation. Aligned to 3GPP spec.

- **UFMC:**

  A sub-band size corresponding to the number of subcarriers in a resource block is assumed, along with a Chebyshev filter with 40 dB of side-lobe attenuation. A predistortion stage is added to compensate for in-band distortion induced by the passband filter, thus, requiring no further processing at the receiver side [22].

- **BF-OFDM:**

  A sub-band size corresponding to the number of subcarriers in a resource block is adopted, along with a Gaussian pulse shape of length KM (K = 4, the filter-bank overlapping factor, M the number of allocated sub-bands/RBs). A predistortion stage is added to compensate the distortion induced by the transmit filter [102].

- **F-OFDM:**

  A pass-band filter with a bandwidth equivalent to the full spectrum allocation is applied. The filter design is based on a sinc truncated to be of length equal to half the FFT size via a Hanning window. An offset of two subcarriers at each extreme is considered so that the filter has a sufficiently flat response over the entire transmission bandwidth, i.e., so the ripples at the edges do not impact the subcarriers allocated at the edges.

- **OTFS:**

  It is implemented with a per frame CP with the TX and RX block illustrated in Figure 35. To make a comparison between the different pulse shaping, in C1 and C3 a rectangular pulse shaping has been considered, while in Q1 a Square Root Raised Cosine (SRRC) with a Roll-Off factor of 0.1 has been applied. At the receiver side, a MP detection scheme is implemented.

6.3 RESULTS

6.3.1 C-band Scenario C1 (downlink)

Table 32 presents an overview of the PAPR and power spectral density over the C1 scenario in downlink. As discussed, the PAPR provides a view of the extent to which the waveform will be compressed by the power amplifier, i.e., the larger the PAPR the greater the compression. On the other hand, the PSD depicts the amount of the out-of-band power emitted as a by-product of such a PA compression.

TABLE 32: PAPR AND PSD FOR SCENARIO C1 IN DL

	PAPR	*Power Spectral Density*
CP-OFDM	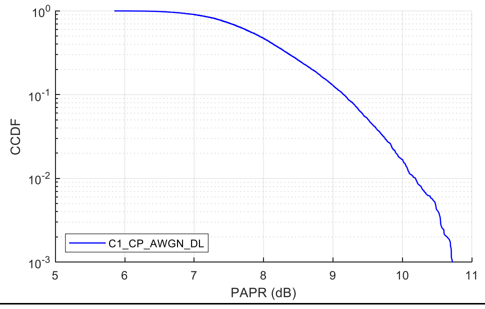	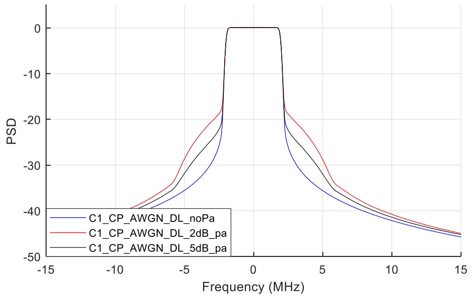
CP-OFDM (ERIS)	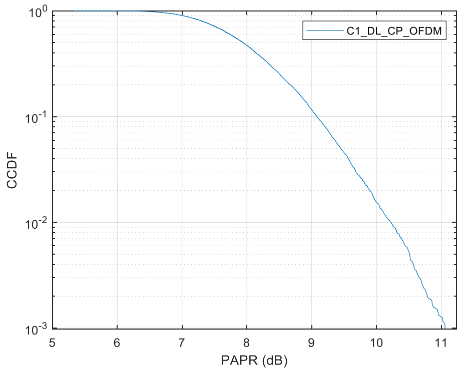	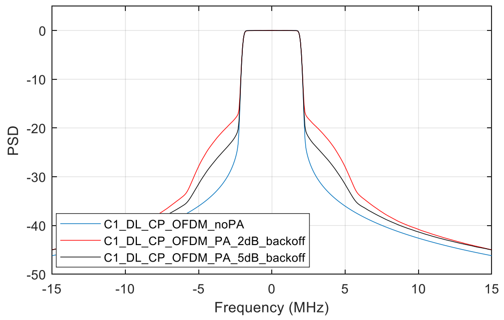
WOLA-OFDM	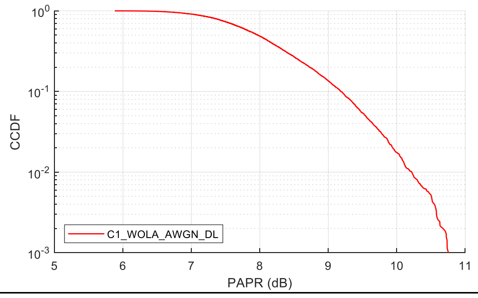	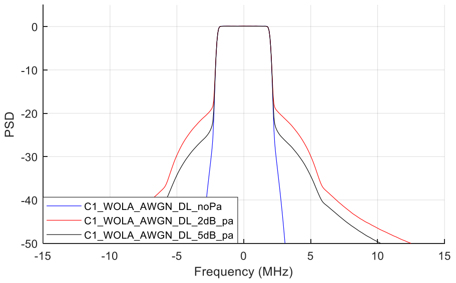
DFT-s-OFDM	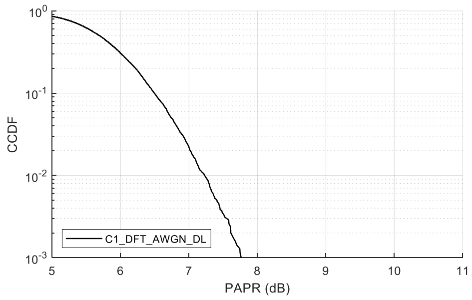	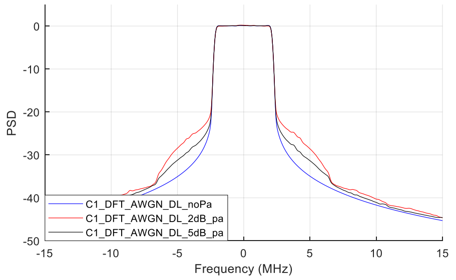

Co-funded by the European Union

UFMC

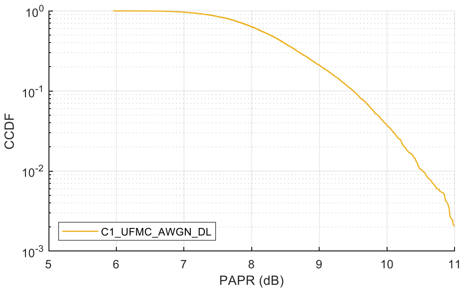

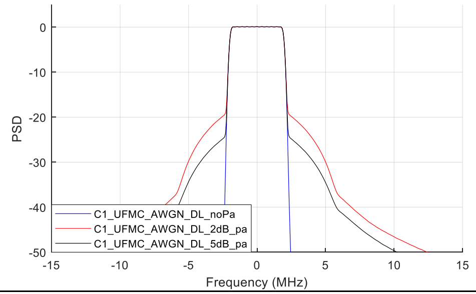

BF-OFDM

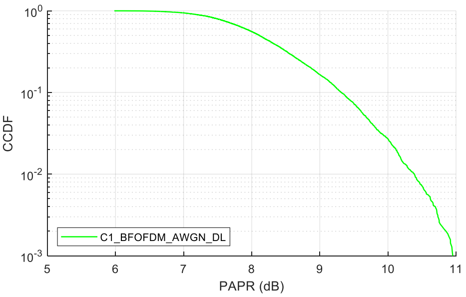

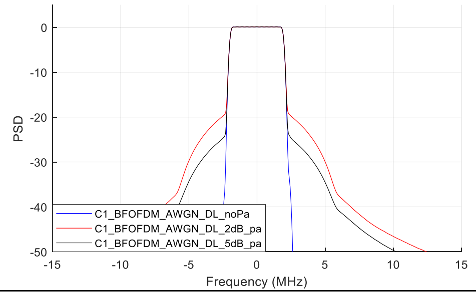

F-OFDM

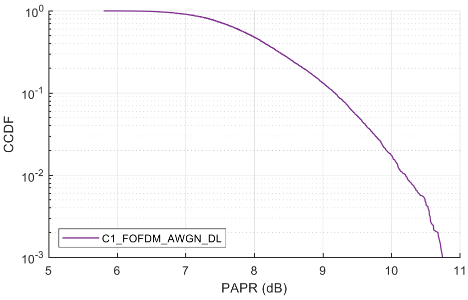

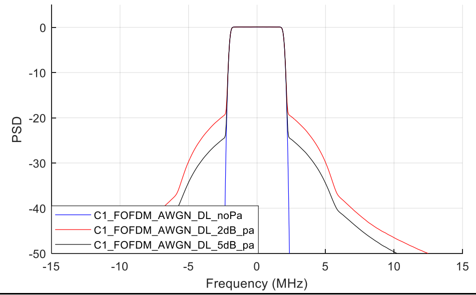

OTFS

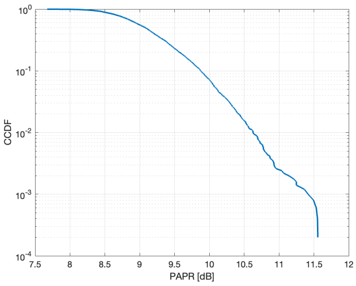

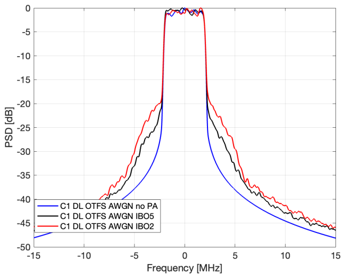

Starting from the left column with the PAPR empirical Complementary Cumulative Distribution Function (CCDF) prior to the amplification stage, it can be observed that most OFDM-based waveforms, namely: CP-based, WOLA-based, UFMC, BF, and F-OFDM, present very similar PAPR profiles across the whole distribution. The same is valid for the OTFS. Fundamentally, varying on the basic pulse adopted with respect to conventional CP-based OFDM, they all suffer from similarly high PAPR. On the contrary, the DFT-s-OFDM exhibits the expected 2-3 dB improvement relative to CP-OFDM [31].

The power spectral distribution on the right column demonstrates the impact of the different waveforms over the produced spectrum up to and beyond the allocated bandwidth. Particularly, looking at the curves before the PA stage (blue), we see that all the filtered OFDM variants, namely: WOLA, UFMC, BF and F-OFDM, fall rapidly below -50 dB relative to the power in the allocated spectrum. Instead, as anticipated, the CP and DFT-s-OFDM and OTFS present a slowly decaying spectrum.

Nevertheless, the out-of-band emissions for all waveforms following the PA stage is evidenced similar and become a strong function of the input backoff value applied. Particularly, and in the best case, a gap of at least 8 MHz to the allocated spectrum is required for the PA-enabled PSDs to fall below -50 dB relative to the respective power density.

TABLE 33: BER AND BLER FOR SCENARIO C1 IN DL

	BER	*BLER*
CP-OFDM (QCM)	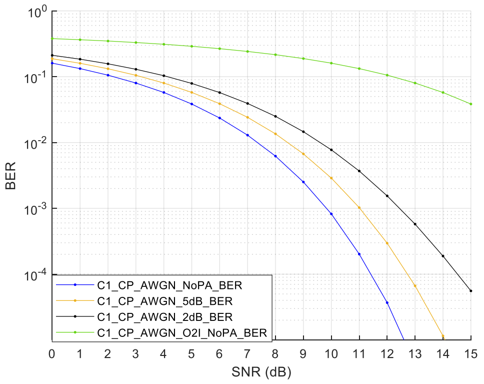	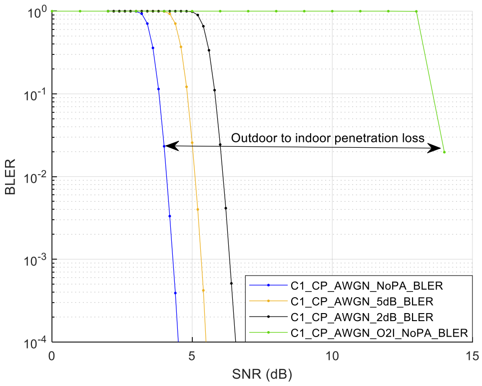
CP-OFDM (ERIS)	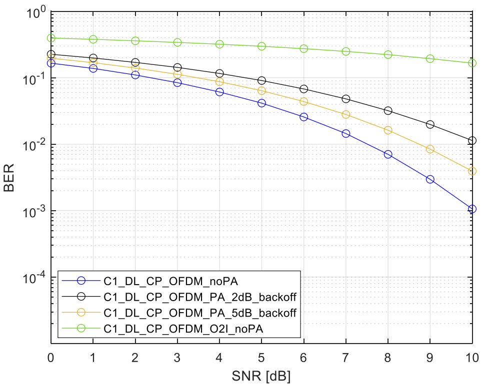	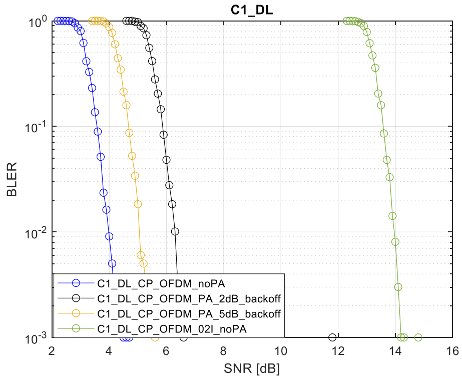
WOLA-OFDM	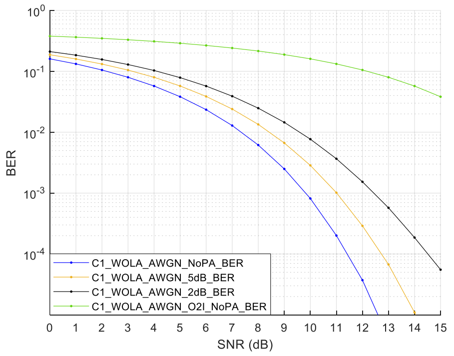	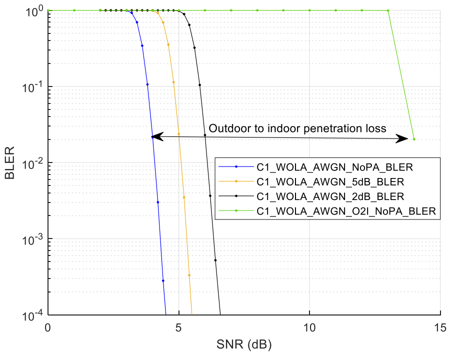
DFT-s-OFDM	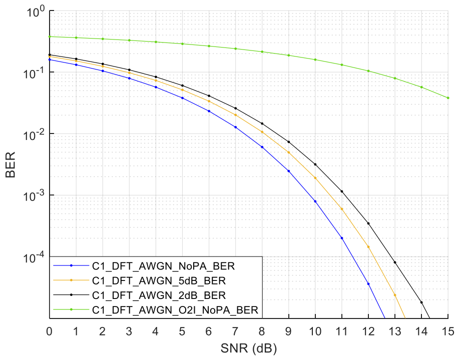	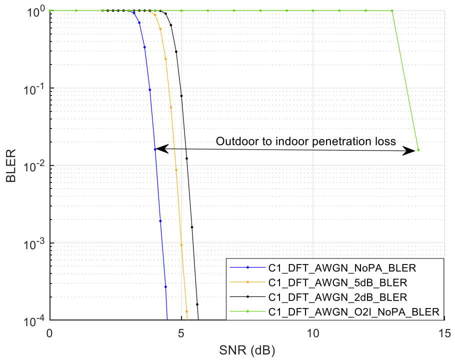

UFMC

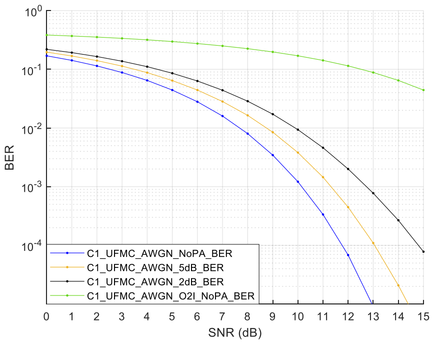

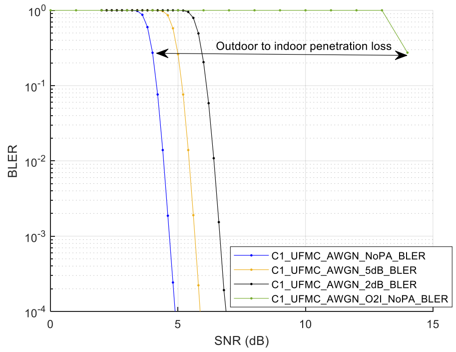

BF-OFDM

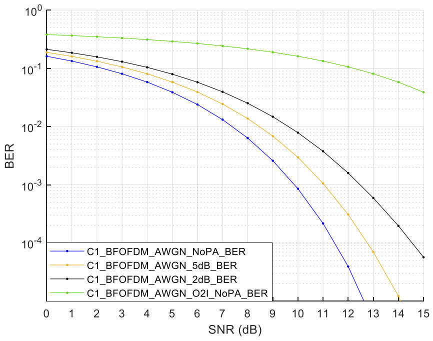

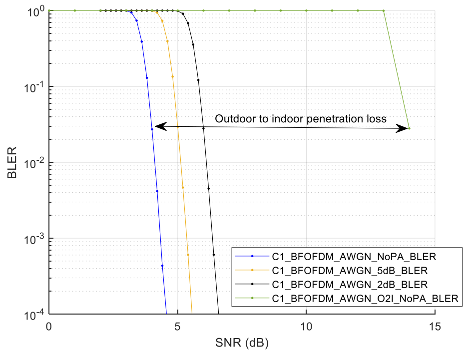

F-OFDM (QCM)

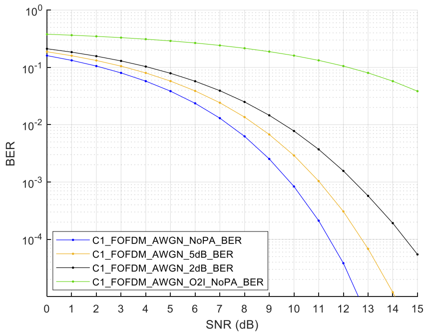

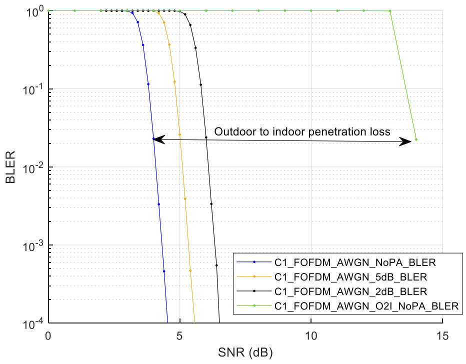

F-OFDM (TH-SIX)

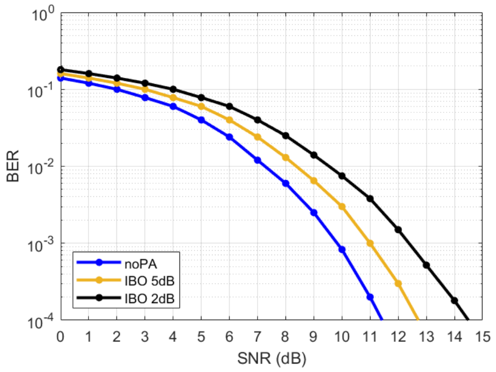

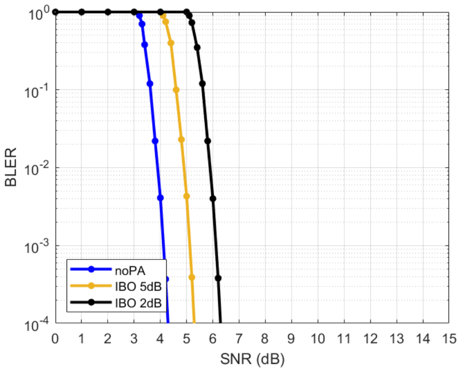

OTFS	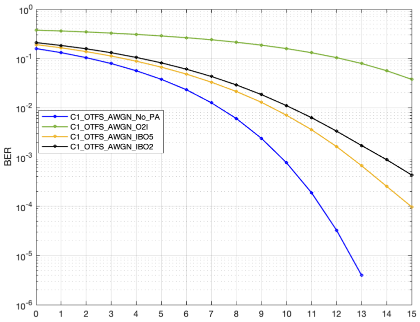	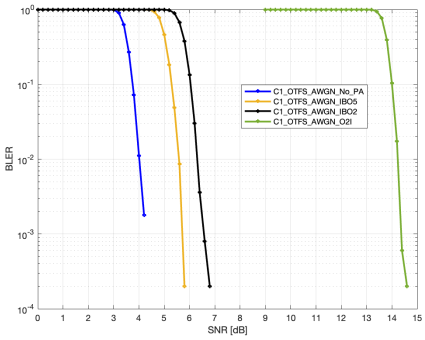
	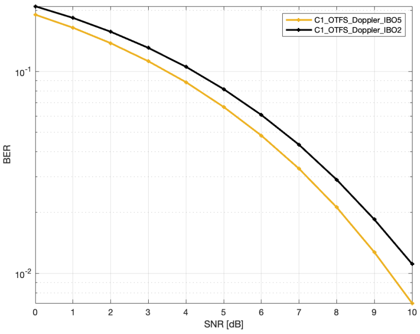	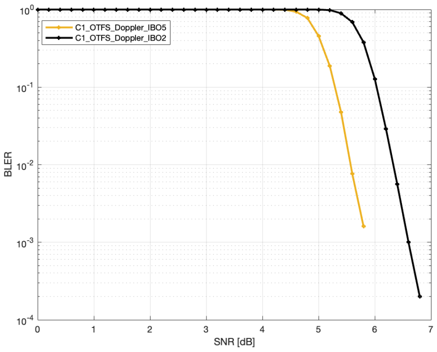

The presented results in Table 33 show a consistent relationship between BER/BLER estimates with the PAPR profile across OFDM-based alternatives. In other words, CP-OFDM, WOLA, UFMC, BF, and F-OFDM degrade similarly following PA stage, in line with their resemblant PAPR characteristics. In contrast, DFT-s-OFDM provides superior bit error rates and block error rates at the evaluated backoff values relative to other OFDM variants because of the comparably lower PAPR-related waveform distortion. Regarding the OTFS, the BER and the BLER have been computed in case of AWGN channel and considering the differential Doppler shift. It can be seen that it follows the same trend of OFDM based waveforms. However, unlike OFDM-based waveforms, it is resilient to Doppler shift and essentially offers the same performance as in the AWGN scenario.

6.3.2 C-band Scenario C1 (uplink)

The complementary uplink C1 scenario is composed of identical parameters, if not for the adoption of the UE PA model and a ~ 50% lower coding rate to cope with the typically inferior transmit specifications of UEs.

TABLE 34: PAPR AND PSD FOR SCENARIO C1 IN UL

	PAPR	*Power Spectral Density*
CP-OFDM	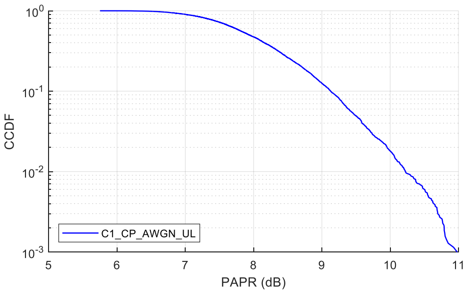	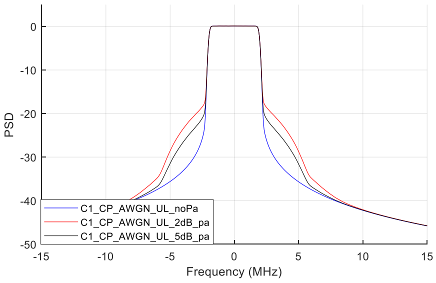

WOLA-OFDM	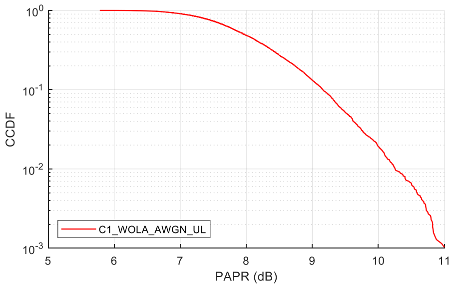	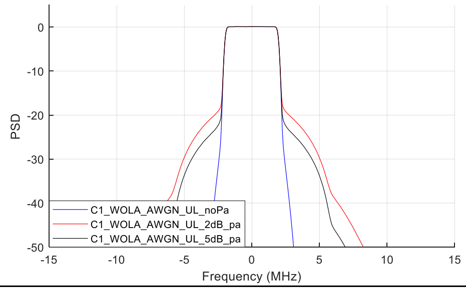
DFT-s-OFDM (QCM)	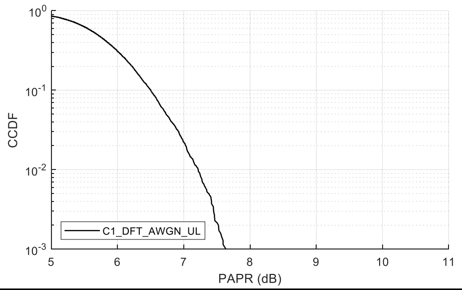	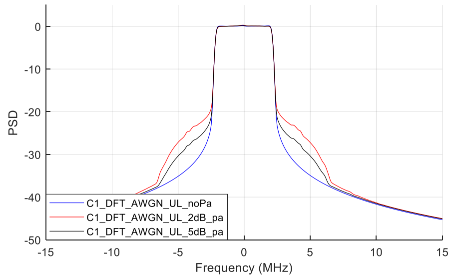
DFT-s-OFDM (ERIS)	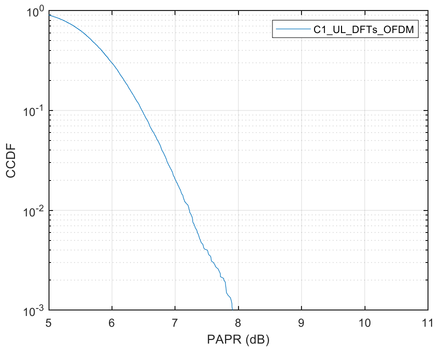	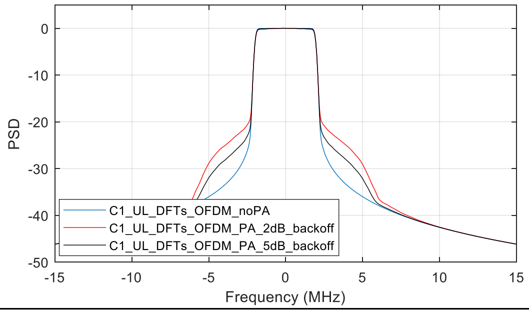
UFMC	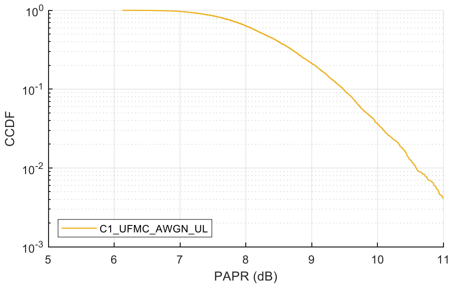	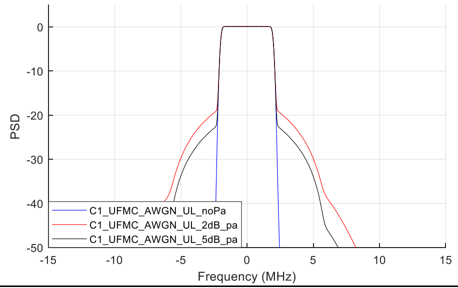
BF-OFDM	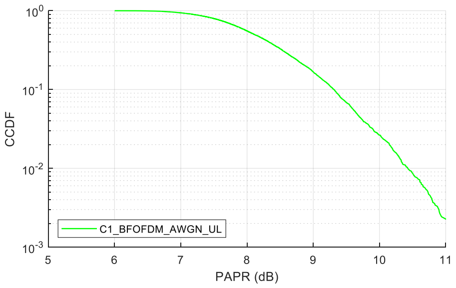	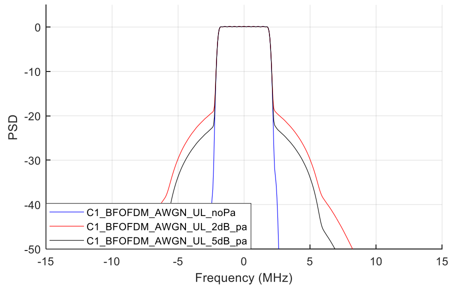

Co-funded by the European Union

F-OFDM	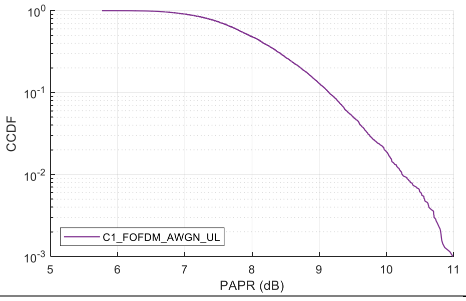	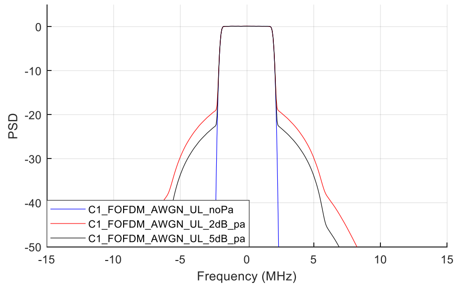
OTFS	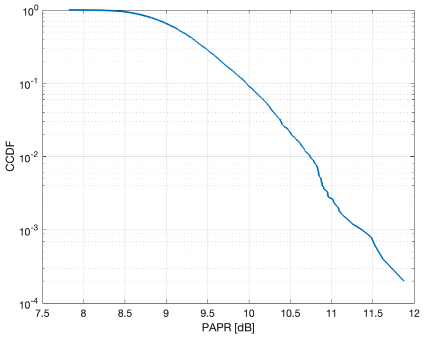	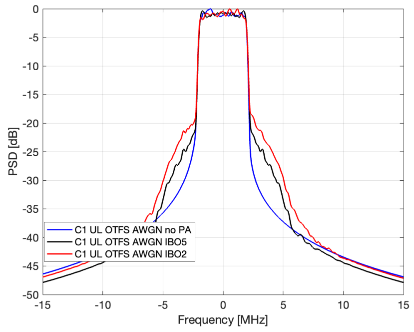

As evidenced from Table 34, both PAPR and out-of-band emission trends remain unchanged with respect to the observed ones in the downlink counterpart over all OFDM-based waveforms and OTFS. Nevertheless, out-of-band emissions decay rapidly in comparison to those in the downlink scenario, even adopting PA models. As an example, the power density falls below the -50 dB reference after 5 MHz of the spectrum allocation (unlike 8 MHz in the downlink case) for most filtered OFDM variants relying on a backoff of 5 dB.

TABLE 35: BER AND BLER FOR SCENARIO C1 IN UL

	BER	*BLER*
CP-OFDM	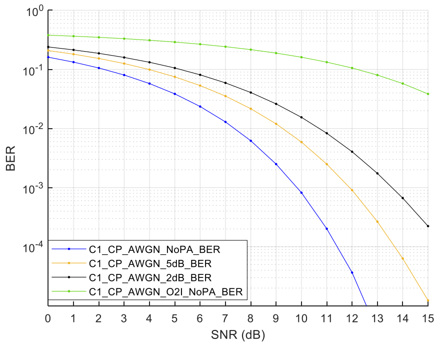	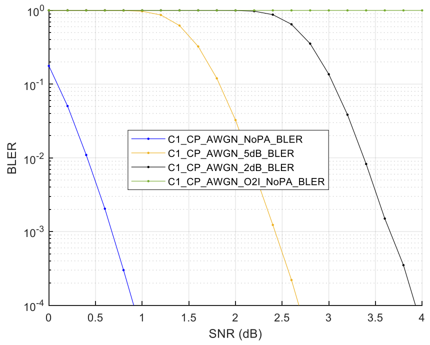
WOLA-OFDM	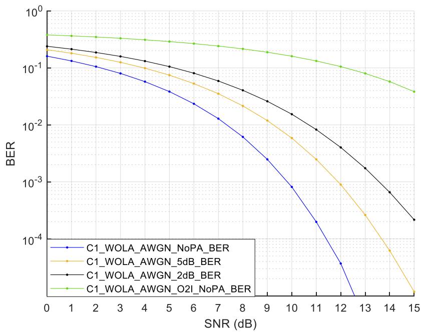	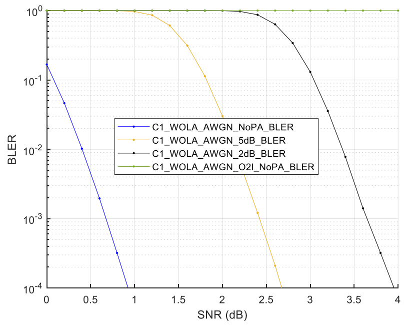

DFT-s-OFDM (QCM)

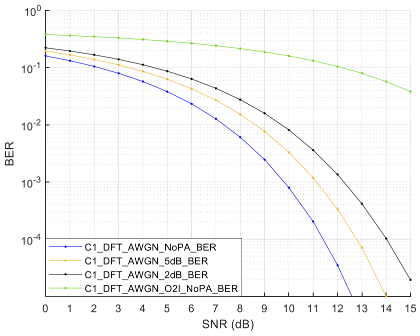

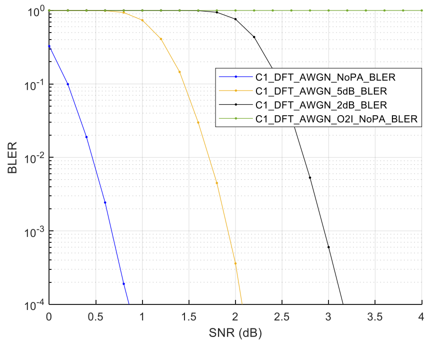

DFT-s-OFDM (ERIS)

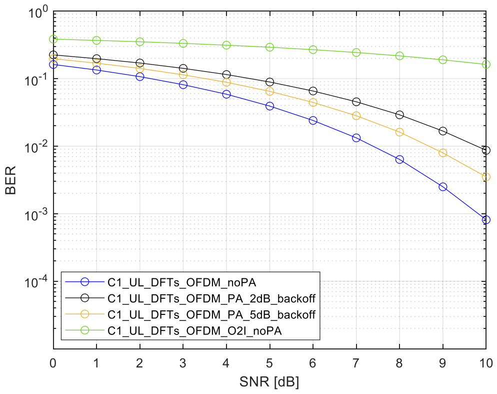

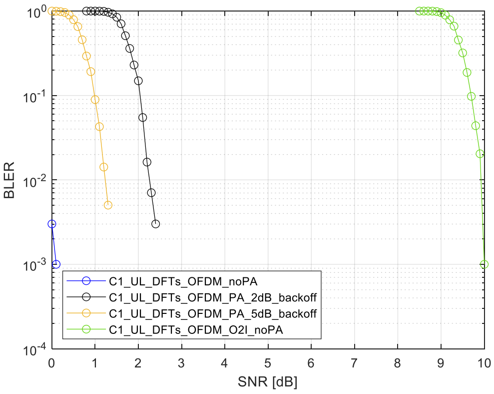

UFMC

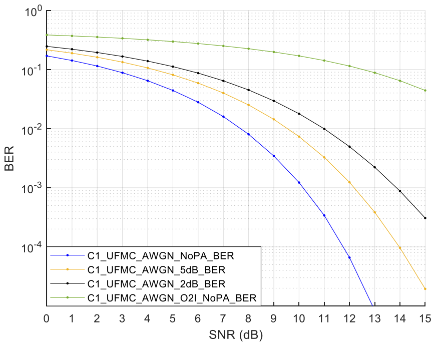

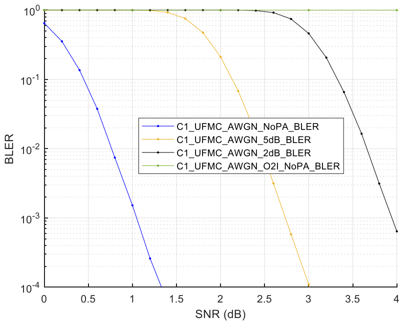

BF-OFDM

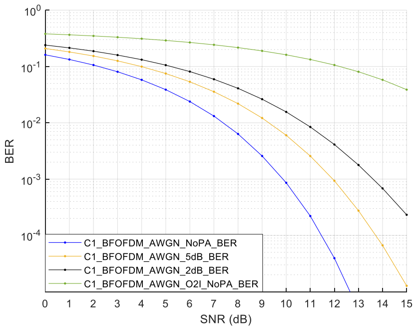

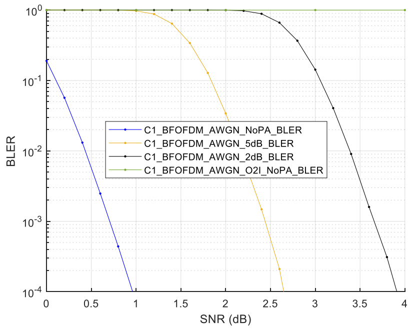

F-OFDM

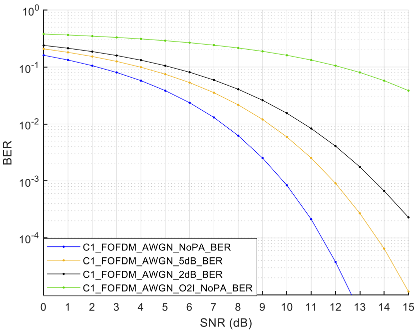

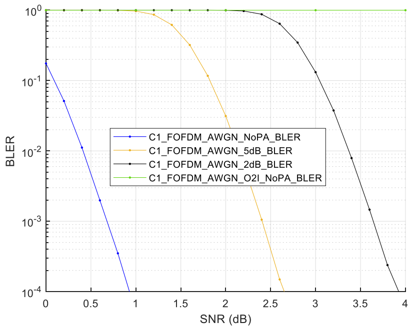

OTFS	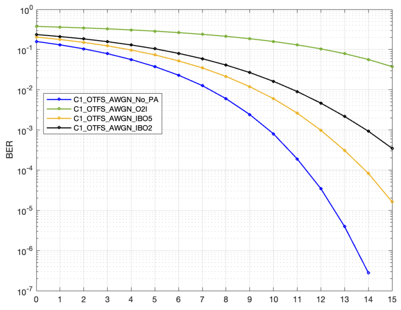	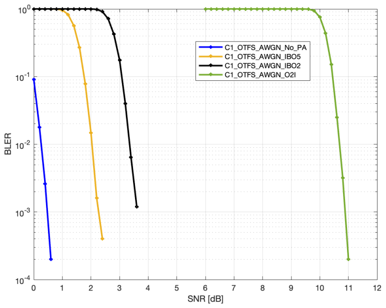
	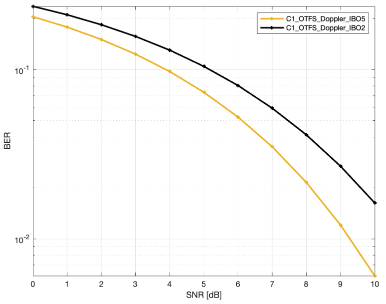	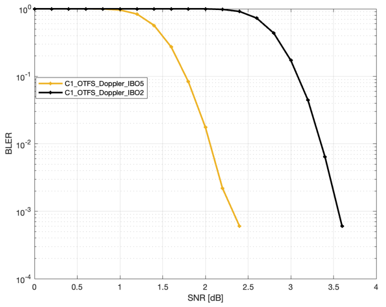

Notably, the BER estimates in uplink show a slight degradation of close to 1 dB with respect to downlink ones owing to the lower compression point of the UE PA relative to the respective satellite one. However, previously observed BER and BLER trends remain unchanged relative to the downlink case, despite a gain in BLER of 3-4 decibels explained by the improved uplink coding rate (as can been from Table 35).

6.3.3 C-band Scenario C3 (downlink)

Contrary to the previous scenarios, the C3 scenario is evaluated over a variety of fading channels, as aforementioned, a LoS TDL-D fading channel with a delay spread of 50 ns, a NLoS TDL-A fading channel with a delay spread of 50 ns, and a NLOS TLD-A fading channel with a delay spread of 100 ns. Additionally, a 10 times larger bandwidth is considered for scenario C3 relative to C1. Results are illustrated in Table 36.

TABLE 36: BER AND BLER FOR SCENARIO C3 IN DL

	BER	*BLER*
CP-OFDM (QCM)	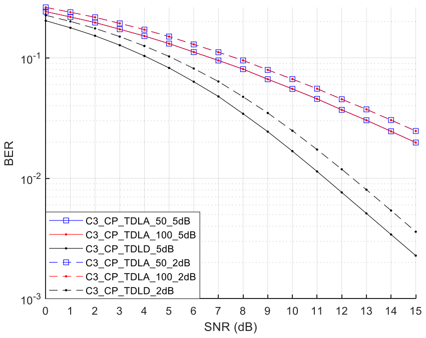	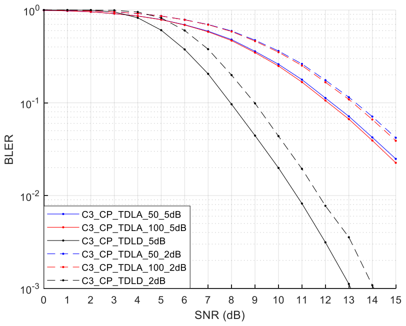

CP-OFDM (ERIS)

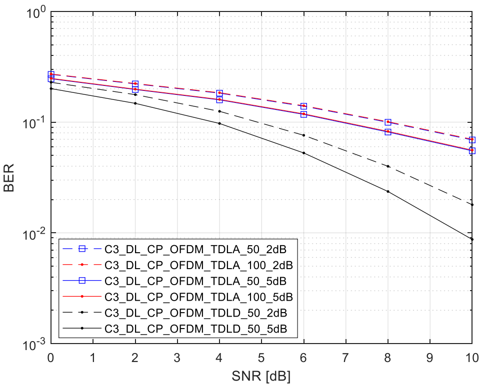

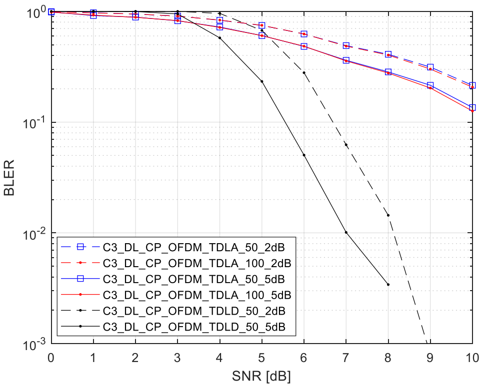

WOLA-OFDM

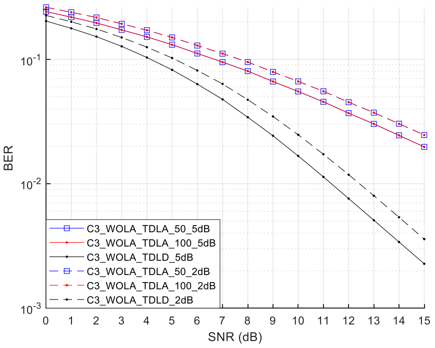

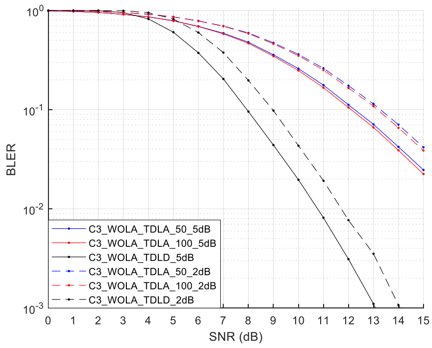

DFT-s-OFDM

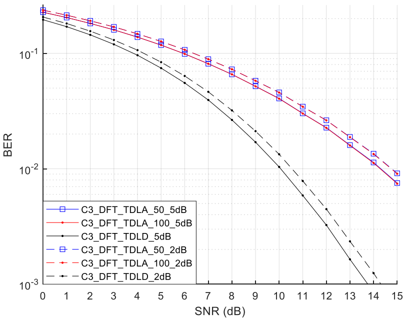

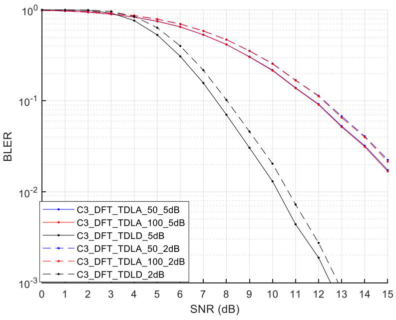

UFMC

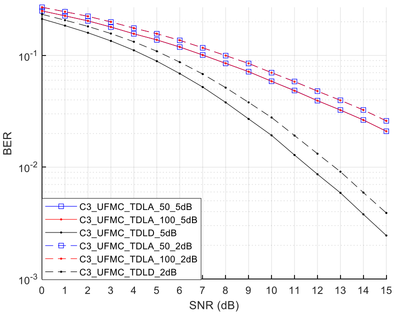

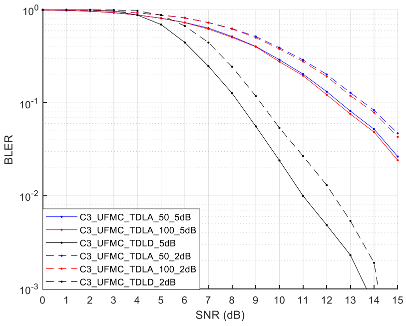

BF-OFDM

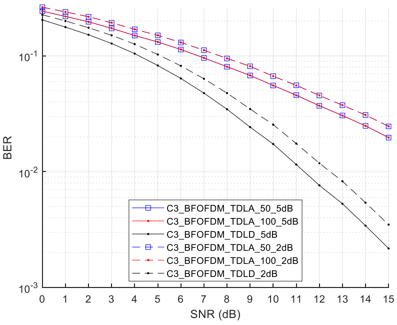

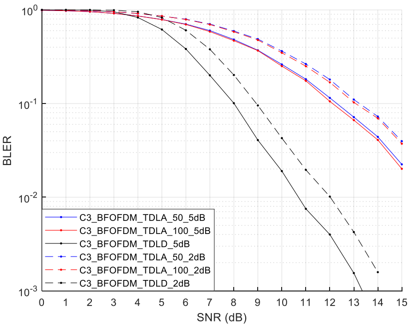

F-OFDM	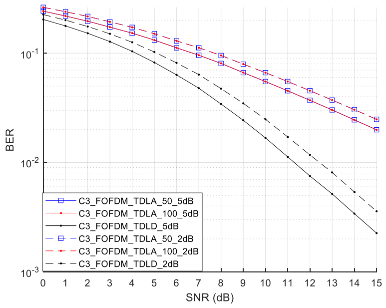 	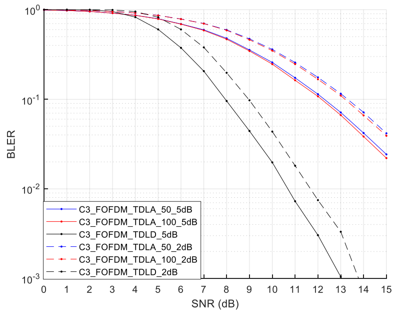
OTFS	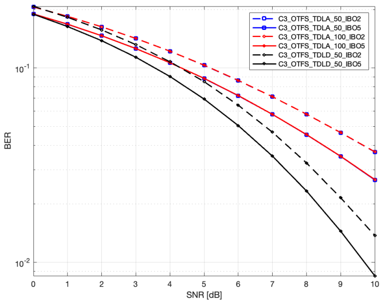 	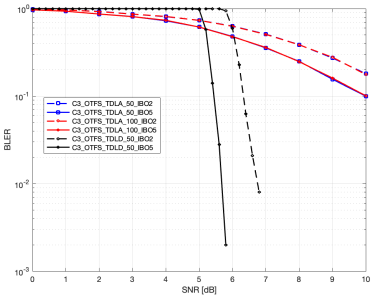

In alignment with the observations over the calibration results section, and in every case, the TDL-D channel model outperform the TDL-A alternative due to the increased reliability of the LoS component. Likewise, the DFT-s-OFDM waveform variant exposes an improved performance thanks to its lower PAPR enabling the PA to operate away from saturation to a greater extent. The OTFS waveform provides better performance than the OFDM based waveforms thanks to the sparse representation of the channel in delay and Doppler domain. However, this gain in performance comes at the expense of the complexity of the MP receiver, which is proportional to number of delay and Doppler bins, the cardinality of the modulation, and the number of iterations required to converge the MP (i.e., 200 for these channels).

6.3.4 C-band Scenario C3 (uplink)

The scenario C3 in uplink differs from the downlink counterpart mainly on the adopted PA model and on the ~50% lower coding rate. Table 37 summarizes the BER/BLER results over the considered waveform variants.

TABLE 37: BER AND BLER FOR SCENARIO C3 IN UL

	BER	*BLER*
CP-OFDM	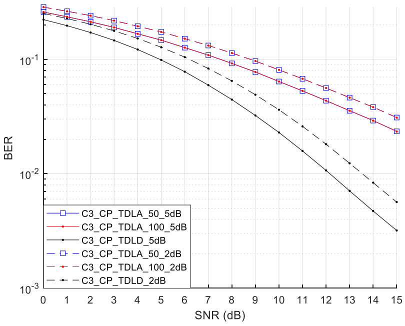 	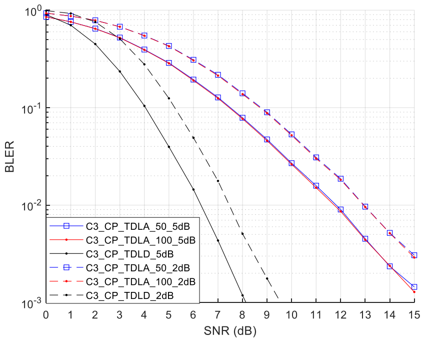

Co-funded by
the European Union

WOLA-OFDM	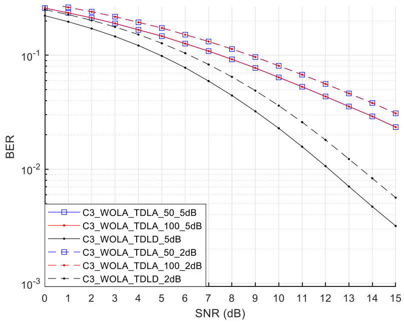	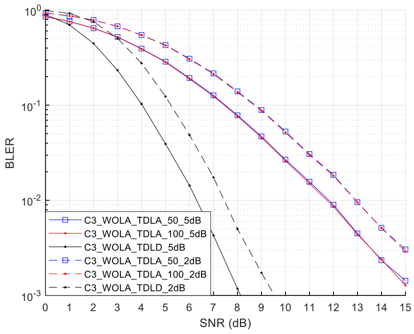
DFT-s-OFDM (QCM)	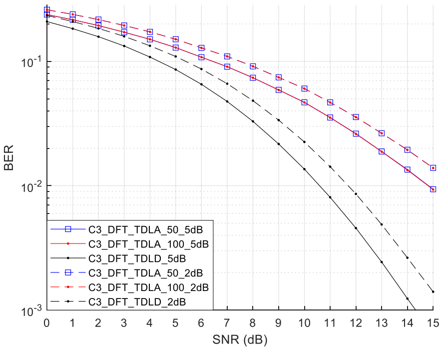	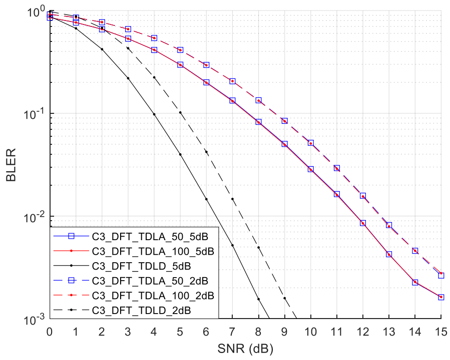
DFT-s-OFDM (ERIS)	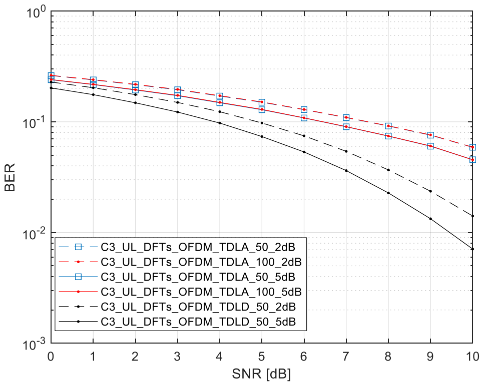	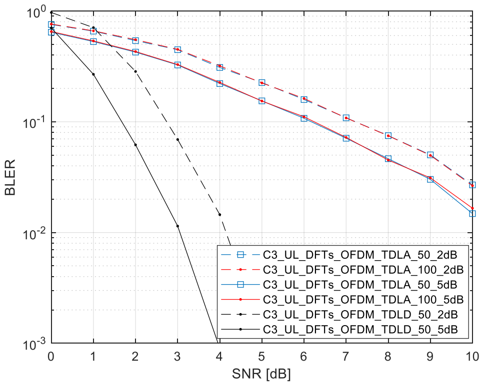
UFMC	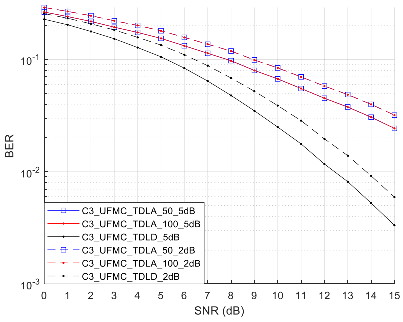	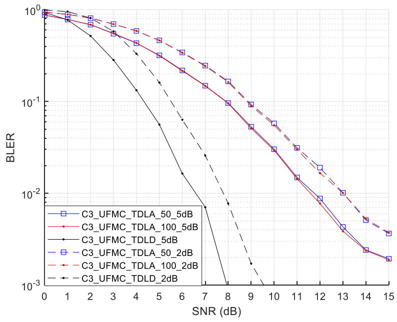

BF-OFDM	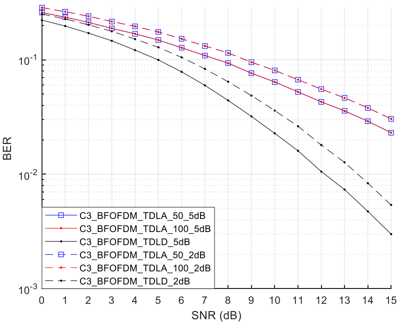	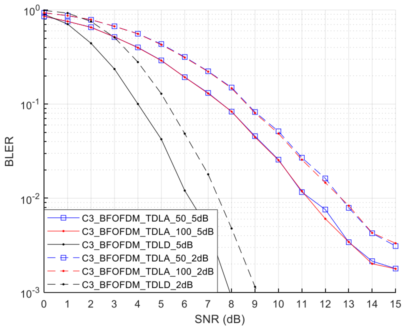
F-OFDM	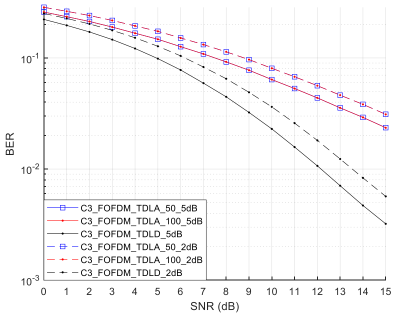	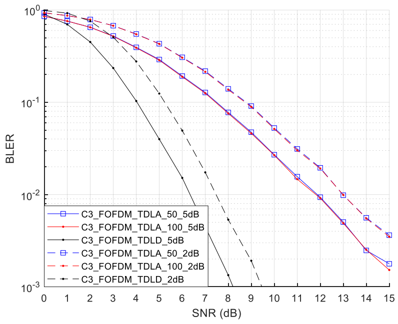
OTFS	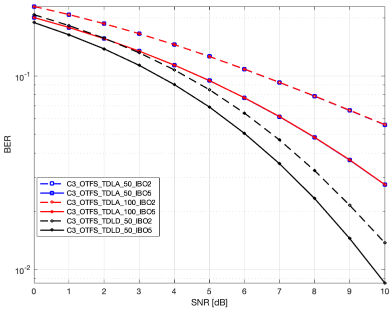	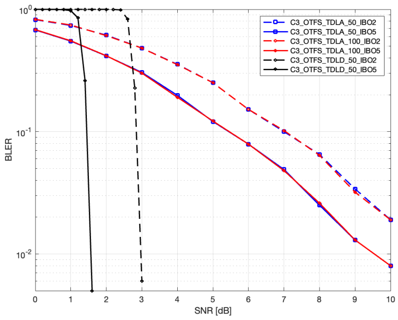

As observed in the calibration section, the BER estimates in uplink exhibit a minor detriment with respect to downlink because of the lower compression point of the UE PA relative to the satellite one. Other observed BER and BLER trends remain as in the downlink case. A gain in the BLER performance of 3-4 decibels is observed thanks to the improved uplink coding rate.

6.3.5 Q-band Scenario Q1 (downlink)

The adopted Q1 scenario encompasses a similar bandwidth allocation as in the preceding scenario C3, unlike its increased subcarrier spacing of 120 kHz. As pointed out, Q-band satellite PA suffers of higher phase distortion relative to other models assumed for the current deliverable. Phase noise is further considered as it becomes especially restrictive in this band.

TABLE 38: PAPR AND PSD FOR SCENARIO Q1 IN DL

	PAPR	*Power Spectral Density*

Co-funded by the European Union

CP-OFDM (QCM)	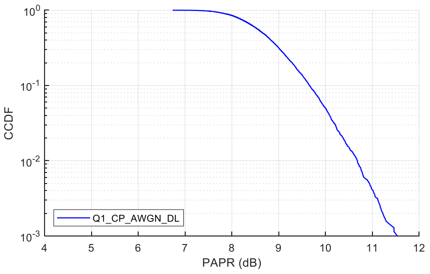	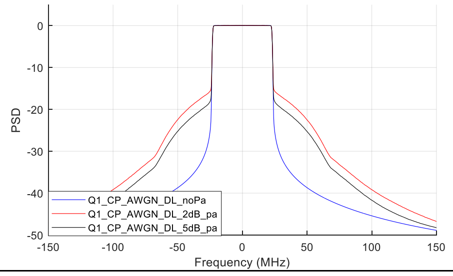
CP-OFDM (ERIS)	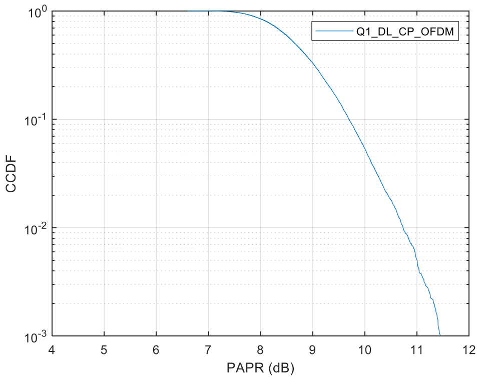	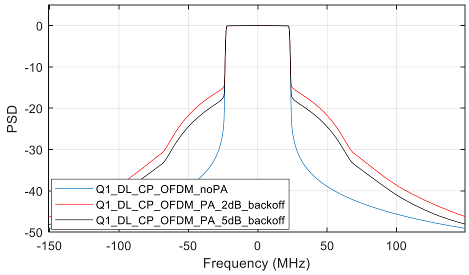
WOLA-OFDM	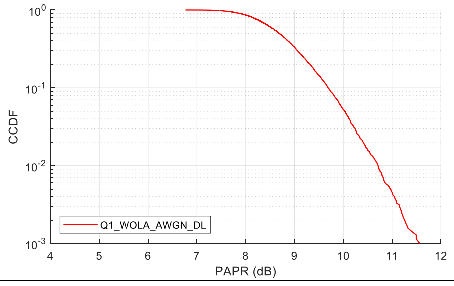	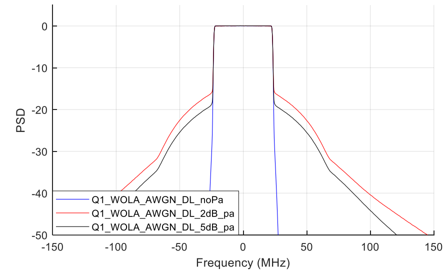
DFT-s-OFDM	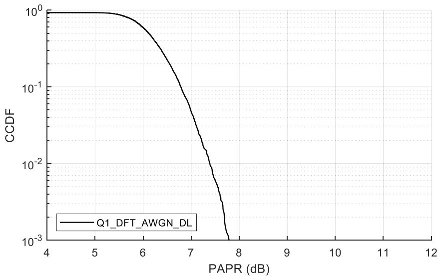	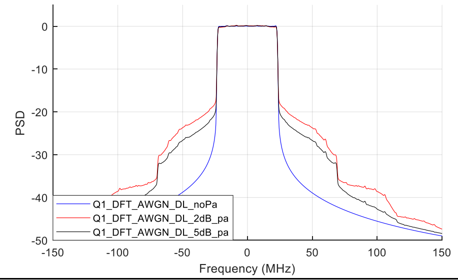
UFMC	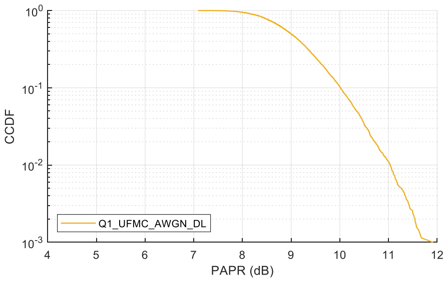	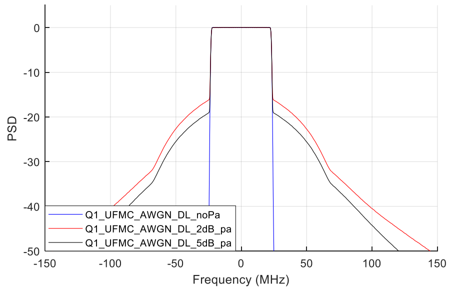

BF-OFDM	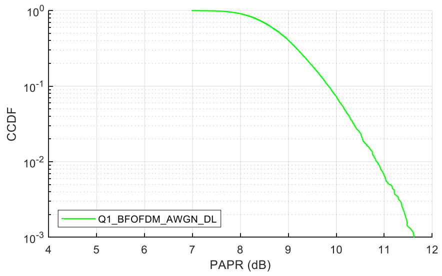	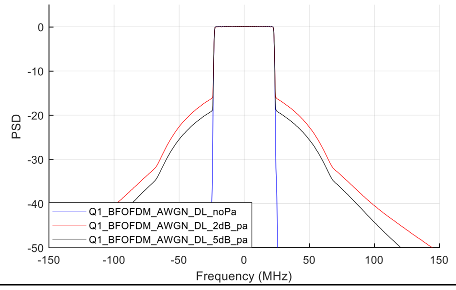
F-OFDM	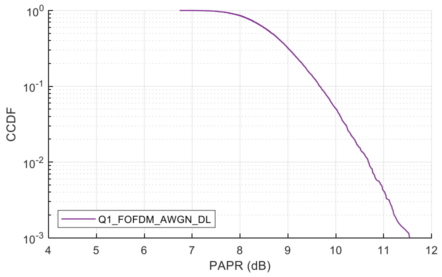	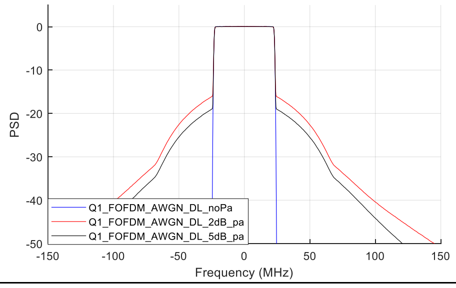
OTFS	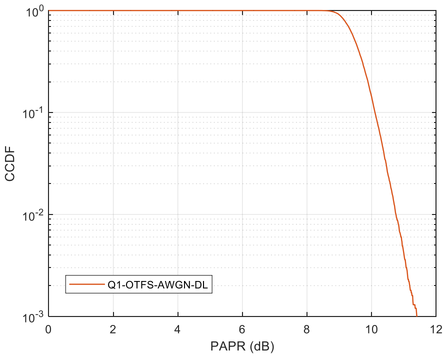	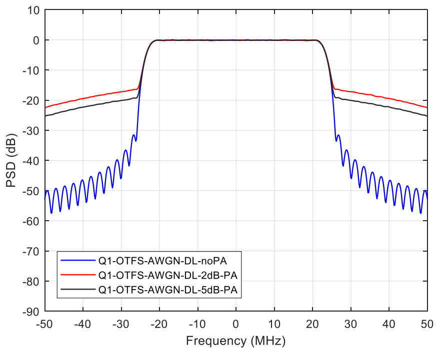

As evidenced from Table 38, pulse shaped OFDM variants, i.e., WOLA, UFMC, BF and F-OFDM, present greater out-of-band emission suppression with their power density falling below -50 dB less than 5 MHz away when neglecting the impact of PA. On the contrary, CP and DFT spread variants require a gap of at least 25 MHz if the -40 dB crossing is assumed a reference under similar circumstances. Similar out-of-band emissions are observed in all cases after the PA stage regardless the waveform specifications.

TABLE 39: BER AND BLER FOR SCENARIO Q1 IN DL

	BER	*BLER*
CP-OFDM (QCM)	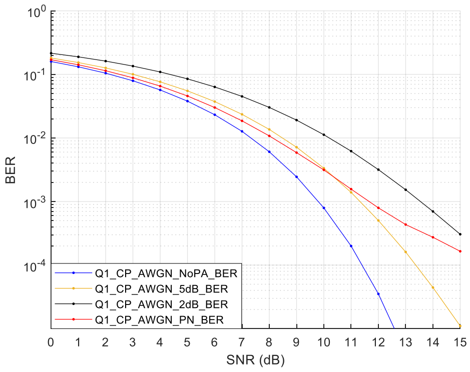	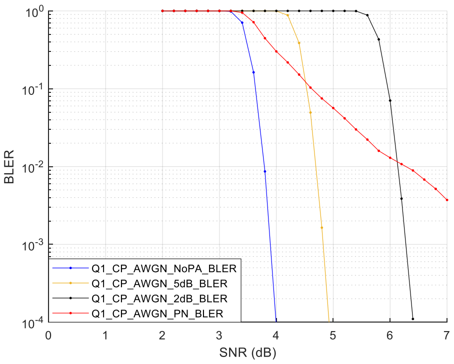

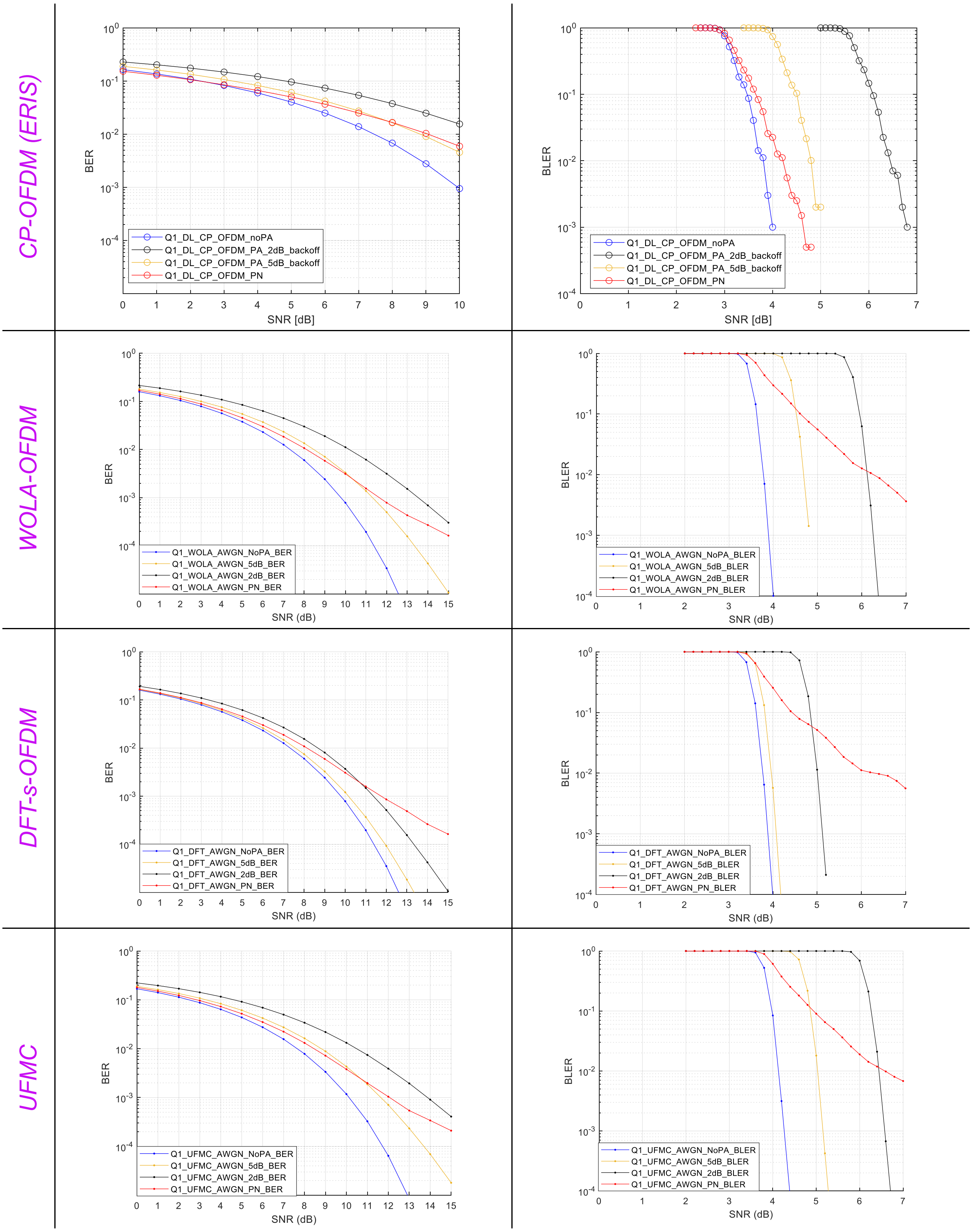
CP-OFDM (ERIS)
WOLA-OFDM
DFT-s-OFDM
UFMC
BER
BLER
SNR [dB]
SNR (dB)
Q1_DL_CP_OFDM_noPA
Q1_DL_CP_OFDM_PA_2dB_backoff
Q1_DL_CP_OFDM_PA_5dB_backoff
Q1_DL_CP_OFDM_PN
Q1_WOLA_AWGN_NoPA_BER
Q1_WOLA_AWGN_5dB_BER
Q1_WOLA_AWGN_2dB_BER
Q1_WOLA_AWGN_PN_BER
Q1_WOLA_AWGN_NoPA_BLER
Q1_WOLA_AWGN_5dB_BLER
Q1_WOLA_AWGN_2dB_BLER
Q1_WOLA_AWGN_PN_BLER
Q1_DFT_AWGN_NoPA_BER
Q1_DFT_AWGN_5dB_BER
Q1_DFT_AWGN_2dB_BER
Q1_DFT_AWGN_PN_BER
Q1_DFT_AWGN_NoPA_BLER
Q1_DFT_AWGN_5dB_BLER
Q1_DFT_AWGN_2dB_BLER
Q1_DFT_AWGN_PN_BLER
Q1_UFMC_AWGN_NoPA_BER
Q1_UFMC_AWGN_5dB_BER
Q1_UFMC_AWGN_2dB_BER
Q1_UFMC_AWGN_PN_BER
Q1_UFMC_AWGN_NoPA_BLER
Q1_UFMC_AWGN_5dB_BLER
Q1_UFMC_AWGN_2dB_BLER
Q1_UFMC_AWGN_PN_BLER

BF-OFDM

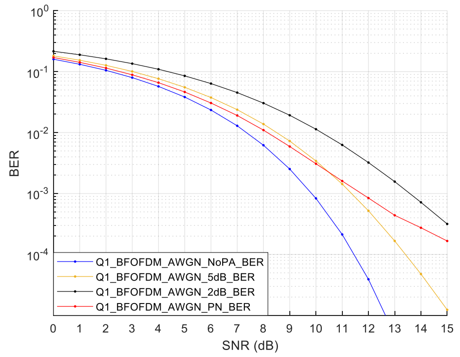

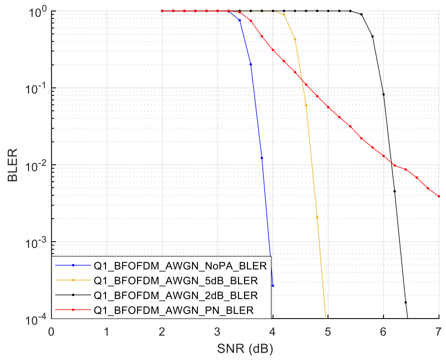

F-OFDM

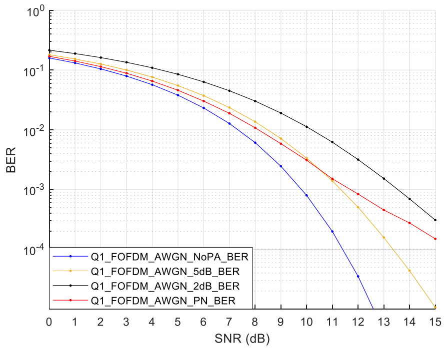

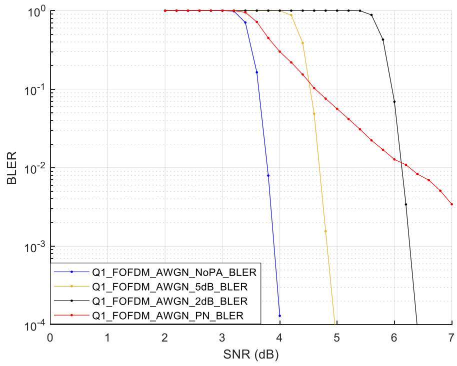

OTFS

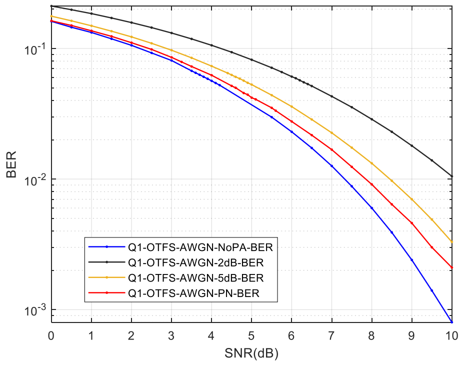

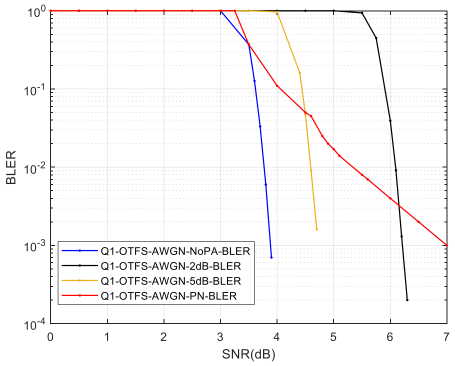

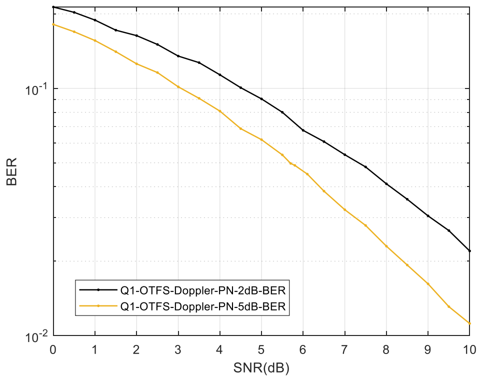

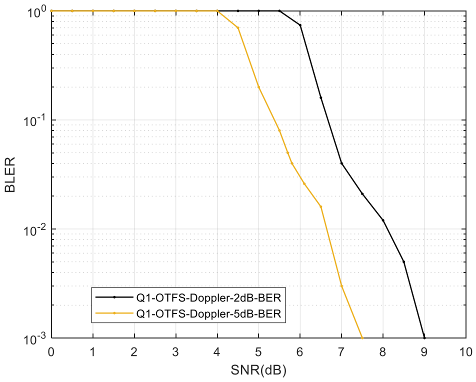

Both BER and BLER estimates (Table 39) show good alignment of OFDM variants in every case, except for the DFT spread alternative that sees an improvement in PA related evaluations because of its reduced PAPR. The performance over the phase noise imperfection is evidenced identical over every OFDM variant.

6.3.6 Q-band Scenario Q1 (uplink)

As aforementioned, the adopted UE PA model presents better amplitude and phase distortion characteristics relative to the satellite one in the Q band. The code rate is decreased by ~50% in uplink relative to downlink in alignment with simulation specifications. Additionally, unlike in downlink for scenario Q1, the return phase noise profile is adopted for uplink. The PAPR and PSD are shown in Table 40, while BER and BLER performance are illustrated in Table 41.

TABLE 40: PAPR AND PSD FOR SCENARIO Q1 IN UL

	PAPR	*Power Spectral Density*
CP-OFDM	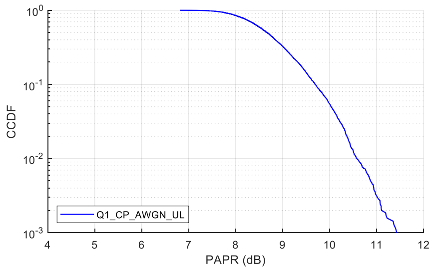	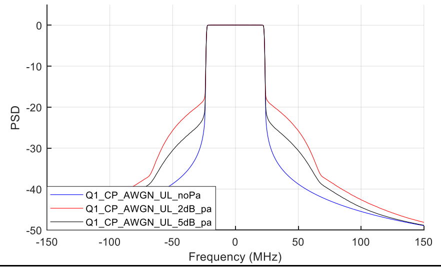
WOLA-OFDM	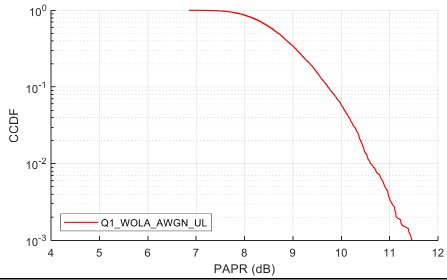	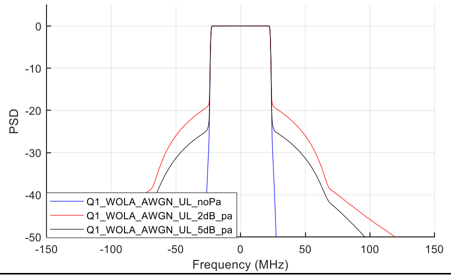
DFT-s-OFDM	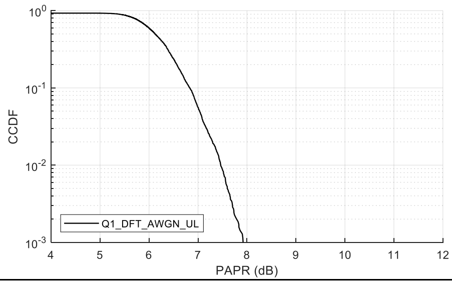	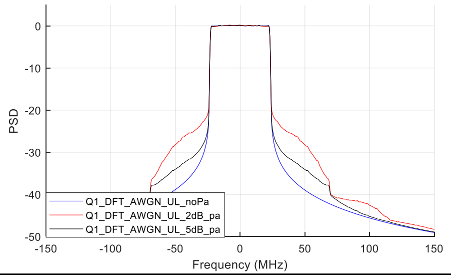
DFT-s-OFDM (ERIS)	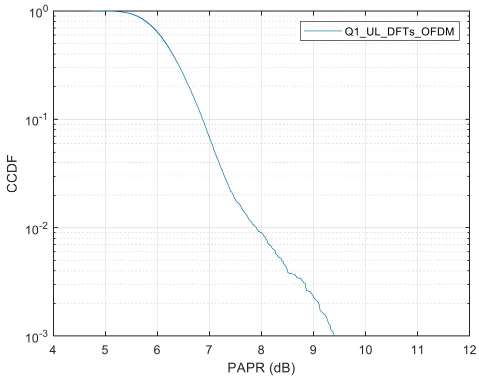	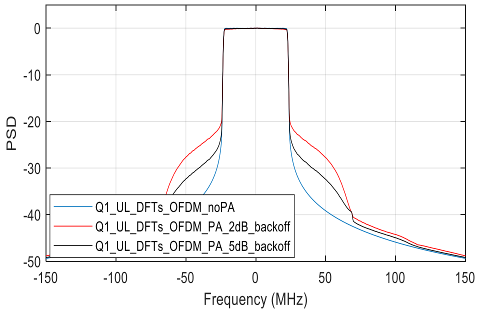

Co-funded by the European Union

UFMC	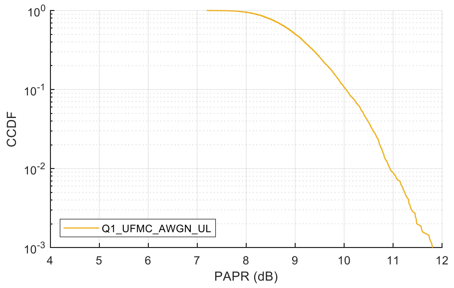	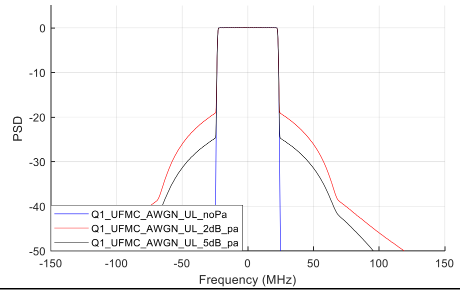
BF-OFDM	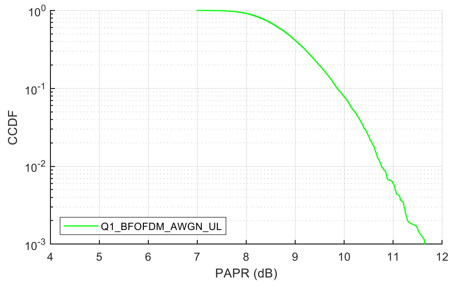	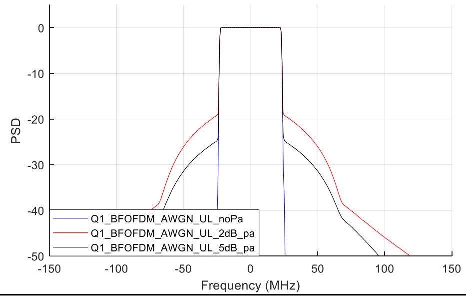
F-OFDM	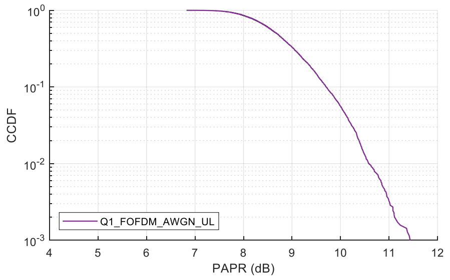	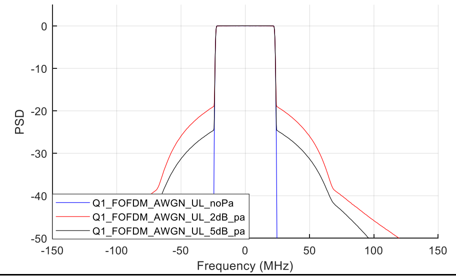
OTFS	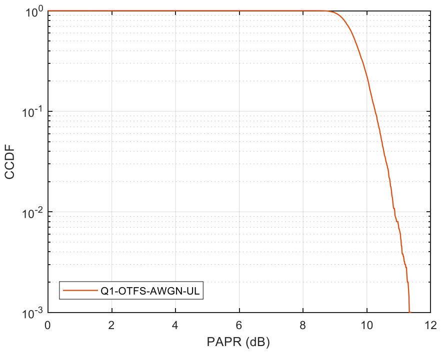	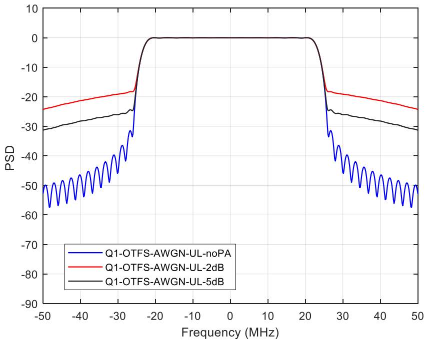

The improved UE PA specifications translate into a reduction of approximately 5 decibels in the spectra regrowth in adjacent channels relative to the downlink scenario Q1 over all OFDM variants. The DFT-spread OFDM variant sees a further improvement of around 5 decibels relative to OFDM-based alternatives.

Co-funded by the European Union

TABLE 41: BER AND BLER FOR SCENARIO Q1 IN UL

	BER	*BLER*
CP-OFDM	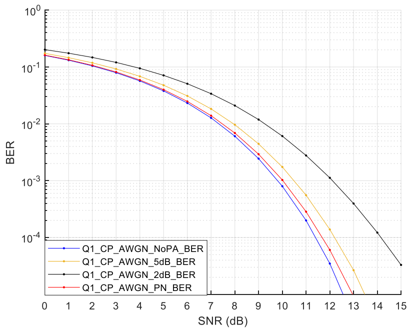	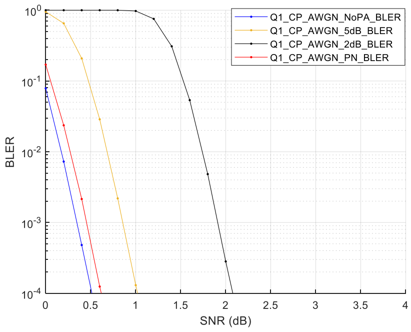
WOLA-OFDM	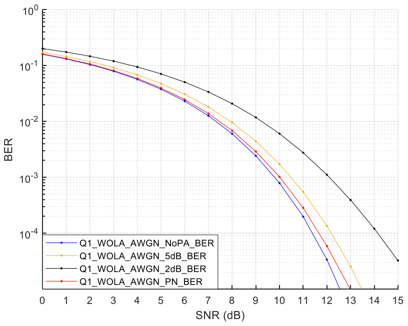	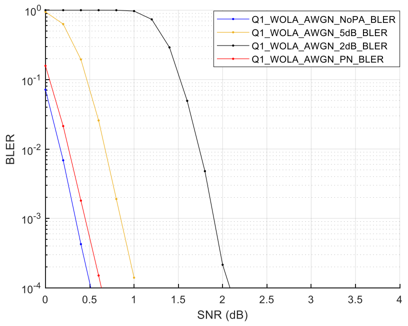
DFT-s-OFDM (QCM)	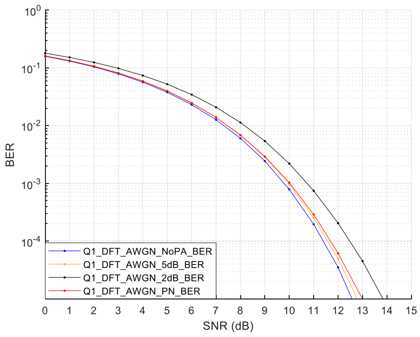	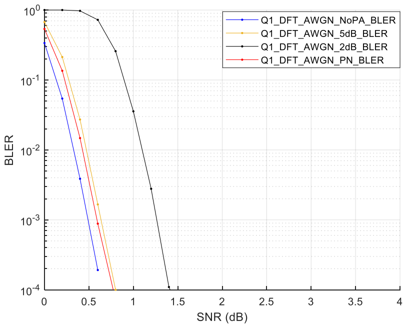
DFT-s-OFDM (ERIS)	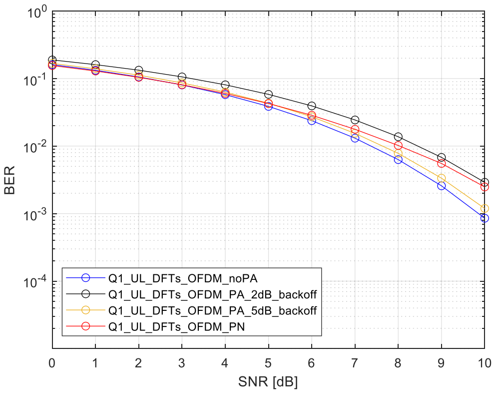	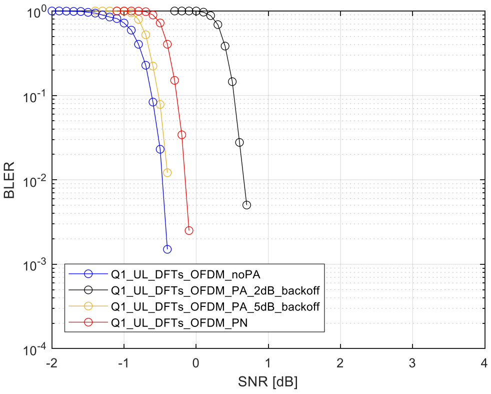

UFMC

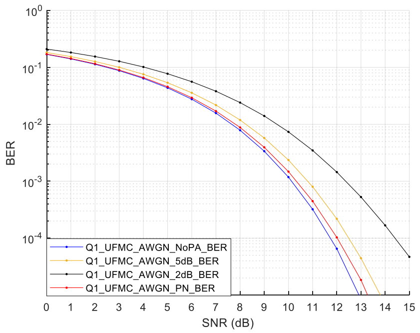

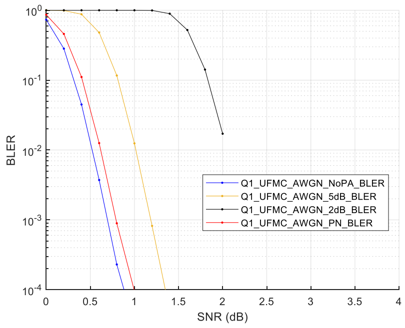

BF-OFDM

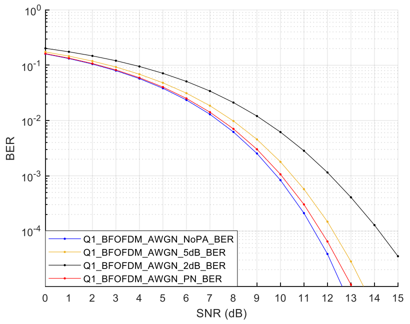

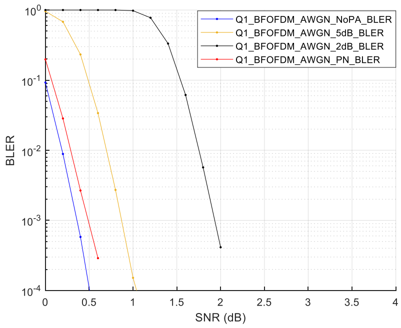

F-OFDM

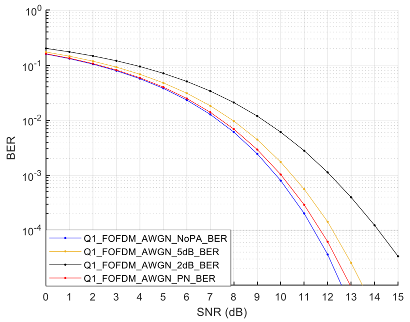

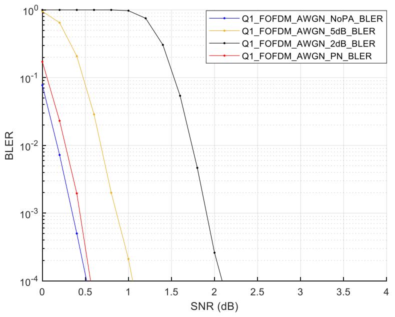

OTFS

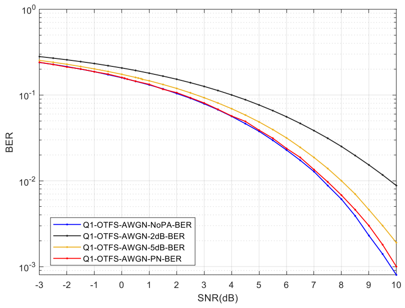

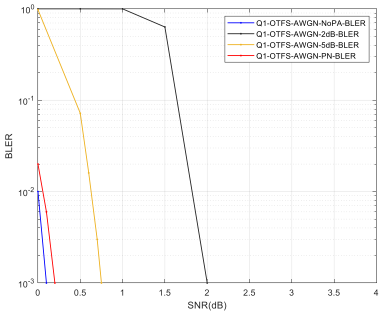

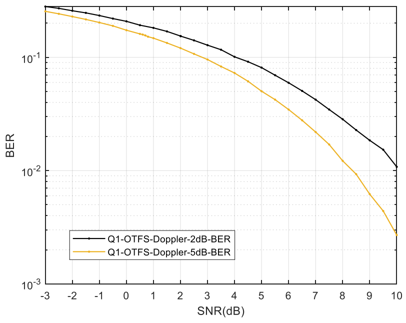

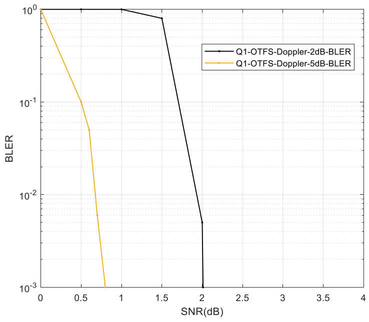

6.4 OBSERVATION

The previous sub-section presented the outcomes of CP-OFDM, WOLA-OFDM, DFT-s-OFDM, F-OFDM, BF-OFDM, UFMC, and OTFS across various scenarios. Notably, different partners analysed same waveforms, and the results were consistent, underscoring the success of the calibration process. Some differences in the BLER can be observed, attributed to the LDPC algorithm. As previously mentioned, receiver optimization has not been addressed in the current release of the deliverable and will be investigated in the final version. On the other hand, the BER, evaluated before the LDPC decoding, is consistent across partners, facilitating the evaluation and comparison of the waveforms.

Regarding the OTFS, it is possible to note that the BER/BLER decreases with the increment of SNR as expected. The best performance is achieved with the cases with no hardware imperfections (i.e., no PA and no PN). The increment in the IBO from 2 dB to 5 dB improves the performance in the simulated scenarios as it leads to better linearity of the PA, which can reduce distortion and ISI in the transmitted signal. Due to the robustness of OTFS to phase noise, the degradation of the performance is moderate. The PAPR of the OTFS is approximately like that of the OFDM-based waveforms. Hence, it can be considered high. OTFS (like OFDM-based waveforms) introduces interference to the neighbouring bands and hence pulse shaping, or guard bands is also needed for the OTFS to reduce the out of band interference. Bearing this in mind, in the Q band scenario, the OTFS scheme shapes the subcarriers with a SRRC filter with a roll-off factor of 10%. The resulting PSDs of the system with different schemes reveal that the PA introduces significant distortion and spectral broadening to the signal.

Overall, OFDM-based waveforms evidence nearly identical BER/BLER performance in AWGN. Likewise, out-of-band emissions are seemingly identical down to -50 dB relative to the PSD at the allocated bandwidth for filtered OFDM variants, i.e., WOLA, UFMC, BF and F-OFDM, when a HPA model is not considered. On the other hand, CP and DFT-spread alternatives present higher emissions as they intrinsically rely on sharp rectangular pulses with a large spectral regrowth. Notably, all OFDM-based waveforms evidence similar out-of-band emissions when the HPA is enabled. Nonetheless, DFT-s-OFDM exposes slightly lower PA-related performance degradation due to its improved PAPR. Thus, additional PAPR reduction and PA predistortion techniques may be relevant of consideration in the following deliverable. Results show that mainly: PAPR, power amplifier specifications and input backoff drive the detriment observed on OOB emissions and BER/BLER performance in every case. Particularly, the smaller the input backoff, the greater the waveform compression and, with it, the performance loss. As evidenced, the lower the PAPR, the higher the robustness to compression. Also, the computational complexity increment related to UFMC and BF-OFDM does not seem supported by qualitative nor quantitative proportionate gains via the studied KPIs, e.g., relative to the lower-complexity WOLA-OFDM alternative. Hence, ACLR may be relied upon in the following deliverable to provide a more granular view of OOB emissions. F-OFDM competitive gains in OOB emissions are inherently hindered by the full-band nature of its employed filter, i.e., as it becomes restrictive if multi-user multiplexing in the frequency domain is to be considered.

After comparing the waveforms in terms of BLER, BER, PAPR, and PSD, we conclude Section 6 providing information on the complexity and the maturity of the waveforms. This analysis is reported in Table 42. Moreover, Table 42 has a fourth column, where we highlight the necessary modifications of the waveforms to meet the design features listed in Table 1. It is worth mentioning that these modifications refer to the waveform and not to the air interface. The complete assessment of the waveform features will be provided in the final deliverable.

The complexity is expressed qualitatively for the transmitter and the receiver of each waveform relative to that of conventional CP-OFDM, while the maturity is rated as follows:

- High, i.e., implemented in the standard;
- Medium, i.e., some prototype exist;
- Low, i.e., assessment by means of simulations or testing with simple assumptions.

TABLE 42: WAVEFORMS COMPLEXITY AND MATURITY

Waveform	**Complexity**	**Maturity**	**Need for further investigation**
CP-OFDM	Reference.	High (LTE, NR)	Combination of multiple techniques for simultaneous pulse shaping, PAPR reduction and PA predistortion may be necessary.
WOLA-OFDM	Low (transmitter): inexpensive additional weighting, overlapping and addition operations. Low (receiver): inexpensive additional weighting, overlapping and addition operations.	High (LTE)	PAPR reduction and/or PA predistortion techniques
DFT-s-OFDM	Medium (transmitter): additional DFT operation; radix-2 FFT not warranted. Medium (receiver): additional IDFT operation; radix-2 FFT not warranted.	High (LTE, NR)	Pulse shaping and PA predistortion techniques. Combining it with pulse-shaped waveform variants.
UFMC	High (transmitter): multiple additional FFT/IFFT operations per RB. Pulse predistortion for simplified receiver implementation. Low (receiver): little or no modification to receiver in spec required.	Medium [124]	PAPR reduction and/or PA predistortion techniques
BF-OFDM	High (transmitter): multiple additional operations (among which: IDFT, up-conversion) per RB; radix-2 FFT not warranted. Pulse predistortion for simplified receiver implementation. Low (receiver): little or no modification to receiver in spec required.	Medium [125]	PAPR reduction and/or PA predistortion techniques

F-OFDM	High (transmitter): complexity increase related to long filter length. Predistortion for simplified receiver implementation. Low (receiver): little or no modification to receiver in spec required.	High	PAPR reduction and/or PA predistortion techniques
OTFS	High (transmitter): ISFT and Heisenberg transforms. High (Receiver): SFT and Wigner transforms.	Low [126]	Pulse shaping, PAPR reduction, and/or PA predistortion techniques

7 CONCLUSIONS

This deliverable provides an initial analysis of the potential candidate waveforms for NTN in 6G that will be completed in the second release of this document, which will be issued at the end of the project, i.e., deliverable D4.5.

In this release of the document, the waveform features and KPIs under which the waveforms will be assessed have been defined, and a comprehensive state of the art of both standardized and non-standardized air interface has been conducted considering multi-carrier and single-carrier waveforms. The comparison between the satellite-native DVB air interface family, i.e., DVB-S2X and DVB-RCS2, and the NR air interface performed in the ETSI SES SCN framework [4] has been also included.

Based on the SoA analysis and on the ETSI SES SCN comparison results that showed that, although the DVB satellite native family is not a potential waveform candidate for NTN in 6G, certain air interface configurations and receiving algorithms used for the DVB satellite-native family can also be considered for OFDM-like waveforms in the context of NTN, we short-listed the candidate waveforms to be further evaluated in the NTN scenarios by numerical simulations into the following set:

- CP-OFDM
- WOLA-OFDM
- DFT-s-OFDM
- F-OFDM
- BF-OFDM
- UFMC
- OTFS

The preliminary simulation analysis of these waveforms, to be further extended in the next release of the document, shows that in AWGN OFDM-based waveforms exhibit nearly identical performance in terms of BER/BLER. Filtered OFDM variants such as WOLA, UFMC, BF, and F-OFDM show also similar out-of-band emissions down to -50 dB relative to the PSD at the allocated bandwidth, while CP and DFT-spread alternatives show higher emissions due to their reliance on sharp rectangular pulses that cause significant spectral regrowth.

When the HPA effects are considered at different IBO and OBO, all OFDM-based waveforms show similar out-of-band emissions, though DFT-s-OFDM demonstrates slightly less HPA-related performance degradation because of its reduced PAPR. Also, the increased computational complexity of UFMC and BF-OFDM does not seem justified by the qualitative and quantitative gains in the studied KPIs, compared to the lower-complexity WOLA-OFDM. Finally, F-OFDM's competitive advantage in OOB emissions is inherently limited by its full-band filter, which becomes restrictive when considering multi-user multiplexing in the frequency domain.

Coming to OTFS, the analysis shows that it provides similar performance to OFDM, except in scenario C3, where it outperforms OFDM thanks to its inherent robustness to the multipath. In scenario C1 and Q1, we provided results for the OTFS also in the presence of Doppler. However, this better performance comes at the expense of high complexity. Indeed, in all the cases a Message Passing Algorithm receiver has been adopted.

Co-funded by the European Union

In support of the waveform assessment and, possibly, of the future standardization actions, the activity has been also focused on an initial, again to be further extended in the second release of the document, analysis and definition of the channel models in the new frequency bands considered in the 6G-NTN project architecture [118]. In particular, the outcome of the ray tracing simulations showed that in C band and Q/V band, the Rice factor exhibits an increasing trend with elevation regardless of the propagation environment, and the opposite trend for the delay spread. The ray tracing results are in line with the observation that larger elevation always means greater LoS probability, i.e., the presence of a powerful, short-delayed received signal contribution, that exactly contributes to increase the Rice factor and to reduce the delay spread. Nonetheless, further investigations are still necessary, e.g. to extend the evaluation to angular dispersion (i.e. channel angle spread), and to improve the description of ground terminal antennas radiation pattern. In fact, isotropic radiators have been considered so far for the sake of simplicity, which is an oversimplified assumption in particular as far as Q and V bands are concerned. In the second release of the document, these assumptions will be removed, and more accurate ones will be adopted.

In conclusions, future work will address the following:

- Extension of the waveform analysis to those KPIs not yet addressed, e.g., ACLR.
- Prioritization and selection of the waveform based on the full fledge KPIs assessment.
- For the selected waveforms, we will consider the SNR ranges (provided by the link budget analysis carried out in WP3) and the channel propagation characteristics (defined in WP4) for the most relevant use cases (elaborated in WP2) and
    - Assessment of the robustness of the waveforms to the residual synchronization and channel estimation errors.
    - Explore Machine Learning (ML)-based end-to-end PHY techniques to further optimize the spectral efficiency, connection diversity, and system availability.
    - Test low bandwidth scenario (e.g., 200 kHz).
    - Perform analysis for the procedure at the PHY and MAC levels.
    - Study coverage improvements techniques to allow light indoor communications.
- Based on these outcomes, a further down selection and possible identification of potential waveform for the NTN in 6G will be performed.

Co-funded by the European Union

REFERENCES

[1] 3GPP TS 38.211 ‘NR Physical channel and modulation’ v18.2.0 (2024-03)

[2] 3GPP TS 38.300 ‘NR and NG-RAN Overall description; Stage-2’ v18.1.0 (2024-03)

[3] A. Bouttier, "A Flexible OFDM-Like DFT-s-OFDM Reference Symbol," 2020 10th Advanced Satellite Multimedia Systems Conference and the 16th Signal Processing for Space Communications Workshop (ASMS/SPSC), Graz, Austria, 2020, pp. 1-7

[4] ETSI TR 103.886 ‘Satellite Earth Station & Systems (SES); DVB-S2x/RCS2 versus 3GPP New Radio protocol technical comparison for broadband satellite systems’ v0.0.5 (2024-05)

[5] Qualcomm Incorporated, "5G Waveform and Multiple Access Techniques," 2015.

[6] Adoum, et.al., "A Comprehensive Survey of Candidate Waveforms for 5G, beyond 5G and 6G Wireless Communication Systems," *Open Journal of Applied Sciences,* pp. 136-161, 2023.

[7] Schaich, et.al., "Waveform contenders for 5G – OFDM vs. FBMC vs. UFMC," in *6th Intl. Symp. Comm., Control and Sig. Proc. (ISCCP)*, 2014.

[8] Schaich, et.al., "Waveform contenders for 5G – suitability for short packet and low latency transmissions," in *IEEE 79th Veh. Tech. Conf.*, 2014.

[9] Huawei and HiSilicon, "R1-162152 - OFDM based flexible waveform for 5G," 3GPP WDG RAN WG1 Mtg #84bis, 2016.

[10] Balint, et.al., "OFDM-Based Multi-Carrier Waveforms Performances in 5G," in *Intl. Symp. Electronics and Telecommunications (ISETC)*, 2018.

[11] B. Farhang-Boroujeny, "OFDM versus filter bank Multicarrier," *IEEE Signal Processing Magazine,* pp. 92-112, May 2011.

[12] Bouttier, "A Flexible OFDM-Like DFT-s-OFDM Reference Symbol," in *10th Advanced Satellite Multimedia Systems Conference and the 16th Signal Processing for Space Communications Workshop (ASMS/SPSC)*, Graz, Austria, 2020.

[13] Berardinelli, "Generalized DFT-s-OFDM waveforms without cyclic prefix," *IEEE Access,* pp. 4677-4689, 2018.

[14] R. Nissel and M. Rupp, "On pilot-symbol aided channel estimation in FBMC-OQAM," in *IEEE International Conference on Acoustics, Speech and Signal Processing (ICASSP)*, Shanghai, China, 2016.

[15] V. Durga and S. Anuradha, "On Channel Estimation in Universal Filtered Multi-Carrier (UFMC) System," in *Photonics & Electromagnetics Research Symposium - Spring (PIERS - Spring)*, Rome, Italy, 2019.

[16] Bellanger, et.al., "FBMC physical layer: a primer," PHYDYAS.

[17] Aminjavaheri, "Prototype filter design for FBMC in Massive MIMO Channels," in *IEEE Intl. Conf. on Communications (ICC)*, 2017.

[18] P. Singh and K. Vasudevan, "MIMO-FBMC Channel Estimation with Limited,

and Imperfect Knowledge of Channel Correlations," in *National Conference on Communications (NCC)*, Bangalore, India, 2019.

[19] D. M. M. T. M. Bellanger, "Lapped-OFDM as an alternative to CP-OFDM for 5G asynchronous access and cognitive radio," in *Vehicular Technology Conference (VTC Spring)*, 2015.

[20] Medjahdi, et.al., "On the Road to 5G: Comparative Study of Physical Layer in MTC Context," 2017.

[21] Demmer, David, et al. "Block-filtered OFDM: A novel waveform for future wireless technologies." 2017 IEEE International Conference on Communications (ICC). IEEE, 2017.

[22] E. Vakilian, "Universal-filtered multi-carrier technique for wireless systems beyond LTE," in *IEEE Globecom workshops*, 2013.

[23] Wild, et.al., "5G Air interface design based on universal filtered (UF-)OFDM," in *19th Intl. Conf. on Digital Sig. Proc.*, 2014.

[24] Ahmed, et.al., "Coexistence of UF-OFDM and CP-OFDM," in *IEEE 83rd Veh. Tech. Conf. (VTC Spring)*, 2016.

[25] Abdoli, et.al., "Filtered OFDM: A new waveform for future wireless systems," in *16th Intl Workshop on Signal Proc Advances in Wireless Comm (SPAWC)*, 2015.

[26] Huawei and HiSilicon, "R1-165425 - f-OFDM scheme and filter design," 3GPP TSG RAN WG1 Mtg #85, 2016.

[27] Michailow, et.al., "Generalized frequency division multiplexing for 5th generation cellular networks," *IEEE Trans. Communications,* pp. 3045-3061, 2014.

[28] Fettweis, et.al., "GFDM – Generalized frequency division multiplexing," in *IEEE 69th Veh. Tech. Conf. (VTC Spring 2009)*, 2009.

[29] Michailow, et.al., "Generalized frequency division multiplexing: analysis of an alternative multi-carrier technique for next generation cellular systems," in *Intl. Symp. Wireless Comm. Systems (ISWCS)*, 2012.

[30] Lamani, et.al., "Generalized frequency division multiplexing for 5G cellular systems: a tutorial paper".

[31] Berardinelli, et.al., "Generalized DFT-spread-OFDM as 5G waveform," *IEEE Communications Mag.,* pp. 99-105, November 2016.

[32] Berardinelli, "On the potential of zero-tail DFT-spread-OFDM in 5G networks," in *IEEE 80th Veh. Tech. Conf (VTC2014-Fall)*, 2014.

[33] Berardinelli, et.al., "On the sensitivity of zero-tail DFT-spread-OFDM to small bandwidth allocations," *IEEE Wireless Comm. Letters,* pp. 452-455, June 2018.

[34] Berardinelli, "Zero-tail DFT-spread-OFDM signals," in *IEEE Globecom Workshops*, 2013.

[35] Sahin, et.al., "An improved unique word DFT-spread OFDM scheme for 5G systems," in *IEEE Globecom Workshops*, 2015.

[36] Kumar, et.al., "A waveform for 5G: Guard interval DFT-s-OFDM," in *IEEE Globecom Workshops*, 2015.

Co-funded by
the European Union

[37] Jawhar, et.al., "A review of partial transmit sequence for PAPR reduction in the OFDM systems," *IEEE Access,* pp. 18021-18041, 2019.

[38] Jiang, et.al., "An overview: peak-to-average power ratio reduction techniques for OFDM signals," *IEEE Trans. Broadcasting,* pp. 257-268, 2008.

[39] Huang, et.al., "Out-of-band emission reduction and a unified framework for precoded OFDM," *IEEE Communications Mag.,* pp. 151-159, June 2015.

[40] Pawar, et.al., "Review of PAPR reduction techniques in wireless communication," in *IEEE Global Conf. Wireless Computing and Networking (GCWCN)*, 2018

[41] Sravanti, et.al., "Precoding PTS scheme for PAPR reduction in OFDM," in *IEEE Intl. Conf. on Innovations in Electrical, Electronics, Instrumentation and Media Tech (ICIEEIMT)*, 2017.

[42] Cimini, et.al., "Peak-to-average power ratio reduction of an OFDM signal using partial transmit sequences with embedded side information," in *Globecom'00*, 2000.

[43] Cimini, et.al., "Peak-to-average power ratio reduction of an OFDM signal using partial transmit sequences," in *Intl. Conf. on Communications*, 1999.

[44] Cimini, et.al., "Peak-to-average power ratio reduction of an OFDM signal using partial transmit sequences," *IEEE Comm. Letters,* pp. 86-88, March 2000.

[45] Laabidi, et.al., "PAPR reduction in FBMC/OQAM systems using active constellation extension and tone reservation approaches," in *IEEE Symp. on Computers and Communication (ISCC)*, 2015.

[46] Kollar, et.al., "Clipping-based iterative PAPR-reduction techniques for FBMC," in *17th Intl. OFDM Workshop (InOWo)*, 2012.

[47] Boontra, et.al., "A PAPR reduction for FBMC-OQAM signals using ABC-OPTS scheme," in *Intl. Conf. on Advanced Comm. Technology (ICACT)*, 2019.

[48] Michailow, et.al., "Low peak-to-average power ratio for next generation cellular systems with generalized frequency division multiplexing," in *Intl. Symp. on Intelligent Sic. Proc. and Comm. Systems*, 2013.

[49] Hadani, R., et.al., “Orthogonal Time Frequency Space Modulation,” in *IEEE Wireless Communications and Networking Conference*, 2017.

[50] P. Raviteja, K. T. Phan, Y. Hong and E. Viterbo, "Interference Cancellation and Iterative Detection for Orthogonal Time Frequency Space Modulation," *IEEE Transactions on Wireless Communications,* vol. 17, no. 10, pp. 6501-6515, Oct. 2018.

[51] A. Farhang, A. RezazadehReyhani, L. E. Doyle and B. Farhang-Boroujeny, "Low Complexity Modem Structure for OFDM-Based Orthogonal Time Frequency Space Modulation," *IEEE Wireless Communications Letters, ,* vol. 7, no. 3, pp. 344-347, 2018.

[52] P. Raviteja, Y. Hong, E. Viterbo and E. Biglieri, "Practical Pulse-Shaping Waveforms for Reduced-Cyclic-Prefix OTFS," *IEEE Transactions on Vehicular Technology,* vol. 68, no. 1, pp. 957-961, Jan. 2019.

[53] G. Surabhi and A. Chockalingam, "Low-complexity linear equalization for OTFS

modulation," *IEEE communications letters,* vol. 24, no. 2, pp. 330--334, 2019.

[54] S. Tiwari, S. S. Das and V. Rangamgari, "Low complexity LMMSE receiver for OTFS," *IEEE communications letters,* vol. 23, no. 12, pp. 2205--2209, 2019.

[55] T. Zou, W. Xu, H. Gao, Z. Bie, Z. Feng and Z. Ding, "Low-complexity linear equalization for OTFS systems with rectangular waveforms," in *IEEE International Conference on Communications Workshops (ICC Workshops)*, 2021.

[56] H. Qu, G. Liu, L. Zhang, S. Wen and M. A. Imran, "Low-complexity symbol detection and interference cancellation for OTFS system," *IEEE transactions on communications,* vol. 69, no. 3, pp. 1524--1537, 2020.

[57] Z. Yuan, F. Liu, W. Yuan, Q. Guo, Z. Wang and J. Yuan, "Iterative detection for orthogonal time frequency space modulation with unitary approximate message passing," *IEEE transactions on wireless communications,* vol. 21, no. 2, pp. 714--725, 2021.

[58] C. Shen, J. Yuan and H. Lin, "Error performance of rectangular pulse-shaped OTFS with practical receivers," *IEEE Wireless Communications Letters,* vol. 11, no. 12, pp. 2690--2694, 2022.

[59] P. Banelli, S. Buzzi, G. Colavolpe, A. Modenini, F. Rusek and A. Ugolini, "Modulation formats and waveforms for 5G networks: Who will be the heir of OFDM?: An overview of alternative modulation schemes for improved spectral efficiency," *IEEE Signal Processing Magazine,* vol. 31, no. 6, pp. 80--93, 2014.

[60] G. Surabhi, R. M. Augustine and A. Chockalingam, "Peak-to-average power ratio of OTFS modulation," *IEEE Communications Letters,* vol. 23, no. 6, pp. 999--1002, 2019.

[61] S. Tiwari and S. S. Das, "Circularly pulse-shaped orthogonal time frequency space modulation," *Electronics Letters,* vol. 56, no. 3, pp. 157--160, 2020.

[62] H. Zhang and T. Zhang, "A low-complexity message passing detector for OTFS modulation with probability clipping," *IEEE wireless communications letters,* vol. 10, no. 10, pp. 1271--1275, 2021.

[63] T. Thaj and E. Viterbo, "Low-complexity linear diversity-combining detector for MIMO-OTFS," *IEEE Wireless Communications Letters,* vol. 11, no. 2, pp. 288--292, 2021.

[64] T. Thaj and E. Viterbo, "Low Complexity Iterative Rake Decision Feedback Equalizer for Zero-Padded OTFS Systems," *IEEE Transactions on Vehicular Technology,* vol. 69, no. 12, pp. 15606--15622.

[65] T. Thaj and E. Viterbo, "Low Complexity Iterative Rake Detector for Orthogonal Time Frequency Space Modulation," in *IEEE Wireless Communications and Networking Conference (WCNC)*, 2020.

[66] C. Jin, Z. Bie, X. Lin, W. Xu and H. Gao, "A Simple Two-Stage Equalizer for OTFS With Rectangular Windows," *IEEE Communications Letters,* vol. 25, no. 4, pp. 1158--1162, 2021.

[67] T. Zemen, M. Hofer, D. Loeschenbrand and C. Pacher, "Iterative detection for orthogonal precoding in doubly selective channels," in *IEEE 29th Annual International Symposium on Personal, Indoor and Mobile Radio Communications (PIMRC)*, 2018.

Co-funded by the European Union

[68] W. Yuan, Z. Wei, J. Yuan and D. W. K. Ng, "A simple variational Bayes detector for orthogonal time frequency space (OTFS) modulation," *IEEE transactions on vehicular technology,* vol. 69, no. 7, pp. 7976--7980, 2020.

[69] Z. Zhang, H. Liu, Q. Wang and P. Fan, "A survey on low complexity detectors for OTFS systems," *ZTE Commun.,* vol. 19, no. 4, pp. 3--15, 2021.

[70] P. Raviteja, K. T. Phan, Y. Hong and E. Viterbo, "Embedded delay-Doppler channel estimation for orthogonal time frequency space modulation," in *IEEE 88th Vehicular Technology Conference (VTC-Fall)*, 2018.

[71] P. Raviteja, K. T. Phan and Y. Hong, "Embedded pilot-aided channel estimation for OTFS in delay--Doppler channels," *IEEE transactions on vehicular technology,* vol. 68, no. 5, pp. 4906--4917, 2019.

[72] T. Thaj, E. Viterbo and Y. Hong, "Orthogonal time sequency multiplexing modulation: Analysis and low-complexity receiver design," *IEEE Transactions on Wireless Communications,* vol. 20, no. 12, pp. 7842--7855, 2021.

[73] W. Yuan, S. Li, Z. Wei, J. Yuan and D. W. K. Ng, "Data-aided channel estimation for OTFS systems with a superimposed pilot and data transmission scheme," *IEEE wireless communications letters,* vol. 10, no. 9, pp. 1954--1958, 2021.

[74] H. B. Mishra, P. Singh, A. K. Prasad and R. Budhiraja, "OTFS channel estimation and data detection designs with superimposed pilots," *IEEE transactions on wireless communications,* vol. 21, no. 4, pp. 2258--2274, 2021.

[75] K. R. Murali and A. Chockalingam, "On OTFS modulation for high-Doppler fading channels," in *Information Theory and Applications Workshop (ITA)*, 2018.

[76] O. K. Rasheed, G. Surabhi and A. Chockalingam, "Sparse delay-Doppler channel estimation in rapidly time-varying channels for multiuser OTFS on the uplink," in *IEEE 91st Vehicular Technology Conference (VTC2020-Spring)*, 2020.

[77] P. a. F. A. Sanoopkumar, "A Practical Pilot for Channel Estimation of OTFS," in *IEEE International Conference on Communications ICC'23*, 2023.

[78] W. Shen, L. Dai, J. An, P. Fan and R. W. Heath, "Channel estimation for orthogonal time frequency space (OTFS) massive MIMO," *IEEE Transactions on Signal Processing,* vol. 67, no. 16, pp. 4204--4217, 2019.

[79] Y. Liu, S. Zhang, F. Gao, J. Ma and X. Wang, "Uplink-aided high mobility downlink channel estimation over massive MIMO-OTFS system," *IEEE Journal on Selected Areas in Communications,* vol. 38, no. 9, pp. 1994--2009, 2020.

[80] Buzzi, Stefano, et al. "LEO Satellite Diversity in 6G Non-Terrestrial Networks: OFDM vs. OTFS." IEEE Communications Letters (2023).

[81] Caus, Màrius, et al. "Reliability Oriented OTFS-based LEO Satellites Joint Transmission Scheme." 2022 IEEE Globecom Workshops (GC Wkshps). IEEE, 2022.

[82] Shi, Jia, et al. "OTFS enabled LEO satellite communications: A promising solution to severe doppler effects." IEEE Network (2023).

[83] Chu, Thi My Chinh, et al. "OTFS Modulation for Non-Terrestrial Networks: Concepts, Applications, Benefits, and Challenges." 2023 16th International Conference on Signal Processing and Communication System (ICSPCS). IEEE,

2023.

[84] Li, Songyan, et al. "Downlink Carrier Frequency Offset Estimation for OTFS-based LEO Satellite Communication System." IEEE Communications Letters (2023).

[85] Wang, Xueyang, et al. "Joint Bayesian channel estimation and data detection for OTFS systems in LEO satellite communications." IEEE Transactions on Communications 70.7 (2022): 4386-4399.

[86] Devarajalu, Senthil Kumaran, and Deepak Jose. "Performance Evaluation of OTFS Under Different Channel Conditions for LEO Satellite Downlink." 2023 10th International Conference on Wireless Networks and Mobile Communications (WINCOM). IEEE, 2023.

[87] Liu, et.al., "Performance evaluation of MSK and OFDM modulations for future GNSS signals," *GPS Solutions,* 2014.

[88] D. Hea, Z. Zhangb, H. Linb, Z. Wub, Y. Huangb and Z. Wang, "Performance comparison of single-carrier and multi-carrier waveforms over terahertz wireless channels," *Digital Communications and Networks,* 2023.

[89] I. Deneire, B. Glyselinckx and M. Engels, "Training sequence versus cyclic prefix-a new look on single carrier communication," *IEEE Communication Letters,* pp. 292-294, 2001

[90] Falconer, D., et.al., "Frequency domain equalization for single-carrier broadband wireless systems".*IEEE Communications Magazine.*

[91] Y.-S. Chen and C. Lin, "Blind-channel identification for MIMO single-carrier zero-padding block-transmission systems," *IEEE Trans. Circuits Syst. I: Regular Papers,* 2008.

[92] R. Rajashekar, K. V. S. Hari and L. Hanzo, "Spatial modulation aided zero-padded single carrier transmission for dispersive channels," *IEEE Trans. Commun.,* 2013.

[93] ETSI, "TR 103 297, Satellite Earth Stations and Systems (SES) SC-FDMA Based Radio Wave- Form Technology for Ku/Ka Band Satellite Service," 2017.

[94] G. Cherubini, E. Eleftheriou, S. Oker and J. M. Cioffi, "Filter bank modulation techniques for very high speed digital subscriber lines," *IEEE Communications Magazine,* May 2000.

[95] F. J. Harris, C. Dick and M. Rice, "Digital receivers and transmitters using polyphase filter banks for wireless communications," *IEEE Transactions on Microwave Theory and Techniques,* pp. 1395-1412, 2003.

[96] Hexa-X-II, "D4.2: Radio design and spectrum access requirements and key enablers for 6G evolution".

[97] Hexa-X, "D2.1: Towards Tbps Communications in 6G: Use Cases and Gap Analysis".

[98] Hexa-X, "D2.3: Radio models and enabling techniques towards ultra-high data rate links and capacity in 6G".

[99] S. Dimitrov, N. Privitera, R. Suffritti, G. Boccolini, A. B. Awoseyila and B. G. Evans, "Spectrally efficient waveforms for the return link in satellite communication

systems," in *European Conference on Networks and Communications (EuCNC)*, Paris, France, 2015.

[100] 5G-ALLSTAR, "D1.4: Final Report".

[101] 5G-ALLSTAR, "D5.2: Integration and system level testing for European testbed of 5G cellular and satellite access networks".

[102] D. Demmer, R. Gerzaguet, J.-B. Doré, D. L. Ruyet and D. Kténas, "Block-filtered OFDM: A novel waveform for future wireless technologies," IEEE International Conference on Communications (ICC), Paris, France, 2017.

[103] 5G CHAMPION, "D5.1: 5G Satellite Communication analysis - intermediate version".

[104] 3GPP, "TR 38.811 “Study on New Radio (NR) to support non-terrestrial networks”," 2020.

[105] E. Lutz, D. Cygan, M. Dippold, F. Dolainsky and W. Papke, "The Land Mobile Satellite Communication Channel – Recording, Statistics, and Channel Model," *IEEE Trans. on Veh. Tech.,* vol. 40, no. 2, pp. 375-386, 1991.

[106] J. Huang, Y. Cao, X. Raimund, A. Cheema and S. Salous, "Rain Statistics Investigation and Rain Attenuation Modeling for Millimeter Wave Short-Range Fixed Links," *IEEE Access,* vol. 7, pp. 156110-156120, 2019.

[107] A. D. Panagopulos, P.-D. M. Arapoglou and P. G. Cottis, "Satellite Communications at Ku, Ka, and V bands: Propagation Impairments and Mitigation Techniques," *IEEE Comm. Surveys & tutorials,* vol. 6, no. 3, pp. 2-14, 2004.

[108] ITU-R, "P.676-11: “Attenuation by atmospheric gases”"

[109] ITU-R, " P.618-14: “Propagation data and prediction methods required for the design of Earth-space telecommunication systems”," 2003.

[110] ITU-R, "P.531-15: “Ionospheric propagation data and prediction methods required for the design of satellite networks and systems”," 2023.

[111] ETSI, "TR 138.901, “Study on channel models for frequencies from 0.5 to 100 GHz”," 2022.

[112] Berens, Friedbert, et al. "UWB car attenuation measurements." 2007 16th IST Mobile and Wireless Communications Summit. IEEE, 2007.

[113] In-car Mobile signal attenuation measurements, OFCOM 2017

[114] Tanghe, Emmeric, et al. "Evaluation of vehicle penetration loss at wireless communication frequencies." IEEE transactions on vehicular technology 57.4 (2008): 2036-2041.

[115] E. M. Vitucci, V. D. Esposti, F. Mani, F. Fuschini, M. Barbiroli, M. Gan, C. Li, J. Zhao and Z. Zhong, "Tuning Ray Tracing for Mm-wave Coverage Prediction in Outdoor Urban Scenarios," *Radio Science,* vol. 54, no. 11, pp. 1112-1128, 2019.

[116] V. D. Esposti, F. Fuschini, E. Vitucci and G. Falciasecca, "Measurement and modelling of scattering from buildings," *IEEE Transactions on Antennas and Propagation,* vol. 55, no. 1, pp. 143-153, 2007.

[117] Ericsson R4-165901 ’ Further elaboration on PA models for NR’, 2016-08

[118] 6G-NTN D4.4 'Spectrum regulation analysis for 6G-NTN scenarios'

[119] Qualcomm Incorporated, "R1-162199 - Waveform candidates," 3GPP TSG-RAN WG1 #84b.

[120] ETSI, "ETSI EN 302 307 - 1 V1.4.1 Digital Video Broadcasting (DVB); Second generation framing structure, channel coding and modulation systems for Broadcasting, Interactive Services, News Gathering and other broadband satellite applications; Part 1: DVB-S2".

[121] A. Morello and V. Mignone, "DVB-S2: the second generation standard for satellite broad-band services," *IEEE proceedings,* pp. 210-227, 2006.

[122] G. Albertazzi, S. Cioni, G. Corazza, M. Neri, R. Pedone, P. Salmi, A. Vanelli-Coralli and M. Villanti, "ON THE ADAPTIVE DVB-S2 PHYSICAL LAYER: DESIGN AND PERFORMANCE".

[123] L. Bai, "Channel Modeling for SatelliteCommunication Channels at Q-Band inHigh Latitude," *IEEE Access.*

[124] V. Kumar, M. Mukherjee and J. Lloret, "A Hardware-Efficient and Reconfigurable UFMC Transmitter Architecture With its FPGA Prototype," in IEEE Embedded Systems Letters, vol. 12, no. 4, pp. 109-112, Dec. 2020, doi: 10.1109/LES.2019.2961850.

[125] J. -B. Doré, M. Laugeois, N. Cassiau and X. Popon, "FPGA Implementation of a Wideband Multi-Gb/s 5G BF-OFDM Transceiver," 2021 Joint European Conference on Networks and Communications & 6G Summit (EuCNC/6G Summit), Porto, Portugal, 2021, pp. 502-507, doi: 10.1109/EuCNC/6GSummit51104.2021.9482424.

[126] T.Thaj and E.Viterbo 'OTFS Modem implementation and experimental study of receiver impairments effects', in IEEE ICC Workshop 2019,doi: 10.1109/ICCW.2019.8757167

[127] Hassan, Shahbaz, Scott L. Linfoot, and Marwan M. Al-Akaidi. "An analysis on the performance of the forward and return interaction channels in DVB-RCS." IEEE Transactions on Consumer Electronics 52.2 (2006): 371-376.

[128] Digital Video Broadcasting (DVB); Second Generation DVB Interactive Satellite System (DVB-RCS2); Part 2: Lower Layers for Satellite standard

Co-funded by the European Union

8 APPENDIX

8.1 APPENDIX A: DVB STANDARD

8.1.1 DVB-S2

The DVB-S2 is a single, very flexible standard and it is characterized by [120]:

- a flexible input stream adapter, suitable for operation with single and multiple input streams of various formats (packetized or continuous);
- a powerful FEC system based on LDPC codes concatenated with BCH codes, allowing Quasi-Error-Free operation at about 0,7 dB to 1 dB from the Shannon limit, depending on the transmission mode (AWGN channel, modulation constrained Shannon limit);
- a wide range of code rates (from 1/4 up to 9/10); 4 constellations, ranging in spectrum efficiency from 2 bit/s/Hz to 5 bit/s/Hz, optimized for operation over non-linear transponders;
- a set of three spectrum shapes with roll-off factors 0,35, 0,25 and 0,20;
- Adaptive Coding and Modulation (ACM) functionality, optimizing channel coding and modulation on a frame-by-frame basis.

The DVB-S2 transmission is structured as a sequence of functional blocks illustrated in Figure 57. The signal generation consists of two level of framing structures:

- BBFRAME at the BB level, carrying different signaling bits in order to configure the receiver in a flexible way according to the application scenario;
- PLFRAME at the PL level, carrying few highly protected signaling bits to provide robust synchronization and signaling at the Physical (PHY) layer.

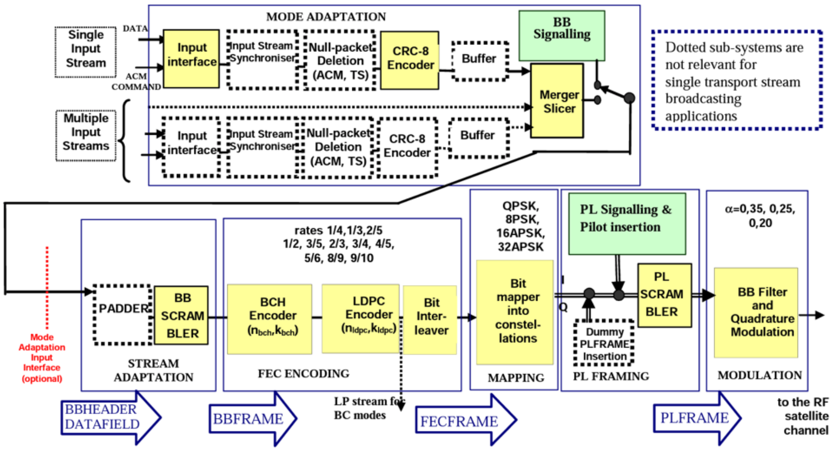

FIGURE 57: FUNCTIONAL BLOCK DIAGRAM OF THE DVB-S2 SYSTEM [120]

The main functional blocks of the DVB-S2 are:

- Mode adaptation, which is application dependent. It provides input stream interfacing, Input Stream Synchronization (optional), null-packet deletion (for ACM and Transport Stream input format only), CRC-8 coding for error detection at packet level in the receiver (for packetized input streams only), merging of input streams (for Multiple Input Stream modes only) and slicing into DATA FIELDs. Finally, base-band signalling is inserted to notify the receiver of the adopted Mode Adaptation format.

  This block takes as input: i)

  single or multiple Transport Streams (TS); and ii) Single or multiple Generic Streams (packetized or continuous). The output sequence is BBHEADER (80 bits) followed by a DATA FIELD.

  The supported interfaces are listed in Table 43.

TABLE 43: SYSTEM INTERFACES

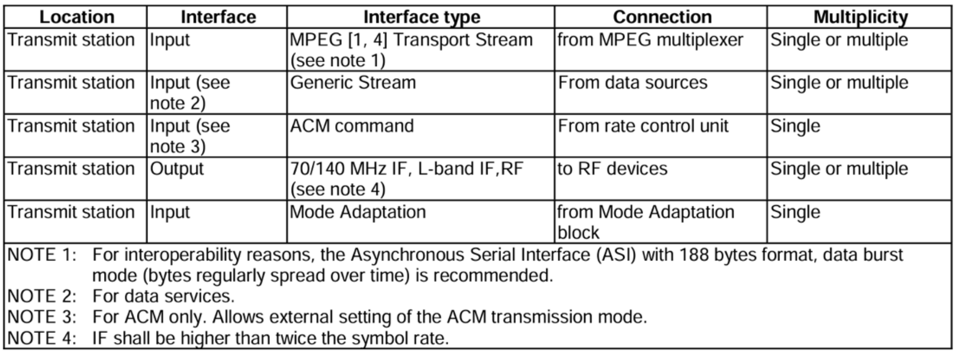

Location	Interface	Interface type	Connection	Multiplicity
Transmit station	Input	MPEG [1, 4] Transport Stream (see note 1)	from MPEG multiplexer	Single or multiple
Transmit station	Input (see note 2)	Generic Stream	From data sources	Single or multiple
Transmit station	Input (see note 3)	ACM command	From rate control unit	Single
Transmit station	Output	70/140 MHz IF, L-band IF,RF (see note 4)	to RF devices	Single or multiple
Transmit station	Input	Mode Adaptation	from Mode Adaptation block	Single
NOTE 1: For interoperability reasons, the Asynchronous Serial Interface (ASI) with 188 bytes format, data burst mode (bytes regularly spread over time) is recommended. NOTE 2: For data services. NOTE 3: For ACM only. Allows external setting of the ACM transmission mode. NOTE 4: IF shall be higher than twice the symbol rate.				

The input interface subsystem maps the input electrical format into internal logical-bit format. The first received bit will be indicated as the Most Significant Bit (MSB). A Transport Stream is characterized by User Packets (UP) of constant length UPL = 188 × 8 bits (one MPEG packet), the first byte being a Sync-byte (47HEX). A Generic Stream is characterized by a continuous bit-stream or a stream of constant-length UP, with length UPL bits (maximum UPL value 64 K, UPL = 0D means continuous stream, see clause 5.1.5). A variable length packet stream, or a constant length packet exceeding 64 kbit, is treated as a continuous stream. For Generic packetized streams, if a synch-byte is the first byte of the UP, it shall be left unchanged, otherwise a sync-byte = 0D shall be inserted before each packet, and UPL shall be increased by eight. UPL information can be derived by static modulator setting. "ACM Command" signalling input allows to set, through an external "transmission mode control unit", the transmission parameters to be adopted by the DVB-S2 modulator, for a specific portion of input data. As previously mentioned, Mode Adaptation (optional input) is a sequence of Data Fields, where each individual Data Field is preceded by a BBHEADER.

The main elements of Mode Adaptation are:

- **Input Synchronizer.** Data processing in the DVB-S2 modulator may produce variable transmission delay on the user information. The Input Stream Synchronizer subsystem provides suitable means to guarantee Constant-Bit-Rate (CBR) and constant end-to-end transmission delay for packetized input streams (e.g., for Transport Streams).

- **Null-Packet Deletion**. For ACM modes and TS input data format, MPEG null-packets is identified (PID = 8191D) and removed. This allows to reduce the information rate and increase the error protection in the modulator. The process is carried-out in a way that the removed null-packets can be re-inserted in the receiver in the exact place where they originally were.
- **CRC-8 encoder.** This sub-system passes forward the input stream without modifications if the latter is a continuous generic stream (UPL = 0_D).

  When the input stream is a sequence of UP of length UPL bits, this sub-system processes the input. In particular, the CRC-8 encoder is applied to packetized streams only. The generator polynomial is:

  $$g(x) = x^8 + x^7 + x^6 + x^4 + x^2 + 1$$

  The CRC encoder output is computed as:

  $$CRC = remainder\ [x^8\, u(x): g(x)]$$

  Where $u(x)$ is the input sequence with length equal to 8 bits to be systematically encoded. The register is initialized to all zeros before the first bit of each sequence enters the circuit. The computed CRC-8 replaces the sync-byte of the following UP and the sync-byte is copied into the SYNC field of the BBHEADER for transmission.
- **Merger/Slicer.** The Merger/Slicer input stream(s) is (are) organized as Generic continuous Stream(s) (with UPL = 0) or Packetized Input Stream(s). The input stream(s) is buffered until the Merger/Slicer can read them. The Slicer reads (i.e., slices) from its input (single input stream), or from one of its inputs (multiple input streams) a DATA FIELD, composed of bits Data Field Length (DFL), where:

  $$K_{bch} - (10 \times 8) \geq DFL\ \geq 0$$

  With K_{bch} being the 80 bits dedicated to the BBHEADER.

  The Merger concatenates, in a single output, different data fields read and sliced from one of its inputs. It should be noted that in presence of a single stream, only the slicing functionality applies. Depending on the applications, the Merger/Slicer can either allocate a number of input bits equal to the maximum DATAFIELD capacity (DFL = K_{bch} -80), thus breaking UPs in subsequent DATAFIELDs, or can allocate an integer number of UPs within the DATAFIELD, making the DFL variable within the above specified boundaries.

  When a DATA FIELD is not available at the merger/slicer request on any input port, the Physical Layer Framing sub-system generates and transmits a DUMMY PLFRAME. After Sync-byte replacing by CRC-8, it is necessary to provide the receiver a method to recover UP synchronization (when the receiver is already synchronized to the DATA FIELD). Therefore, the number of bits from the beginning of the DATA FIELD and the beginning of the first complete UP (first bit of the CRC-8) must be detected by the Merger/Slicer and stored in SYNCD field (i.e., SYNC Distance) of the BBHeader. As an example, SYNCD = 0_D means that the first UP is aligned to the DATA FIELD.

  Figure 58 provides the stream format at the output of Mode Adapter.

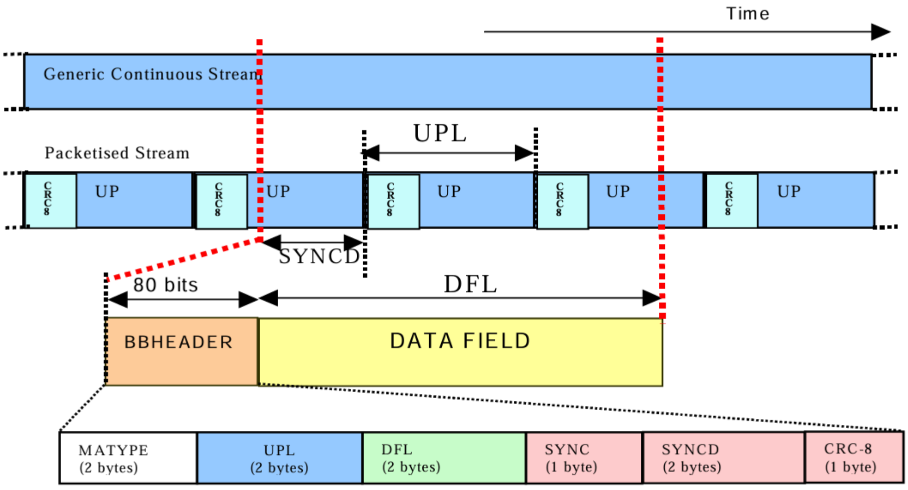

FIGURE 58: STREAM FORMAT AT THE OUTPUT OF MODE ADAPTER

- **BBHEADER insertion.** Finally, a fixed length BBHEADER of 10 bytes is inserted in front of the DATA FIELD, describing its format. Referring to Figure 58, MATYPE (2 bytes): describes the input stream(s) format, the type of Mode Adaptation and the transmission Roll-off factor.

➲ Stream adaptation provides padding to complete a constant length (k_{bch} bits) BBFRAME and scrambling. k_{bch} depends on the FEC rate. Padding may be applied in circumstances when the user data available for transmission are not sufficient to completely fill a BBFRAME, or when an integer number of UPs has to be allocated in a BBFRAME. The input stream is a BBHEADER followed by a DATA FIELD. The output stream is a BBFRAME.

The main elements of the stream adaptation are:

- **BB Scrambling.** The complete BBFRAME needs to be randomized and the randomization sequence shall be synchronous with the BBFRAME, starting from the MSB and ending after k_{bch} bits. The scrambling sequence is generated by the feed-back shift and the polynomial for the Pseudo Random Binary Sequence (PRBS) generator is: $1 + x^{14} + x^{15}$.
- **FEC encoding.** Finally, the FEC Encoding is performed by the concatenation of Bose-Chaudhuri-Hocquenghem (BCH) outer codes, LDPC (Low Density Parity Check) inner codes (rates 1/4, 1/3, 2/5, 1/2, 3/5, 2/3, 3/4, 4/5, 5/6, 8/9, 9/10), and bit interleaving.

  The input stream is composed of BBFRAMEs and the output stream of FECFRAMEs. Each BBFRAME (k_{bch} bits) is processed by the FEC coding subsystem, to generate a FECFRAME (n_{ldpc} bits). The parity check bits (BCHFEC) of the systematic BCH outer code are appended after the BBFRAME, and the parity check bits (LDPCFEC) of the inner LDPC encoder after the BCHFEC field.

  Depending on the application area, the FEC coded block shall have length n_{ldpc}= 64800 bits or 16200 bits. When ACM is used, FEC and modulation mode may be changed in different frames but remains constant within a frame. Bit interleaving is then applied to FEC-coded bits in 8PSK, 16APSK, and 32APSK to separate, from each other, bits mapped onto the same transmission signal. In particular, for these modulation formats, the output of the LDPC encoder shall be bit interleaved using a block interleaver. Data is serially written into the interleaver column-wise, and serially read out row-wise (the MSB of BBHEADER is read out first, except 8PSK rate 3/5 case where MSB of BBHEADER is read out third). Error rate requirements for DVB-S2 are very stringent, 10^{-7} MPEG Transport Streams (TS) packet error rate (PER),

- <u>Mapping</u>: four modulation modes can be selected for the transmitted payload, which are QPSK, 8PSK, 16APSK and 32APSK constellations depending on the application area. Each FECFRAME (which is a sequence of 64 800 bits for normal FECFRAME, or 16 200 bits for short FECFRAME) is serial-to-parallel converted (parallelism level = η_{MOD} 2 for QPSK, 3 for 8PSK, 4 for 16APSK, 5 for 32APSK) the MSB of the FECFRAME is mapped into the MSB of the first parallel sequence. Each parallel sequence is mapped into constellation, generating a (I,Q) sequence of variable length depending on the selected modulation efficiency η_{MOD}. The output sequence is a XFECFRAME (compleX FECFRAME), composed of 64 800/ η_{MOD} (normal XFECFRAME) or 16 200/η_{MOD} (short XFECFRAME) modulation symbols. Each modulation symbol can be organized either in a complex vector in the format (I,Q) (I being the in-phase component and Q the quadrature component) or in the equivalent format polar form $\rho \cdot e^{j\phi}$(with ρ the modulus of the vector and ϕ being its phase).

  Gray mapping of constellations is used for QPSK and 8PSK. By selecting the modulation constellation and code rates, spectrum efficiencies from 0.5 to 4.5 bits per symbol are available and can be chosen dependent on the capabilities of the satellite transponder used. The 16APSK constellation is composed of two concentric rings of uniformly spaced 4 and 12 PSK points, respectively in the inner ring of radius R_1 and outer ring of radius R_2. The ratio of the outer circle radius to the inner circle radius $\gamma = R_2/R_1$ is provided in Table 44.

TABLE 44: OPTIMUM CONSTELLATION RADIUS Γ FOR 16 APSK (LINEAR CHANNEL)

Code rate	Modulation/coding spectral efficiency	γ
2/3	2,66	3,15
3/4	2,99	2,85
4/5	3,19	2,75
5/6	3,32	2,70
8/9	3,55	2,60
9/10	3,59	2,57

The 32APSK modulation constellation consists of three concentric rings of uniformly spaced 4, 12 and 16 PSK points, respectively in the inner ring of radius R_1, the intermediate ring of radius R_2 and the outer ring or radius R_3. Table 45 defines the values of γ_1 = R_2/ R_1 and γ_2 = R_3/ R_1.

TABLE 45: OPTIMUM CONSTELLATION RADIUS γ_1 AND γ_2 FOR 32 APSK (LINEAR CHANNEL)

Code rate	Modulation/coding spectral efficiency	γ_1	γ_2
3/4	3,74	2,84	5,27
4/5	3,99	2,72	4,87
5/6	4,15	2,64	4,64
8/9	4,43	2,54	4,33
9/10	4,49	2,53	4,30

The 16 and 32APSK constellations have been optimized for nonlinear transponders by placing the points on circles; nevertheless their performance in the AWGN channel is comparable with those of 16QAM or 32QAM respectively. QPSK and 8PSK are typically proposed for broadcast applications, since they are virtually constant envelope modulations and can be used in nonlinear satellite transponders driven near saturation. The 16APSK and 32APSK modes are mainly targeted at professional applications, due to the higher requirements in terms of available SNR, but they can also be used for broadcasting. While these modes are not as power efficient as the other modes, the spectrum efficiency is much greater. They need to operate the satellite transponder in a quasi-linear region or, alternatively, to adopt advanced predistortion methods in the uplink station to minimize the effect of transponder nonlinearity [121].

- Physical layer framing generates a physical layer frame (named PLFRAME) by performing the following processes: i) Dummy PLFRAME generation when no XFECFRAME is ready to be processed and transmitted; ii) XFECFRAME slicing into an integer number S of constant length SLOTs (length: M = 90 symbols each); iii) PLHEADER generation and insertion before the XFECFRAME for receiver configuration. PLHEADER shall occupy exactly one SLOT (length: M = 90 Symbols); iv) Pilot Block insertion (for modes requiring pilots) every 16 SLOTS, to help receiver synchronization. The Pilot Block shall be composed of P = 36 pilot symbols; and v) Randomization of the (I, Q) modulated symbols by means of a physical layer scrambler.

The input stream of the sub-system is a XFECFRAME and the output a scrambled PLFRAME.

Dummy PLFRAMEs are transmitted when no useful data is ready to be sent on the channel and it composed of a PLHEADER and of 36 SLOTS of un-modulated carriers (I = $^1/_{\sqrt{2}}$, Q = $^1/_{\sqrt{2}}$). The PLHEADER is intended for receiver synchronization and physical layer signalling. Indeed, after decoding the PLHEADER, the receiver knows the PLFRAME duration and structure, the modulation and coding scheme of the XFECFRAME, the presence or absence of pilot symbols. The PLHEADER (one SLOT of 90 symbols) is of the following fields: i) SOF (26 symbols), identifying the Start of Frame; and ii) PLS code (64 symbol): PLS (Physical Layer Signalling) code shall be a non-systematic binary code of length 64 and dimension 7 with minimum distance dmin = 32. It is equivalent to the first order Reed-Muller under permutation. It transmits 7 bits for physical layer signalling purpose. These 7 bits consists of two fields: MODCOD identifying the XFECFRAME modulation and FEC rate and TYPE defined identifying the FECFRAME length (64 800 bits or 16 200 bits) and the presence/absence of pilots. Two PLFRAME configurations shall be possible: with and without pilots. In the former case a PILOT BLOCK must be composed of P = 36 pilot symbols. Each pilot shall be an un-modulated symbol, identified by I = $1/\sqrt{2}$, Q = $1/\sqrt{2}$. The first PILOT BLOCK is inserted 16 SLOTs after the PLHEADER, the second after 32 SLOTs. It shall be noticed that the pilot presence/absence in VCM and ACM can be changed on a frame-by-frame basis. Prior to modulation, each PLFRAME, excluding the PLHEADER, is randomized for energy dispersal by multiplying the (I+jQ) samples by a complex randomization sequence (C_I+jC_Q):

$$I_{scrambled} = IC_I - QC_Q$$

$$Q_{scrambled} = IC_Q - QC_I$$

The randomization sequence rate corresponds to the I-Q PLFRAME symbol rate; thus, it has no impact on the occupied signal bandwidth. The randomization sequence has a period greater than the maximum required duration of about 70 000 symbols. The randomization sequence is reinitialized at the end of each PLHEADER. The PLFRAME duration depends on the modulation selected, thus the randomization sequence length shall be truncated to the current PLFRAME length.

The scrambling code sequences is constructed by combining two real m-sequences (generated by means of two generator polynomials of degree 18) into a complex sequence. The resulting sequences thus constitute segments of a set of Gold sequences.

- Base-Band Filtering and Quadrature Modulation is applied, after the randomization, to shape the signal spectrum (squared-root raised cosine, roll-off factors 0,35 or 0,25 or 0,20) and to generate the RF signal. After randomization, the signals shall be square root raised cosine filtered. The baseband square root raised cosine filter has a theoretical function defined by the following expression:

$$H(f) = 1, for\ |f| < f_n(1-\alpha)$$

$$H(f) = 0\ for\ |f| > f_n(1-\alpha)$$

$$H(f) = \sqrt{\frac{1}{2} + \frac{1}{2}\sin\frac{\pi}{2f_n}[\frac{f_n - |f|}{\alpha}]}\ for\ |f| = f_n(1-\alpha)$$

With $f_n = \frac{R_s}{2} = \frac{1}{2T_s}$ is the Nyquist frequency and α is the roll-off factor.

Quadrature modulation is performed by multiplying the in-phase and quadrature samples (after baseband filtering) by $\sin(2\pi f_o t)$ and $\cos(2\pi f_o t)$, respectively (where f_o is the carrier frequency). The two resulting signals are then added to obtain the modulator output signal.

Table 46 maps the system configurations to the applications areas.

TABLE 46: SYSTEM CONFIGURATIONS AND APPLICATION AREAS

System configurations		**Broadcast services**	**Interactive services**	**DSNG**	**Professional services**
QPSK	1/4,1/3, 2/5	O	N	N	N
	1/2, 3/5, 2/3, 3/4, 4/5, 5/6, 8/9, 9/10	N	N	N	N
8PSK	3/5, 2/3, 3/4, 5/6, 8/9, 9/10	N	N	N	N
16APSK	2/3, 3/4, 4/5, 5/6, 8/9, 9/10	O	N	N	N
32APSK	3/4, 4/5, 5/6, 8/9, 9/10	O	N	N	N
CCM		N	N (see note 1)	N	N
VCM		O	O	O	O
ACM		NA	N (see note 2)	O	O
FECFRAME (normal)	64 800 (bits)	N	N	N	N
FECFRAME (short)	16 200 (bits)	NA	N	O	N
Single Transport Stream		N	N (see note 1)	N	N
Multiple Transport Streams		O	O (see note 2)	O	O
Single Generic Stream		NA	O (see note 2)	NA	O
Multiple Generic Streams		NA	O (see note 2)	NA	O
Roll-off 0,35, 0,25 and 0,20		N	N	N	N
Input Stream Synchronizer		NA except (see note 3)	O (see note 3)	O (see note 3)	O (see note 3)
Null Packet Deletion		NA except (see note 3)	O (see note 3)	O (see note 3)	O (see note 3)
Dummy Frame insertion		NA except (see note 3)	N	N	N
N = normative, O = optional, NA = not applicable.					
NOTE 1: Interactive service receivers shall implement CCM and Single Transport Stream. NOTE 2: Interactive Service Receivers shall implement ACM at least in one of the two options: Multiple Transport Streams or Generic Stream (single/multiple input). NOTE 3: Normative for single/multiple TS input stream(s) combined with ACM/VCM or for multiple TS input streams combined with CCM.					

8.1.1.1 Digital receiver implementation

Figure 59 shows a possible DVB-S2 digital receiver architecture [122].

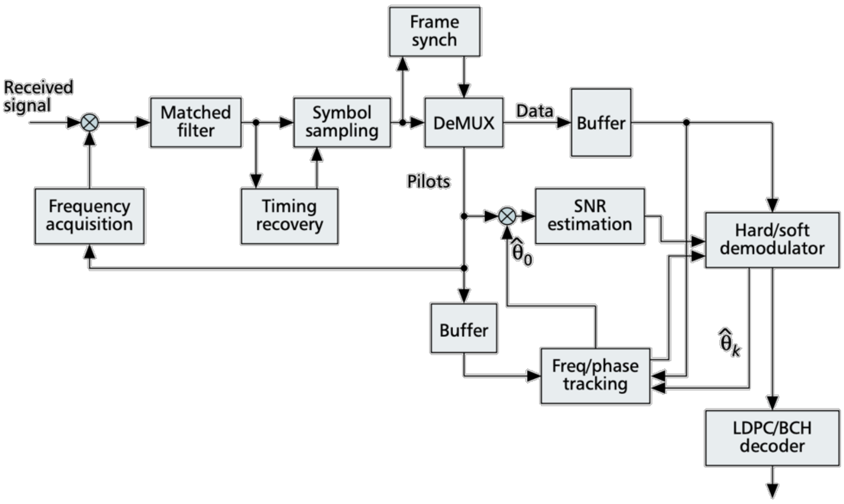

FIGURE 59: DIGITAL RECEIVER BLOCK DIAGRAM [122]

Several subsystems are involved in the recovery of information. Following a sequential functional order from startup, the first operation after matched filtering is clock recovery, followed by frame synchronization, which exploits the PLFRAME header. Both operations must be performed in the presence of large carrier frequency errors. After this initial synchronization procedure, a demultiplexer is used to separate pilots from data symbols in a PLFRAME. The pilot symbol stream is used by the following three

subsystems: the coarse frequency acquisition loop, the signal-to-noise level estimator, and finally a phase-locked loop (PLL) for tracking the residual frequency offset and carrier phase. Once all auxiliary parameters are recovered, the data symbols can be detected by the hard/soft demodulator. The hard decisions are fed back to the PLL, while the soft initial a posteriori probabilities (APPs) on the received information bits are passed on to the LDPC-BCH decoder.

Symbol timing recovery

A suitable algorithm for timing recovery in DVB-S2 is the Gardner estimator [122]. In fact, this is a non-data-aided (NDA) circuit that is virtually insensitive to modulation format (from QPSK to 32-APSK) and performs efficiently even in the presence of quite large carrier frequency errors over the range of E_s/N_0 of interest. After the Gardner timing adjustment, the sampled symbol is indicated as:

$$r_k = d_k e^{j\varphi_k} + n_k$$

where d_k is the transmitted symbol, φ_k contains the carrier frequency and phase offsets, and n_k represents the AWGN sample. In terms of achievable performance, with an oversample factor equal to 4, the overall acquisition transient can be completed in around 10^5 symbols (2–3 PLFRAMEs) independent from the modulation format, while at steady state the normalized residual timing jitter is less than 10^{-2}, which is more than satisfactory.

Frame synchronization

Frame synchronization for DVB-S2 can be divided into acquisition and tracking. DVB-S2 frame acquisition is performed by exploiting the autocorrelation properties of the PLFRAME header, which is a sequence of 26 π/2-binary PSK (BPSK) symbols, identified as start of frame (SOF). The received signal is correlated with locally generated SOF replicas shifted by discrete offsets. Therefore, the frame epoch estimation problem is translated into a detection problem that has to discriminate between hypotheses or cells in a discretized uncertainty region. Frame acquisition in DVB-S2 suffers from two major impairments: the extremely low SNR, which can indeed assume negative values in dB, and the unknown carrier frequency offset and phase. In addition, at terminal startup the uncertainty region equals the entire frame length, TF, which in the worst case is as large as 33282 QPSK symbols. At first glance, one could hope to improve performance by exploiting multidwell procedures (i.e., collecting information from multiple frames before making a final decision). Unfortunately, this approach cannot be used in DVB-S2, where the frame length depends on the selected coding/modulation pair. In particular, the frame format is signaled to the receiver by a 64-symbol physical layer signaling (PLS) field. Since the PLS field cannot be decoded accurately prior to frame synchronization, the latter must be performed in single-dwell fashion. The frame acquisition performance is measured in terms of mean acquisition time, for which a practical performance specification of 2 s can be assumed at terminal startup. In the proposed design, a serial search procedure is considered where possible false alarms are recovered by a tracking circuit that restarts the procedure after a penalty time of Tp s. Passive correlation (SOF matched filtering) is used for coherent integration to reduce delay at the price of increased complexity.

Coarse carrier frequency recovery

After frame synchronization is achieved, the coarse carrier synchronization is performed by exploiting the pilot fields introduced in the DVB-S2 PLFRAME. In particular, the specified length for the pilot field is 36. In these conditions, a pilot-aided Mengali and Morelli (M&M) algorithm appears to be a valid candidate, because it allows to have low estimation error variance (approaching the Cramer-Rao bound) and a sufficiently large pull-in range, according to the requirements.

SNR estimation

Adaptive physical layer receivers require accurate estimation of the received SNR, for two basic reasons: first, this estimate can be fed back to the network to determine the most suitable coding/modulation pair according to the channel conditions experienced by the specific user; second, this information is needed by the soft demodulator to compute the A Priori Probabilities (APPs) on the received symbols. A suitable algorithm to this purpose is the SNR Estimator (SNORE), which is performed in a data-aided fashion over the pilot field after frequency and timing corrections have taken place.

Fine carrier frequency and phase tracking

The residual frequency offset after coarse acquisition and phase estimation (penalized by strong phase noise) is performed through a second order PLL that exploits all possible aiding mechanisms, using a hybrid data-aided and decision-directed approach. The initial phase estimate is obtained by a maximum likelihood (MLL) feedforward estimator over a pilot sequence, and is employed by a decision-directed second-order PLL. Within a PLFRAME, whenever a new pilot field occurs, the PLL operates according to a data-aided approach exploiting the known pilot symbols.

LDPC decoding

LDPC decoding is performed through the iterative sum-product algorithm, which updates the APP values after each iteration, exploiting the Tanner graph.

8.1.2 DVB-S2X

The DVB-S2X is an extension of the DVB-S2 standard and, accordingly, it retains DVB-S2's architecture, in order to facilitate rapid implementation and launch on the market, but it is not backward compatible to it [120]. Nevertheless, new DVB-S2X receivers are required to decode DVB-S2X and legacy DVB-S2 transmissions. The main new elements of DVB-S2X consist of: the introduction of very-low SNR range (VL-SNR) and the very-high SNR range (VHSNR), improved physical layer signalling allowing finer SNR granularity (and, thus, finer MODCOD steps), reduced roll-off factors (decreasing the occupied bandwidth) and defined linear channel modes (for use in for example Ka-band and for multicarrier per transponder configurations).

The main features to enable these enhancements are: i) an optional periodic super-frame structure with signalling of the format of the super-frame content and further benefits like simplifying synch recovery at VL-SNR and allowing periodic pilot structures and PL-Scramblers; ii) an extended PLHEADER signalling scheme to support the additional MODCODs; iii) an extended PLHEADER signalling scheme to support Mobile Frames; iv) a high efficiency BBFRAME mode (Generic Stream Encapsulation – High Efficiency Mode (GSE-HEM)); and v) signalling of streams which are GSE-Lite compliant. Depending on the frame length, the MODCODs span from a BPSK to a 256 A-PSK. A comparison between the spectral efficiency provided by DVB-S2 and DVB-S2X is shown in Figure 60, where the extended range of SNR are well highlighted along with the improved efficiency in the common SNR range, achieved with a smaller roll-off value than the one use by the DVB-S2.

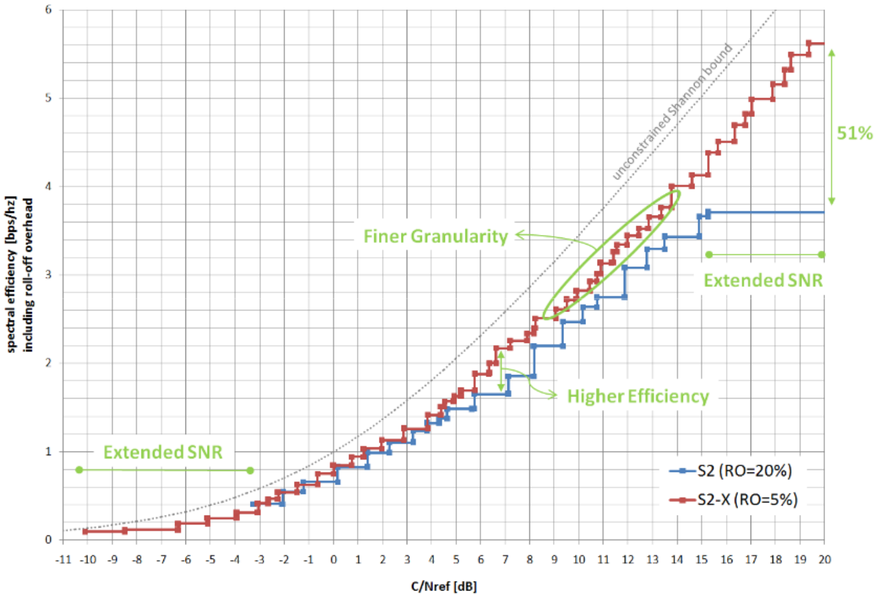

FIGURE 60: COMPARISON OF DVB-S2 AND DVB-S2X. EFFICIENCY VERSUS C/N REF FOR THE SAME OCCUPIED BANDWIDTH

The transmitter of the DVB-S2X is based on the same building blocks of the DVB-S2, however some modifications are introduced in order to support the new features of the standard. In the following, these modifications are described.

In the mode adaptation block, the main changes are related to the support of the GSE-HEM. Indeed, GSE variable-length or constant length UPs may be transmitted in GSE-HEM. In GSE-HEM, slicing of GSE packets is performed and SYNCD is be computed. The receiver may derive the length of the UPs from the packet header, therefore UPL transmission in BBHEADER is not performed. UP is not sliced when there is a BBFRAME from a different stream following and the splitting is only possible with the immediately following BBFRAME. The optional ISSY field is transmitted in the BBHEADER. Therefore, the Mode Adaptation unit shall perform the following sequence of operations.

- Optional input stream synchronization relevant to the first transmitted UP which starts in the data field; ISSY field inserted in the UPL and SYNC fields of the BBHEADER;
- Null-packet Deletion and CRC-8 at UP level shall not be computed nor inserted.
- SYNCD computation (pointing at the first bit of the first transmitted UP which starts in the Data Field) and storage in BBHEADER. The transmitted UP corresponds exactly to the original UP itself. Hence SYNCD points to the first bit of the original UP.
- CRC8_MODE computation. This is the EXOR of the CRC-8 (1-byte) field with the MODE (1-byte) field. CRC-8 is the error detection code applied to the first 9 bytes of the BBHEADER. MODE (8 bits) shall be 1_D for GSE-HEM.
- UPL not computed nor transmitted.
- GSE-Lite compliance of the stream shall be signalled in the 6th bit of the MATYPE-1 field. GSE-Lite=1 means a GSE-Lite compliant signal is transmitted. GSE-Lite=0 means that the transmitted GSE stream may not meet the definition of a GSE-Lite signal.

Another difference lies in the channel bonding. Channel bonding allows for example to avoid unused capacity in a transponder in case of Constant Bit-Rate video programes, and /or to maximize the statistical multiplexing gain in case of Variable Bit-Rate (VBR) video programes.

The Channel bonding for the TS allows a single "big-Transport-Stream" to be carried in parallel over L transponders ($L \leq 3$). This requires that the receivers are equipped with L tuners/S2X decoders, receiving in parallel the L "partial" Transport Streams from the L transponders, and reconstructing the original "big-Transport-Stream". The L S2X modulators are allowed to adopt the same symbol-rate and MODCOD or different ones. The number of bonded transponders and their carrier frequencies are signalled in the System Information (SI) tables according to ETSI EN 300 468. These SI tables are transmitted in parallel over each of the bonded transponders. This allows an initial signal scan with a single tuner to extract SI tables. The principle of the S2X transmitting side shall be according to Figure 61, where the L S2X modulators use the same modulo 2^{22} Input-Stream Synchronization (ISSY) counter, clocked by the symbol-rate of a master channel (in Figure 61, modulator number 1 as example), to implement ISSY. The correspondence between the RF channel and master channel shall be signalled to the receivers via the SI. Null-Packet deletion is implemented in all modulators. The input "big-TS" shall be split at TS-packet level over L branches, as follows:

- For PIDs $\notin$ {SI tables}, when a TS packet is routed into a branch, corresponding Null Packets shall be generated on the other output branches.
- For PIDs $\in$ {SI tables}, the packet shall be copied in all the output branches.

Each input packet with PID $\notin$ {SI tables} is routed into a branch such that the interval between two useful packets with PIDs $\notin$ {SI tables} (in terms of TS packets) which are separated by Null Packets, not including packets with PIDs $\in$ {SI tables}, generated in the SPLIT block, is kept to a minimum and as uniform as possible. The useful packet intervals shall be according to the ratio of the total bitrate of the bonded channels to the TS rate of each channel. For L = 2 channels, this can be fulfilled if the useful packet interval of transponder k takes on only two different values: floor (total TS rate/TS rate of transponder k) and/or ceil(total TS rate/TS rate of transponder k), in which floor(x) and ceil(x) denote the flooring and ceiling operation, respectively. The useful packet interval is defined as the number of Null Packets, not including packets with PIDs $\in$ {SI tables}, inserted into two useful packets in the SPLIT block plus 1.

The TS rate of each transponder k = 1, 2…, L is the rate used for transferring packets with PIDs $\notin${SI tables} in channel bonding on this transponder. This corresponds to the total TS rate of the transponder minus the data rate occupied by PIDs $\in${SI tables}. The total TS rate in above equations is the sum of such TS rates of all transponders. Each S2X modulator shall activate Input Stream Synchronization by setting the suitable ISSY field. Transport Stream rate-adapters (i.e. adding or deleting Null-Packets and adjusting the MPEG time-stamps) is not inserted after the split.

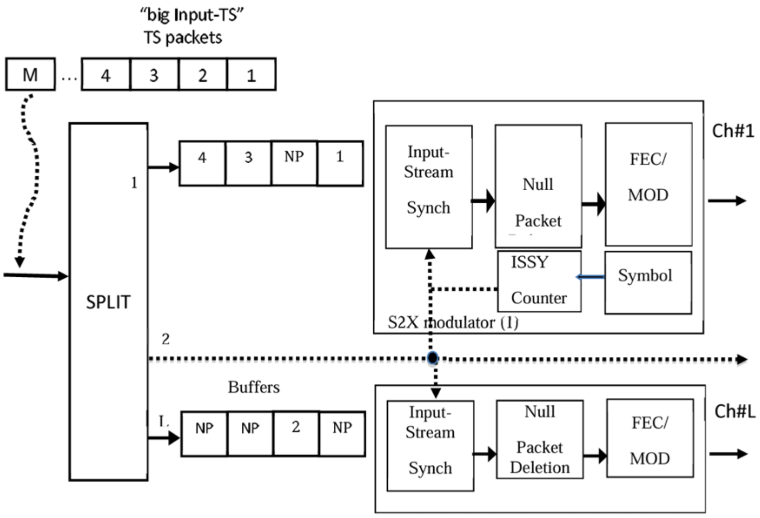

FIGURE 61: PRINCIPLE OF THE TRANSMITTING MODULATORS CONFIGURATIONS FOR CHANNEL BONDING

Generic Stream Encapsulation is an extremely flexible method to transmit any kind of data, including popular formats such as IP packets or TS packets where the data can be of fixed or variable length. GSE can be used for bonded channels to support a higher data rate than can be carried in a single RF channel. A maximum of L channels (L ≤ 3) is supported. The number of bonded transponders and associated information is signalled in the GSE-LLC tables according to ETSI TS 102 606-2. These GSE-LLC tables shall be transmitted in parallel over each of the bonded transponders. To ensure maximum efficiency in S2X, it is recommended to use GSE-HEM.

Channel bonding for GSE transmission is like the TS method of bonding, using the ISCR timing data in the ISSY field to allow the receiver to align packets from different Radio Frequency (RF) channels. However, ISSY is not added per UP, but per BBFRAME. ISSY is always used for bonded GSE channels. In the ISSY field, ISCR is transmitted every BBFRAME. BUFS and BUFSTAT shall not be transmitted. At the modulator, input UPs (GSE packets) are continuously added to the Data Field of a single BBFRAME until it is complete. Appropriate ISSY information is added to the baseband frame header (BBHEADER) of each BBFRAME. ISSY information refers to the first transmitted UP which starts in the Data Field. UPs shall be transparently sliced between BBFRAMEs on different RF channels as necessary - it is not required to slice UPs on BBFRAMEs using the same RF channel. The order of input UPs shall be maintained in the bonding process. Each BBFRAME is constructed with a length that is derived according to the modulation and coding parameters for that RF channel. Each RF channel may have different modulation and coding parameters. To reduce buffering requirements, BBFRAMEs is created for each RF channel according to the ratio of the bitrate of each RF channel. For example, if the bitrates of two bonded RF channels are equal, BBFRAMEs for each RF channel shall occur in alternating fashion. At the receiver side, each GSE bonded RF channel is demodulated according to the modulation and coding parameters for that RF channel. Thus, the output from each demodulator is then combined at the Merger using the ISSY information contained in the BBHEADER of each BBFRAME. The ISSY information provides the timing information to recover the order of the BBRAMES from different demodulators. Since ISSY information applies to each BBFRAME, and the packet order of UPs within each BBFRAME is maintained, the overall order of UPs is maintained at the Merger output. Split UPs are reconstructed in the Merger. In comparison to the TS method, the output bitrate of each demodulator is no greater than the bitrate of the channel, which can significantly reduce the processing burden at the Merger. Furthermore, since ISSY information need only be processed per BBFRAME, the merging operation processing burden is also reduced. A maximum tolerance of one BBFRAME of delay shall be allowed between the different

Co-funded by the European Union

receivers. After merging, additional processing such as filtering of GSE packets, output of IP or TS packets rather than GSE packets, and so on may be undertaken at the receiver as necessary.

The other modifications occur in the FEC Encoding module, as new coding rates and modulation formats are available. For VL-SNR support an additional FECFRAMEs (shown in Table 47) is defined with n_{ldpc}= 32 400 bits covering only BPSK modulation, coding rates 1/5, 11/45, 1/3 and requiring puncturing and shortening.

TABLE 47: CODING PARAMETERS FOR MEDIUM FECFRAME n_{ldpc}= 32 400

LDPC Code Identifier	BCH uncoded block K_{bch}	BCH coded block N_{bch} LDPC uncoded block k_{ldpc}	BCH t-error correction	LDPC coded block n_{ldpc}
1/5	5 660 (note)	5 840 (note)	12	30 780 (note)
11/45	7 740	7 920	12	30 780 (note)
1/3	10 620	10 800	12	30 780 (note)
NOTE: VL-SNR puncturing and shortening is defined in clause 5.5.2.6.				

Following the FEC Enconding module, also the Constellation and Bit Mapping module foresees changes due to the presence of the new modulations. Each FECFRAME (which is a sequence of 64 800 bits for normal FECFRAME, or 16 200 bits for short FECFRAME, or 32 400 bits for medium FECFRAME), is serial-to-parallel converted (parallelism level = η_{MOD} 1 for π/2BPSK; 2 for QPSK, 3 for 8PSK, 4 for 16APSK, 5 for 32APSK, 6 for 64APSK, 7 for 128APSK, 8 for 256APSK). Then, each parallel sequence is mapped into constellation, generating an (I,Q) sequence of variable length depending on the selected modulation efficiency η_{MOD}. For 128 APSK padding is introduced to have an integer number of constellation points in a FECFRAME; thus, 6 zeros are appended at the end of the FECFRAME after FEC encoding.

VL-SNR modes shall include π/2BPSK modulation. For "Spreading Factor 2" modes, FECFRAME bits shall be repeated twice before mapping into constellation. π/2BPSK symbols shall be generated according to the rule:

$$I_{2i-1} = Q_{2i-1} = \frac{1}{\sqrt{2}}(1-2y_{2i-1}), I_{2i-1} = -Q_{2i-1} = -\frac{1}{\sqrt{2}}(1-2y_{2i-1}), for\ i = 1, \dots, N$$

Where $N = n_{ldpc}/2$ for π/2BPSK modes, $N = n_{ldpc}$ for π/2BPSK spreading factor 2 modes, and N = 450 for VL-SNR header.

Constellations with 8 points can be 8PSK (as DVB-S2 standard) and 8APSK, with constellation points on 3 rings, 2 on the 1st ring, 4 on the 2nd ring, and 2 on the 3rd ring (2+4+2).

In addition to the 16APSK constellation defined in DVB-S2 standard, that has 4 points on the first ring and 12 on the second ring (4+12), another constellation is defined, with 8 points on the first ring and 8 points on the second ring (8+8).

In addition to the 32APSK constellation defined in DVB-S2 standard, that has 4 points on the first ring, 12 on the second ring and 16 on the third ring (4+12+16), a further constellation is introduced with 4 points on the first ring, 12 on the second ring and 16 on the third ring (4+12+16), and another constellation, with 4 rings and 4 points on the first ring, 8 on the second ring, 4 on the third ring and 16 on the fourth ring (4+8+4+16).

Three different 64APSK constellations are introduced, the first with 16 points on the first ring, 16 on the second ring, 16 on the third ring and 16 on the fourth ring (16+16+16+16), the second with 8 points on the first ring, 16 on the second ring, 20 on the third ring and 20 on the fourth ring (8+16+20+20), the third with 4 points on the first ring, 12 on the second ring, 20 on the third ring and 28 on the fourth ring (4+12+20+28).

One 128APSK constellation is introduced, with 6 rings and 128 constellation points, while two different 256APSK constellations are introduced, with 256 constellation points.

The Physical layer framing foresees modification regarding the VL-SNR FRAMES, where the VL-SNR Dummy PLFRAME shall be composed of PLS header with code decimal value of 131 followed by VL SNR Header which is then followed by 15696 unmodulated symbols. In addition to conventional PLFRAME where a PLHEADER is appended to each XFECFRAME, S2

can transport VL-SNR XFECFRAMEs. In this case, after the conventional PLHEADER, an additional VL-SNR Header is transmitted.

VL-SNR XFECFRAMEs shall be two sets:

- Set 1 characterized by XFECFRAMEs of 33 282 modulated symbols including the header and pilot symbols.
- Set 2 characterized by XFECFRAMEs of 16 686 modulated symbols including the header and pilot symbols.

In specific cases VL-SNR frames may be inserted in a S2 transmission without disturbing the regular reception of the S2-frames by legacy receivers capable of ACM/VCM operation (these simply ignore the VL-SNR frames). To make this feasible, the PLHEADERs of the VL-SNR frames shall indicate an un-used (by S2 services) MODCOD and TYPE configuration, corresponding to the suitable XFECFRAME length (i.e. 32 400 symbols for VL-SNR-frames of Set-1 or 16 200 symbols for Set-2). In addition to the regular 36 symbol pilots of S2-frames, VL-SNR frames insert additional pilot symbols which are either 32, 34, or 36 symbols long. In particular for VL-SNR frames of Set-1, additional 34 symbol pilots shall be inserted within the groups 1 through 18, and additional 36 symbol pilots shall be inserted within the groups 19 through 21. For VL-SNR frames of Set-2, additional 32 symbol pilots shall be inserted within the groups 1 trough 9, and additional 36 symbol pilots shall be inserted within the group 10.

The PLHEADER (one SLOT of 90 symbols) is composed of the following fields: i) SOF (26 symbols), identifying the Start of Frame and ii) PLS code (64 symbol): PLS (Physical Layer Signalling) code, carrying 1+7 signalling bits denoted as (b0, b1, …, b7), where b0 is the Most Significant Bit (MSB) and b7 is the Least Significant Bit (LSB). The most significant bit indicates whether the PL header refers to regular DVB-S2 MODCODs (b0= 0) or whether the PL header refers to DVB-S2X MODCODs (b0 = 1).

In order for VL-SNR frames to be compatible with legacy DVB-S2 VCM receivers, the PLFRAME length including the mobile header and increased pilot symbols shall be the same as in DVB-S2 PLFRAME. This requires reducing the information carrying symbols of VL-SNR frames through shortening and puncturing. If an LDPC block is shortened, the first X_s information bits are set to zero before encoding, and they will not be transmitted. If an LDPC block is punctured, every p^{th} parity bit starting with the first parity bit, p_0, (i.e., p_0, p_p, p_{2p} …) will not be transmitted until the desired number of punctured bits, X_p, is achieved.

8.1.3 DVB-RCS2

The Return Channel Satellite Terminal (RCST) or Satellite Interactive Terminal (SIT) is the user terminal receiving the broadcast channel and the forward interaction channel and transmitting return channel. The RCST access the satellite transponder in Multiple Channels Per Carrier (MCPC) way using Multi FrequencyTime Division Multiple Access (MF-TDMA) with a set of carrier frequencies, each of which is divided into time slots for different user terminals. The return transmission is in burst format either in Asynchronous Transfer Mode (ATM) cell of 53-octets (48 octet information payload and 6 octets signaling information) or in Moving Picture Experts Group-Transport Stream (MPEG2-TS) of 188-octets (182 octets of information payload and 6 octets signaling information) [127].

Figure 62 provides the generic digital signal processing to be performed at the RCST transmitter side from the burst formatting of the serial information bit-stream to the modulation representing the digital to analogue conversion [128].

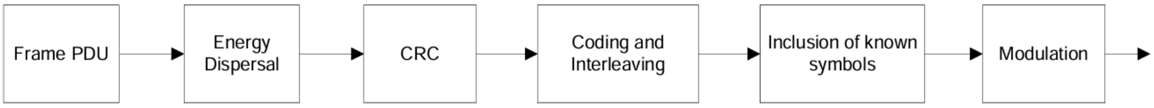

FIGURE 62: BLOCK DIAGRAM OF THE RCTS RETURN LINK BASEBAND SIGNAL PROCESSING

Each transmission burst belongs to a transmission type that is assigned a specific content type. This is determined by the specification of the transmission type in the Return Link Broadcast Configuration Table (BCT). The format and syntax of the burst payload is determined by the content type, the transmission context, when the format and syntax is context variant. Four content types are defined: 1) logon (non-configurable context variant frame payload format); 2) control (non-configurable context variant frame payload format); 3) traffic/control (configurable context variant transmission frame payload format); and 4) traffic (configurable context variant transmission frame payload format).

Burst Waveform

The burst waveform generation is applied to the Frame PDU. The generation consists of the following functions: i) energy dispersal, addition of the cyclic redundancy check (CRC); coding and interleaving techniques; unique word and/or known pilot insertion; and linear modulator or continuous phase modulator.

Energy Dispersal

The MF-TDMA return link data stream is organized in bursts. In order to ensure adequate binary transitions, the bit stream in a burst shall be varied by scrambling to reduce the probability of monotonic bit sequences. The used polynomial of the Pseudo Random Binary Sequence (PRBS) is:

$$1 + x^{14} + x^{15}$$

The data is randomized using the 15 register Linear Feedback Shift Register (LFSR) to randomize the distribution of ones and zeroes. The randomizer performs modulo-2 addition of the data with the pseudo-random sequence.

Payload CRC

The frame CRC is calculated for the bit sequence output from PRBS Randomizer. Two CRC are considered depending on the type of payload, i.e., for traffic payload the CRC is 32, while for control burst payload the CRC is 16.

The CRC16 polynomial is $x^{16} + x^{15} + \ x^2 + 1$ and it is the remainder of the division of the burst payload by the polynomial.

While the polynomial for CRC 32 is:

$$x^{32} + x^{26} + x^{23} + x^{22} + x^{16} + x^{12} + x^{11} + x^{10} + x^{8} + x^{7} + x^{5} + x^{4} + x^{2} + x + 1$$

Coding and Interleaving

In the standard two transmitter configuration are specified: i) one using turbo coding and linear modulation, and ii) one using convolutional coding and continuous phase modulation.

The first one uses a double binary Circular Recursive Systematic Convolutional (CRSC) code. The MSB bit of the first byte after the burst preamble is assigned to A, the next bit to B and so on for the remaining of the burst content. The encoder (shown in Figure 63) is fed by blocks of K bits or N couples (K = 2*N bits), where N is a multiple of 4 and K is a multiple of 8.

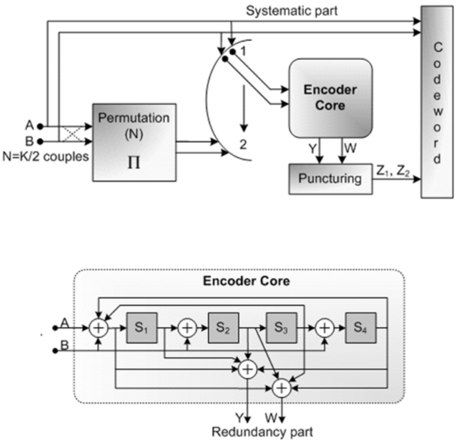

FIGURE 63: ENCODER BLOCK DIAGRAM (TURBO CODE)

The Feedback branch is given by the polynomial $1 + x^3 + x^4$ in symbolic notation. The first parity bits Y are given by the polynomial $1 + x^1 + x^2 + x^4$ and the second parity bits W by the polynomial $1 + x^2 + x^3 + x^4$. The input A bit is connected to tap 1 of the shift register. The input B bit is connected to the taps 1, S1 and S3. First, the encoder (after initialization by the circulation state C1) is fed by the sequence in the natural order (switch in position 1) from incrementing position i=0,...N-1. This first encoding output sequence after puncturing is called Z1. Then the encoder (after initialization by the circulation state C2) is fed by the interleaved order sequence (switch in position 2) with incremental address j=0,...N-1. This second encoding output sequence after puncturing is called Z2. The interleaver function Π(j) gives the natural order index i reference for the considered couple. The encoder core is run four times, first to find the initial circulation states C1 and C2 and then to generate the redundancy couples (Y,W).

The permutation is done in two parts. One part is permutation inside the bit couple and the second part is permutation between couples. A0 is the first information bit that enters the encoder, B0 the second information bit of the first couple with input order index i=0.

The state of the turbo encoder is denoted S with:

$$S = 8 \cdot S1 + 4 \cdot S2 + 2 \cdot S3 + S4, \quad with\ 0 \leq S \leq 15$$

The circulation states C1 and C2 are determined by the following operations:

- The encoder is initialized by the state S=0.

- The sequence is encoded in the natural order for the determination of C1 and in the interleaved order for the determination of C2.
- The last state of the encoder (i.e., the state of the encoder after all the N couples have been encoded) and the N mod 15 determine the initial circulation state (C1 or C2) according to Table 48.

TABLE 48: INITIAL CIRCULATION STATE AS A FUNCTION OF LAST ENCODER STATE S AND N MODE 15

N mod 15	**Last Encoder State**															
	0	**1**	**2**	**3**	**4**	**5**	**6**	**7**	**8**	**9**	**10**	**11**	**12**	**13**	**14**	**15**
1	0	14	3	13	7	9	4	10	15	1	12	2	8	6	11	5
2	0	11	13	6	10	1	7	12	5	14	8	3	15	4	2	9
3	0	8	9	1	2	10	11	3	4	12	13	5	6	14	15	7
4	0	3	4	7	8	11	12	15	1	2	5	6	9	10	13	14
5	0	12	5	9	11	7	14	2	6	10	3	15	13	1	8	4
6	0	4	12	8	9	13	5	1	2	6	14	10	11	15	7	3
7	0	6	10	12	5	3	15	9	11	13	1	7	14	8	4	2
8	0	7	8	15	1	6	9	14	3	4	11	12	2	5	10	13
9	0	5	14	11	13	8	3	6	10	15	4	1	7	2	9	12
10	0	13	7	10	15	2	8	5	14	3	9	4	1	12	6	11
11	0	2	6	4	12	14	10	8	9	11	15	13	5	7	3	1
12	0	9	11	2	6	15	13	4	12	5	7	14	10	3	1	8
13	0	10	15	5	14	4	1	11	13	7	2	8	3	9	12	6
14	0	15	1	14	3	12	2	13	7	8	6	9	4	11	5	10

Each burst has a FEC code rate determined by a specific puncturing period and puncturing pattern, for each of the bit streams of the redundancy bits Y and W. The different rates are achieved through generating parity bits by selectively deleting the redundancy bits (puncturing). The chosen puncturing patterns are applied. These patterns are identical for both the natural order and the interleaved order encoder outputs. They are also independent of the modulation (depends only on the code rate). The output sequences of the puncturing are named Z1 and Z2, respectively for the natural-order encoding and the interleaved-order encoding. They each consist of the Y parity bits that remain after puncturing, followed by the W parity bits that remain after puncturing.

The convolutional coding for continuous phase modulation consists of the convolutional coder, bit interleaving, bit-to-symbol mapping, and the CPM modulator, as shown in Figure 64.

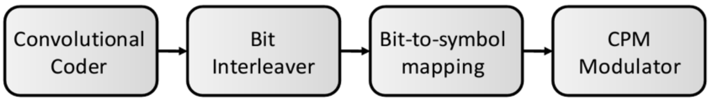

FIGURE 64: BLOCK DIAGRAM OF THE CC-CPM TRANSMITTER COMPONENTS

The FEC encoder for the CPM uses binary, non-systematic, non-recursive convolutional codes. The constraint length K is either 3 or 4. The generator polynomials for the rate 1/2 constraint length 3 code are GNS1 = $1 + x^2$ and GNS2 = $1 + x + x^2$. While the generator polynomials for the rate 1/2 constraint length 4 code are GNS1 = $1 + x + x^3$ and GNS2 = $1 + x + x^2 + x^3$.

Code rates >1/2 are obtained by puncturing the rate ½ code. The puncturing pattern is periodically applied to the serialized bit stream at the rate 1/2 convolutional encoder's output. When the puncturing pattern is 1 the corresponding encoder output is transmitted and when it is 0, the encoder output is deleted.

After the encoding of information bits is complete, the convolutional encoder states are flushed to all zero values by feeding tail bits t0=0, t1=0 for the constraint length 3 code, and t0=0, t1=0, t2=0 for the constraint length 4 code. After that the bit interleaver is performed by means of a permutation indices.

Inclusion of known symbols

The transmission bursts are constructed by combining the payload symbols with symbols known to the receiver in advance, including a unique word. The burst construction rules differ for a TC-LM transmitter and a CC-CPM transmitter.

The burst construction for linear modulation implies preamble and postamble at the beginning and the end of the burst and in the middle. When direct-sequence spreading is employed, this user payload is obtained from the sequence of symbol values by repetition of the representation of each symbol a number of times equal to the spreading factor. The other components are section types with predetermined content known as preamble (pre), pilot block (p) and postamble (post). A preamble is typically present in every burst. The repetitions, the size, the interval, and the content of the pilot block are configurable. The pilot blocks are evenly distributed with evenly sized payload sections in between. A postamble may be present.

The generic CC-CPM burst implies the insertion of a unique word (UW) in each CC-CPM burst to support frequency and timing recovery in the receiver, and decoder initialization. The total length of this unique word shall be less than or equal to 256 unique word symbols. The unique word is divided in nbr_uw_segments segments of specific length that are located in specific positions in the burst.

Regarding the modulation, two schemes are supported by the RCST: i) linear modulation for the turbo coded (TC-LM) Frame PDU and ii) continuous phase modulation for the convolutionally coded (CC-CPM) Frame PDU.

The transmission burst of TC-LM is constituted by three sections of symbols, the preamble section, the payload section, and the postamble section.

Prior to modulation, the I and Q signals (mathematically represented by a succession of Dirac delta functions, multiplied by the amplitudes I and Q, spaced by the symbol duration TS = 1/RS) are filter through a square root raised cosine filter with a roll-off factor shall be 20%. For the payload modulation format, there are four TC-LM modulation formats, π/2-BPSK, QPSK, 8PSK and 16QAM.

In the case of π/2-BPSK modulation, all couples of systematic bits (A,B) are transmitted first, followed by all couples of systematic parity bits (Z1,Z2) that result after puncturing. The format is given in Table 49.

TABLE 49: BIT TO SYMBOL MAPPING FOR PI/2-BPSK MODULATION

Symbol index	u_0
0	A_0
1	B_0
2	A_1
3	B_1
…	
N-2	$A_{N/2-1}$
N-1	$B_{N/2-1}$
N	$Z_{1,0}$
N+1	$Z_{2,0}$
N+2	$Z_{1,1}$
N+3	$Z_{2,1}$
…	
N+M-2	$Z_{1,M/2-1}$
N+M-1	$Z_{2,M/2-1}$

The value of u_0 is first BPSK mapped with +1 representing a '0' encoder output bit and –1 representing a '1' encoder output bit. All symbols in the frame are further mapped to π /2-BPSK modulation. This mapping is done by the outer phase rotation:

$$s(n) = u(n)e^{(\frac{j2\pi n}{2}+\frac{j\pi}{4})}$$

Where u(n) denotes BPSK symbol number n in the burst, and the resulting s(n) symbol is placed in one of the four possible s_k positions. The integer value n to apply for the very first symbol in the burst is arbitrary. The additional π /4 term in the phase rotation equation is a convenience factor, in order to place the symbols as for QPSK modulation.

In the case of the modulation QPSK, all couples of systematic bits (A,B) are transmitted first, followed by all couples of systematic parity bits (Z1,Z2) that result after puncturing.

For the 8 PSSK, the parity bits are always assigned to the bit u_0 ($u_0$and $u_1$are most protected by the constellation than u_2). The systematic bits A and B are assigned respectively to u_1 andu_2. The bits are assigned to symbols in the natural encoder output order. The ordering of the A and B bits are following the puncturing pattern (given by the configured puncturing map).

A 16-QAM constellation can be decomposed into two independent 4-Pulse Amplitude Modulation constellations, respectively on I and Q axis (denoted I-PAM and Q-PAM). The symbol mapping for 16QAM is specified for code rates 3/4 and higher. The parity bits are assigned to the most protected bit position u_1-bit of the Q-PAM. For rates > 3/4, the number of symbols is higher than the number of Z-bits in the frame. Once all Z-bits have been assigned to the first 2M symbols, the remaining A and B bits are used to fill the remaining symbols, in the order they are coming out from the encoder. If the pattern is incomplete, the I-PAM is fed by 0. If the last 16QAM symbol resulting from this mapping is only required for transmission of a solitary trailing parity bit, this 16QAM symbol is omitted from the waveform.

When direct-sequence spreading is employed, the entire burst, including preamble, pilots and postamble, is scrambled by chip-by-chip multiplication by a pseudo-random sequence. The sequence is re-set to its beginning at the start of each burst and shall be repeated as required to scramble the complete burst.

The complex baseband CPM signal is given by:

$$s(t) = \sqrt{\frac{2E_s}{T_s}}\, e^{j\varphi(t)}$$

Where T_s is the symbol duration. The CPM phase (t) is given by:

$$\varphi(t) = 2\pi h \sum_{i=0}^{\infty} a_i q(t - iT_s), t \ \geq 0$$

With:

- a_i indicating the input symbol to the demodulator, such that $a_i \in \{\pm 1, \pm 3\}$
- h indicating the modulation index and is a rational number
- $q(t)$ is the CPM phase response and it is a continuous function, such that:

$$= 0, t \ < 0$$

$$\begin{aligned} q(t) \quad &= \int_0^t g(\tau)d\tau, \;\; 0 \; \leq t \leq LT_s \\ &= 0.5, t \; > LT_s \end{aligned}$$

Where L is the memory of the modulation, and it is set to L = 2.

The pulse shape, known as the weighted average (AV) CPM pulse shape is a linear combination of the raised-cosine (RC) and rectangular (REC) pulse shapes, such that:

$$g_{AV} = \alpha_{RC} g_{RC} + (1 - \alpha_{RC}) g_{REC}$$

With:

$$g_{RC}(t) = \frac{1}{4T_s}\left(1 - cos\,\frac{\pi t}{T_s}\right), 0 \leq t \leq 2T_s$$

$$g_{RC}(t) = 0, otherwise$$

$$g_{REC}(t) = \frac{1}{4T_s}, 0 \leq t \leq 2T_s$$

$$g_{REC}(t) = 0, otherwise$$

The FEC encoded bit sequence, after interleaving, is mapped to symbols. When the modulation index h = 1/3 the bit to symbol mapping is given by Table 50. For the remaining modulation indices, Gray mapping is used as indicated in Table 51. If the length of the bit sequence at the interleaver output is not exactly divisible by $log_2(M)$, a bit 0 is appended at the end of the interleaved bit sequence prior to applying the bit to symbol mapping.

TABLE 50: BIT TO SYMBOL MAPPING FOR H = 1/3

MSB	LSB	Symbol value
0	0	−3
0	1	−1
1	0	1
1	1	3

TABLE 51: BIT TO SYMBOL MAPPING FOR H ≠ 1/3

MSB	LSB	Symbol value
0	0	−3
0	1	−1
1	1	1
1	0	3

TRANSMISSION BURST TIMING.

Accurate synchronization of the RCST transmissions is an important feature of the satellite interactive network. Constraints are imposed on the RCSTs to obtain an efficient TDMA system with minimum interference between RCSTs and maximum throughput (although these constraints may be relaxed if the receiver performs tasks such as satellite frequency translation error and common-mode Doppler compensation for RCST carrier frequency). For this reason, the synchronization scheme is based on information contained within the Forward Link Signalling as follows:

- Broadcast of the Network Clock Reference (NCR).

- Broadcast of the return link satellite position in the SPT.
- Optional broadcast of nominal timing offset in the initial transmission timing in the FAT.
- Broadcast of the burst time plan in the SCT, FCT2, BCT and TBTP2.
- Transmission timing adjustment for each RCST transmitted in TIM-U and CMT.

The forward link that carries the Forward Link Signalling contains an NCR counter which provides a 27 MHz clock reference as well as a time reference to the RCSTs connected to the forward link. The NCR is fed on the forward link with an accuracy of 5 ppm or better. The minimum NCR value injection frequency is 10 pps. The RCST uses the NCR as the timing reference for the burst transmission. To minimize truncation errors, the N LSB bits of the scaled value in the transmission timing adjustments are set to an approximate mid-range value of "1" followed by "0"s, with N being the value of the Burst_time_scaling field.

The transmission of the logon burst shall accurately adapt to the timing indicated for the superframe sequence as referenced to the NCR received from the forward link, as if the NCR propagated from the return link satellite, offset by the optional Timing Offset Descriptor if this is provided in the FAT (or as part of the NCR TS packet, when considering a TS Packet stream). The propagation delay compensation shall nominally reflect the propagation delay between the nominal position of the RCST as provided to the RCST and the nominal position of the return link satellite as indicated by the NCC via the SPT. Before issuing the logon burst, the RCST calculates the satellite ranges for both forward and return links using the satellite ephemeris data contained within the most recent Satellite Position Table (SPT) plus knowledge of its own location (latitude, longitude and height above sea level). It shall use these ranges to calculate the corresponding satellite to RCST and RCST to satellite propagation delays. A nominal satellite position that may be found in the NIT shall be used if the NCC does not transmit the SPT.

The RCST additively offsets transmission start of succeeding transmission bursts as instructed by the NCC in the Correction Message Descriptor provided in TIM-U and the Correction Message Table. Moreover, the RCST supports a control resolution of 1 NCR tick in this process. The RCST shall take into account all timing corrections received at least 90 ms in advance of transmission start. The TIM-U may contain multiple CMDs that each has independent scaling factors. All the corrections of the CMDs of a TIM-U shall be used for adjustment of the timing. Burst transmission time start accuracy shall for any burst be within 50 % of a symbol period relative to the nominal start time. The burst transmission time accuracy is the worst case deviation between the scheduled start of a burst transmission and the actual start of the burst transmission. The scheduled start of burst transmission is the nominal point in time where the RCST should start transmission according to the NCR, the BTP and the received timing corrections.

Symbol clock accuracy shall be within 20 ppm from the nominal symbol rate. The symbol clock rate shall have a short term stability that limits the time error of any symbol within a burst to 1/20 symbol duration.

The carrier frequency accuracy shall be better than 10^{-8}(root mean square) relative to the nominal carrier frequency. Each logon burst shall be issued at the nominal carrier frequency indicated by the SCT/FCT2 for the specific logon timeslot. Other bursts shall be issued at a nominal carrier frequency offset relative to SCT/FCT2 resulting from the accrued frequency corrections received in CMD in TIM-U and CMT, and in a Satellite Return Link descriptor in TIM-U if the operational SFS is assigned this way. The RCST shall take into account all frequency corrections received at least 90 ms in advance of transmission start.

8.1.3.1 The Return Link Structure (MF-TDMA)

MF-TDMA allows e.g., a group of RCSTs to communicate with a gateway sharing a set of carrier frequencies, each of which is divided into timeslots for burst transmission. A burst is defined by carrier frequency, bandwidth, start time, duration, the type of burst payload content to be issued and other characteristics.

The timeslots of the MF-TDMA carriers are organized and numbered so that the NCC easily and efficiently can refer to individual timeslots in the allocation process. The largest entity is the super-frame, composed of frames that are again composed of timeslots. Each timeslot is constructed from a number of equal Bandwidth-Time Units (BTU). Each frame is constructed of timeslots that are constructed of multiples of one BTU type.

A superframe is composed of frames themselves composed of slots limited in time and frequency, called timeslots. The frame is at an intermediate level between the superframe and the timeslots and it is introduced for reasons of signalling efficiency (forward link signalling). The superframe may be implemented with frames in non-adjacent frequency bands.

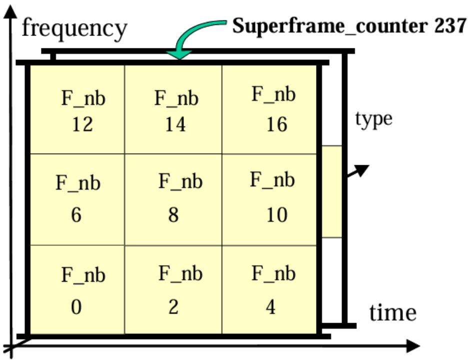

FIGURE 65: EXAMPLE OF SUPERFRAME COMPOSITION

Figure 65 provides an example of superframe composition.

In a superframe, the frames are numbered from 0 (lowest burst centre frequency, first in start time, lowest in frame type ID) to N (highest carrier frequency, last in start time, highest in frame type), ordered, with falling precedence, according to ascending lowest burst centre frequency, ascending start time and then ascending frame type as shown in the example in Figure 65. N shall be less than or equal to 255. The superframe and its frames may have the same duration, in which case each frame is constricted to a frequency sub-band of the superframe. The frames of a superframe may also differ in duration as well as bandwidth and timeslot composition, and Figure 65 shows an example of a superframe with a duration 3 times a unified frame duration as well as with frames occupying the same time and frequency space. The superframe duration is system dependent. An RCST shall support operation in superframes ranging in duration from 25 ms to 750 ms and may support operation with superframe durations outside this range.

A superframe sequence (SFS) is a portion of frequency bandwidth of the return link, not necessarily contiguous, constituted by a consecutive sequence of superframes of a dedicated superframe type. Each superframe of the superframe sequence is equally delimited in duration and bandwidth occupation as specified for the associated superframe type. The SFS identifies a set of MF-TDMA resources within the network. The MF-TDMA capacity may be segmented by allocating RCSTs to different superframe sequences, and the interactive network will then manage several concurrent superframe sequences. The RCST shall be able to keep track of dynamically assigned timeslots for raffic assigned up to 1 second in advance of its use, referring to operation on a superframe sequence. This concerns the operational interactive state control timeslots and traffic timeslots for random access as well as dedicated access to the specific RCST.

A frame is delimited in time equal to or shorter than the duration of the parent superframe and may span several frequency bands that do not have to be adjacent. Each frame is dedicated to a specific transmission format class. The frame is composed of Bandwidth-Time Units (BTU) of one single type organized as one or more BW limited time sequences of contiguous BTUs, each sequence spanning the duration of the frame in one frequency sub-band. The timeslots in the frame are composed of one BTU or several BTUs adjacent in time. The symbol rate is determined by the BTU. Thus, all the timeslots of the frame use equal symbol rate and spans equal BW. A frame type identifies a particular relative arrangement of timeslots aggregated from one type of BTU. For example, frame_type = 1 could identify a sequence of 10 "user traffic" timeslots on the same carrier, and frame_type = 2 a sequence of 4 "control" timeslots followed by 8 "user traffic" timeslots, all on the same carrier. A frame type may also span several carriers with a relative offset. A frame type may refer to consecutive timeslots, each of a single BTU that are not allocated to a specific transmission type in advance but instead aggregated in consecutive sequences and each timeslot aggregate mapped to a specific transmission type matching the aggregate, indicated to the RCST just in time by using the TBTP2.

Separation of consecutive transmission bursts on the same carrier is intended supported by a nominal guard time, to allow for RCST power ramping transients and errors in the transmission timing. Guard time is allocated by the NCC and may differ for the timeslots. The required guard time is system dependant, and it is determined by the system design. The leading and trailing guard time for a specific burst are determined by the combination of the size of the burst, the size of the two adjacent bursts, the size of the timeslots associated to the bursts and the nominal burst offset for each of the bursts. The NCC controls these parameters via the FCT2, the BCT and the TBTP2. The BCT specifies the alignment of a burst in a block of consecutive BTUs.

transmission channel allows a group of RCSTs to communicate using a set of carrier frequencies, each of which is divided into timeslots. The NCC will allocate to each active RCST a number of timeslots/bursts pairs, each defined by a number of parameters including modulation scheme, coding rate, frequency, symbol rate, start time and duration. This constitutes the Transmission Channel for an RCST. Any of these characteristics may change between successive bursts, provided the sets of parameters are among those made available for the current BTP (SCT, FCT2, and BCT).

The RCST may not be capable of switching dynamically between linear modulation and constant-envelope modulation during a log-on session. The frequency agility of an RCST is specified in terms of long-term frequency tuning and rapid burst-to-burst carrier switching. Long-term frequency tuning represents a change in centre frequency of the carrier switching band. The settling time for a long-term frequency tuning shall not exceed 1 s. The different transmission formats are grouped in transmission format classes where each class is distinguished by some shared major characteristics of the transmission format. The different variants of transmission format classes that are recognized are listed in Table 52.

The ability of the RCST to perform burst-to-burst carrier switching within a burst-based transmission format class is distinguished as "fast" or "slow". "Fast" carrier switching is defined as the ability to transmit in adjoining timeslots on any frequency within the switching band. "Slow" carrier switching is defined as the ability to transmit on any frequency within the switching band when the transmitter is allowed at least a minimum idle interval between transmission timeslots as indicated in Table 53.

TABLE 52: TRANSMISSION FORMAT CLASS VARIANTS

Transmission format class	Classes application for switching to/from
Linear Modulation Bursts	Continuous Transmission, Spread-Spectrum Linear Modulation Bursts
Continuous Phase Modulation Bursts	
Continuous Transmission	Linear Modulation Bursts, Spread-Spectrum Linear Modulation Bursts
Spread-Spectrum Linear Modulation Bursts	Linear Modulation Bursts, Continuous Transmission
User defined Format Classes	

TABLE 53: MINIMUM GUARD INTERVAL AS A FUNCTION OF CARRIER FREQUENCY CHANGE

Transmission format class	Classes application for switching to/from
Linear Modulation Bursts	Continuous Transmission, Spread-Spectrum Linear Modulation Bursts
Continuous Phase Modulation Bursts	
Continuous Transmission	Linear Modulation Bursts, Spread-Spectrum Linear Modulation Bursts
Spread-Spectrum Linear Modulation Bursts	Linear Modulation Bursts, Continuous Transmission
User defined Format Classes	

An RCST shall indicate its ability to perform either fast or slow carrier switching, and also its switching band for doing this. When switching to a transmission type belonging to another transmission format class than the one currently used, the switching latency is implementation dependent and may even imply a reboot of the RCST. The latency shall however not exceed 2 s for switching to and from the optional continuous carrier transmission, when this is supported. An RCST has a well-defined minimum band for the carrier frequency switching from time-slot to time-slot. Change to a frequency outside this minimum band may be implemented by the slower carrier frequency tuning mechanism. The RCST indicates the size of the switching band to the NCC. The minimum carrier frequency switching step supported by an RCST shall be at least ±50 % of the minimum band for the switching class claimed supported, aligned with the centre frequency of the band in use, for the different classes of carrier switching ranges defined in Table 54.

TABLE 54: THE DIFFERENT CARRIER SWITCHING CLASSES

Carrier switching class	Minimum band size
Class 1	36 MHz
Class 2	125 MHz
Class 3	250 MHz
Class 4	500 MHz

Change of carrier frequency in excess of this range is considered retuning and out of scope for the fast and slow carrier frequency switching performance requirements. The RCST can as an option employ a continuous carrier mode of transmission in accordance with the provisions in this clause. The ability to operate in this manner shall be signalled in the logon PDU. An RCST declaring support for continuous carrier operation shall be capable of transmitting either a continuous carrier or an MF-TDMA signal as instructed but need not be able to transmit both simultaneously.

The RCST shall limit adjacent channel power emission for continuous transmission. The autonomous back-off level indicated to the NCC at logon also applies to continuous transmission. There are two variants of continuous-carrier operation. In the so-called "non-persistent mode", the RCST will autonomously revert to TDMA operation when the continuous carrier assignment expires without renewal and following log-off and TX Disable instructions. In "persistent mode", the RCST will not autonomously revert to TDMA, even following a power cycle, and will autonomously resume CC transmission unless it receives an explicit carrier revocation.

Continuous return link carriers are specified and referred to by the same means as used for MF-TDMA timeslots. In the FCT2, a frame_type can define one or more carriers for continuous transmission, all with the same symbol-rate. A frame_type cannot define a mix of continuous carriers and MF-TDMA carriers. A superframe with multiple frames can however apply a mix of such frame_types. Assignment of any timeslot on a carrier of a frame for continuous transmission shall be understood to apply to the entire carrier. Such frames form part of a Superframe Sequence in the same manner as other frames. A pair of frames in the same superframe may refer to the same frequency BW, one being specified for continuous transmission and the other for burst transmission. The BCT contains specifications/references for continuous carrier waveforms with identification of their respective tx_types, parallel to burst waveform specifications/references and corresponding tx_types. The continuous carrier is organized in carrier frames. Each carrier frame consists of a number of code words with uniform size, code rate, modulation and spreading factor, corresponding to a particular tx_type. The carrier frame further contains a number of known symbols, organized in a preamble and distributed pilot blocks. Subsequent carrier frames may use different tx_types. The carrier frame is distinct from the frame implicitly referred to by the term "Frame PDU", as it may hold a number of Frame PDUs.

The carrier frame is constructed as follows:

1. User data SDUs and control PDUs are encapsulated and organized in code block payloads. Each code block payload corresponds to one Frame PDU.
2. Each code block payload is scrambled for energy dispersal and the CRC is appended
3. Each scrambled block appended with CRC is FEC encoded using the turbo code.
4. The coded bits of each block are mapped to modulation symbols.
5. The carrier frame payload is constructed by concatenating the required number of blocks of modulated symbols.
6. The symbols are each repeated SF times, where SF is the desired spreading factor. Operation with SF > 1 shall be supported if spread spectrum TDMA operation is supported. The sequence is further extended by a number of padding chips. The padding chips are pseudo-random, drawn from the symbol alphabet of the chip sequence. It is worth mentioning that padding chips may be used to achieve a uniform carrier frame duration among several combinations of block payload size, code rate, number of blocks, modulation and spreading factor.
7. A preamble is pre-pended and pilot chip blocks are inserted with the modification that references to bursts in said clause shall be understood to apply to carrier frames of the continuous carrier.
8. If so specified, the sequence of chips is multiplied by a (±1) binary scrambling sequence. This sequence is reset at the beginning of every carrier frame. This scrambling sequence is a section of a PN-sequence, generated according to a specified polynomial and initial condition in the same manner as for spread-spectrum bursts.

8.2 APPENDIX B: OTHER HW IMPAIRMENTS

The end-to-end filter profile to be taken into consideration can be obtained from the aggregation of three type of profiles (linear, parabolic and sinusoidal ripple) defined in the Table 55 [4].

TABLE 55: GAIN FLATNESS AND GROUP DELAY ACCORDING TO THE THREE TYPES OF PROFILE

Profiles	**Gain flatness profile**	**Group delay profile**
Linear $\boldsymbol{f_0}$ **:** channel center frequency	GF=$\frac{\Delta G}{\Delta F} * (f - f_0)$ [dB] $\frac{\Delta G}{\Delta F}$ = [0,25 dB/MHz] (worst case local slope) $\frac{\Delta G}{\Delta F}$ = [-0,0085 dB/MHz] (typical slope observed on channel bandwidth)	GD=$\frac{\Delta T}{\Delta F} * (f - f_0)$ [ns] $\frac{\Delta T}{\Delta F}$ =[2 ns/MHz] (worst case local slope) $\frac{\Delta T}{\Delta F}$ =[0,0080 ns/MHz] (typical slope observed on channel bandwidth)
Parabolic $\boldsymbol{f_0}$:channel center frequency B: channel bandwidth	GF=$4\Delta G * (f - f_0)^2/B^2$ [dB] $\Delta G = [2{,}4 \text{ dB}]$ for B=500 MHz	GD=$4\Delta T * (f - f_0)^2/B^2$[ns] $\Delta T = [20 \text{ ns}]$ for B=500 MHz
Sinusoidal ripple $\boldsymbol{\Delta f}$: ripple period $\boldsymbol{f_0}$: channel center frequency	GF$= \Delta G \cos\left(\frac{2\pi(f-f_0)}{\Delta f}\right)$ [dB] within 90% of the band ΔG =[0,3 dB] Δf = 15 MHz; 30 MHz; 75 MHz	GD=$\Delta T \cos\left(\frac{2\pi(f-f_0)}{\Delta f}\right)$ [ns] within 90% of the band ΔT= [1,5 ns] $\Delta f = 15 \text{ MHz};\ 30 \text{ MHz};\ 75 \text{ MHz}$

These profiles can be used in FWD and RTN links.

From the previous table, several end-to-end filter profiles can be calculated and considered as reference for link level simulations.

The end-to-end gain response (shown in Figure 66) is derived as follows:

- The gain response includes:
  - A parabolic response, with minimum relative gain of -2,4dB at the edge of the channel.
  - A sinusoidal ripple with 0,3dB amplitude and 30MHz period is added within 90% of the bandwidth.
  - A smooth slope of -0,0085 dB/MHz within all the channel bandwidth.
- The total response is the addition (in dB) of above 3 contributions.
- The response is normalised so that the maximum gain is 0dB.

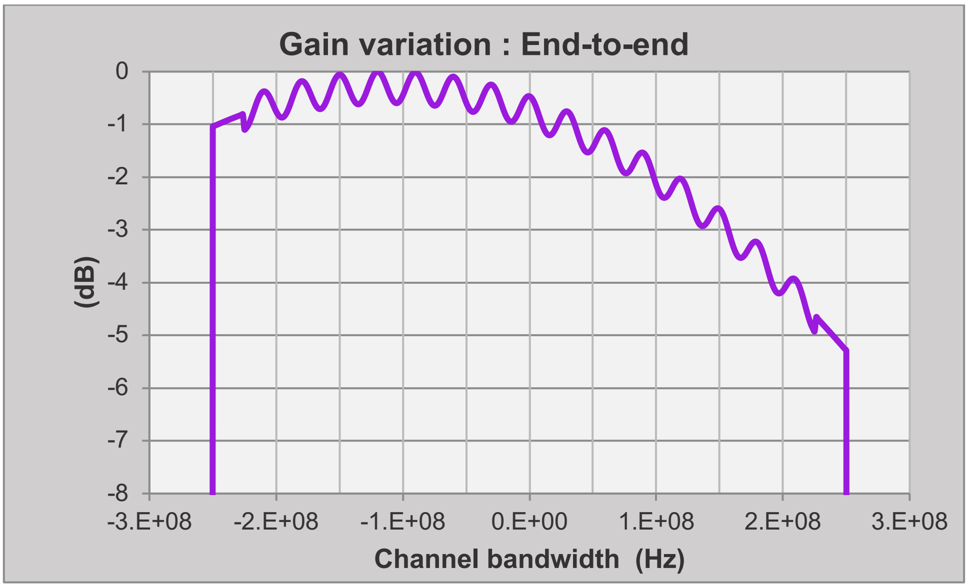

FIGURE 66: END-TO-END GAIN VARIATION

The end-to-end group delay (illustrated in Figure 67) response is derived as follows:

- The group delay response includes:
  - A parabolic response, with maximum value of 20 ns at the edge of the channel.
  - A sinusoidal ripple with 1,5 ns amplitude and 30MHz period is added within 90% of the bandwidth.
  - A smooth slope of 0,0080 ns/MHz within all the channel bandwidth.
- The total response is the addition (in ns) of above 3 contributions.
- The response is normalised so that the minimum group delay is 0ns.

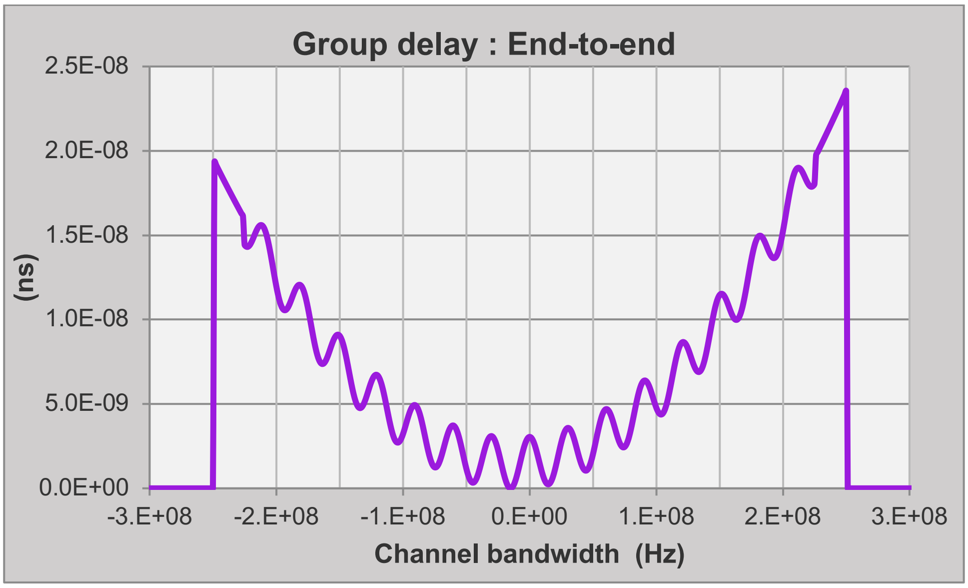

FIGURE 67: END-TO-END GROUP DELAY

Co-funded by the European Union